



University
of Glasgow

<https://theses.gla.ac.uk/>

Theses Digitisation:

<https://www.gla.ac.uk/myglasgow/research/enlighten/theses/digitisation/>

This is a digitised version of the original print thesis.

Copyright and moral rights for this work are retained by the author

A copy can be downloaded for personal non-commercial research or study, without prior permission or charge

This work cannot be reproduced or quoted extensively from without first obtaining permission in writing from the author

The content must not be changed in any way or sold commercially in any format or medium without the formal permission of the author

When referring to this work, full bibliographic details including the author, title, awarding institution and date of the thesis must be given

Enlighten: Theses

<https://theses.gla.ac.uk/>
research-enlighten@glasgow.ac.uk

UNIVERSITY OF GLASGOW

DEPARTMENT OF CHEMISTRY

PHYSICAL AND INORGANIC CHEMICAL STUDIES
OF SOME RUTHENIUM COMPLEXES

being

A thesis submitted in part fulfilment of the requirements

for the

DEGREE OF DOCTOR OF PHILOSOPHY

by

MUHAMMED JASIM BADER AL-ASSADI

January, 1987

ProQuest Number: 10991904

All rights reserved

INFORMATION TO ALL USERS

The quality of this reproduction is dependent upon the quality of the copy submitted.

In the unlikely event that the author did not send a complete manuscript and there are missing pages, these will be noted. Also, if material had to be removed, a note will indicate the deletion.



ProQuest 10991904

Published by ProQuest LLC (2018). Copyright of the Dissertation is held by the Author.

All rights reserved.

This work is protected against unauthorized copying under Title 17, United States Code
Microform Edition © ProQuest LLC.

ProQuest LLC.
789 East Eisenhower Parkway
P.O. Box 1346
Ann Arbor, MI 48106 – 1346

TO

MY

MUM AND DAD

ACKNOWLEDGEMENTS

I would like to express my deep thanks to my supervisor, Dr. A.L. Porte, for his helpful and constant guidance throughout this work.

I thank Professor G.A. Sim in whose laboratories the work was carried out.

I would also like to express my gratitude to all technicians who work in the microanalysis, infrared, n.m.r., e.p.r., and mass spectroscopy laboratories in the Chemistry Department of the University of Glasgow, for their helpful assistance.

Finally, I would like to thank the University of Basra for study leave, thereby enabling this work to be carried out.

PREFACE

This thesis is concerned with an attempt to develop a very detailed knowledge and understanding of the electronic, magnetic, optical, and chemical properties of nd^5 transition-metal ions and their complexes, particularly Ru^{3+} and its complexes. The link between these properties is the Tanabe-Sugano diagram whose development is described in the first part of the thesis.

The thesis is subdivided into two major parts, a theoretical part represented by Chapters One to Four, and a practical part represented by Chapters Five and Six. Chapter One explains how, by taking interelectronic repulsion effects on term energies into account, an energy level diagram for the nd^5 configuration of the isolated Ru^{3+} ion can be derived. Chapter Two describes the effects of crystal fields on isolated nd^5 ions, and shows how the electronic wave functions of these ions change on going from a strong octahedral crystal field \rightarrow to the "spin cross-over" point \rightarrow to a weak octahedral field. The derivation of the Tanabe-Sugano diagram for an nd^5 ion is described in this chapter and the effects of crystal fields of different symmetries are also described in detail. In Chapter Three, the magnetic properties of nd^5 ions, including the Ru^{3+} ion, are related to the Tanabe-Sugano diagram, and their characteristic, and complex magnetic behaviour in a strong octahedral field, in a weak octahedral field, and at the "spin cross-over" point is considered, as is the effect of changing the geometry of the transition-metal ion complex.

Chapter Four shows how electron paramagnetic resonance measurements can be used to obtain information about the electronic ground states of nd^5 ions in complexes. The very intricate and very sensitive relationships connecting electron paramagnetic resonance data with geometrical properties of complexes is considered in great detail.

In the second part of this thesis, the theoretical knowledge built up from the first part is used to identify two ruthenium complexes.

The first of these was prepared from a solid state reaction between benzoin and "commercial ruthenium trichloride", $\text{RuCl}_3 \cdot x\text{H}_2\text{O}$. The complex was identified as $\text{RuC}_{56}\text{H}_{42}\text{O}_2$. It possesses very interesting spectroscopic properties which are described in detail and used to characterise the molecular structure of the compound. Its formation must involve interesting redox reactions followed by polymerization, and these are described in detail in Chapter Five of the thesis.

The last chapter describes the reaction of dithiobenzoin with ruthenium(II)-chloride. This produces a mixture of two closely similar substances, $\text{Ru}_2^{\text{II}}\text{S}_2(\text{S}_2\text{C}_2\text{Ph}_2)_2$ and $\text{Ru}^{\text{II}}\text{Ru}^{\text{III}}\text{S}_2(\text{S}_2\text{HC}_2\text{Ph}_2)_2$. The rather interesting spectroscopic and magnetic properties of these substances are described in detail in this chapter and along with other physio-chemical properties, are used to characterise the compounds.

M.J.B. Al-Assadi

January, 1987.

TABLE OF CONTENTS

CHAPTER ONE

THE TERMS OF THE $4d^5$ CONFIGURATION OF THE ISOLATED Ru^{3+} ION

	Page
INTRODUCTION	1
1.1 THE EIGENFUNCTIONS AND EIGENVALUES OF THE FREE- ION HAMILTONIAN, $\mathcal{H} = V_F$	2
1.2 ELECTRON CONFIGURATIONS AND TERMS	6
1.2.a Electron configurations and terms for nd^5 ions	7
1.2.b The eigenfunctions of V_F : the term wavefunctions	11
1.2.c Interelectronic repulsions and term energies	17
1.2.d Term energies for the $4d^5$ configuration of the isolated Ru^{3+} ion	24
1.3 SPIN-ORBIT COUPLING IN FREE IONS	25
APPENDIX I	35

CHAPTER TWO

THE EFFECTS OF CRYSTAL FIELDS ON THE nd^5 CONFIGURATION

2.1 THE ELECTROSTATIC POTENTIAL GENERATED BY LIGANDS	39
2.1.a Electrostatic interactions in transition metal-ion complexes	42

	Page
2.2 THE nd^N ION IN A CRYSTAL FIELD	44
2.2.a The weak octahedral crystal field case	49
2.2.a.1 Electronic eigenfunctions for an nd^5 ion in a weak crystal field	51
2.2.a.2 The energy levels of an nd^5 ion in a weak crystal field	55
2.2.a.3 Term interactions in the nd^5 systems perturbed by an octahedral crystal field	60
2.2.b The strong octahedral crystal field case	66
2.2.b.1 Electronic eigenfunctions for an nd^5 ion in a strong crystal field	69
2.2.b.2 The energy levels of an nd^5 ion in a strong crystal field	71
2.2.c The "spin cross-over point" for an nd^5 ion in an octahedral crystal field.	78
2.3 THE TANABE-SUGANO DIAGRAM FOR AN nd^5 ION IN AN OCTAHEDRAL CRYSTAL FIELD	80
2.4 THE JAHN-TELLER EFFECT AND THE nd^5 IONS	82
2.5 COMPLEXES OF THE $4d^5$ ION Ru^{3+}	82
2.6 SPIN-ORBIT COUPLING IN TRANSITION-METAL ION COMPLEXES	85
2.6.a Spin-orbit coupling in complexes of the nd^5 ions	86

	Page
2.7 CRYSTAL FIELDS OF LOWER SYMMETRIES	88
2.7.a The nd^5 ion in a tetragonal, or orthorhombic crystal field	90
2.7.b The nd^5 ion in a trigonal crystal field	92
2.7.c The nd^5 ion in crystal fields of point group symmetries C_{4v} and C_{2v}	97
2.7.d The nd^5 ion in a tetrahedral crystal field	98

CHAPTER THREE

THE MAGNETIC PROPERTIES OF nd^5 IONS IN TRANSITION

METAL-ION COMPLEXES

3.1 MAGNETIC PROPERTIES OF ELECTRONS AND NUCLEI IN COMPLEXES	99
3.2 THE MAGNETIC PROPERTIES OF nd^5 SYSTEMS	104
3.2.a The weak field case	104
3.2.b The strong field case	107
3.2.b.1 Splitting by spin-orbit coupling	107
3.2.b.2 Estimation of the g-factor, the molar magnetic susceptibility, χ_M , and the magnetic dipole moment, μ_{eff} , of the ${}^2T_{2g}$ term	109
3.2.b.3 Low symmetry crystal field components and magnetic properties of nd^5 ions	111
3.2.b.4 Electron delocalization and magnetic properties of ${}^2T_{2g}$ terms	113

	Page
3.2.3 Spin free-spin paired equilibria ${}^6A_{1g} \rightleftharpoons {}^2T_{2g}$ in an nd^5 system	115
3.2.4 The magnetic properties of complexes of Ru^{3+}	117
3.3 ADDITIONAL, WEAKER, CONTRIBUTIONS TO THE GENERAL "THEORETICAL HAMILTONIAN"	121

CHAPTER FOUR

ELECTRON PARAMAGNETIC RESONANCE OF nd^5 IONS

IN TRANSITION METAL-ION COMPLEXES

4.1 THE GENERAL SPIN-HAMILTONIAN	123
4.2 THE ELECTRON PARAMAGNETIC RESONANCE PARAMETERS OF HIGH SPIN, $S = 5/2$, nd^5 IONS	127
4.3 THE ELECTRON PARAMAGNETIC RESONANCE PARAMETERS OF LOW SPIN, $S = 1/2$, nd^5 IONS	135
4.4 THE ELECTRON PARAMAGNETIC RESONANCE SPECTRA OF THE nd^5 IONS NEAR TO THE "SPIN CROSS-OVER" POINT	144
4.4.a High-spin \leftrightarrow low-spin equilibrium in planar nd^5 complexes	145
4.4.b "Mixed-spin" systems	151
4.5 ELECTRON PARAMAGNETIC RESONANCE DATA FOR Ru^{3+} COMPLEXES	156

CHAPTER FIVETHE REACTION OF SOLID "RUTHENIUM TRICHLORIDE", $\text{RuCl}_3 \cdot x\text{H}_2\text{O}$, AND SOLID BENZOIN, Ph-CO-CH(OH)Ph

5.1	INTRODUCTION	164
5.2	THE SOLID STATE REACTION : THE EXPERIMENTAL PROCEDURE	165
5.3	THE PROTON MAGNETIC RESONANCE SPECTRUM OF OLIVE-GREEN $\text{RuC}_{56}\text{H}_{42}\text{O}_2$	167
5.4	THE ^{13}C NUCLEAR MAGNETIC RESONANCE SPECTRUM OF OLIVE-GREEN $\text{RuC}_{56}\text{H}_{42}\text{O}_2$	172
5.5	THE INFRARED SPECTRUM OF OLIVE-GREEN $\text{RuC}_{56}\text{H}_{42}\text{O}_2$	180
5.6	THE ELECTRON IMPACT MASS SPECTRUM OF OLIVE- GREEN $\text{RuC}_{56}\text{H}_{42}\text{O}_2$	187
5.7	THE MAGNETIC PROPERTIES OF OLIVE-GREEN $\text{RuC}_{56}\text{H}_{42}\text{O}_2$	196
5.8	THE VISIBLE-ULTRAVIOLET SPECTRUM OF OLIVE- GREEN $\text{RuC}_{56}\text{H}_{42}\text{O}_2$	200
5.9	THE REACTION MECHANISMS INVOLVED IN THE FORMATION OF OLIVE-GREEN $\text{RuC}_{56}\text{H}_{42}\text{O}_2$	207

CHAPTER SIXBIS[μ -THIO(1,2-DIPHENYLETHANE)DITHIONE]-RUTHENIUM(II,III)]

6.1	INTRODUCTION	212
6.2	PREPARATION OF $\text{Ru}_2\text{S}_2(\text{S}_2\text{C}_2\text{Ph}_2)_2$	214
6.3	THE INFRARED SPECTRUM OF BLACK $\text{Ru}_2\text{S}_2(\text{S}_2\text{C}_2\text{Ph}_2)_2$	214
6.4	THE ELECTRON IMPACT MASS SPECTRUM OF BLACK $\text{Ru}_2\text{S}_2(\text{S}_2\text{C}_2\text{Ph}_2)_2$	222
6.5	THE MAGNETIC SUSCEPTIBILITIES OF BLACK $\text{Ru}_2\text{S}_2(\text{S}_2\text{C}_2\text{Ph}_2)_2$	232
6.6	THE X-BAND ELECTRON PARAMAGNETIC RESONANCE SPECTRA OF BLACK $\text{Ru}_2\text{S}_2(\text{S}_2\text{C}_2\text{Ph}_2)_2$	236
6.7	THE HIGH RESOLUTION PROTON MAGNETIC RESONANCE SPECTRUM OF BLACK $\text{Ru}_2\text{S}_2(\text{S}_2\text{C}_2\text{Ph}_2)_2$	249
6.8	THE VISIBLE-ULTRAVIOLET SPECTRUM OF BLACK $\text{Ru}_2\text{S}_2(\text{S}_2\text{C}_2\text{Ph}_2)_2$	253
6.9	THE d-ELECTRON DISTRIBUTION IN BLACK $\text{Ru}_2\text{S}_2(\text{S}_2\text{C}_2\text{Ph}_2)_2$	256

REFERENCES

- CHAPTER ONE -

THE TERMS OF THE $4d^5$ CONFIGURATION OF THE
ISOLATED Ru^{3+} ION

To develop a full picture of the nature of the bonding between central metal ion and ligands in a transition metal-ion complex, and to set the energy levels associated with it, it is necessary to construct a general Hamiltonian, and then solve the proper Schrödinger equation for that complex. However, this is not a simple matter, and in order to simplify the problem it is necessary to tackle it stepwise, i.e. to divide the general Hamiltonian of the system into its several components, starting with the free ion Hamiltonian, finding its proper wave functions and their corresponding eigenvalues, then incorporating the crystal field contribution to the Hamiltonian,.... and so on until the nuclear Zeeman contribution to the Hamiltonian is taken into account, as shown below. Provided the different contributions are written in descending order of magnitude, each successive contribution can be considered to perturb the eigenvalues and eigenfunctions of the preceding contributions, and the problem then becomes a series of exercises in the application of perturbation theory.

The general Hamiltonian is

$$\mathcal{H} = V_F + V_{x\ell} + V_{SO} + V_Z + V_{SS} + V_{SI} \quad (1.1)$$

where

V_F is the free ion energy, including only the

electronic kinetic energies, and all the electronic

electrostatic interactions in the free ion; $V_F \approx 10^5 \text{ cm}^{-1}$;

$V_{x\ell}$ is the crystal field interaction energy; $V_{x\ell} \approx 10^4 \text{ cm}^{-1}$;

V_{SO} is the spin-orbit interaction energy; $V_{SO} \approx 10^3 - 10^2 \text{ cm}^{-1}$;

V_Z is the electronic Zeeman interaction energy; $V_Z < 100 \text{ cm}^{-1}$;

V_{SS} is the spin-spin interaction energy; $V_{SS} \approx 1 \cdot 10^{-1} \text{ cm}^{-1}$;
 V_{SI} is the nuclear Zeeman interaction energy; $V_{SI} \approx 10^{-1} \cdot 10^{-3} \text{ cm}^{-1}$.

In general, the last five terms in equation (1.1) are small compared to V_F , i.e. they can be considered as perturbations to V_F .

1.1 THE EIGENFUNCTIONS AND EIGENVALUES OF THE FREE ION

HAMILTONIAN $\mathcal{H} = V_F^{1-7}$

To find the energy levels available to N equivalent electrons moving in a central field, assuming the single electron approximation in which the N electrons distribute themselves among single electron orbitals, it is necessary to start with the appropriate Hamiltonian and the Schrödinger equation $V_F \Psi = E\Psi$, i.e., in c.g.s. units,

$$\left[-\frac{\hbar^2}{2m} \sum_{i=1}^N \nabla_i^2 - \sum_{i=1}^N \frac{Ze^2}{r_i} + \frac{1}{2} \sum_{i=1}^N \sum_{\substack{j=1 \\ i \neq j}}^N \frac{e^2}{r_{ij}} \right] \Psi = E\Psi \quad (1.2)$$

where

$+Ze$ is the atomic, or ionic, nuclear charge; m and $-e$ are the mass and charge of the electron respectively; ∇_i^2 is the Laplacian operator which operates on the spatial coordinates (r_i, θ_i, ϕ_i) of the i th electron; $-(Ze^2/r_i)$ is the Coulomb interaction between the atomic nucleus and the i th electron, where r_i is the distance between the i th electron and the nucleus; e^2/r_{ij} is the Coulomb interaction between the i th and j th electrons; Ψ is the wave function for the N electrons, and its form depends upon the space and the spin coordinates of all N electrons

$$\Psi = \Psi(\vec{r}_1, \sigma_1; \vec{r}_2, \sigma_2; \dots; \vec{r}_N, \sigma_N)$$

\vec{r}_i is an abbreviation for r_i, θ_i, ϕ_i , the spherical polar coordinates of electron i ; σ_i is the spin coordinate of electron i ; E is the total energy of the N electrons.

Equation (1.2) can not be solved exactly for $N > 1$. Therefore to find the wave function Ψ and the energies E for a many-electron system, for example one consisting of five electrons, approximation methods must be used. Using the so-called central-field approximation in conjunction with a perturbation calculation gives rise to the procedure known in the literature as the "Slater theory of atoms and ions".⁷

At this point it is convenient to add the quantity $\sum_{i=1}^N eV(r_i) - \sum_{i=1}^N eV(r_i)$ to the Hamiltonian in equation (1.2) where $V(r_i)$ is the "shielding potential", i.e. a spherically symmetrized averaged electrostatic potential generated at electron i by all other electrons. V_F is then subsequently divided into two parts $\mathcal{H}^0 + \mathcal{H}'$, i.e.

$$V_F = \mathcal{H}^0 + \mathcal{H}' \quad (1.3)$$

with

$$\mathcal{H}^0 = -\frac{\hbar^2}{2m} \sum_{i=1}^N \nabla_i^2 - \sum_{i=1}^N eV(r_i) \quad (1.4)$$

and

$$\mathcal{H}' = -\sum_{i=1}^N \left[\frac{Ze^2}{r_i} - eV(r_i) \right] + \frac{1}{2} \sum_{i=1}^N \sum_{j=1, j \neq i}^N \frac{e^2}{r_{ij}} \quad (1.5)$$

If the shielding potential, $V(r_i)$, is chosen such that \mathcal{H}' , everywhere in coordinate space, is as small as possible, then \mathcal{H}' may be treated as a perturbation operator acting on the unperturbed system that is described by the Shrödinger equation

$$\mathcal{H}^0 \Psi^0 = E \Psi^0 \quad (1.6)$$

The effect of \mathcal{H}' on the system will be discussed in section (1.2.c). The differential equation (1.6) can be solved to give solutions for Ψ^0 which are products of one-electron functions $\psi_{a_i}(\vec{r}_i, \sigma_i)$ where

$$\psi_{a_i}(i) = \psi_{n_i, \ell_i, m_{\ell_i}, m_{s_i}}(\vec{r}, \sigma) = R_{n_i, \ell_i}(r) Y_{\ell_i, m_{\ell_i}}(\theta, \phi) \begin{Bmatrix} \alpha(\sigma) \\ \beta(\sigma) \end{Bmatrix} \quad (1.7)$$

$$a_i = n_i, \ell_i, m_{\ell_i}, m_{s_i}$$

The wave functions Ψ^0 in equation (1.6) can be written in the form

$$\Psi^0 = \psi_{a_1}(1) \cdot \psi_{a_2}(2) \dots \psi_{a_N} \quad (1.8)$$

and the corresponding energy is given by

$$E = \varepsilon_{n_1, \ell_1} + \varepsilon_{n_2, \ell_2} + \dots + \varepsilon_{n_N, \ell_N} \quad (1.9)$$

Equation (1.8) does not take exchange of the coordinates of the electrons in the system into account. There are in total $N!$ different product functions which can be obtained from equation (1.8) by performing all possible permutations of the electron coordinates. Every linear combination of these $N!$ functions is an eigenfunction of the unperturbed Hamiltonian of (1.6) with the eigenvalue (1.9). Hence, when exchange is taken into account, the most general eigenfunction, Φ , of \mathcal{H}^0 , equation (1.4), is⁷

$$\Phi = (1/\sqrt{N!}) \sum_P (-1)^P P \Psi^0 \quad (1.10)$$

$(1/\sqrt{N!})$ is a normalization factor and the summation is taken over all permutations P of the electron coordinates. The antisymmetric function Φ , (1.10), is called the Heisenberg-Slater function, HS-function, and in abbreviated form it is usually written as

$$\Phi(a_1; a_2; \dots; a_N)$$

or

$$\Phi(n_1, \ell_1, m_{\ell_1}, m_{s_1}; n_2, \ell_2, m_{\ell_2}, m_{s_2}; \dots; n_N, \ell_N, m_{\ell_N}, m_{s_N}) \quad (1.11)$$

For electrons belonging to the same subshell, i.e. electrons possessing the same n and ℓ values, Φ can be written as

$$\Phi(m_{\ell_1}, m_{s_1}; m_{\ell_2}, m_{s_2}; \dots; m_{\ell_N}, m_{s_N}) \quad (1.12)$$

or

$$\Phi(\overset{+}{m}_{\ell_1}; \bar{m}_{\ell_2}; \dots; \overset{+}{m}_{\ell_N}) \quad (1.13)$$

The positive sign being used when $m_s = +\frac{1}{2}$ and the negative sign when $m_s = -\frac{1}{2}$. The function Φ , equation (1.10), can also be written in determinantal form;^{2,7} It is a normalized and orthogonalized function.

Before investigating which energy values, E , an atomic N -electron system is allowed to have in the central-field approximation, it is necessary to establish clearly the significance of two quantities, configuration and term, and to distinguish between them.

1.2 ELECTRON CONFIGURATION AND TERMS

A configuration is an assignment of a given number of electrons to a set of orbitals, each of the form $\psi_a(i)$, equation (1.7), and it can be written symbolically as, $(n_1\ell_1)^a, (n_2\ell_2)^b, \dots, (n_i\ell_i)^N$, where a, b, \dots, N are the number of electrons which occupy one electron orbital of energy, $\epsilon_{n,\ell}$, equation (1.9). For example $1s^2, 2s^2, 2p^2, \dots, nd^5$. It is important to realise that a given configuration gives rise to a number of energy levels.

Possible eigenfunctions of \mathcal{H}^0 , Φ , associated with a particular electron configuration are obtained when within this electron configuration all the possible orbital occupations allowed by the Pauli Exclusion Principle are taken into account. For instance, to find the Φ functions allowed for the nd^5 configuration, the five (nd) valence electrons are to be distributed over the $2(2\ell+1)$, i.e., 10-degenerate d-orbitals taking the Pauli Principle into consideration. If, for example, four electrons are placed in the orbitals $(m_{\ell_1}, m_{s_1}) = \frac{1}{2}, (m_{\ell_2}, m_{s_2}) = \bar{2}, (m_{\ell_3}, m_{s_3}) = \bar{1}$, and $(m_{\ell_4}, m_{s_4}) = \bar{1}$, then the fifth electron can occupy only one of the orbitals $(m_{\ell_5}, m_{s_5}) = 0, 0, -1, -1, -2$ or -2 . From this, it follows that the following functions are acceptable eigenfunctions Φ of \mathcal{H}^0 , equation (1.4).

$$\begin{aligned} \Phi[(m_{\ell_1}, m_{s_1}); (m_{\ell_2}, m_{s_2}); (m_{\ell_3}, m_{s_3}); (m_{\ell_4}, m_{s_4}); (m_{\ell_5}, m_{s_5})] = \\ \Phi(\overset{+}{2}, \overset{-}{2}, \overset{+}{1}, \overset{-}{1}, \overset{+}{0}) \text{ or } \Phi(\overset{+}{2}, \overset{-}{2}, \overset{+}{1}, \overset{-}{1}, \overset{-}{0}) \text{ or } \Phi(\overset{+}{2}, \overset{-}{2}, \overset{+}{1}, \overset{-}{1}, \overset{-}{2}) \\ \Phi(\overset{+}{2}, \overset{-}{2}, \overset{+}{1}, \overset{-}{1}, \overset{-}{-1}) \text{ or } \Phi(\overset{+}{2}, \overset{-}{2}, \overset{+}{1}, \overset{-}{1}, \overset{-}{-2}) \text{ or } \Phi(\overset{+}{2}, \overset{-}{2}, \overset{+}{1}, \overset{-}{1}, \overset{-}{-2}) \end{aligned}$$

The remaining acceptable Φ functions can be similarly derived by considering all other possible occupations of the d orbitals.

1.2.a ELECTRON CONFIGURATIONS AND TERMS FOR nd^5 IONS

All physically different Φ functions can then be ordered according to the quantities $M_L = (m_{\ell_1} + m_{\ell_2} + m_{\ell_3} + m_{\ell_4} + m_{\ell_5})$ and $M_S = (m_{s_1} + m_{s_2} + m_{s_3} + m_{s_4} + m_{s_5})$ and tabulated as in Table (1.1). It can be shown in this way that there are 252 physically different Φ functions belonging to the nd^5 -configuration. Table (1.1) shows the general scheme involved in drawing up the M_L, M_S table and lists the number of possible Φ functions in each box for the possible values $M_L = 6, 5, 4, 3, 2, 1, 0, -1, -2, -3, -4, -5, -6$ and $M_S = \frac{5}{2}, \frac{3}{2}, \frac{1}{2}, -\frac{1}{2}, -\frac{3}{2}, -\frac{5}{2}$. Table (1.2) is an expansion of the main table, for the $M_L=0, M_S=\frac{1}{2}$ box with its proper Φ functions. The nd^5 configuration is 252-fold degenerate in the central-field approximation.

The determinantal functions Φ are eigenfunctions of \mathcal{H}^0 , equation (1.4). They are not generally eigenfunctions of the free ion Hamiltonian V_F , equation (1.3). These Φ functions are known as "microstates". They are degenerate. The perturbation term \mathcal{H}^1 , equation (1.5), perturbs \mathcal{H}^0 and according to degenerate perturbation theory in principle it mixes the degenerate functions Φ , and removes their degeneracy.

The total angular momentum and its allowed z-axis components, must always be constants of the motion for all the electrons in an isolated atom or ion. However, in equation (1.3) there are no inter-

Table (1.1)

$M_L \backslash M_S$	$+\frac{5}{2}$	$+\frac{3}{2}$	$+\frac{1}{2}$	$-\frac{1}{2}$	$-\frac{3}{2}$	$-\frac{5}{2}$
6			1	1		
5			2	2		
4		1	5	5	1	
3		2	8	8	2	
2		3	12	12	3	
1		4	14	14	4	
0	1	5	16	16	5	1
-1		4	14	14	4	
-2		3	12	12	3	
-3		2	8	8	2	
-4		1	5	5	1	
-5			2	2		
-6			1	1		

Table (1.2)

$M_L \backslash M_S$	$+\frac{1}{2}$									
0	Φ_1	$\begin{smallmatrix} + & - & + & + & - \\ (2, & 2, & 0, & -2, & -2) \end{smallmatrix}$	Φ_2	$\begin{smallmatrix} + & - & + & + & - \\ (1, & 1, & 0, & -1, & -1) \end{smallmatrix}$						
	Φ_3	$\begin{smallmatrix} + & + & + & - & - \\ (2, & 1, & 0, & -1, & -2) \end{smallmatrix}$	Φ_4	$\begin{smallmatrix} - & - & + & + & + \\ (2, & 1, & 0, & -1, & -2) \end{smallmatrix}$						
	Φ_5	$\begin{smallmatrix} + & - & + & + & - \\ (2, & 1, & 0, & -1, & -2) \end{smallmatrix}$	Φ_6	$\begin{smallmatrix} - & + & + & - & + \\ (2, & 1, & 0, & -1, & -2) \end{smallmatrix}$						
	Φ_7	$\begin{smallmatrix} - & + & + & + & - \\ (2, & 1, & 0, & -1, & -2) \end{smallmatrix}$	Φ_8	$\begin{smallmatrix} + & - & + & - & + \\ (2, & 1, & 0, & -1, & -2) \end{smallmatrix}$						
	Φ_9	$\begin{smallmatrix} + & + & - & + & - \\ (2, & 1, & 0, & -1, & -2) \end{smallmatrix}$	Φ_{10}	$\begin{smallmatrix} + & + & - & - & + \\ (2, & 1, & 0, & -1, & -2) \end{smallmatrix}$						
	Φ_{11}	$\begin{smallmatrix} + & - & - & + & + \\ (2, & 1, & 0, & -1, & -2) \end{smallmatrix}$	Φ_{12}	$\begin{smallmatrix} - & + & - & + & + \\ (2, & 1, & 0, & -1, & -2) \end{smallmatrix}$						
	Φ_{13}	$\begin{smallmatrix} + & + & - & + & - \\ (2, & 0, & 0, & -1, & -1) \end{smallmatrix}$	Φ_{14}	$\begin{smallmatrix} + & - & + & - & + \\ (1, & 1, & 0, & 0, & -2) \end{smallmatrix}$						
	Φ_{15}	$\begin{smallmatrix} + & - & + & - & + \\ (2, & 2, & -1, & -1, & -2) \end{smallmatrix}$	Φ_{16}	$\begin{smallmatrix} + & + & - & + & - \\ (2, & 1, & 1, & -2, & -2) \end{smallmatrix}$						

actions that couple the space and spin coordinates of the electrons, so it follows that eigenfunctions of V_F can be obtained which are simultaneous eigenfunctions of the total orbital angular momentum, and the total spin angular momentum of the electrons, and of their allowed z-axis components. From the quantum mechanics of angular momentum and its operators, the total orbital and spin angular momenta can be defined by quantum numbers L and S , and their z-axis components by the quantum numbers M_L and M_S respectively. The total orbital and spin angular momenta are $\sqrt{L(L+1)} \hbar$ and $\sqrt{S(S+1)} \hbar$ respectively. Their corresponding z-axis components are given by $M_L \hbar$ and $M_S \hbar$. The total orbital angular momentum of the electron distribution is similarly defined by a total angular momentum quantum number J , and is given by $\sqrt{J(J+1)} \hbar$.

The eigenvalues of V_F , equation (1.3), i.e. the energy levels, or terms, for the free ion can thence be denoted by specifying the term symbol $^{2S+1}L_J$, where $(2S+1)$ is the spin multiplicity, and when $L=0;1;2;3;4;5;6;\dots$ the L quantum number is denoted by $S;P;D;F;G;H;I;\dots$, respectively. The degeneracy of the term is $(2L+1)(2S+1)$, i.e. each value of M_L , where $M_L = L, (L-1), \dots, \text{or } -L$, occurs $(2S+1)$ times and each value of M_S , where $M_S = S, S-1, \dots, \text{or } -S$, occurs $(2L+1)$ times in the term. For example, a 4G term is 36-fold degenerate.

It has already been pointed out that for the nd^5 -configuration, there are 252 "microstates", eigenfunctions, Φ , of \mathcal{H}^0 . It therefore follows that there are 252 eigenstates of V_F for the nd^5 -ions. These are substates of all possible terms $^{2S+1}L_J$ for the nd^5 -ions, and it is

important at this point to determine which linear combination of the "microstates", Φ , correspond to the eigenfunctions of the substates labelled by the possible M_L, M_S quantum numbers of each of the terms in the term symbol ^{2S+1}L . It turns out that the nd^5 -configuration gives rise to 16-terms whose L and S values and term symbols are listed in Table (1.3). The number of "microstates" that contribute to each of these terms are also listed in this table.

1.2.b THE EIGENFUNCTIONS OF V_F : THE TERM WAVEFUNCTIONS

In equation (1.3) the operators $\hat{L}, \hat{S}, \hat{L}_z = \sum_i (\hat{l}_i)_z$ and $\hat{S}_z = \sum_i (\hat{s}_i)_z$, all commute with V_F and with each other. Eigenfunctions Ψ of the wave-equation (1.2) can therefore be found which are simultaneous eigenfunctions of these operators.^{2,3,7} These functions are denoted by $\Psi(L, M_L, S, M_S)$ and from angular momentum theory, the following algebraic relationships now follow:

$$\begin{aligned} \hat{L}^2 \Psi(L, M_L, S, M_S) &= L(L+1) \hbar^2 \Psi(L, M_L, S, M_S) \\ L &= 0, 1, 2, 3, 4, \dots \end{aligned} \quad (1.14)$$

$$\begin{aligned} \hat{L}_z \Psi(L, M_L, S, M_S) &= M_L \hbar \Psi(L, M_L, S, M_S) \\ M_L &= L, (L-1), \dots, \text{ or } -L \end{aligned} \quad (1.15)$$

$$\begin{aligned} \hat{S}^2 \Psi(L, M_L, S, M_S) &= S(S+1) \hbar^2 \Psi(L, M_L, S, M_S) \\ S &= 0, \frac{1}{2}, 1, \frac{3}{2}, 2, \frac{5}{2}, 3, \dots \end{aligned} \quad (1.16)$$

Table (1.3)

L	S	Term	Number of microstates, Φ $= (2L + 1)(2S + 1)$
0	5/2	6S	6
4	3/2	4G	36
3	3/2	4F	28
2	3/2	4D	20
1	3/2	4P	12
6	1/2	2I	26
5	1/2	2H	22
4	1/2	$2x {}^2G$	$2x18$
3	1/2	$2x {}^2F$	$2x14$
2	1/2	$3x {}^2D$	$3x10$
1	1/2	2P	6
0	1/2	2S	2
Total = 252			

$$\hat{S}_z \Psi(L, M_L, S, M_S) = M_S \hbar \Psi(L, M_L, S, M_S)$$

$$M_S = S, (S-1), \dots, \text{ or } -S \quad (1.17)$$

$$(\hat{L}_x \pm i\hat{L}_y) \Psi(L, M_L, S, M_S) = \hbar \sqrt{(L \pm M_L + 1)(L \mp M_L)} \Psi(L, M_L \pm 1, S, M_S) \quad (1.18)$$

$$(\hat{S}_x \pm i\hat{S}_y) \Psi(L, M_L, S, M_S) = \hbar \sqrt{(S \pm M_S + 1)(S \mp M_S)} \Psi(L, M_L, S, M_S \pm 1) \quad (1.19)$$

It should be noted that if a function $\Psi(L, M_L, S, M_S)$ is known then all other functions $\Psi(L, M'_L, S, M'_S)$ with $M'_L = L, (L-1), \dots, \text{ or } -L$ and $M'_S = S, (S-1), \dots, \text{ or } -S$, can be determined by repeated application of the shift operator relationships in equations (1.18) and (1.19).⁷

In general, the term eigenfunctions $\Psi(L, M_L, S, M_S)$ are linear combinations of "microstates" Φ , with the same M_L and M_S values. In general, the "microstates", Φ , are not term eigenfunctions, and it is only when one "microstate", Φ , is in a given box in Table (1.1) that Φ "microstate" is an acceptable term wavefunction. Thus, Table (1.1) shows that the function $\Phi(2, 1, 0, -1, -2)$ is a term eigenfunction with $M_L = 0$, $M_S = \frac{5}{2}$, belonging to the 6S term.

$$(\hat{L}_x + i\hat{L}_y) = \sum_i (\hat{\ell}_x)_i + i \sum_i (\hat{\ell}_y)_i = \sum_i (\hat{\ell}_x + i\hat{\ell}_y)_i, \dots, \text{ etc.},$$

and therefore, the antisymmetrized product functions Φ of the "microstates" satisfy the relationships

$$\begin{aligned}
& (\hat{L}_x \pm i \hat{L}_y) \Phi(m_{\ell_1}, m_{s_1}, \dots, m_{\ell_N}, m_{s_N}) \\
&= \hbar \sum_{i=1}^N \sqrt{(\ell_i \pm m_{\ell_i} + 1)(\ell_i \mp m_{\ell_i})} \Phi(m_{\ell_1}, m_{s_1}; \dots (m_{\ell_i} \pm 1), m_{s_i}; \dots m_{\ell_N}, m_{s_N})
\end{aligned}
\tag{1.20}$$

$$\begin{aligned}
& (\hat{S}_x \pm i \hat{S}_y) \Phi(m_{\ell_1}, m_{s_1}; \dots; m_{\ell_N}, m_{s_N}) \\
&= \hbar \sum_{i=1}^N \sqrt{\left(\frac{3}{2} \pm m_{s_i}\right) \left(\frac{1}{2} \mp m_{s_i}\right)} \Phi(m_{\ell_1}, m_{s_1}; \dots; m_{\ell_i}, (m_{s_i} \pm 1); \dots; m_{\ell_N}, m_{s_N})
\end{aligned}
\tag{1.21}$$

The Φ functions are eigenfunctions of \hat{L}_z and \hat{S}_z with sharply defined eigenvalues $\hbar M_L = \hbar(m_{\ell_1} + m_{\ell_2} + \dots + m_{\ell_N})$ and $\hbar M_S = \hbar(m_{s_1} + m_{s_2} + \dots + m_{s_N})$ for these operators.

The most useful procedure⁸ for determining the term eigenfunctions $\Psi(L, M_L, S, M_S)$ is as follows:

- 1) The functions $\Psi(L, M_L, S, M_S)$ are represented by linear combinations of the Φ functions in the appropriate M_L, M_S box in Tables (1.1) and (1.2).
- 2) If a function $\Psi(L, M_L, S, M_S)$ is known, then all the other functions $\Psi(L, M'_L, S, M'_S)$ that belong to the same term ^{2S+1}L are generated by repeated application of the shift relationships given in equations (1.18)-(1.21).
- 3) The functions $\Psi(L, M_L, S, M_S)$ are orthogonal and they are now normalized, i.e.

$$\langle \Psi(L, M_L, S, M_S) \mid \Psi(L', M'_L, S', M'_S) \rangle = \delta_{L, L'} \cdot \delta_{M_L, M'_L} \cdot \delta_{S, S'} \cdot \delta_{M_S, M'_S}$$

For example, as already explained, the "microstate" $\Phi(2,2,1,0,-1)^{+-++}$ is the only "microstate" in its box in Table (1.1). It is therefore an eigenfunction $\Psi(L, M_L, S, M_S)$ for which $M_L = 4$, and $M_S = \frac{3}{2}$. The 4G -term for which $L = 4$, $S = \frac{3}{2}$ generates a substate for which $M_L = 4$ and $M_S = \frac{3}{2}$. It therefore follows, from Table (1.1) that this "microstate" is an eigenfunction of V_F and

$$\Psi(4,4,\frac{3}{2},\frac{3}{2}) = \Phi(2,2,1,0,-1)^{+-++} \quad (1.22)$$

The other eigenfunctions belonging to the 4G -term, i.e. the other $\Psi(4, M_L, \frac{3}{2}, M_S)$ functions where $M_L = 3, 2, 1, 0, -1, -2, -3$ and $M_S = \frac{3}{2}, \frac{1}{2}, -\frac{1}{2}, -\frac{3}{2}$, 35-states in all can be generated with the aid of the lowering operators $(\hat{L}_x - i \hat{L}_y)$ and $(\hat{S}_x - i \hat{S}_y)$. For example, application of the first of these to both sides of equation (1.22) gives

$$\begin{aligned} (\hat{L}_x - i \hat{L}_y) \Psi(4,4,\frac{3}{2},\frac{3}{2}) &= \hbar \sqrt{(4-4+1)(4+4)} \Psi(4,3,\frac{3}{2},\frac{3}{2}) \\ &= 2 \sqrt{2} \hbar \Psi(4,3,\frac{3}{2},\frac{3}{2}) \end{aligned} \quad (1.23)$$

and

$$\begin{aligned} (\hat{L}_x - i \hat{L}_y) \Phi(2,2,1,0,-1)^{+-++} &= [\sqrt{(2-2+1)(2+2)} \Phi(1,2,1,0,-1)^{+-++} \\ &+ \sqrt{(2-2+1)(2+2)} \Phi(2,1,1,0,-1)^{+-++} \\ &+ \sqrt{(1-1+1)(1+1)} \Phi(2,2,0,0,-1)^{+-++} \\ &+ \sqrt{(0-0+1)(0+0)} \Phi(2,2,1,-1,-1)^{+-++} \\ &+ \sqrt{(1-1+1)(1+0)} \Phi(2,2,1,0,-2)^{+-++}] \hbar \end{aligned} \quad (1.24)$$

For the same reasons that lead to the Pauli Exclusion Principle, the first, the third and the fourth terms of the right hand side of equation (1.24) are zero, therefore

$$(\hat{L}_x - i \hat{L}_y) \phi(\overset{+}{2}, \overset{-}{2}, \overset{+}{1}, \overset{+}{0}, \overset{-}{1}) = \hbar [2\phi(\overset{+}{2}, \overset{-}{1}, \overset{+}{1}, \overset{+}{0}, \overset{-}{1}) + \phi(\overset{+}{2}, \overset{-}{2}, \overset{+}{1}, \overset{+}{0}, \overset{-}{2})]$$

and it now follows that

$$\Psi(4, 3, \frac{3}{2}, \frac{3}{2}) = \frac{1}{\sqrt{2}} \phi(\overset{+}{2}, \overset{-}{1}, \overset{+}{1}, \overset{+}{0}, \overset{-}{1}) + 2 \frac{1}{\sqrt{2}} \phi(\overset{+}{2}, \overset{-}{2}, \overset{+}{1}, \overset{+}{0}, \overset{-}{2}) \quad (1.25)$$

i.e. a second eigenfunction $\Psi(4, 3, \frac{3}{2}, \frac{3}{2})$ associated with the 4G -term has been derived, and shown to be one of the linear combinations of the two "microstates" belonging to the box in Table (1.1) for which $M_L = 3$, $M_S = \frac{3}{2}$. The complete list of 36-states of the 4G -term can be derived in a similar way, and similar arguments eventually lead to a list of all possible eigenfunctions of the terms derived from the nd^5 -configuration.

For example, some of the eigenfunctions of V_F for which $M_L = 0$, $M_S = \frac{1}{2}$, in terms of the determinantal "microstates" ϕ for the nd^5 -configuration are given below. These functions are taken from reference 2, page 335.

$$\Psi(0,0,\frac{5}{2},\frac{1}{2})[{}^6S]$$

$$= (10)^{-\frac{1}{2}} (-\phi_3 - \phi_4 - \phi_5 - \phi_6 - \phi_7 - \phi_8 - \phi_9 - \phi_{10} - \phi_{11} - \phi_{12})$$

$$\Psi(4,0,1,\frac{1}{2})[{}^4G]$$

$$= (210)^{-\frac{1}{2}} (3\phi_3 + 3\phi_4 + 3\phi_5 + 3\phi_6 - 2\phi_7 + 8\phi_8 - 7\phi_9 - 2\phi_{10} - 2\phi_{11} - 7\phi_{12})$$

$$\Psi(3,0,1,\frac{1}{2})[{}^4F]$$

$$= (30)^{-\frac{1}{2}} (\phi_3 - \phi_4 - 3\phi_5 + 3\phi_6 - \phi_9 + 2\phi_{10} - 2\phi_{11} + \phi_{12})$$

Slater gives a complete list of the eigenfunctions V_F of the form $\Psi(L,0,S,\frac{1}{2})$ for each of the terms of the nd^5 -configuration.² The other eigenfunctions can be generated from these by using the shift operators as described above.

1.2.c INTERELECTRONIC REPULSIONS AND TERM ENERGIES

The term of lowest energy for any electronic configuration can always be determined by applying Hund's rules. Accordingly, the 6S -term is the ground term of the nd^5 configuration. In order to find the energies of the other terms, however, it is necessary to go back to equations (1.3) and (1.5) and consider the effects of the perturbation term \mathcal{H}' on the degenerate eigenfunctions of \mathcal{H}^0 . According to time-independent degenerate perturbation theory, \mathcal{H}' formally mixes together all of the 252 eigenfunctions of \mathcal{H}^0 and perturbs their energies by

ΔE . In applying perturbation theory either the $\phi_1, \phi_2, \dots, \phi_{252}$ or $\psi_1(L, M_L, S, M_S), \psi_2(L, M_L, S, M_S), \dots, \psi_{252}(L, M_L, S, M_S)$ bases can be used, and no matter which is used a 252×252 secular determinant

$$\left| \begin{array}{ccc} H_{11} - \Delta E & H_{12} & \dots \dots \dots H_{1,252} \\ H_{21} & H_{22} - \Delta E & \dots \dots \dots H_{2,252} \\ \vdots & \vdots & \ddots \ddots \ddots \ddots \ddots \ddots \\ H_{252,1} & H_{252,2} & \dots \dots \dots H_{252,252} - \Delta E \end{array} \right| = 0 \quad (1.26)$$

is obtained. If one begins with the ϕ bases then the matrix elements

H_{ij} are defined by the integrals $H_{ij} = \langle \phi_i | \mathcal{H}' | \phi_j \rangle$. If the $\psi(L, M_L, S, M_S)$ basis is used then $H_{ij} = \langle \psi_i | \mathcal{H}' | \psi_j \rangle$.

In principal the determinantal equation (1.26) can be expanded in the polynomial form

$$(\Delta E)^{252} - (H_{11} + H_{22} + \dots + H_{252,252}) (\Delta E)^{251} + \dots + (H_{11} H_{22} \dots H_{252,252}) = 0 \quad (1.27)$$

and the 252 roots, ΔE , extracted by standard methods. This would result in $252 \times 252 = 63504$ matrix elements, H_{ij} being calculated, but the work involved can be considerably reduced by using the

$\psi(L, M_L, S, M_S)$ functions and making use of the so-called "diagonal-sum rule".^{4,5} Since \mathcal{H}' commutes with \hat{L}^2 , \hat{S}^2 , \hat{L}_Z and \hat{S}_Z , it follows that the secular determinant (1.26) will factorize into a number of smaller determinants, one for each possible pair of values M_L , M_S , and for each

of these $\Delta E_1 + \Delta E_2 + \dots + \Delta E_r = \sum_{i=1}^r H_{ii} + \dots$. Hence, the sum of the roots, ΔE , for those terms that contribute to each of these smaller sub-determinants is just $\sum_{i=1}^r H_{ii}$.

This diagonal-sum rule is important because it follows from it that, the sum of the H_{ii} for all the functions Ψ (or Φ) that contribute to a given box of the M_L, M_S table, for example Tables (1.1) and (1.2) for the nd^5 -configuration, gives the sum of the energies of the terms that contribute to that M_L, M_S box. Subtracting similar sums for suitable adjacent boxes then gives the energy of any term that occurs only once in the configuration. However, if a term appears more than once in the configuration, for example the ${}^2G, {}^2F$ and 2D terms of the nd^5 -configuration, then some of the off-diagonal elements H_{ij} will need to be determined and a secular determinant will then have to be solved.⁹

To evaluate the matrix element H_{ij} , it is important to remember that the $\Psi(L, M_L, S, M_S)$ functions are linear combinations of the Slater-determinants $\Phi_r = \Phi_r[a_1^{(r)}, a_2^{(r)}, \dots, a_N^{(r)}]$, the a_i being symbols for the four quantum numbers $n_i, \ell_i, m_{\ell_i}, m_{s_i}$, equation (1.11) i.e.

$$\Psi_i = c_{i1}\Phi_1 + c_{i2}\Phi_2 + \dots + c_{ir}\Phi_r + \dots,$$

and

$$\Psi_j = c_{j1}\Phi_1 + c_{j2}\Phi_2 + \dots + c_{js}\Phi_s + \dots$$

so that an integral $\langle \Psi_i | \mathcal{H} | \Psi_j \rangle$ is made up additively of sub-integrals of the form

$$h_{rs} = \langle \Phi_r | \mathcal{H} | \Phi_s \rangle \quad (1.28a)$$

The perturbation operator, \mathcal{H}' , equation (1.5) may be recast to give

$$\mathcal{H}' = \sum_{i=1}^N U_i + \frac{1}{2} \sum_{i=1}^N \sum_{\substack{j=1 \\ i \neq j}}^N Q_{ij} \quad (1.28b)$$

where U_i is the one-electron operator

$$U_i = -(Ze^2/r_i) + eV(r_i)$$

and

Q_{ij} is the two-electron operator,

$$Q_{ij} = e^2/r_{ij}$$

The integral h_{rs} can itself be expressed in terms of integrals involving the one-electron functions ψ_{a_i} , equation (1.7). The most general form of the integral involving the two-electron operator $\frac{1}{r_{ij}}$ having the form $V(a_i, a_j, a_p, a_q)$ where

$$\begin{aligned} & V(a_i, a_j, a_p, a_q) \\ &= \langle a_i a_j | \frac{1}{r_{ij}} | a_p a_q \rangle \\ &= \delta_{m_{s_i}, m_{s_p}} \delta_{m_{s_j}, m_{s_q}} \delta_{m_{\ell_i} + m_{\ell_j}, m_{\ell_p} + m_{\ell_q}} \times \\ & \times \sum_{k=0}^{\infty} c^k(\ell_i, m_{\ell_i}; \ell_p, m_{\ell_p}) c^k(\ell_q, m_{\ell_q}; \ell_j, m_{\ell_j}) \times \\ & \times R^k(n_i, \ell_i; n_j, \ell_j; n_p, \ell_p; n_q, \ell_q) \end{aligned} \quad (1.29)$$

with

$$c^k(\ell_i, m_{\ell_i}; \ell_j, m_{\ell_j}) = \left(\frac{4\pi}{2k+1}\right)^{\frac{1}{2}} \int_0^\pi \int_0^{2\pi} Y_{\ell_i, m_{\ell_i}}^*(\theta, \phi) Y_{k, m_{\ell_i} - m_{\ell_j}}(\theta, \phi) \times \\ \times Y_{\ell_j, m_{\ell_j}}(\theta, \phi) \sin\theta d\theta d\phi \quad (1.30a)$$

and

$$R^k(n_i, \ell_i; n_j, \ell_j; n_p, \ell_p; n_q, \ell_q) \\ = e^2 \int_0^\infty \int_0^\infty R_{n_i, \ell_i}^*(r_i) R_{n_j, \ell_j}^*(r_j) \frac{r_{<}^k}{r_{>}^{k+1}} R_{n_p, \ell_p}(r_i) R_{n_q, \ell_q}(r_j) r_i^2 r_j^2 dr_i dr_j \quad (1.30b)$$

where Y_{ℓ, m_ℓ} are normalized spherical harmonics, $R_{n, \ell}(r)$ are the radial parts of the one-electron functions $\psi_{n, \ell, m_\ell, m_s}$ and $r_{<}$ and $r_{>}$ are, respectively, the smaller and the larger of r_i and r_j .

When $p=i$ and $q=j$, the general radial integral defined in (1.30b) become identical with the Slater-Condon parameters, F^k , that are encountered in the literature.^{3,4,5}

$$R^k(n_i, \ell_i; n_j, \ell_j; n_i, \ell_i; n_j, \ell_j) = F^k(n_i, \ell_i; n_j, \ell_j) \quad (1.31)$$

Other, more useful forms of radial integrals of this kind, are encountered in the literature: for example, the Slater-Condon Parameters, F_k .

When $\ell_i = \ell_j = 2$, the relationships between the two sets of parameters are:

$$F_0 = F^0, \quad F_2 = \frac{1}{49} F^2; \quad F_4 = \frac{1}{441} F^4 \quad (1.32)$$

In the ligand field calculations it is customary to use the so-called Racah parameters¹⁰ A, B and C which are defined through the relationships:

$$A = F_0 - 49F_4, \quad B = F_2 - 5F_4, \quad C = 35F_4 \quad (1.33)$$

The radial integrals (1.30b) are most commonly encountered in the literature in the form of the Slater-Condon parameters F_k and the Racah parameters A, B and C: these are all positive.

The Racah parameters are slightly more useful because it turns out that if they are used, then the separation between the terms of the same multiplicity within the configuration involve only the parameter B: separations between terms of different multiplicities, however, involve both B and C. If Slater-Condon parameters are used, then the separation between the terms, even with the same multiplicity, in general are functions of both F_2 and F_4 .

Systematic evaluation of these one-electron repulsive integrals, use of the "diagonal-sum rule", and use of relationships developed by Racah^{4,10} connecting term energies of the nd^5 -configuration with term energies of the nd^2 -configuration (cf. appendix I), eventually lead to the theoretical energies for the terms of the nd^5 -configuration. These are listed in Table (1.4),^{3,4} in terms of both the Slater-Condon and the Racah forms of the various electronic repulsion parameters.

Table (1.4)

Term	Energies	
	Racah parameters ⁽⁴⁾	Slater Condon parameters ⁽³⁾
6S	$10A - 35B$	$10F_0 - 35F_2 - 315F_4$
4G	$10A - 25B + 5C$	$10F_0 - 25F_2 - 190F_4$
4F	$10A - 13B + 7C$	$10F_0 - 13F_2 - 180F_4$
4D	$10A - 18B + 5C$	$10F_0 - 18F_2 - 225F_4$
4P	$10A - 28B + 7C$	$10F_0 - 28F_2 - 105F_4$
2I	$10A - 24B + 8C$	$10F_0 - 24F_2 - 90F_4$
2H	$10A - 22B + 10C$	$10F_0 - 22F_2 - 30F_4$
2G	$10A - 13B + 8C$	$10F_0 - 13F_2 - 145F_4$
${}^2G'$	$10A + 3B + 10C$	$10F_0 - 3F_2 - 155F_4$
2F	$10A - 9B + 8C$	$10F_0 - 25F_2 - 15F_4$
${}^2F'$	$10A - 25B + 10C$	$10F_0 - 9F_2 - 165F_4$
2D	$10A - 4B + 10C$	$10F_0 - 4F_2 - 120F_4$
${}^2D'_{\pm}$	$10A - 3B + 11C$	$10F_0 - 3F_2 - 90F_4$
	$\pm 3(57B^2 + 2BC + C^2)^{\frac{1}{2}}$	$\pm (513F_2^2 - 4500F_2F_4 + 20,700F_4^2)^{\frac{1}{2}}$
2P	$10A + 20B + 10C$	$10F_0 + 20F_2 - 240F_4$
2S	$10A - 3B + 8C$	$10F_0 - 3F_2 - 195F_4$

1.2.d TERM ENERGIES FOR THE $4d^5$ CONFIGURATION OF THE
ISOLATED Ru^{3+} ION

Theoretical expressions similar to those listed in Table (1.4) can be derived for other nd^N configurations, and experimental values for the Racah and Slater-Condon parameters can be obtained by equating differences in such tables with absorption and/or emission spectral data.¹¹ Experimentally determined semi-empirical B and C/B values for Ru, Ru^+ , Ru^{2+} are listed in Table (1.5).^{1,4} Experimental parameters for Ru^{3+} do not seem to be available in the literature. However, theoretical values of F^k and of the 4G and 4P term energies of the $4d^5$ configuration of Ru^{3+} have been listed by Fraga, Karwowski and Saxena.¹² Conversion of these to F_k and then to A, B and C, using equations (1.32) and (1.33) gives the parameters listed for Ru^{3+} in Table (1.5)

Table (1.5)

atom/ion	B (cm^{-1})	C/B
Ru	600	5.4
Ru^+	670	3.5
Ru^{2+}	620 (474) ⁴	6.5 (3.8) ⁴
* Ru^{3+}	(929.21) ¹²	(4.03) ¹²

* Theoretical values¹²: $A=135254.4\text{ cm}^{-1}$ and $C=3744.9\text{ cm}^{-1}$.

Combining the data for Ru^{3+} in Table (1.5) with the theoretical expressions listed in Table (1.4) leads to the free ion term energies, relative to the ^6S term, for the $4d^5$ configuration of Ru^{3+} listed in Table (1.6) and shown in Figure (1.1).

Figure (1.2) shows in more general form, how the energy level diagram for an isolated nd^5 -configuration changes as the ratio of (B/C) is changed. For Ru^{3+} $(B/C) = 0.248$, and it should be noted that the energies of the ^4F , $^2\text{D}'$, $^2\text{F}'$, ^2G and ^2H terms are very close together for this ratio.

1.3 SPIN-ORBIT COUPLING IN FREE IONS

In order to understand the magnetic properties of free ions, or for that matter of ions in chemically interesting systems, it is necessary to consider the effects of spin-orbit coupling on the eigenfunctions and eigenvalues of the free ions or of the ion in a ligand field. Both spin and orbital angular momenta contribute to the magnetic dipole of the electron. Furthermore, the spin and orbital magnetic moments are coupled together, the interaction being known as, "spin-orbit coupling", and it changes the energy of the ion. Spin-orbit interaction energies vary between $100\text{-}5000\text{ cm}^{-1}$ in the transition series of elements.¹

Classically, the energy associated with spin-orbit coupling is proportional to the orbital angular momentum vector, spin angular momentum vector and the cosine of the angle between these two vectors, i.e. the contribution to the electronic Hamiltonian arising from spin-orbit coupling can be written in the form

Table (1.6)

Term	Energy (cm ⁻¹)
⁶ S	0
⁴ G	28016.6
⁴ F	46657.0
⁴ D	34521.1
⁴ P	32718.8
² I	40180.5
² H	49528.8
² G	50401.9
² G'	72759.1
² F	54118.8
² F'	46741.1
² D	66254.7
² D' ₊	96064.4
² D' ₋	45793.2
² P	88555.8
² S	59694.1

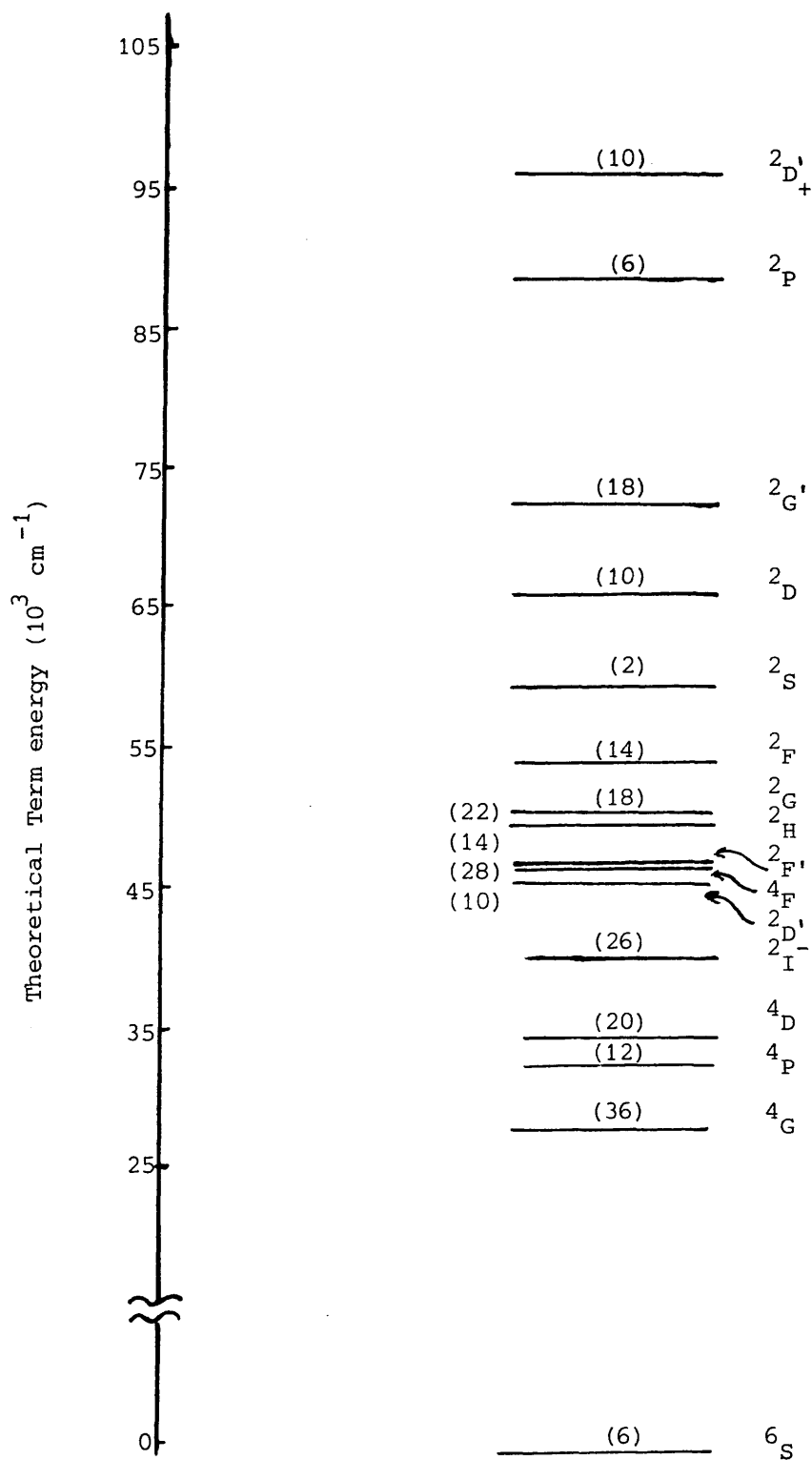


Figure (1.1). The term energies in cm^{-1} of Ru^{3+} ion, $4d^5$ configuration, relative to $6S$ assuming $B/C = 0.2481$. Numbers between parentheses represent number of Φ (micro states) in each term

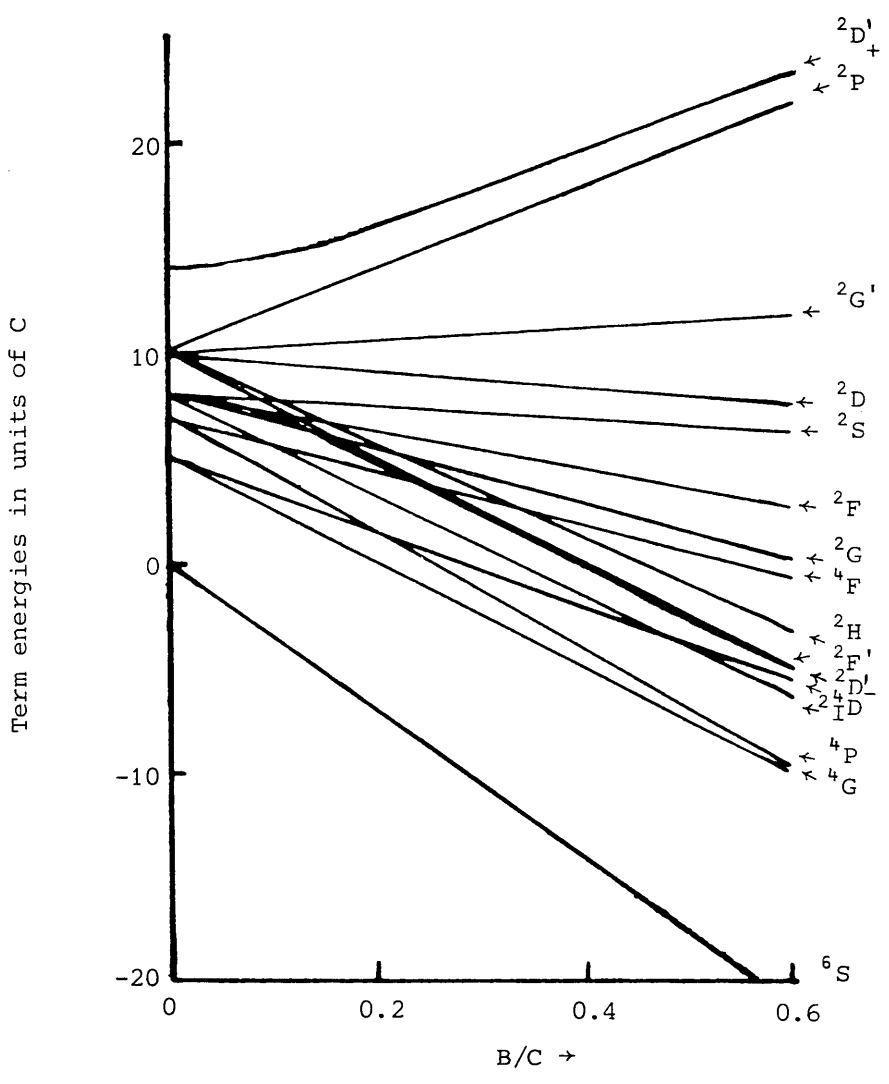


Figure (1.2). Energy level diagram for nd^5 configuration

$$\mathcal{H}_{SO} = \zeta(r) \hat{l} \cdot \hat{s} \quad (1.34)$$

Relativistic quantum mechanics applied to an electron moving in a central field, the electrostatic potential being $V(r)$, shows that the one electron spin-orbit coupling $\zeta(r)$ is given by

$$\zeta(r) = -\frac{e}{2m^2 c^2} \frac{1}{r} \frac{\partial V(r)}{\partial r} \quad (1.35)$$

where c is the velocity of light. The direct product of $\hat{l} \cdot \hat{s}$ is

$$\hat{l} \cdot \hat{s} = \hat{l}_z \hat{s}_z + \hat{l}_x \hat{s}_x + \hat{l}_y \hat{s}_y \quad (1.36)$$

$$= \hat{l}_z \hat{s}_z + \frac{1}{2} \hat{l}_+ \hat{s}_- + \frac{1}{2} \hat{l}_- \hat{s}_+ \quad (1.37)$$

When more than one electron is present, it is usual to neglect the interaction of the spins with orbitals other than their own, this is a valid approximation as long as the central field is stronger than the inter-electronic interactions, and equation (1.34) becomes

$$\mathcal{H}_{SO} = \sum_i \zeta(r_i) \hat{l}_i \cdot \hat{s}_i \quad (1.38)$$

This is often recast in the form

$$\mathcal{H}_{SO} = \lambda \mathbf{L} \cdot \mathbf{S} \quad (1.39)$$

where \mathbf{L} and \mathbf{S} are the operators for the total electronic orbital and the total electronic spin angular momenta respectively.

The total Hamiltonian at this stage, then becomes

$$\mathcal{H} = \mathcal{H}^0 + \mathcal{H}_{SO} \quad (1.40)$$

where, from equations (1.4) and (1.5)

$$\mathcal{H}^0 = \sum_{i=1}^N \left[-\frac{\hbar^2}{2m} \nabla_i^2 - \frac{Ze^2}{r_i} \right] + \frac{1}{2} \sum_i^N < \sum_j^N \frac{e^2}{r_{ij}} + \sum_{i=1}^N eV(r_i) \quad (1.41)$$

Exact solutions for the eigenfunctions and the eigenvalues of the Hamiltonian of (1.40) cannot be given and so usually the spin-orbit coupling \mathcal{H}_{SO} is treated as a perturbation of the unperturbed Hamiltonian of (1.41). This is a reasonable approximation even in complexes of the second and third transition metal-ion series. The solutions for the unperturbed system (1.41) are those described in section 1.2 and if the free ion basis function, (L, M_L, S, M_S) -scheme is used then the spin-orbit coupling matrix elements E_{SO} become

$$E_{SO} = < \Psi(L, M_L, S, M_S) | \mathcal{H}_{SO} | \Psi'(L, M'_L, S, M'_S) > \quad (1.42)$$

and inserting equation (1.39), this gives

$$E_{SO} = \lambda < \Psi(L, M_L, S, M_S) | L.S | \Psi'(L, M'_L, S, M'_S) > \quad (1.43)$$

The one-electron spin-orbit coupling parameter $\zeta(r)$ defined in equation (1.35) depends only on the radial distribution function of the electron. However, when the spin-orbit coupling constant λ ,

equation (1.43), for the many electron system is evaluated⁵ this turns out to depend on the two quantum numbers L and S and is found to be

$$\lambda = \pm \xi_{n,\ell} / (2S) \quad (1.44)$$

where

$$\xi_{n,\ell} = \hbar^2 \int_0^\infty R_{n,\ell}^2 \zeta(r) r^2 dr \quad (1.45)$$

the positive sign is used for a less than half-full shell and the negative sign is used for a more than half-full shell. When the shell is half-full, for example in high spin nd^5 ions, $L = 0$ and therefore $\lambda = 0$ for the ground states.

Spin-orbit coupling parameters estimated from electronic wave functions are very sensitive to the precise details of the wave functions that are used and need to be treated with caution. Thus, for example, the one electron spin-orbit coupling parameter $\xi_{n\ell}$ for Ru^{3+} has been estimated by various authors to be 1500 cm^{-1} ,⁷ 1250 cm^{-1} ,¹ and 1180 cm^{-1} ¹³ respectively.

For a given LS-term the matrix elements (1.38) are proportional to the matrix elements $\hat{L} \cdot \hat{S}$. It therefore follows that the matrix elements (1.43) differ from zero only if

$$M_L + M_S = M'_L + M'_S = M_J \quad (1.46)$$

Since the Hamiltonian operator commutes with \hat{L}^2 , \hat{S}^2 , \hat{J}^2 and \hat{J}_z it follows that the corresponding quantum numbers can be chosen to characterize the states which can, now, be designated in the form

(L, S, J, M_J) . Furthermore,

$$\hat{J}^2 = (\hat{L} + \hat{S})^2$$

therefore

$$\hat{L} \cdot \hat{S} = \frac{1}{2} (\hat{J}^2 - \hat{L}^2 - \hat{S}^2) \quad (1.47)$$

and on neglecting the off-diagonal terms, the energy of a state (L, S, J, M_J) is now given by

$$E = E(L, S) + \frac{1}{2} \lambda [J(J+1) - L(L+1) - S(S+1)] \quad (1.48)$$

The energy difference between similar levels J and $J-1$ is

$$\Delta E = E(L, S, J, M_J) - E(L, S, J-1, M_J) = \lambda J \quad (1.49)$$

and this is the so-called Landé interval rule.³

Each LS-term in Figure (1.1) is split by spin-orbit coupling into states which can be labelled by the quantum number J , where J ranges from $|L+S|$, $|L+S-1|$, ..., $|L-S|$, and it is easy to show that $(2S+1)(2L+1)$ states originate from a given LS-term. Table (1.7) shows the effects of spin-orbit coupling on the sextet, quartet, and 2I terms of the nd^5 configuration.

Since $L = 0$ in the 6S -term, it follows that this term does not split under spin-orbit coupling to any order. However, off-diagonal matrix elements of the spin-orbit coupling operator can mix excited levels of the nd^5 configuration into this ground state and can modify its eigen-

Table (1.7)

Term	Degeneracy (2S+1)(2L+1)	J	Number of states at J level = (2J+1)	Energy of state including spin- orbit coupling*
6S	6	5/2	6	$E({}^6S) + 0$
4G	36	11/2	12	$E({}^4G) + 6\lambda$
		9/2	10	$E({}^4G) + \frac{1}{2}\lambda$
		7/2	8	$E({}^4G) - 4\lambda$
		5/2	6	$E({}^4G) - \frac{15}{2}\lambda$
4F	28	9/2	10	$E({}^4F) + \frac{9}{2}\lambda$
		7/2	8	$E({}^4F) + 0$
		5/2	6	$E({}^4F) - \frac{7}{2}\lambda$
		3/2	4	$E({}^4F) - 6\lambda$
4D	20	7/2	8	$E({}^4D) + 3\lambda$
		5/2	6	$E({}^4D) - \frac{1}{2}\lambda$
		3/2	4	$E({}^4D) - 3\lambda$
		1/2	2	$E({}^4D) - 6\lambda$
4P	12	5/2	6	$E({}^4P) + \frac{3}{2}\lambda$
		3/2	4	$E({}^4P) - \lambda$
		1/2	2	$E({}^4P) - \frac{5}{2}\lambda$
2I	26	13/2	14	$E({}^2I) + 3\lambda$
		11/2	12	$E({}^2I) - \frac{7}{2}\lambda$

* Energies in cm^{-1} , and are derived from equation (1.48). Energies for free ion terms $E(L,S)$ can be obtained from Table (1.4).

function and eigenvalue.⁴ In the presence of spin-orbit coupling, therefore, the ground state is not exactly 6S but contains admixture of some nd^5 excited level i.e.

$$\Psi = c_o \Psi({}^6S) + \sum_i c_i X_i \tag{1.50}$$

where

$$\Psi({}^6S) = \Psi(0, \frac{5}{2}, \frac{5}{2}, M_J)[{}^6S],$$

c_o and c_i are mixing coefficients and X_i are wave functions for the excited level i .

It turns out that the ${}^4P_{5/2}$ level is the only level of the nd^5 configuration that is mixed in with 6S by spin-orbit coupling, and full calculations⁴ show that in the presence of spin-orbit coupling the eigenfunction of the lowest level of nd^5 configuration is given approximately by

$$\psi = \Psi({}^6S) - \frac{\zeta \sqrt{5}}{\Delta E({}^6S-{}^4P)} \Psi(1, \frac{3}{2}, \frac{5}{2}, \frac{5}{2})[{}^4P] \tag{1.51}$$

where

$$\Psi(1, \frac{3}{2}, \frac{5}{2}, \frac{5}{2})[{}^4P] = X_i$$

and from Table (1.4)

$$\Delta E({}^6S-{}^4P) = 7(B + C)$$

APPENDIX I

SEXTET AND QUARTET TERM ENERGIES OF THE

nd⁵ CONFIGURATION^{4,10}

The interelectronic repulsion parameters, F_k or A , B and C can be related to the Coulomb integral, J , and the exchange integral, K , between the d-electrons where

$$J(\psi_{a_i}, \psi_{a_j}) = \langle \psi_{a_i} \psi_{a_j} | V | \psi_{a_i} \psi_{a_j} \rangle$$

(I.1)

and

$$K(\psi_{a_i}, \psi_{a_j}) = \langle \psi_{a_i} \psi_{a_j} | V | \psi_{a_j} \psi_{a_i} \rangle$$

The resultant relations are shown, for the nd^2 configuration, in Table (I.1).

Most of the term energies of the nd^5 configuration, including the sextet and the quartet terms, can be determined by using the "diagonal-sum rule" procedure outlined in section (1.2.c). The energies of the sextet and quartet terms can also be determined by means of the following general procedure established by Racah,^{4,10} in which the energies of the terms with $S = \ell - \frac{1}{2}$ and $S = \ell + \frac{1}{2}$ in the configuration $(n\ell)^{2\ell+1}$ are related to the energies of $(n\ell)^2$, especially when $\ell = 2$. According to this argument, terms with $S = 5/2$ and $S = 3/2$ in the nd^5 configuration are related to the energies of terms arising from the nd^2 configuration. The energies of the terms, (¹G, ³F, ¹D, ³P and ¹S) that

Table (I.1)

m_ℓ values		J	K
± 2	± 2	$A + 4B + 2C$	$A + 4B + 2C$
± 2	∓ 2	$A + 4B + 2C$	$2C$
± 2	± 1	$A - 2B + C$	$6B + C$
± 2	∓ 1	$A - 2B + C$	C
± 2	0	$A - 4B + C$	$4B + C$
± 1	± 1	$A + B + 2C$	$A + B + 2C$
± 1	∓ 1	$A + B + 2C$	$6B + 2C$
± 1	0	$A + 2B + C$	$B + C$
0	0	$A + 4B + 3C$	$A + 4B + 3C$

arise from the nd^2 configuration are first worked out, using the "diagonal-sum rule" procedure, and then the sextet and quartet energies belonging to the nd^5 configuration can be determined in the following manner. From the M_L, M_S table for the nd^2 configuration,^{3,7} and from Table (I.1), one obtains

$$E(^1G) = E(\overset{+}{2}, \overset{-}{2}) = J(2, 2) = A + 4B + 2C$$

$$\begin{aligned} E(^3F) + E(^1G) &= E(\overset{+}{2}, \overset{+}{1}) + E(\overset{+}{2}, \overset{+}{1}) \\ &= 2J(2, 1) \\ &= A - 4B + 2C \end{aligned}$$

$$\begin{aligned} E(^1D) + E(^3F) + E(^1G) &= E(\overset{+}{2}, \overset{-}{0}) + E(\overset{+}{2}, \overset{-}{0}) + E(\overset{+}{1}, \overset{-}{1}) \\ &= 2J(2, 0) + J(1, 1) \\ &= 3A - 7B + 4C \end{aligned}$$

$$\begin{aligned} E(^3P) + E(^1D) + E(^3F) + E(^1G) &= E(\overset{+}{2}, \overset{+}{-1}) + E(\overset{+}{2}, \overset{+}{-1}) + E(\overset{+}{1}, \overset{+}{0}) + E(\overset{+}{1}, \overset{+}{0}) \\ &= 2J(2, -1) + 2J(1, 0) \\ &= 4A + 4C \end{aligned}$$

$$\begin{aligned} E(^1S) + E(^3P) + E(^1D) + E(^3F) + E(^1G) &= \\ &= E(\overset{+}{2}, \overset{-}{-2}) + E(\overset{-}{2}, \overset{+}{-2}) + E(\overset{+}{1}, \overset{-}{-1}) + E(\overset{-}{1}, \overset{+}{-1}) + E(\overset{+}{0}, \overset{-}{0}) \\ &= 2J(2, -2) + 2J(1, -1) + J(0, 0) \\ &= 5A + 14B + 11C \end{aligned}$$

From these equations, one deduces immediately the first-order electrostatic energies for terms that arise from nd^2 configuration. Thus,

$$\begin{aligned}
E(^1S) &= A + 14B + 7C \\
E(^1D) &= A - 3B + 2C \\
E(^1G) &= A + 4B + 2C \\
E(^3P) &= A + 7B \\
E(^3F) &= A - 8B
\end{aligned}
\tag{I.2}$$

The energies of the five terms (6S , 4P , 4D , 4F and 4G) that arise from the nd^5 configuration are then related to the corresponding energies, listed in equations (I.2), with the same L value. In terms of the Racah A , B and C parameters, these turn out to be

$$E(d^5, ^6 \text{ or } ^4L) = 11A - 21B + 7C - E(d^2, ^{2S+1}L) \tag{I.3}$$

Equation (I.3) then gives the energies of the sextet and quartet terms of nd^5 configuration, thus

$$\begin{aligned}
E(^6S) &= 10A - 35B \\
E(^4P) &= 10A - 28B + 7C \\
E(^4D) &= 10A - 18B + 5C \\
E(^4F) &= 10A - 13B + 7C \\
E(^4G) &= 10A - 25B + 5C
\end{aligned}
\tag{I.4}$$

- CHAPTER TWO -

THE EFFECTS OF CRYSTAL FIELDS ON THE
nd⁵ CONFIGURATION

In crystal field theory, the central metal ion of an inorganic complex is subjected to an electric field originating from the surrounding ions, atoms, or molecules, i.e. the ligands, and this crystal field destroys the spherical symmetry of the free atom. Furthermore, in crystal field theory, electrons on the ligand are not allowed to overlap and mix with the electrons of the metal ion, and ligand-ligand and next neighbouring interactions are neglected.^{1-4,7,9,14-18}

2.1 THE ELECTROSTATIC POTENTIAL GENERATED BY LIGANDS

If the distribution of charge density of all the ligands in a given complex is given by $\rho(\vec{R}) \equiv \rho(x', y', z') \equiv \rho(R, \theta', \phi')$, where \vec{R} is the vector joining the central metal ion to a point whose coordinates are x', y', z' or R, θ', ϕ' , as shown in Figure (2.1), then

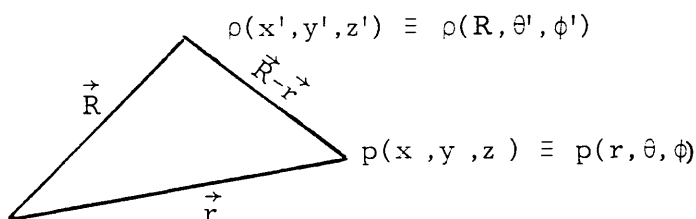


Figure (2.1)

the total charge on the ligand produces at the reference point $p(\vec{r}) \equiv p(x, y, z) \equiv p(r, \theta, \phi)$, an electrostatic potential given by

$$V(\vec{r}) = \int \frac{\rho(\vec{R})}{|\vec{R} - \vec{r}|} d\tau_{\vec{R}} \quad (2.1)$$

where the integration is taken over the entire space covered by the ligand charge distribution. Equation (2.1) can be expanded out in

terms of an infinite series of spherical harmonics

$$V(\vec{r}) = V(r, \theta, \phi) = \sum_{k=0}^{\infty} \sum_{\alpha=-k}^{+k} A_{k,\alpha} r^k Y_{k,\alpha}(\theta, \phi) \quad (2.2)$$

where

$$A_{k,\alpha} = \frac{4\pi}{2k+1} \int \frac{\rho(\vec{R}) Y_{k,\alpha}^*(\theta', \phi')}{R^{k+1}} d\tau_{\vec{R}} \quad (2.3)$$

$A_{k,\alpha}$ is obviously just a number which is characteristic of the distribution of charge in the ligand.

Although equation (2.2) is an infinite series in fact only a very few terms are important in crystal field theory of transition-metal ion complexes, and it is worthwhile to bear the following points in mind: (a) the electrostatic potential function $V(\vec{r})$ must possess the same symmetry properties as the ligand charge distribution $\rho(\vec{R})$, (b) it can be shown that, terms in which $k > 4$, and terms for which k is odd do not affect the energy of d-electrons. It therefore follows that when considering crystal field theory of transition metal complexes that one only needs to use the abbreviated form

$$V(\vec{r}) = A_{0,0} r^0 Y_{0,0} + \sum_{\alpha=-2}^{+2} A_{2,\alpha} r^2 Y_{2,\alpha} + \sum_{\alpha=-4}^{+4} A_{4,\alpha} r^4 Y_{4,\alpha} \quad (2.4)$$

for the electrostatic ligand potential when considering crystal field contributions to the electronic energies. However, it should always be remembered that (2.4) does not describe the complete potential but only that part which plays a role in crystal field theory of d-electrons.

Equation (2.4) is valid for all d-electron systems and it is independent

of the symmetry properties of the ligand system which generates the potential. Symmetry considerations, in general, lead to further simplifications of the expression for the ligand potential function, as will be seen later on in this chapter.

In the ionic crystal field theory, the charge distributions of individual ligands are approximated by point charges or by point dipoles. With such an approximation the integral (2.3) becomes a sum over the ligand charges and is given by

$$A_{k,\alpha}^{(L)} = \frac{4\pi}{2k+1} \sum_i \frac{-q'_i Y_{k,\alpha}^*(\theta'_i, \phi'_i)}{R^{k+1}} \quad (2.5)$$

where $-q'_i$ is the charge on ligand i , and superscript (L) indicates that the ligand acts as a point charge, not as a point dipole. If all ligands possess the same charge $-q'$ and are at the same distance R from the nucleus of the central ion then

$$A_{k,\alpha}^{(L)} = -\frac{4\pi}{2k+1} \frac{q'}{R^{k+1}} \sum_i Y_{k,\alpha}^*(\theta'_i, \phi'_i) \quad (2.6)$$

$$\text{i.e.} \quad A_{k,\alpha}^{(L)} = a_k^{(L)} \sum_i Y_{k,\alpha}^*(\theta'_i, \phi'_i) \quad (2.7a)$$

$$\text{where} \quad a_k^{(L)} = -\frac{4\pi}{2k+1} \frac{q'}{R^{k+1}} \quad (2.7b)$$

2.1.a ELECTROSTATIC INTERACTIONS IN TRANSITION METAL-ION COMPLEXES

Let a transition metal-ion, at the origin of a coordinate system be surrounded by six point charges, $-q'$, at the vertices of a regular octahedron and lying along the coordinate axes at a distance R from the central ion, as shown in Figure (2.2).

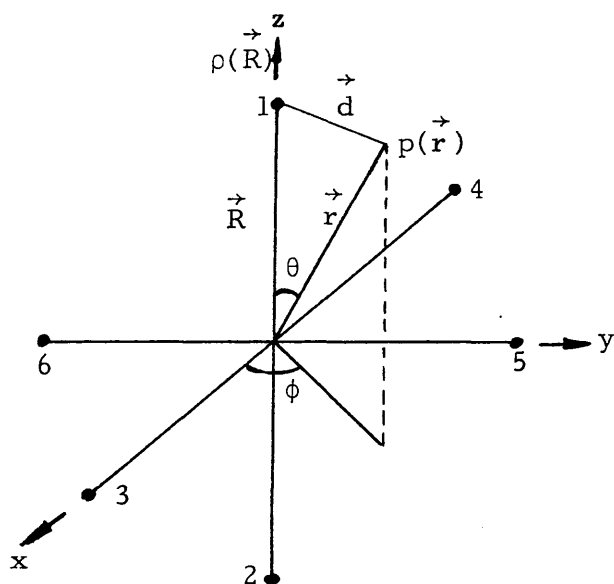


Figure (2.2)

A transition metal ion electron, charge $-e$, at the point p at a distance d from $-q'$ interacts with the potential generated by $-q'$ and its potential energy, $V_{x\ell}$, is altered by an amount

$$V_{x\ell} = q'e/d \quad (2.8)$$

and when the interactions with all six ligand charges are taken into account, it is quite easy to show that the potential energy of this

electron is altered by amount

$$\sum_{i=1}^N V_{x\ell}^i = \frac{6q'e}{R} + D(x^4 + y^4 + z^4 - \frac{3}{5} r^4) \quad (2.9)$$

when the parameter D is $35q'e/(4R^5)$.^{15,18} Equation (2.9) can also be recast in terms of spherical harmonics $Y_{k,\alpha}$

$$V_{x\ell}^{\text{oct}}(\vec{r}) = \frac{3}{\sqrt{\pi}} a_0 Y_{0,0} + \frac{21}{4\sqrt{\pi}} a_4 r^4 \{Y_{4,0} + \sqrt{\frac{5}{14}}(Y_{4,4} + Y_{4,-4})\} \quad (2.10)$$

where

$$a_0 = \frac{-4\pi q'}{R} \quad \text{and} \quad a_4 = \frac{-4\pi}{9} \frac{q'}{R^5} \quad (2.11)$$

The first terms in equations (2.9) and (2.10) depend only on the distance, R , of the ligands from the transition metal ion. They do not depend on the symmetry properties of the ligand field. However, the second terms in these equations do depend on, and reflect the stereochemistry of the six ligands, in this case at the vertices of the octahedron. It is these last terms in these equations that are responsible for the removal of the electron d -orbital degeneracy. Since the electron will prefer to avoid regions in space where the electron density is greatest, the extent to which orbital alignments are determined by these last terms obviously depends upon the number of transition metal ion electrons present and their correlating interactions with one another.

Expressions for ligand electrostatic contributions to the potential energy of a transition metal-ion electron, can be derived for other symmetries, and the results^{3,4,7} for the most important cases are

given in Table (2.1). It should be noticed that, (i) in each of these expressions the first term has a similar form, (ii) the angular dependence for octahedral, cubic, and tetrahedral complexes is identical, (iii) the D_{4h} complexes have additional $Y_{2,0}$ terms, and (iv) the trigonal complexes have additional $Y_{4,\pm 3}$ terms.

2.2 THE nd^N ION IN A CRYSTAL FIELD

If free ion interactions, crystal field interactions, and spin-orbit interactions are all taken into account then the electronic Hamiltonian for a system containing N electrons, for example $N=5$, in its outermost shell becomes

$$\mathcal{H} = \sum_{i=1}^N \left[-\frac{\hbar^2}{2m} \nabla_i^2 - \frac{Ze^2}{r_i} \right] + \frac{1}{2} \sum_{i=1}^N \sum_{j=1, i \neq j}^N \frac{e^2}{r_{ij}} + \sum_{i=1}^N V_{x\ell}(\vec{r}_i) + \sum_{i=1}^N V_{SO}(i) \quad (2.12)$$

Exact eigenfunctions and exact eigenvalues of the Hamiltonian (2.12) can not be obtained, but an approximate solution can be deduced by means of appropriate perturbation calculations. Equation (2.12) can be recast into the form

$$\mathcal{H} = \mathcal{H}_{00} + \mathcal{H}_1 \quad (2.13)$$

where

$$\mathcal{H}_{00} = \sum_{i=1}^N \left[-\frac{\hbar^2}{2m} \nabla_i^2 - \frac{Ze^2}{r_i} \right] \quad (2.14)$$

and

$$\mathcal{H}_1 = \frac{1}{2} \sum_{i=1}^N \sum_{j=1, i \neq j}^N \frac{e^2}{r_{ij}} + \sum_{i=1}^N V_{x\ell}(\vec{r}_i) + \sum_{i=1}^N V_{SO}(i) \quad (2.15)$$

Table (2.1)^{4,7}

Symmetry	Crystal field contributions to potential energy of a transition metal-ion electron
6 ligands, octahedron, O _h	$V_{xl}^{oct}(\vec{r}) = \frac{3}{\sqrt{\pi}} a_0 Y_{0,0} + \frac{21}{4\sqrt{\pi}} a_4 r^4 \{Y_{4,0} + \sqrt{\frac{5}{14}} (Y_{4,4} + Y_{4,-4})\}$
8 ligands, cube, O _h	$V_{xl}^{cub}(\vec{r}) = \frac{4}{\sqrt{\pi}} a_0 Y_{0,0} - \frac{14}{3\sqrt{\pi}} a_4 r^4 \{Y_{4,0} + \sqrt{\frac{5}{14}} (Y_{4,4} + Y_{4,-4})\}$
4 ligands, tetrahedron, T _d	$V_{xl}^{td}(\vec{r}) = \frac{2}{\sqrt{\pi}} a_0 Y_{0,0} - \frac{7}{3\sqrt{\pi}} a_4 r^4 \{Y_{4,0} + \sqrt{\frac{5}{14}} (Y_{4,4} + Y_{4,-4})\}$
4 ligands, square, D _{4h}	$V_{xl}^{sq}(\vec{r}) = \frac{2}{\sqrt{\pi}} a_0 Y_{0,0} - \frac{\sqrt{5}}{\sqrt{\pi}} a_2 r^2 Y_{2,0} + \frac{9}{4\sqrt{\pi}} a_4 r^4 \{Y_{4,0} + \sqrt{\frac{35}{18}} (Y_{4,4} + Y_{4,-4})\}$
$a_0 = -4\pi q' / R, \quad a_2 = -\frac{4\pi q'}{5R^3}, \quad a_4 = -\frac{4\pi q'}{9R^5}$	

Table (2.1) contd.

Symmetry	Crystal field contributions to potential energy of a transition metal-ion electron
general, D_{4h}	$V_{x\ell}^{te}(\vec{r}) = A_{0,0} Y_{0,0} + A_{2,0} r^2 Y_{2,0} + A_{4,0} r^4 Y_{4,0} + A_{4,4} r^4 (Y_{4,4} + Y_{4,-4})$
general trigonal, D_{3d} or C_{3v}	$V_{x\ell}^{tri}(\vec{r}) = A_{0,0} Y_{0,0} + A_{2,0} r^2 Y_{2,0} + A_{4,0} r^4 Y_{4,0} + A_{4,3} r^4 (Y_{4,3} - Y_{4,-3})$

Eigenfunctions and eigenvalues of \mathcal{H}_{00} have already been considered in chapter one, where it has been shown that its eigenvalues for an nd^5 system are $E_{00} = 5\epsilon_{nd}$, and its eigenfunctions are the 252 anti-symmetrized one-electron product functions $\Phi[(m_{\ell_1}, m_{s_1}), \dots, (m_{\ell_5}, m_{s_5})]$, cf. Tables (1.1) and (1.2). These 252 Φ functions are degenerate, i.e. their energies $5\epsilon_{nd}$ are identical.

A complete perturbation calculation involving \mathcal{H}_1 , can, in principle, be carried out. However, it is extremely difficult to do and it is conventional to divide the perturbation calculation into a sequence of well-defined separate steps in which the expression on the right hand side of the perturbation operator (2.15) are ordered according to their magnitudes.

Three different distinguishable cases with regards to the relative magnitudes of the three terms in (2.15) can be recognised at this point.

(i) The weak crystal field case, where the d electron-electron repulsion interactions are strongest, i.e.

$$\frac{1}{2} \sum_{i=1}^N \sum_{j=1, j \neq i}^N \frac{e^2}{r_{ij}} > \sum_i^N V_{x\ell}(\vec{r}_i) > \sum_i^N V_{SO}(i)$$

(ii) The strong crystal field case, very commonly encountered in complexes of the second and third transition series, where the crystal field interactions are strongest, i.e.

$$\sum_i^N V_{x\ell}(\vec{r}_i) > \frac{1}{2} \sum_{i=1}^N \sum_{j=1, j \neq i}^N \frac{e^2}{r_{ij}} > \sum_i^N V_{SO}(i)$$

(iii) The strong spin-orbit coupling case, encountered in the complexes of rare-earth ions, where the spin-orbit interactions are strongest, i.e.

$$\sum_i^N V_{SO}(i) > \sum_i^N V_{x\ell}(\vec{r}_i), \quad \frac{1}{2} \sum_{i=1}^N \sum_{i \neq j}^N \frac{e^2}{r_{ij}}$$

Since this account is concerned with transition metal-ion complexes, spin-orbit coupling interactions for the moment will be neglected and the Hamiltonian \mathcal{H}_1 then becomes more manageable for,

$$\begin{aligned} \mathcal{H}_1 &= \frac{1}{2} \sum_{i=1}^N \sum_{i \neq j}^N \frac{e^2}{r_{ij}} + \sum_{i=1}^N V_{x\ell}(\vec{r}_i) \\ &= \mathcal{H}_{el} + \mathcal{H}_{lig} \end{aligned} \quad (2.16)$$

If the d electron-electron repulsion interactions and d-electron-ligand interactions are of the same order of magnitude then complete perturbation analysis involving secular equations that include \mathcal{H}_1 must be solved, but if one of these contributions dominates then one or other of the two limiting cases of (i) weak field or (ii) strong field complexes is encountered.

2.2.a THE WEAK OCTAHEDRAL CRYSTAL FIELD CASE

In the weak crystal field case, \mathcal{H}_{lig} effectively perturbs \mathcal{H}_{el} . The quantum numbers L and S of the central ion then retain their validity and the problem then degenerates to deciding how a given LS-scheme is split by the ligand-field, i.e. the Hamiltonian of equation (2.12) can be recast into the form

$$\mathcal{H} = \mathcal{H}_{ion} + \mathcal{H}_{lig}$$

where

$$\begin{aligned}\mathcal{H}_{\text{ion}} &= \sum_{i=1}^N \left[-\frac{\hbar^2}{2m} \nabla_i^2 - \frac{Ze^2}{r_i} \right] + \frac{1}{2} \sum_{i=1}^N \sum_{j=1, i \neq j}^N \frac{e^2}{r_{ij}} \\ &= \mathcal{H}_{00} + \mathcal{H}_{\text{el}}\end{aligned}\quad (2.17)$$

and the perturbation term

$$\mathcal{H}_{\text{lig}} = \sum_{i=1}^N V_{\text{xel}}(\vec{r}_i) \quad (2.18)$$

The eigenfunctions of \mathcal{H}_{ion} are the $(2S+1)(2L+1)$ free ion eigenfunctions $\Psi(L, M_L, S, M_S)$ already discussed in section 1.2.c and detailed results of the nd^5 configuration, for example, are listed in Table (1.4).

In principle the crystal field perturbation of \mathcal{H}_{lig} mixes these basis functions and the eigenfunctions of $\mathcal{H} = \mathcal{H}_{\text{ion}} + \mathcal{H}_{\text{lig}}$ can be obtained by solving the secular equations (2.19).

$$|| \langle \Theta_r | \mathcal{H}_{\text{lig}} | \Theta_s \rangle - \Delta E_{\text{lig}} \delta_{r,s} || = 0 \quad (2.19)$$

where Θ_x is either the basis $\Psi(L, M_L, S, M_S)$ or some linear combination of these Ψ .

The solutions of the secular equations (2.19) can be greatly simplified by making use of group theoretical arguments, in which the appropriate irreducible representations of the terms ^{2S+1}L are found and then linear combinations Θ_x of the $\Psi(L, M_L, S, M_S)$ which transform as the irreducible representations, i.e. appropriate symmetry adapted linear combinations of $\Psi(L, M_L, S, M_S)$ functions, are then used to calculate the magnitudes of the ligand field splitting. Table (2.2) lists the symmetry species of the irreducible representations that arise from

Term $2S+1L$ free ion, $\mathcal{H}=V_F$	Orbital degeneracy in free ion ($2L+1$)	Irreducible species under O_h symmetry
$6S$	1	$6A_{1g}$
$4G$	9	$4A_{1g} + 4E_g + 4T_{1g} + 4T_{2g}$
$4F$	7	$4A_{2g} + 4T_{1g} + 4T_{2g}$
$4D$	5	$4E_g + 4T_{2g}$
$4P$	3	$4T_{1g}$
$2I$	13	$2A_{1g} + 2A_{2g} + 2E_g + 2T_{1g} + 2T_{2g}$
$2H$	11	$2E_g + 2T_{1g} + 2T_{2g}$
$2x^2G$	$2x \ 9$	$2x(^2A_{1g} + ^2E_g + ^2T_{1g} + ^2T_{2g})$
$2x^2F$	$2x \ 7$	$2x(^2A_{2g} + ^2T_{1g} + ^2T_{2g})$
$3x^2D$	$2x \ 5$	$3x(^2E_g + ^2T_{2g})$
$2P$	3	$2T_{1g}$
$2S$	1	$2A_{1g}$

the terms ^{2S+1}L of the configuration nd^5 for the point group O_h .

2.2.a.1 ELECTRONIC EIGENFUNCTIONS FOR AN nd^5 ION IN A WEAK CRYSTAL FIELD

The functions $\Psi(L, M_L, S, M_S)$ have the same transformation properties as spherical harmonics except for the fact that the $\Psi(L, M_L, S, M_S)$ functions for an nd^N system must always have even parity. Correct symmetry adapted linear combinations of the functions $\Psi(L, M_L, S, M_S)$ can, therefore, be taken directly from the symmetry adapted linear combinations of the spherical harmonics Y_{ℓ, m_ℓ} for the appropriate point group - cf. for example, reference 3, pages 93-95; reference 4, Table A19; and reference 7, pages 305-309.

The wave function for the i th irreducible representation, $^{2S+1}\Gamma_i$ in a weak ligand field with O symmetry, derived from the free ion terms ^{2S+1}L with an M_S value of M_S is denoted²⁰ by the symbol $(^{2S+1}\Gamma_i | ^{2S+1}L, M_S)$. For example, for the nd^5 configuration in a weak field octahedral complex it can be shown that the wave function of the 6A_1 irreducible representation is identical with the wave function of the $M_S = 5/2$ level of the 6S free ion term,²¹ i.e.

$$\Theta(^6A_1 | ^6S, \frac{5}{2}) = \Psi(0, 0, \frac{5}{2}, \frac{5}{2})$$

This same wave function can, now, be expanded out in terms of the corresponding Φ functions, as outlined in section 1.2.b. Table (2.3) lists some of the wave functions for the nd^5 ion in a weak crystal field with point group symmetry O .

Table (2.3)

Wave functions of an nd^5 ion in a weak crystal field of O-symmetry

Term of free ion	Wave functions in a weak field
4G	$\begin{aligned} \Theta_1 (^4A_1 ^4G, \frac{3}{2}) &= \sqrt{\frac{7}{12}} \Psi (4, 0, \frac{3}{2}, \frac{3}{2}) + \sqrt{\frac{5}{24}} \{\Psi (4, 4, \frac{3}{2}, \frac{3}{2}) + \Psi (4, -4, \frac{3}{2}, \frac{3}{2})\} \\ \Theta_2 (^4E(a) ^4G, \frac{3}{2}) &= -\sqrt{\frac{5}{12}} \Psi (4, 0, \frac{3}{2}, \frac{3}{2}) + \sqrt{\frac{7}{24}} \{\Psi (4, 4, \frac{3}{2}, \frac{3}{2}) + \Psi (4, -4, \frac{3}{2}, \frac{3}{2})\} \\ \Theta_3 (^4E(b) ^4G, \frac{3}{2}) &= \frac{1}{\sqrt{2}} \{\Psi (4, 2, \frac{3}{2}, \frac{3}{2}) + \Psi (4, -2, \frac{3}{2}, \frac{3}{2})\} \\ \Theta_4 (^4T_1(a) ^4G, \frac{3}{2}) &= -\frac{1}{\sqrt{8}} \Psi (4, -3, \frac{3}{2}, \frac{3}{2}) - \sqrt{\frac{7}{8}} \Psi (4, 1, \frac{3}{2}, \frac{3}{2}) \\ \Theta_5 (^4T_1(b) ^4G, \frac{3}{2}) &= \frac{1}{\sqrt{2}} \{\Psi (4, 4, \frac{3}{2}, \frac{3}{2}) - \Psi (4, -4, \frac{3}{2}, \frac{3}{2})\} \\ \Theta_6 (^4T_1(c) ^4G, \frac{3}{2}) &= \sqrt{\frac{1}{8}} \Psi (4, 3, \frac{3}{2}, \frac{3}{2}) + \sqrt{\frac{7}{8}} \Psi (4, -1, \frac{3}{2}, \frac{3}{2}) \\ \Theta_7 (^4T_2(a) ^4G, \frac{3}{2}) &= \sqrt{\frac{7}{8}} \Psi (4, 3, \frac{3}{2}, \frac{3}{2}) - \frac{1}{\sqrt{8}} \Psi (4, -1, \frac{3}{2}, \frac{3}{2}) \\ \Theta_8 (^4T_2(b) ^4G, \frac{3}{2}) &= \frac{1}{\sqrt{2}} \{\Psi (4, 2, \frac{3}{2}, \frac{3}{2}) - \Psi (4, -2, \frac{3}{2}, \frac{3}{2})\} \\ \Theta_9 (^4T_2(c) ^4G, \frac{3}{2}) &= \sqrt{\frac{1}{8}} \Psi (4, 1, \frac{3}{2}, \frac{3}{2}) - \sqrt{\frac{7}{8}} \Psi (4, -3, \frac{3}{2}, \frac{3}{2}) \end{aligned}$

Table (2.3) contd.

Term of free ion	Wave functions in a weak field
$4F$	$\Theta_1 ({}^4A_2 {}^4F, \frac{3}{2}) = \frac{1}{\sqrt{2}} \{ \Psi (3, 2, \frac{3}{2}, \frac{3}{2}) - \Psi (3, -2, \frac{3}{2}, \frac{3}{2}) \}$ $\Theta_2 ({}^4T_1^{(a)} {}^4F, \frac{3}{2}) = \sqrt{\frac{5}{8}} \Psi (3, -3, \frac{3}{2}, \frac{3}{2}) - \sqrt{\frac{3}{8}} \Psi (3, 1, \frac{3}{2}, \frac{3}{2})$ $\Theta_3 ({}^4T_1^{(b)} {}^4F, \frac{3}{2}) = \Psi (3, 0, \frac{3}{2}, \frac{3}{2})$ $\Theta_4 ({}^4T_1^{(c)} {}^4F, \frac{3}{2}) = -\sqrt{\frac{5}{8}} \Psi (3, 3, \frac{3}{2}, \frac{3}{2}) - \sqrt{\frac{3}{8}} \Psi (3, -1, \frac{3}{2}, \frac{3}{2})$
$4D$	$\Theta_1 ({}^4E^{(a)} {}^4D, \frac{3}{2}) = \Psi (2, 0, \frac{3}{2}, \frac{3}{2})$ $\Theta_2 ({}^4E^{(b)} {}^4D, \frac{3}{2}) = \frac{1}{\sqrt{2}} \{ \Psi (2, -2, \frac{3}{2}, \frac{3}{2}) - \Psi (2, -2, \frac{3}{2}, \frac{3}{2}) \}$ $\Theta_3 ({}^4T_2^{(a)} {}^4D, \frac{3}{2}) = \Psi (2, -1, \frac{3}{2}, \frac{3}{2})$ $\Theta_4 ({}^4T_2^{(b)} {}^4D, \frac{3}{2}) = \frac{1}{\sqrt{2}} \{ \Psi (2, 2, \frac{3}{2}, \frac{3}{2}) - \Psi (2, -2, \frac{3}{2}, \frac{3}{2}) \}$ $\Theta_5 ({}^4T_2^{(c)} {}^4D, \frac{3}{2}) = -\Psi (2, 1, \frac{3}{2}, \frac{3}{2})$

Table (2.3) contd.

Term of free ion	Wave functions in a weak field
$4P$	$\Theta_1 \ ({}^4T_1(a) \mid {}^4P, \frac{3}{2}) = \psi \ (1, 1, \frac{3}{2}, \frac{3}{2})$
	$\Theta_2 \ ({}^4T_1(b) \mid {}^4P, \frac{3}{2}) = \psi \ (1, 0, \frac{3}{2}, \frac{3}{2})$
	$\Theta_3 \ ({}^4T_1(c) \mid {}^4P, \frac{3}{2}) = \psi \ (1, -1, \frac{3}{2}, \frac{3}{2})$
$2S$	$\Theta \ ({}^2A_1 \mid {}^2S, \frac{3}{2}) = \psi \ (0, 0, \frac{1}{2}, \frac{1}{2})$

Similar procedures also enable appropriate wave functions for the nd^5 ion in other weak fields of other symmetries to be derived.

2.2.a.2 THE ENERGY LEVELS OF AN nd^5 ION IN A WEAK CRYSTAL FIELD

The energies of the progeny terms in Table (2.2) relative to the corresponding free ion terms from which they originate can be determined by standard perturbation procedures in this case. In this, the crystal field contribution to the Hamiltonian, \mathcal{H}_{lig} , formally mixes all the eigenfunctions of all the free ion terms, and in principle a very large perturbation secular determinant has to be solved. However, this can be considerably simplified when it is realised that there are no off-diagonal matrix elements connecting symmetry adapted linear combinations of the $\Psi(L, M_L, S, M_S)$ functions,

$$\theta_i(^{2S+1}\Gamma_i | ^{2S+1}L, M_S)$$

which belong to different symmetry species. Furthermore, the crystal field operator, \mathcal{H}_{lig} , has no effect on spin coordinates. Hence, off-diagonal matrix elements connecting $\theta_i(^{2S+1}\Gamma_i | ^{2S+1}L, M_S)$ functions with different S or with different M_S values are zero.

It therefore follows that the eigenfunction of the free ion term 6S is also an eigenfunction of the nd^5 ion in an octahedral crystal field, i.e.

$$\begin{aligned} \theta(^6A_{1g} | ^6S, \frac{5}{2}) &= \Psi(0, 0, \frac{5}{2}, \frac{5}{2}) \\ &= \Phi(\overset{+}{2}, \overset{+}{1}, \overset{+}{0}, -\overset{+}{1}, -\overset{+}{2}) \end{aligned} \quad (2.20)$$

and this, for reasons which have just been explained, can not mix with any other free ion eigenfunction. Hence, the change in energy of this function when the crystal field interaction is taken into account is given by

$$\Delta E_{\text{lig}}(^6A_{1g} | ^6S, \frac{5}{2}) = \langle \Theta(^6A_{1g} | ^6S, \frac{5}{2}) | \mathcal{H}_{\text{lig}} | \Theta(^6A_{1g} | ^6S, \frac{5}{2}) \rangle \quad (2.21)$$

and when equation (2.20) is substituted into this, bearing in mind that, \mathcal{H}_{lig} , is a sum of one-electron operators

$$\mathcal{H}_{\text{lig}} = \sum_{i=1}^5 V_{\text{x}\ell}^{\text{oct}}(\vec{r}_i),$$

it can be shown that

$$\Delta E_{\text{lig}}(^6A_{1g} | ^6S, \frac{5}{2}) = 2\langle 2 | V_{\text{x}\ell}^{\text{oct}}(\vec{r}) | 2 \rangle + 2\langle 1 | V_{\text{x}\ell}^{\text{oct}}(\vec{r}) | 1 \rangle + \langle 0 | V_{\text{x}\ell}^{\text{oct}}(\vec{r}) | 0 \rangle \quad (2.22)$$

The one-electron integrals can, then, be evaluated by substitution in the appropriate form (2.10) for the octahedral crystal field. For example

$$\begin{aligned} \langle 2 | V_{\text{x}\ell}^{\text{oct}}(\vec{r}) | 2 \rangle &= -A_{0,0} \bar{r}^0 \int_0^\pi \int_0^{2\pi} Y_{2,2}^* Y_{0,0} Y_{2,2} \sin\theta d\theta d\phi \\ &\quad - A_{4,0} \bar{r}^4 \int_0^\pi \int_0^{2\pi} Y_{2,2}^* [Y_{4,0} + \sqrt{\frac{5}{14}}(Y_{4,4} + Y_{4,-4})] Y_{2,2} \sin\theta d\theta d\phi \end{aligned} \quad (2.23)$$

where

$$\bar{r}^k = \int_0^\infty R_{n,2}^* R_{n,2} r^k dr$$

The angular integrals are listed in Table (2.4).⁷ Using these values then gives

$$\begin{aligned} \langle 2 | V_{x\ell}^{\text{oct}}(\vec{r}) | 2 \rangle &= -A_{0,0} \bar{r}^0 \frac{1}{2\sqrt{\pi}} - A_{4,0} \bar{r}^4 \left[\frac{1}{14\sqrt{\pi}} + \sqrt{\frac{5}{14}} (0+0) \right] \\ &= -A_{0,0} \bar{r}^0 \frac{1}{2\sqrt{\pi}} - A_{4,0} \bar{r}^4 \frac{1}{14\sqrt{\pi}} \end{aligned} \quad (2.24)$$

The first term in equation (2.24) is often denoted in the literature by ϵ_0 . It comes from the angular independent part of the potential energy function $V_{x\ell}^{\text{oct}}(\vec{r})$, cf. page 41, and it shifts all of the progeny terms $^{2S+1}\Gamma_i$ that belong to same ^{2S+1}L free ion term to the same degree. The second term on the right hand side of equation (2.24), in the literature of octahedral complexes is usually written as $10Dq$ or Δ , where $10Dq$ is the so-called field-strength parameter. Dq is positive and is given by

$$D = \frac{35}{4} \frac{q^1 e}{R^5} \quad \text{and} \quad q = \frac{2}{105} \int R_{nd}^2(r) r^6 dr.$$

Equation (2.24) can, then, be recast in the form

$$\langle 2 | V_{x\ell}^{\text{oct}}(\vec{r}) | 2 \rangle = -\epsilon_0 + Dq \quad (2.25)$$

It can be similarly shown that the one-electron integrals $\langle 1 | V_{x\ell}^{\text{oct}}(\vec{r}) | 1 \rangle$ and $\langle 0 | V_{x\ell}^{\text{oct}}(\vec{r}) | 0 \rangle$ are given by

$$\langle 1 | V_{x\ell}^{\text{oct}}(\vec{r}) | 1 \rangle = -\epsilon_0 - 4Dq \quad \text{and} \quad \langle 0 | V_{x\ell}^{\text{oct}}(\vec{r}) | 0 \rangle = -\epsilon_0 + 6Dq \quad (2.26)$$

Table (2.4)⁷

Values of the integrals

$$\int_0^\pi \int_0^{2\pi} Y_{2,m_\ell}^* (\theta, \phi) Y_{k,\alpha} (\theta, \phi) Y_{2,m'_\ell} (\theta, \phi) \sin \theta d\theta d\phi$$

	k=0	k=2	k=4
$2\sqrt{\pi} (Y_{2,0}, Y_{k,0}, Y_{2,0})$	1	$2\sqrt{5}/7$	$6/7$
$2\sqrt{\pi} (Y_{2,\pm 1}, Y_{k,0}, Y_{2,\pm 1})$	1	$\sqrt{5}/7$	$-4/7$
$2\sqrt{\pi} (Y_{2,\pm 2}, Y_{k,0}, Y_{2,\pm 2})$	1	$-2\sqrt{5}/7$	$1/7$
$2\sqrt{\pi} (Y_{2,\pm 2}, Y_{k,\pm 4}, Y_{2,\mp 2})$	0	0	$\sqrt{70}/7$

Substitution of expressions (2.25) and (2.26) into equation (2.22) gives

$$\begin{aligned}\Delta E_{\text{lig}}(^6A_{1g} | ^6S, \frac{5}{2}) &= 2(-\epsilon_0 + Dq) + 2(-\epsilon_0 - 4Dq) - \epsilon_0 + 6Dq \\ &= -5\epsilon_0\end{aligned}\quad (2.27)$$

The effects of the octahedral crystal field on the other free ion energies of the nd^5 configuration are more complicated but can nevertheless be evaluated without too much difficulty.

In the case of quartet terms the symmetry adapted functions Θ_i that are derived from the free ion quartet term, 4L , can be subdivided into four sets of functions, $\Theta(^4\Gamma_i | ^4L, \frac{3}{2})$; $\Theta(^4\Gamma_i | ^4L, \frac{1}{2})$; $\Theta(^4\Gamma_i | ^4L, -\frac{1}{2})$; and $\Theta(^4\Gamma_i | ^4L, -\frac{3}{2})$, which are eigenfunctions of different eigenvalues M_S^h of the operator \hat{S} . These can not be mixed by the operator \mathcal{H}_{lig} . It therefore follows that the block of the perturbation determinant originating from a free ion quartet term, 4L , splits into four subdeterminants which have identical roots. Accordingly, in deriving crystal field perturbation energies, it is only necessary to obtain the roots of one of these subdeterminants.

For example, the octahedral crystal field splits the 4D free ion term into the progeny terms 4E_g and $^4T_{2g}$. The 5×5 subdeterminant block in this case, then, for symmetry reasons splits into a 2×2 determinant involving the symmetry adapted basis functions $\Theta_1(^4E_g | ^4D, \frac{3}{2})$, $\Theta_2(^4E_g | ^4D, \frac{3}{2})$ and a 3×3 determinant involving the basis functions $\Theta_1(^4T_{2g} | ^4D, \frac{3}{2})$, $\Theta_2(^4T_{2g} | ^4D, \frac{3}{2})$, and $\Theta_3(^4T_{2g} | ^4D, \frac{3}{2})$. It turns out that, (i) the diagonal elements in the 2×2 determinant are the same, (ii) the

diagonal elements in the 3x3 determinant are the same, and (iii) that all off-diagonal elements in these determinants are zero. Hence, the crystal field perturbations to the 4E_g and ${}^4T_{2g}$ energies are

$$\begin{aligned}
 \Delta E_{\text{lig}}({}^4E_g | {}^4D, \frac{3}{2}) &= \langle \theta_1({}^4E_g | {}^4D, \frac{3}{2}) | \mathcal{H}_{\text{lig}} | \theta_1({}^4E_g | {}^4D, \frac{3}{2}) \rangle \\
 &= \langle \theta_2({}^4E_g | {}^4D, \frac{3}{2}) | \mathcal{H}_{\text{lig}} | \theta_2({}^4E_g | {}^4D, \frac{3}{2}) \rangle \\
 \Delta E_{\text{lig}}({}^4T_{2g} | {}^4D, \frac{3}{2}) &= \langle \theta_1({}^4T_{2g} | {}^4D, \frac{3}{2}) | \mathcal{H}_{\text{lig}} | \theta_1({}^4T_{2g} | {}^4D, \frac{3}{2}) \rangle \\
 &= \langle \theta_2({}^4T_{2g} | {}^4D, \frac{3}{2}) | \mathcal{H}_{\text{lig}} | \theta_2({}^4T_{2g} | {}^4D, \frac{3}{2}) \rangle \\
 &= \langle \theta_3({}^4T_{2g} | {}^4D, \frac{3}{2}) | \mathcal{H}_{\text{lig}} | \theta_3({}^4T_{2g} | {}^4D, \frac{3}{2}) \rangle
 \end{aligned}$$

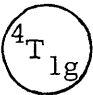

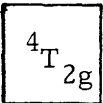
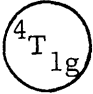
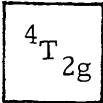
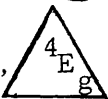
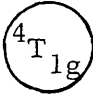
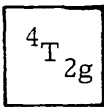
By proceeding in this way, it can be shown that an octahedral crystal field shifts, for example, each of the progeny terms of the nd^5 ion by $-5\varepsilon_0$. Table (2.5) shows this shift of the progeny terms those arise from the sextet and quartet free ion terms.

2.2.a.3 TERM INTERACTIONS IN THE nd^5 SYSTEMS PERTURBED BY AN OCTAHEDRAL CRYSTAL FIELD

The procedures already described are valid for estimating the energies of the progeny terms in a weak octahedral crystal field, if it is assumed that there are no interactions between the same progeny terms which arise from different free ion terms, i.e. interactions between those terms enclosed in a circle, square or triangle in Table (2.5).

Off-diagonal matrix elements of the crystal field interaction connecting symmetry adapted $\theta_i({}^{2S+1}\Gamma_i | {}^{2S+1}L, M_S)$ functions with the

Table (2.5)

Free Ion	Progeny Terms	Energy in weak O _h field
⁶ S	⁶ A _{1g}	10A-35B-5ε ₀
⁴ P		10A-28B+7C-5ε ₀
⁴ D	 , 	10A-18B+5C-5ε ₀
⁴ F	⁴ A _{2g} ,  , 	10A-13B+7C-5ε ₀
⁴ G	⁴ A _{1g} ,  ,  , 	10A-25B+5C-5ε ₀

same spin and with the same symmetry properties are different from zero. Those progeny terms, which are involved in term interactions, therefore, can no longer be assigned to only one free ion term belonging to a particular L value: they belong to all the isolated terms which give rise to such progenies. Thus, the ${}^4T_{2g}$ progenies in an octahedral field are linear combinations of the original 4D , 4F and 4G free ion terms. Orgel²² and Jorgensen²³ have shown that crystal field mixing of these free ion terms leads to the block shown in (2.28) in the perturbation secular determinant in this case

$$\begin{array}{c}
 {}^4G \\
 {}^4F \\
 {}^4D
 \end{array}
 \begin{vmatrix}
 & {}^4G & & {}^4F & & {}^4D \\
 {}^4G-E & & 10(\sqrt{3/7})Dq & & 0 \\
 10(\sqrt{3/7})Dq & & {}^4F-E & & (20/\sqrt{7})Dq \\
 0 & & (20/\sqrt{7})Dq & & {}^4D-E
 \end{vmatrix} = 0 \quad (2.28)$$

where E leads to three roots, the ${}^4T_{2g}$ energies in the octahedral crystal field, and thence to three eigenfunctions for this system.

Similarly, ${}^4T_{1g}$ progenies are derived from linear combinations of the free ion terms 4P , 4F , and 4G . These lead to the off-diagonal matrix elements listed in (2.29), from Table (2.3).

$$\begin{aligned}
\langle \theta_1 (^4P) | \mathcal{H}_{\text{lig}} | \theta_4 (^4G) \rangle &= 4 \sqrt{5} Dq \\
\langle \theta_2 (^4F) | \mathcal{H}_{\text{lig}} | \theta_4 (^4G) \rangle &= -2 \sqrt{5} Dq \\
\langle \theta_2 (^4P) | \mathcal{H}_{\text{lig}} | \theta_5 (^4G) \rangle &= -4 \sqrt{5} Dq \\
\langle \theta_3 (^4F) | \mathcal{H}_{\text{lig}} | \theta_5 (^4G) \rangle &= -2 \sqrt{5} Dq \\
\langle \theta_3 (^4P) | \mathcal{H}_{\text{lig}} | \theta_6 (^4G) \rangle &= -4 \sqrt{5} Dq \\
\langle \theta_4 (^4F) | \mathcal{H}_{\text{lig}} | \theta_6 (^4G) \rangle &= 2 \sqrt{5} Dq
\end{aligned} \tag{2.29}$$

Although in principle the 4E_g progenies are linear combinations of the 4D and 4G free ion terms, in fact^{22,23} it turns out that off-diagonal matrix elements of the octahedral crystal field Hamiltonian are zero in this particular case.

Jorgensen²³ has expressed the matrix elements in (2.28) and (2.29) in terms of the free ion parameters A, B and C, or F_0 , F_2 and F_4 . However, Slater theoretical free ion energies do not agree very well with the experimental distribution of the multiplet energies for 4G , 4F , 4D , and 4P terms of the free ion of most of gaseous nd^5 free ions. For this reason, the experimental energies, known from atomic spectroscopy, of the free ions are usually used in these "Orgel determinants" for ions in weak fields.

Two schematic diagrams for the energy levels available to an nd^5 ion in a weak crystal field are shown in Figures (2.3) and (2.4). Figure (2.3) shows the effect of a fixed octahedral field on the term energies, both with and without term interactions being taken into account. Figure (2.4) shows, the energy level diagram as a function

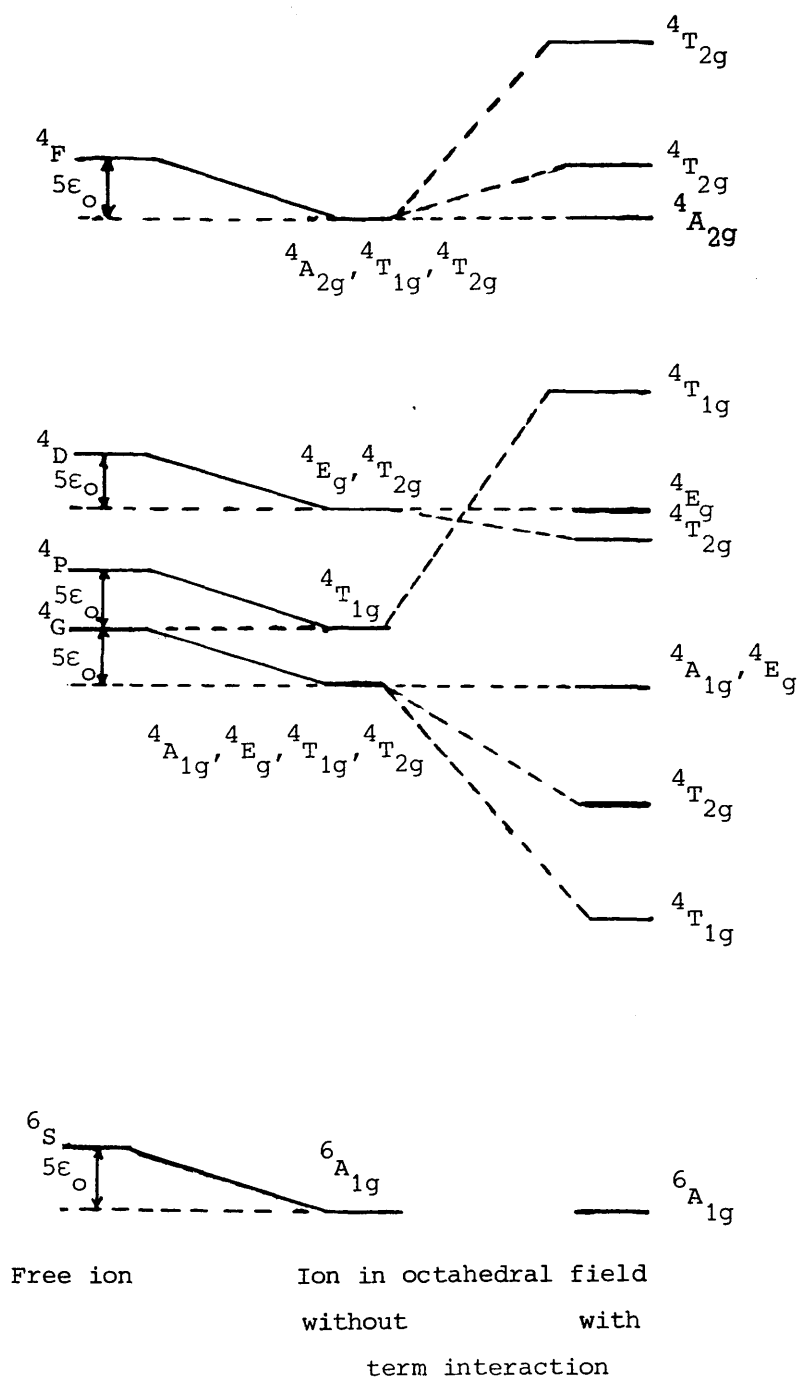


Figure (2.3). Term system of nd^5 configuration in an octahedral field

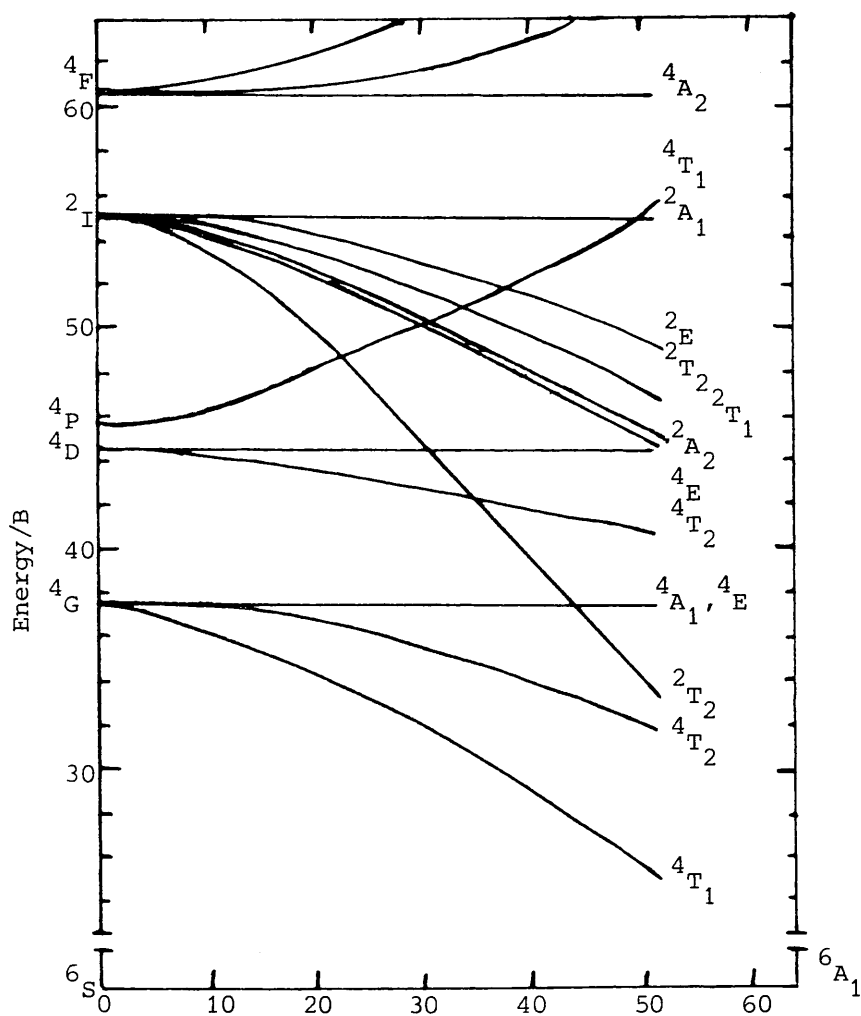


Figure (2.4). An octahedral ligand field splitting diagram for an nd^5 system expressed in terms of DQ/B , $DQ=6\sqrt{30} Dq$, $B=660 \text{ cm}^{-1}$, $C/B=5.5$. The 2I state is included, as are the quartet states

of varying ratio of (DQ/B) where $DQ = 6\sqrt{30} Dq$, for $(C/B) = 5.5$ and $B = 660 \text{ cm}^{-1}$, i.e. a diagram appropriate for Mn^{2+} .

2.2.b THE STRONG OCTAHEDRAL CRYSTAL-FIELD CASE

In "strong-field" complexes, the d electron-electron interaction energy is small compared to the electrostatic interactions between the transition metal-ion d-electrons and the ligands in the complex, i.e.

$$\sum_{i=1}^N V_{x\ell}(\vec{r}) > \sum_{i=1}^N \sum_{j=1, j \neq i}^N \frac{e^2}{r_{ij}}.$$

In such complexes, therefore, the crystal field interaction is considered to perturb the spherically symmetrized one-electron eigenfunctions $|+2\rangle$, $|+1\rangle$, $|0\rangle$, $|-1\rangle$, $|-2\rangle$ and corresponding eigenvalues of the isolated transition-metal ion. These perturbed solutions are then themselves finally perturbed by the d electron-electron interactions.

Calculations show that an octahedral crystal field in this way separates the d-orbitals into two sets, t_{2g} and e_g , which have energies $-5\epsilon_0 - 4Dq$ (or $-5\epsilon_0 - \frac{2}{5} \Delta$) and $-5\epsilon_0 + 6Dq$ (or $-5\epsilon_0 + \frac{3}{5} \Delta$), respectively, so the t_{2g} and e_g sets are separated by $10Dq$ or Δ . The eigenfunctions corresponding to these two sets are as follows.^{2,3,4,23}

t_{2g} eigenfunctions

$$\xi = \frac{1}{i\sqrt{2}} (|+1\rangle + |-1\rangle) = \sqrt{3} (yz)$$

$$\eta = \frac{1}{\sqrt{2}} (|+1\rangle - |-1\rangle) = \sqrt{3} (xz)$$

$$\zeta = \frac{1}{i\sqrt{2}} (|+2\rangle - |-2\rangle) = \sqrt{3} (xy)$$

e_g eigenfunction

$$\begin{aligned}\mu &= |0\rangle = \frac{1}{\sqrt{2}}(3z^2 - r^2) \\ \nu &= \frac{1}{\sqrt{2}}(|+2\rangle + |-2\rangle) = \sqrt{\frac{3}{2}}(x^2 - y^2)\end{aligned}\quad (2.30)$$

If a strong field complex contains m electrons in the t_2 set of orbital and n electrons in the e set then it is said to have the strong-field configuration, $t_2^m e^n$. As explained earlier each configuration gives rise to a number of terms, which can be denoted by the strong field term symbol $^{2S+1}\Gamma_i$ in this case, which are eigenfunctions of the free ion spherically symmetrized interactions and of the crystal field interactions, but not necessarily of the Hamiltonian which includes these plus the d electron-electron interactions. The possible strong field terms that originate from a given configuration can be obtained from group theoretical arguments⁴ by taking direct products of the symmetry species of e^n and the symmetry species of t_2^m . It can be shown, that the allowed terms for an nd^5 ion in a strong field originating from the configuration $t_2^m e^n$ are as listed in Table (2.6).³ It should be noted that the general form of any term function in the strong field approximation has the form⁴

$$|t_2^m (S'\Gamma') e^n (S''\Gamma'') S\Gamma, M_S\rangle$$

where the irreducible representation Γ' and Γ'' of the t_2^m and e^n electrons respectively are coupled to give an irreducible representation Γ for the term and the spin quantum numbers S' and S'' of the t_2^m and

Table (2.6)³

Strong-field configuration	Allowed terms	Total sum of degeneracy numbers
t_2^5	2T_2	6
$t_2^4 e$	${}^2A_1 + {}^2A_2 + 2{}^2E + 2{}^2T_1 + {}^4T_1 + 2{}^2T_2 + {}^4T_2$	60
$t_2^3 e^2$	$2{}^2A_1 + {}^4A_1 + {}^6A_1 + {}^2A_2 + {}^4A_2 + 3{}^2E + 2{}^4E$ $+ 4{}^2T_1 + {}^4T_1 + 4{}^2T_2 + {}^4T_2$	120
$t_2^2 e^3$	${}^2A_1 + {}^2A_2 + 2{}^2E + 2{}^2T_1 + {}^4T_1 + 2{}^2T_2 + {}^4T_2$	60
$t_2 e^4$	2T_2	6

e^n electrons couple together to give spin quantum number S . d electron-electron interactions then perturb these terms and formally mix all of them together.

2.2.b.1 ELECTRONIC EIGENFUNCTIONS FOR AN nd^5 ION IN A STRONG CRYSTAL FIELD

Inspection of Table (2.6) shows that the 6A_1 term arises only from configuration $t_2^3 e^2$, it therefore follows that electron-electron interactions can not mix this term with any of the other (251) terms allowed for nd^5 configuration. It therefore follows that the wave function corresponding to the ${}^6A_{1g}$ term of the nd^5 ion in an octahedral crystal field is given by^{20,25,26}

$$\begin{aligned} {}^6A_{1g} &: |t_{2g}^3 ({}^4A_{2g}) e_g^2 ({}^3A_{2g}) {}^6A_{1g}, \frac{5}{2} \rangle \\ &\equiv |{}^6A_{1g} (t_{2g}^3 e_g^2), \frac{5}{2} \rangle = [\xi^+ \eta^+ \zeta^+ \mu^+ \nu] \end{aligned} \quad (2.31)$$

where bracket $[]$ stands for a Slater determinant, ξ, η, ζ, μ and ν are defined in equations (2.30) and the positive and negative signs refer to the electronic spin quantum numbers $m_s = +\frac{1}{2}$ and $-\frac{1}{2}$, respectively.

Only the $t_{2g}^3 e_g^2$ configuration gives rise to a ${}^4A_{2g}$ term and its corresponding wave function is

$$\begin{aligned} {}^4A_{2g} &: |t_{2g}^3 ({}^4A_{2g}) e_g^2 ({}^3A_{1g}) {}^4A_{2g}, \frac{3}{2} \rangle \equiv |{}^4A_{2g} (t_{2g}^3 e_g^2), \frac{3}{2} \rangle \\ &= \frac{1}{\sqrt{2}} \{ [\xi^+ \eta^+ \zeta^+ \mu^+] + [\xi^+ \eta^+ \zeta^- \nu] \} \end{aligned} \quad (2.32)$$

The $t_{2g}^3 e_g^2$ configuration, also, gives rise to ${}^4A_{1g}$ and furthermore to 4E_g terms. Their corresponding wave functions are

$$\begin{aligned}
 {}^4A_{1g} : & \quad | t_{2g}^3 ({}^4A_{2g}) e_g^2 ({}^3A_{2g}), {}^4A_{1g}, \frac{3}{2} \rangle \equiv | {}^4A_{1g} (t_{2g}^3 e_g^2), \frac{3}{2} \rangle \\
 & = \frac{1}{\sqrt{30}} \{ 3([\xi^+ \eta^+ \zeta^+ \mu^- \nu] + [\xi^+ \eta^+ \zeta^- \mu^+ \nu]) \\
 & \quad - 2([\xi^- \eta^+ \zeta^+ \mu^+ \nu] + [\xi^+ \eta^- \zeta^+ \mu^+ \nu] + [\xi^+ \eta^+ \zeta^- \mu^+ \nu]) \} \quad (2.33)
 \end{aligned}$$

$$\begin{aligned}
 {}^4E_g : & \quad | t_{2g}^3 ({}^2E_g) e_g^2 ({}^3A_{2g}), {}^4E_g^{(a)}, \frac{3}{2} \rangle \equiv | {}^4E_g^{(a)} (t_{2g}^3 e_g^2), \frac{3}{2} \rangle \\
 & = \frac{\alpha'}{\sqrt{6}} \{ 2[\xi^+ \eta^+ \zeta^- \mu^+ \nu] - [\xi^- \eta^+ \zeta^+ \mu^+ \nu] - [\xi^+ \eta^- \zeta^+ \mu^+ \nu] \} \\
 & \quad + \frac{\beta}{\sqrt{2}} \{ [\xi^+ \eta^+ \zeta^+ \mu^- \nu] - [\xi^+ \eta^+ \zeta^- \mu^+ \nu] \} \quad (2.34a)
 \end{aligned}$$

and

$$\begin{aligned}
 & \quad | t_{2g}^3 ({}^4A_{2g}) e_g^2 ({}^1E_g), {}^4E_g^{(b)}, \frac{3}{2} \rangle \equiv | {}^4E_g^{(b)} (t_{2g}^3 e_g^2), \frac{3}{2} \rangle \\
 & = \frac{\alpha'}{\sqrt{2}} \{ [\xi^- \eta^+ \zeta^+ \mu^+ \nu] - [\xi^+ \eta^- \zeta^+ \mu^+ \nu] \} \\
 & \quad + \frac{\beta}{\sqrt{2}} \{ [\xi^+ \eta^+ \zeta^+ \mu^-] - [\xi^+ \eta^+ \zeta^- \nu] \} \quad (2.34b)
 \end{aligned}$$

It can be shown that one of these 4E_g terms whose energy, relative to the free ion ground state, is $10B+5C$ correlates with the free ion level 4G of Table (1.4). For this level $\alpha' = \sqrt{\frac{4}{7}}$ and $\beta = \sqrt{\frac{3}{7}}$. The other 4E_g term whose relative energy is $17B+5C$, correlates with the free ion level 4D and in this case $\alpha' = \sqrt{\frac{3}{7}}$ and $\beta = -\sqrt{\frac{4}{7}}$.

The other terms listed in Table (2.6) correlate with more than one strong-field configuration. d electron-electron perturbation interactions mix these terms together, i.e. d electron-electron repulsions cause terms of the same ${}^2S+1\Gamma_1$ belonging to different configurations to mix together leading to the so-called configuration-interactions which will be considered shortly.

2.2.b.2 THE ENERGY LEVELS OF AN nd^5 ION IN A STRONG CRYSTAL FIELD

In the weak-field scheme, section 2.2.a, ${}^4A_{1g}$ and one of the 4E_g terms are progenies of 4G free ion term, the ${}^4A_{2g}$ term is a progeny of the free ion 4F and the second 4E_g term is a progeny of 4D . It turns out that the energies of these terms in a weak crystal field, are the same as those of the free ion terms from which they arise minus $5\epsilon_0$, as shown in Figures (2.3) and (2.4). Thus

$$\left. \begin{aligned} E({}^4A_{1g}) &= E({}^4E_g^{(a)}) = E({}^4G) - 5\epsilon_0 = 10A - 25B + 5C - 5\epsilon_0 \\ E({}^4A_{2g}) &= E({}^4F) - 5\epsilon_0 = 10A - 13B + 7C - 5\epsilon_0 \\ E({}^4E_g^{(b)}) &= E({}^4D) - 5\epsilon_0 = 10A - 18B + 5C - 5\epsilon_0 \end{aligned} \right\} \quad (2.35)$$

However, in the strong-field case, the states ${}^4A_{1g}$, ${}^4E_g^{(a)}$, and ${}^4E_g^{(b)}$ have the same energy, $10B + 5C$ measured from the ground state ${}^6A_{1g}$.²⁵

There are three ${}^4T_{2g}$ terms belonging to the nd^5 configuration. As shown in Table (2.6), these are derived from $t_{2g}^4({}^3T_{1g}) \times e_g({}^2E_g)$, $t_{2g}^3({}^2T_{1g}) \times e_g({}^3A_{2g})$, and $t_{2g}^2({}^3T_{1g}) \times e_g({}^3E_g)$. These basis wave functions are given by the expressions ψ_1 , ψ_2 , and ψ_3 listed in (2.36)

$$\begin{aligned}
 \psi_1 &= | t_{2g}^4({}^3T_{1g}) e_g({}^2E_g) {}^4T_{2g}, \frac{3}{2} \rangle = | \overset{+}{\xi} \overset{+}{\eta} \overset{\pm}{\zeta} \overset{+}{\nu} \rangle \\
 \psi_2 &= | t_{2g}^3({}^2T_{1g}) e_g({}^3A_{2g}) {}^4T_{2g}, \frac{3}{2} \rangle \\
 &= \frac{1}{\sqrt{2}} | \overset{+}{\xi} \overset{+}{\zeta} \overset{+}{\mu} \overset{+}{\nu} \rangle - \frac{1}{\sqrt{2}} | \overset{\pm}{\eta} \overset{+}{\zeta} \overset{+}{\mu} \overset{+}{\nu} \rangle \\
 \psi_3 &= | t_{2g}^2({}^3T_{1g}) e_g({}^3E_g) {}^4T_{2g}, \frac{3}{2} \rangle = | \overset{+}{\eta} \overset{+}{\xi} \overset{\pm}{\mu} \overset{+}{\nu} \rangle
 \end{aligned} \tag{2.36}$$

with relative crystal field energies of $-10 Dq$, 0 , and $+10 Dq$, respectively. d electron-electron repulsion interactions mix these together and it can be shown that the corresponding matrix elements are, for example, $V_{12} = B\sqrt{6}$ and $V_{13} = -(4B+C)$.⁴ Solutions to the appropriate 3×3 perturbation equation, then, give the wave functions and energy levels of these ${}^4T_{2g}$ terms of the nd^5 system, including both crystal field interactions and configuration interactions.

The energies of ${}^4T_{1g}$, ${}^2T_{2g}$, ${}^2A_{1g}$... etc. terms in Table (2.6), can be handled in a similar manner. The resulting sets of interaction matrices for the nd^5 ion in a strong octahedral field can be obtained from, for example, reference 4, page 414; reference 27, page 767; and reference 28, page 67.

The energies of pure configurations for an nd^5 ion in an octahedral complex are listed in Table (2.7). These are the energies that would be obtained if electron configuration interactions could be neglected. The energies are given by $[a(10Dq)+bB+cC]$ and the atomic ground state, 6S , energy is chosen as zero energy.^{18,23}

It should be carefully noted that in strong crystal fields there must be contribution from covalent bonding, i.e. in such complexes d-electron orbitals must be somewhat distorted from those of free ion, by covalent bonding between the central metal ion and the ligands.^{25,26} To a first approximation only σ bonding needs to be considered in most cases. Only the e_g orbital set is then affected. One can then substitute μ and ν with $\mu \cdot \cos\theta$ and $\nu \cdot \cos\theta$, respectively, where the covalency parameter is $(1-\cos^2\theta)$. When covalent effects are taken into account, then the degeneracy of the energy levels may be partly removed and the matrix elements of the electrostatic interactions now must be written with modified B and C, i.e. B_n and C_n where $B_n = B \cos^n\theta$ and $C_n = C \cos^n\theta$, respectively. For example^{25,26}

$^4E_g(^4D, ^4G)$:

$$\begin{array}{l} t_{2g}^3(^2E_g)e_g^2(^3A_{2g}) \\ t_{2g}^3(^4A_{2g})e_g^2(^1E_g) \end{array} \left| \begin{array}{cc} t_{2g}^3(^2E_g)e_g^2(^3A_{2g}) & t_{2g}^3(^4A_{2g})e_g^2(^1E_g) \\ 9B_0+3C_0+4B_2+2C_2 & -2\sqrt{3}B_2 \\ -2\sqrt{3}B_2 & 6B_2+3C_2+8B_4+2C_4 \end{array} \right|$$

also

Table (2.7)^{18,23}

Configuration	Term	a	b	c
t_{2g}^5	${}^2T_{2g}$	-2.0	15	10
$t_{2g}^4 e_g$	${}^4T_{1g}$	-1.0	10	6
	${}^4T_{2g}$	-1.0	18	6
	${}^2A_{2g}$	-1.0	12	9
$t_{2g}^3 e_g^2$	${}^6A_{1g}$	0.0	0.0	0.0
	${}^4A_{1g}$	0.0	10	5
	${}^4E_g(a)$	0.0	10	5
	${}^4T_{2g}$	0.0	13	5
	${}^4E_g(b)$	0.0	17	5
	${}^4T_{1g}$	0.0	19	7
	${}^4A_{2g}$	0.0	22	7
$t_{2g}^2 e_g^3$	${}^4T_{1g}$	1.0	10	6
	${}^4T_{2g}$	1.0	18	6

${}^4A_{1g}({}^4G):$

$$t_{2g}^3({}^4A_{2g})e_g^2({}^3A_{2g}) = 10B_2 + 5C_2$$

where $B_2=B_0\cos^2\theta$, $B_4=B_0\cos^4\theta$, $C_2=C_0\cos^2\theta$, and $C_4=C_0\cos^4\theta$.

A detailed correlation diagram showing how the free ion terms of an nd^5 ion split in crystal fields of varying strength is shown in Figure (2.5) and the relative energies of the terms for a whole range of ratios of (Dq/B) is shown in Figure (2.6). It should be noticed from these diagrams, that the energy of the ${}^2T_{2g}$ progeny of the free ion term 2I is extremely sensitive to this ratio and that the plot of this progeny's energy vs. (Dq/B) has a large negative slope. For very strong crystal fields, in fact, the ${}^2T_{2g}$ term is the ground term of the nd^5 ion in an octahedral environment. The energy of this ${}^2T_{2g}$ term can be shown to be $(10A-20B+10C)$ or $(10F_0-20F_2-40F_4)$. The "promotional energy", is defined as the difference in energy of the ground state of the free ion compared with the ground state of the ion subjected to the crystal field. For an nd^5 ion in a strong octahedral field this promotional energy is $(15B+10C)$ or $(15F_2+275F_4)$. This is not the same as the stabilization energy. Stabilization energy for an nd^5 ion in a strong octahedral crystal field is $-20 Dq$ (or 2Δ).^{3,29,30}

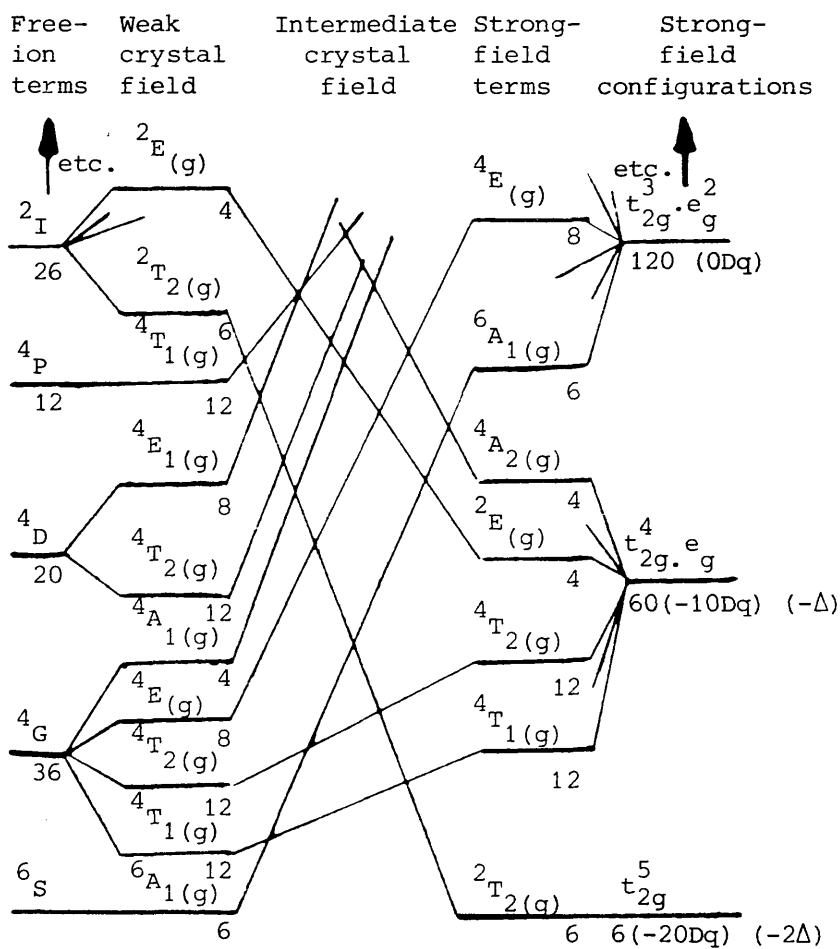


Figure (2.5). Correlation diagram for,
 free-ion terms \rightarrow strong octahedral field
 configuration, for an nd^5 ion

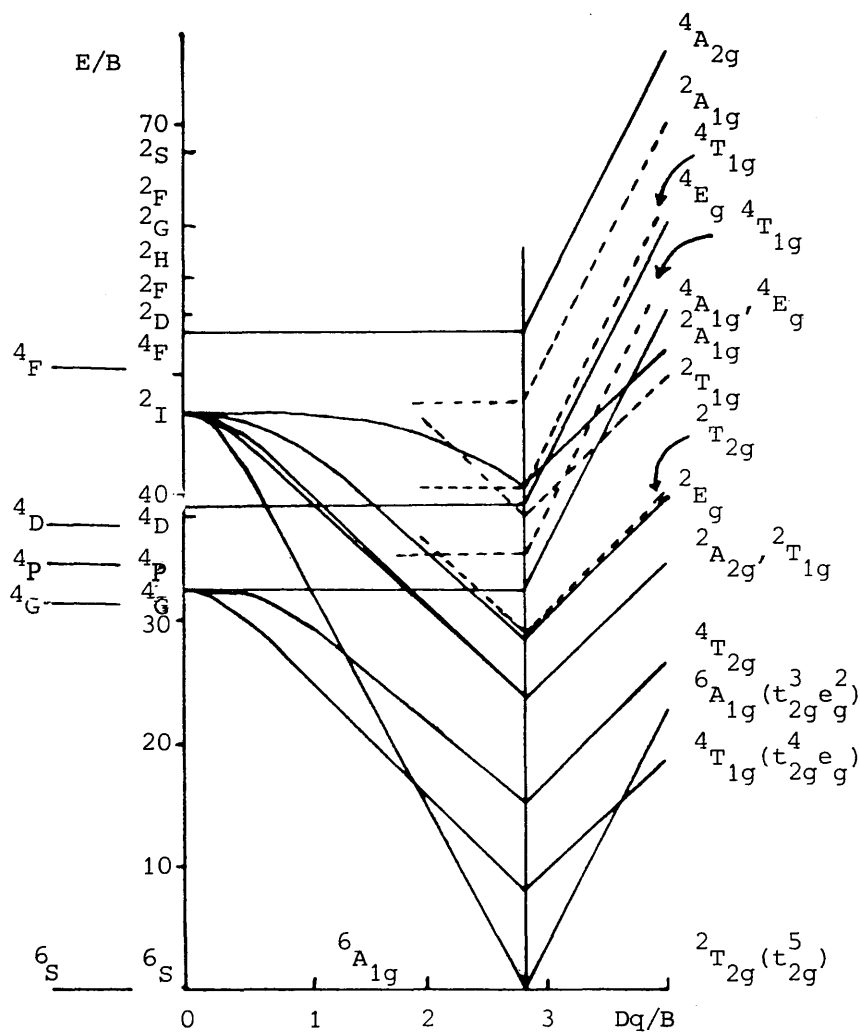


Figure (2.6). Splitting of states of the nd^5 configuration by an octahedral field (Tanabe-Sugano diagram).
 $B = 860 \text{ cm}^{-1}$, $C/B = 4.48$

2.2.c THE "SPIN CROSS-OVER" POINT FOR AN nd^5 ION IN AN OCTAHEDRAL CRYSTAL FIELD

For small values of Δ , ($10 Dq$), the ground term of the nd^5 ion in an octahedral complex is ${}^6A_{1g}$. However, as Δ increases the ${}^2T_{2g}$ progeny of the 2I free ion term is progressively stabilized relative to the ${}^6A_{1g}$ term, and in due course as Δ continues to increase the energy of the ${}^2T_{2g}$ term falls below that of ${}^6A_{1g}$. The value of Δ at which the spin of the ground term changes, is called the "Spin cross-over point".

At the "spin cross-over point", the energies of the high-spin and low-spin terms are the same, therefore, from sections 2.2.a and 2.2.b

$$E({}^6A_{1g}) = E({}^2T_{2g})$$

$$\therefore 10A - 35B = 10A - 20B + 10C - 2\Delta \quad (2.37)$$

Hence, at the "spin cross-over point", the crystal field parameter, Δ , and the free ion parameters B and C are related by

$$\Delta = \frac{15}{2} B + 5C \quad (2.38)$$

The relative fall of the ${}^2T_{2g}$ term relative to the ${}^6A_{1g}$ term is shown in the left-hand side of Figure (2.5).

The ${}^6A_{1g}$ term belongs to the configuration $t_{2g}^3 e_g^2$

$$| t_{2g}^3 ({}^4A_{2g}) e_g^2 ({}^3A_{2g}), {}^6A_{1g}, M_S \rangle$$

whereas the ${}^2T_{2g}$ term belongs to the t_{2g}^5 configuration $| t_{2g}^5, {}^2T_{2g}, M_S \rangle$.

The change in the ground state at the "spin cross-over point", therefore involves taking two electrons out of the e_g orbitals, placing them into

t_{2g} orbitals, and inverting their spin orientations. The change in

electrostatic energy in this process, $15B+10C$, may usefully be regarded as a pairing energy and one-half of this, then, becomes the mean pairing energy, Π , when one of these electrons is transferred from e_g to t_{2g}

orbitals, therefore $\Pi = \frac{15}{2}B+5C$, for an nd^5 ion, i.e. $\Pi = \Delta$ at the "spin cross-over point": when $\Delta < \Pi$, the complex is in the high-spin state

${}^6A_{1g}(t_{2g}^3 e_g^2)$: when $\Delta > \Pi$, the complex is in the low-spin state,

${}^2T_{2g}(t_{2g}^5)$ with one unpaired electron. Π is a threshold value above which

Δ must lie in order to lower the spin state.

It is important to note that a quartet spin state can never be the lowest state of an nd^5 complex. The lowest quartet turns out to be

${}^4T_{1g}$ term of the $t_{2g}^4 e_g$ configuration, and its energy is $E({}^4T_{1g}) \equiv 10A -$

$25B+6C-\Delta$. The mean energy of the ${}^2T_{2g}$ and ${}^6A_{1g}$ terms, listed in

(2.37), is

$$\begin{aligned} \frac{1}{2} [E({}^2T_{2g}) + E({}^6A_{1g})] &= 10A - \frac{55}{2}B + 5C - \Delta \\ &= E({}^4T_{1g}) - \frac{5}{2}B - C \end{aligned}$$

Thus the ${}^4T_{1g}$ term can never be the ground term because one, at least, of the ${}^6A_{1g}$ and ${}^2T_{2g}$ terms must lie $\frac{5}{2}B+C$ or more below this lowest quartet.⁴

The correlation diagram for the nd^5 ion on going from the free ion through the weak, intermediate, and the strong octahedral field cases, is shown in Figure (2.5). It should be noted that the ion gains an amount of energy of 2Δ (or $20 Dq$) on going from the high-spin (low field) to the low-spin (high field) configuration.

2.3 THE TANABE-SUGANO DIAGRAM FOR AN nd^5 ION IN AN OCTAHEDRAL CRYSTAL FIELD

The energies of the terms of the nd^5 ion as its environment varies from the free-ion, section 1.2.c; to the weak-crystal field, section 2.2.a.2; to the "cross-over point", section 2.2.c; and then to the strong crystal field, section 2.2.b.2, can be summarized in the so-called "Tanabe-Sugano diagram" shown in Figure (2.6).^{1,4,27} In this diagram the term energies are plotted on the vertical coordinate, in units of the interelectronic repulsion parameter, B , and the crystal field strength is plotted along the horizontal coordinate in units of (Dq/B) . It should be noted that the usefulness of this diagram is restricted since it requires two parameters B and C to describe the electronic repulsion. Figure (2.6) is drawn for a specific ratio of (C/B) of 4.48, however the diagram is not very sensitive to this ratio.

In the Tanabe-Sugano diagram the zero energy is always taken to be the energy of the lowest term, and since the ground term of the

nd⁵ configuration changes, the diagram shows a discontinuity at the "cross-over point", which takes the form of an increase in the slope of term energies above the cross-over value of (Dq/B) . The ${}^2T_{2g}$ progeny of the free ion term 2I has a very large negative slope before $(Dq/B) = 2.99$, i.e. $(\Delta/B) = 29.9$. It therefore follows that the ${}^6A_{1g}$ progeny of the free ion term 6S has a very large positive slope after $(Dq/B) = 2.99$.

The Tanabe-Sugano diagram emphasizes the change in the ground state from the high-spin ${}^6A_{1g}$ term of the Hund's rule $t_{2g}^3 e_g^2$ configuration to the low-spin ground state ${}^2T_{2g}$ term of the t_{2g}^5 configuration in a strong octahedral crystal field. This cross-over plays a crucial role in understanding the chemical stability, the thermodynamics, the spectroscopy, and the magnetic properties of the nd⁵ ions. At the "cross-over point" the high-spin and low-spin configurations are in equilibrium, and small changes of Δ , or $10Dq$, can have a marked effect on this equilibrium, shifting it in one direction or another. Small changes in temperature, in pressure, in solvent interactions, or in ligand interactions, or in all of these, can have quite dramatic effects and can switch the configuration from a high to low spin configuration and vice versa. Furthermore, small changes in the environment of the ion in the region of the "cross-over point" markedly effect the spatial distribution of the five nd-electrons, and therefore markedly effect the spatial properties of the optical, magnetic, catalytic, and chemical properties of the nd⁵ complexes in this region.

2.4 THE JAHN-TELLER EFFECT AND THE nd^5 IONS

The Tanabe-Sugano diagram can be used to predict whether or not the nd^5 ion undergoes Jahn-Teller distortion.³¹ Van Vleck³² showed that ions in orbitally degenerate T_{1g} and T_{2g} ground states are unstable in the symmetrical configuration, and that in octahedral crystal fields, such ions should gain about 100 cm^{-1} of energy by distorting the octahedron and thereby removing the electronic orbital degeneracy. Ions in non-degenerate orbital states are, of course, stable in the symmetrical configuration, the high-spin weak field ground state, $^6A_{1g}$, therefore does not undergo Jahn-Teller distortion, but the ground state of the strong field complex, $^2T_{2g}$, must exhibit a Jahn-Teller effect. More detailed considerations of the energetics and distortions involved show that the high-spin nd^5 complexes are relatively stable compared to the low-spin nd^5 complexes towards oxidation-reduction reactions.

2.5 COMPLEXES OF THE $4d^5$ ION, Ru^{3+}

For the free $4d^5$ ion Ru^{3+} , the Racah parameters, B and C, are 929.21 cm^{-1} and 3744.9 cm^{-1} , Table (1.5), i.e. $(C/B) = 4.03$. If these values are appropriate to a Ru^{3+} complex then the crystal field parameter Δ at the high-spin \rightarrow low-spin, "cross-over point" is predicted to be $25,700\text{ cm}^{-1}$. However, with such a large positive charge on the central metal ion, covalent effects ought to be allowed for, and the values of B and C would then be rather smaller than those of the free ion and values of B_n and C_n appropriate the complex should be

really used in the relationship $\Delta = \frac{15}{2} B_n + 5C_n$. If B_n and C_n are lowered to 743 cm^{-1} and 2995 cm^{-1} respectively, i.e. about 80% of the free ion values, then the Δ value at the "cross-over point" would be predicted to be $20,500 \text{ cm}^{-1}$.

The only high-spin, weak-field complex containing the Ru^{3+} ion reported in the literature appears to be the molecular complex ammonium pentachloronitrosyl ruthenium(III), $\text{NH}_4 [\text{Ru}(\text{NO})\text{Cl}_5]$.³³

All other Ru^{3+} "octahedral complexes" appear to be low-spin forms.³⁴ The optical and magnetic³⁵ properties of the red species $[\text{RuCl}_6]^{3-}$ and $[\text{RuBr}_6]^{3-}$ show that these are low-spin t_{2g}^5 complexes, so their ground states are ${}^2T_{2g}(t_{2g}^5)$, and the lowest excited doublet levels are ${}^2A_{2g}(t_{2g}^4 e_g)$, and ${}^2T_{1g}(t_{2g}^4 e_g)$, respectively. The first absorption band of $[\text{RuCl}_6]^{3-}$, found at $19,200 \text{ cm}^{-1}$, can therefore be assigned to the transition ${}^2T_{2g} \rightarrow {}^2T_{1g}, {}^2A_{2g}$. Assuming the high field limit to be valid, i.e. assuming pure t_{2g}, e_g quantizations, this energy difference should amount to $10Dq - 3F_2 - 20F_4$, or $10Dq - B - C$: cf. section 2.2.b.2. If $F_2 = 10F_4$ is taken to be 1000 cm^{-1} (or $7B = C$ is taken to be 1000 cm^{-1}) then these optical transitions predict a value of Dq of 2400 cm^{-1} , i.e. $\Delta = 24,000 \text{ cm}^{-1}$. The corresponding experimental value for $[\text{RuBr}_6]^{3-}$ turns out to be $15,300 \text{ cm}^{-1}$.

The optical transition energies for several other low-spin Ru^{3+} complexes are listed in Table (2.8).

It should be noted that the Tanabe-Sugano diagram, shown in Figure (2.6), predicts the first spin-allowed doublet band to be at $18,000 \text{ cm}^{-1}$ and the spin-forbidden quartet band ${}^2T_{2g}(t_{2g}^5) \rightarrow {}^4T_{1g}(t_{2g}^4 e_g)$

Table (2.8)

Complex	${}^2T_{2g} \rightarrow {}^2A_{2g}, {}^2T_{1g}$ transition	Reference
$[RuCl_6]^{3-}$	19,200	35
$[RuBr_6]^{3-}$	15,300	35
* $Ru(acac)_3$	19,600	36
* $Ru(bacac)_3$	19,100	36
* $Ru(dbm)_3$	18,500	36
$RuCl_2AsPh_2$	20,000	37

* $acac \equiv$ acetylacetone; $bacac \equiv$ benzoylacetone; $dbm \equiv$ dibenzoyl-methane.

to be at $11,800 \text{ cm}^{-1}$ for the parameters listed above for $[\text{RuCl}_6]^{3-}$.

2.6 SPIN-ORBIT COUPLING IN TRANSITION METAL-ION COMPLEXES

In complexes of the first series of transition elements, spin-orbit coupling interactions, in general, are so small in comparison with crystal field effects that, as already mentioned on page 47, and equations (2.15) and (2.16), it may be neglected to a first approximation.

However, spin-orbit coupling in complexes of the second and third transition-metal series are much larger than in the first series and therefore, spin-orbit interactions then ought to be considered.

As in the case of the free ion, section 1.3; when spin-orbit coupling is much larger than the crystal field splitting then the total orbital angular momentum \underline{L} , couples with the total spin angular momentum \underline{S} , to produce states which can be labelled by the total orbital angular momentum quantum number, J .²⁸

In the transition-metal ion series this extreme situation is never encountered, but nevertheless to a first approximation the splitting by spin-orbit coupling of the energy levels in a cubic crystal field may be obtained by using Landé-type formulae similar to equations (1.47) and (1.48), with a fictitious L -value, L' , where $L' = 1$ for T_1 or T_2 states. A_1 , A_2 , and E states are not split by spin-orbit coupling. The contribution of spin-orbit coupling to the energies of T_1 or T_2 states is then given by

$$E_{J'} = a[J'(J' + 1) - L'(L' + 1) - S(S + 1)] \quad (2.39)$$

where

$$a = \frac{1}{2} \lambda \text{ and } J' = |L'+S|, |L'+S-1|, \dots, |L'-S|, \text{ and the constant}$$

"a" must be determined in each particular case.

2.6.a SPIN-ORBIT COUPLING IN COMPLEXES OF THE nd^5 IONS

The effects of spin-orbit coupling on the eigenvalues and eigenfunctions of, for example, the lowest ${}^4T_{1g}$ state, can be estimated in the following way.²¹ As outlined in sections 2.2.a.1, 2.2.a.3, and equations (2.29), basis wave functions for the states of this term, ${}^4T_{1g}$, including the effect of term-interactions can be constructed from data given in Table (2.3). Thus, for example, the basis wave function, not including spin-orbit interactions, for the ${}^4T_{1g}(1, \frac{3}{2})$ is given by

$${}^4T_{1g}(1, \frac{3}{2}) = N'' [\theta_4({}^4G) - \frac{4\sqrt{5}Dq}{E({}^4P) - E} \theta_1({}^4P) + \frac{2\sqrt{5}Dq}{E({}^4F) - E} \theta_2({}^4F)] \quad (2.40)$$

where E is the energy of the lowest root of the secular equations, and

$$N''^2(1 + \alpha_P'^2 + \alpha_F'^2) = 1, \text{ and } \alpha_P' = \frac{4\sqrt{5}Dq}{E({}^4P) - E}, \text{ and } \alpha_F' = \frac{2\sqrt{5}Dq}{E({}^4F) - E}.$$

Similar wave functions can be constructed for the ${}^4T_{1g}(0, \frac{3}{2})$ and ${}^4T_{1g}(-1, \frac{3}{2})$ basis functions, and these basis functions are then used in perturbation calculations to compute the matrix elements of the spin-orbit interaction using the operator $\sum_{i=1}^5 V_{SO}(i)$ of page 29. The ${}^4T_{1g}$ level is three-fold orbitally degenerate and four-fold spin degenerate, so that this secular determinant is of the order 12×12 . Diagonalization of this problem^{4,21} leads to the spin-orbit coupling energies which turn out to be, cf. equation (2.39)

$$E_{SO} = 3a(6\text{-fold}),$$

$$\text{or} \quad = -2a(4\text{-fold}),$$

$$\text{or} \quad = -5a(2\text{-fold}).$$

where

$$a = -\frac{\sqrt{5}}{2} N''^2 \alpha_F^1 \xi \quad (2.41)$$

and $\xi = \hbar^2 \int_0^\infty R_{n,\ell}^2 \zeta(r) r^2 dr$, compare with equation (1.45).

It should be noted that the spin-orbit splitting of the ${}^4T_{1g}$ term depends on both α_F^1 and ξ . Furthermore, since ξ in equation (2.41) is positive, it follows that "a" must be negative for an nd^5 ion on an octahedral site with positive Dq , and hence the six-fold levels, therefore, lie lowest in that case. If Dq is known then "a" can be calculated. The twelve-fold degeneracy of the lowest ${}^4T_{1g}$ level of Figures (2.3) and (2.4) is therefore resolved by spin-orbit coupling into a sextet, a quartet, and a doublet, as shown in Figure (2.7).

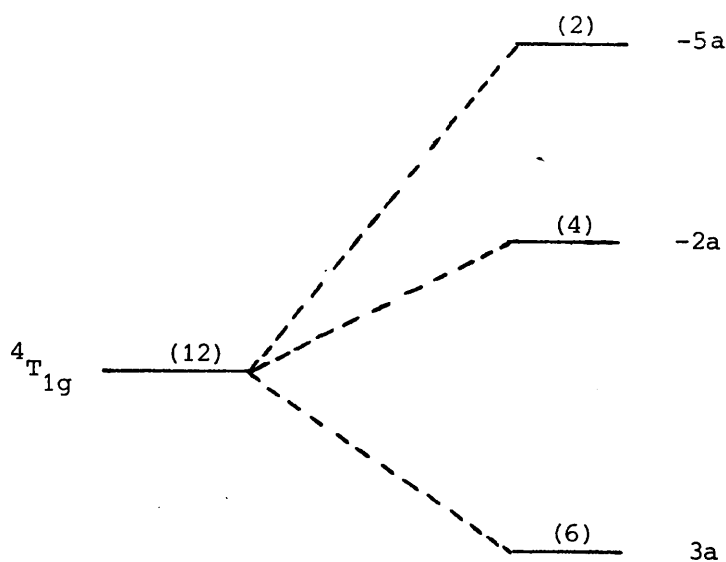


Figure (2.7)

By similar arguments it can be shown that spin-orbit interactions split the energies of both the $^{2S+1}T_1$ and $^{2S+1}T_2$ terms into three-levels with degeneracies $(2S-1)$, $(2S+1)$, and $(2S+3)$, respectively.

The $^6A_{1g}$ ground state of the high spin nd^5 configuration has no orbital angular momentum. In principle spin-orbit coupling can mix some of the excited states into this, and thence reinstate some orbital angular momentum, but theoretical calculations show that, the effect is very small.^{38,39,40} Van Vleck and Penny,³⁸ for example, have found that it is necessary to go to higher order perturbations in order to remove the spin six-fold degeneracy of the $^6A_{1g}$ term and this will be considered in more detail in chapter three. Detailed calculations of the energy levels of nd^5 configuration including the effect of spin-orbit perturbations, for ions in cubic crystal fields can be found in references 41 and 42.

2.7 CRYSTAL FIELDS OF LOWER SYMMETRY

Many transition-ion complexes are not octahedral. It has already been pointed out, even when six ligands are identical, several factors can destroy their most regular arrangement around the central metal-ion, and such complexes exhibit both optical and magnetic anisotropy. Deviation from octahedral symmetry can often be treated as a perturbation superimposed upon the higher symmetry, and the effects of some of the most common distortion of the octahedral field will now be considered. The correlation Table (2.9),¹⁹ lists the relationships between the irreducible representations of the different point group symmetries.

Table (2.9)¹⁹

O _h	O	T _d	D _{4h}	C _{4v}	C _{2v}	D ₃
A _{1g}	A ₁	A ₁	A _{1g}	A ₁	A ₁	A ₁
A _{2g}	A ₂	A ₂	B _{1g}	B ₁	A ₂	A ₂
E _g	E	E	A _{1g} +B _{1g}	A ₁ +B ₁	A ₁ +A ₂	E
T _{1g}	T ₁	T ₁	A _{2g} +E _g	A ₂ +E	A ₂ +B ₁ +B ₂	A ₂ +E
T _{2g}	T ₂	T ₂	B _{2g} +E _g	B ₂ +E	A ₁ +B ₁ +B ₂	A ₁ +E

2.7.a THE nd^5 ION IN A TETRAGONAL, OR ORTHORHOMBIC CRYSTAL FIELD

Inspection of Table (2.9) shows that, except for ${}^6A_{1g}$, the symmetry species of the octahedral terms are altered by tetragonal distortions. The Hamiltonian for an ion in a site possessing tetragonal symmetry can be written in the form

$$\mathcal{H} = \sum_{i=1}^5 V_F(i) + \sum_{i=1}^5 V_{x\ell}(\vec{r}_i) + \sum_{i=1}^5 V_{SO}(i) \quad (2.42)$$

where V_F and V_{SO} have already been discussed in chapter one, and section 2.6.a, respectively. The crystal field contribution can be decomposed into two components

$$\sum_{i=1}^5 V_{x\ell}(\vec{r}_i) = \sum_{i=1}^5 V_{x\ell}^{\text{oct}}(\vec{r}_i) + \sum_{i=1}^5 V_{x\ell}^{\text{te}}(\vec{r}_i) \quad (2.43)$$

where $V_{x\ell}^{\text{oct}}(\vec{r})$ is the contribution from a perfect octahedral crystal field that has already been discussed in length in sections 2.2.a and 2.2.b, and $V_{x\ell}^{\text{te}}(\vec{r})$ is the tetragonal perturbation energy operator. Provided $V_{x\ell}^{\text{te}}(\vec{r})$ is large compared to V_{SO} then, for the moment, spin-orbit coupling effects in (2.42) can be neglected and

$V_{x\ell}^{te}(\vec{r})$ can be considered to perturb the states of the octahedral crystal field. To first order the $V_{x\ell}^{te}$ does not distort the octahedral orbitals, but only changes their energies.

The perturbation calculations can be carried out using either the weak-field or strong-field wave functions. For tetragonal complexes, the matrix elements of $V_{x\ell}^{te}(\vec{r})$ can be expanded out in the form listed in Table (2.1), and are most easily evaluated using the operator technique, described in reference 3, page 100.

For the more general complexes of lower point group symmetry, i.e. for orthorhombic crystal fields, the non-cubic part of the crystal field contribution to the Hamiltonian can be expanded to give^{25,26}

$$\mathcal{H}_{te'} = \sum_{i=1}^5 V_{x\ell}^{te'}(\vec{r}_i) \quad (2.44)$$

where

$$\begin{aligned} \sqrt{\frac{5}{4\pi}} V_{x\ell}^{te'}(\vec{r}) = & A_{2,0} r^2 Y_{2,0} + \sqrt{\frac{5}{12}} A_{4,0} r^4 Y_{4,0} - \sqrt{\frac{7}{24}} A_{4,4} r^4 (Y_{4,4} + Y_{4,-4}) \\ & + B_{2,2} r^2 (Y_{2,2} + Y_{2,-2}) / (\sqrt{2}) + B_{4,2} r^4 (Y_{4,2} + Y_{4,-2}) / (\sqrt{2}) \end{aligned} \quad (2.45)$$

and $B_{k,\alpha}$ are suitable functions of R that satisfy the relationship

$$A_{k,\alpha} = -\frac{4\pi}{2k+1} \int \frac{B_{k,\alpha}}{R^{k-1}} dR \quad (2.46)$$

(compare with equation 2.3). For tetragonal complexes $B_{2,2}=B_{4,2}=0$, but these are different from zero for orthorhombic distortions. It can be shown that the effects of tetragonal and orthorhombic distortions, for example, the three orbital states $^4A_{1g}$, 4E_g , that originate from the

free ion 4G level can be summarized in the following statements:

- (i) Neither tetragonal nor orthorhombic distortions affect the ${}^4A_{1g}$ state.
- (ii) If the distortion is tetragonal then only the energy of ${}^4E_g^{(b)}$ term, cf. Table (2.3), is depressed.
- (iii) For orthorhombic distortion the energy of only one of ${}^4E_g^{(a)}$ or ${}^4E_g^{(b)}$ is depressed.

The weak field ground state, ${}^6A_{1g}$, is not affected by either tetragonal or orthorhombic distortions.^{39,41,43}

If the spin-orbit coupling interactions in equations (2.42) is now taken into account then it can be shown that there are no matrix elements that connect basis functions within the manifolds ${}^6A_{1g}({}^6S)$ and $\{{}^4A_{1g}, {}^4E_g\}({}^4G)$. Hence, in order to work out the effects of spin-orbit coupling, second-order perturbation, or even high-order perturbation^{25, 38,39,41} techniques must be used.

2.7.b THE nd^5 ION IN A TRIGONAL CRYSTAL FIELD

When the octahedron is distorted along a trigonal axis, the point group symmetry will be reduced from O_h to D_{3d} , D_3 , C_{3v} or C_3 . The symmetry species of the resultant levels are as listed in Table (2.9), and the crystal field contribution to the energy of the complex can be decomposed into its components.

$$\sum_{i=1}^5 V_{x\ell}(\vec{r}_i) = \sum_{i=1}^5 V_{x\ell}^{\text{oct}}(\vec{r}_i) + \sum_{i=1}^5 V_{x\ell}^{\text{tri}}(\vec{r}_i) \quad (2.47)$$

where $V_{x\ell}^{\text{tri}}(\vec{r})$ is the contribution from the trigonal perturbation. Equation (2.47) can be recast in the normal way in terms of normalized spherical harmonics,^{24,43-45} and in this process the operators for trigonal symmetry, result in the introduction of the parameters DSIG, DQ, and DTAU, defined by the relationships

$$\begin{aligned} D\sigma &= \text{DSIG} / \sqrt{70} \quad , \quad Dq = \frac{1}{6} \sqrt{\frac{1}{30}} DQ + \frac{1}{60} \sqrt{\frac{7}{6}} \text{DTAU} \quad , \\ D\tau &= -\left(\frac{3}{10}\right) \sqrt{\frac{1}{42}} \text{DTAU} \quad , \end{aligned} \quad (2.48)$$

where the crystal field parameters $D\sigma$ and $D\tau$ are related to the radial potential forms by

$$\begin{aligned} D\sigma &= -\frac{1}{14} \sqrt{\frac{5}{\pi}} \left\langle \frac{4}{5} \sqrt{5\pi} B_{2,2} r_i^2 \right\rangle \\ D\tau &= -\frac{1}{14} \frac{1}{\sqrt{\pi}} \left\langle \frac{16}{3} \sqrt{\pi} B_{4,2} r_i^4 \right\rangle \end{aligned} \quad (2.49)$$

The parameters DSIG and DTAU reflect the trigonal component of the electrostatic fields due to the presence of the ligands.

The energies for complexes D_3 symmetry have been calculated,²⁴ using representation of the Hamiltonian, shown in (2.42) i.e. using symmetry adapted basis functions,^{4,46,47} $|d^5, J M_J \rangle$. These calculations can also be used for point group symmetries D_3 , D_{3d} , C_3 and C_{3v} by making appropriate correlations of the irreducible representations of these point groups.^{19,47} The results of such calculations are shown schematically in Figures (2.8) and (2.9) and these should be compared with Figure (2.4). Trigonal distortion splits the octahedral orbital triplet states, T, in Figure (2.4), into an orbitally degenerate, E doublet plus an

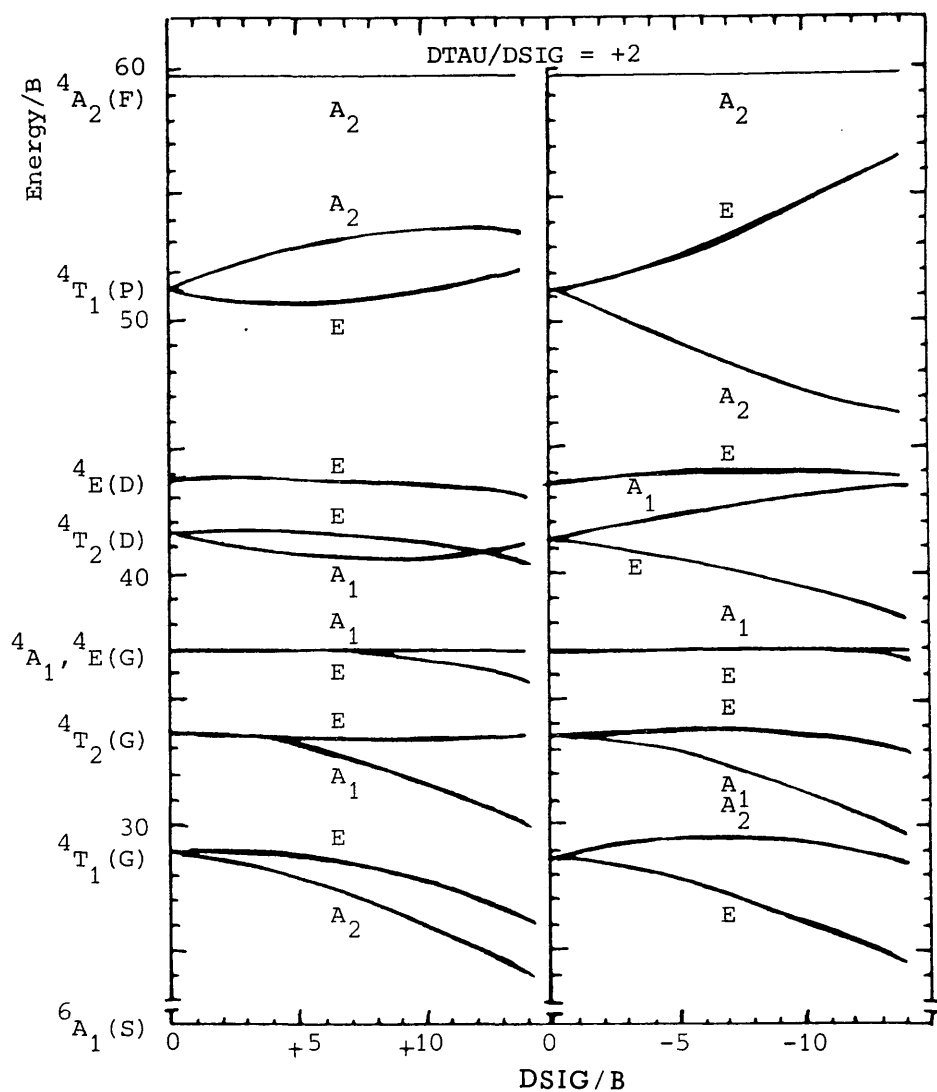


Figure (2.8). Trigonal ligand field splitting diagram for the quartet states of the nd^5 system, $B=670\text{ cm}^{-1}$, $C/B=5.4$, $DQ=26,291\text{ cm}^{-1}$ and $DTAU/DSIG=+2$.
 D_3 symmetry

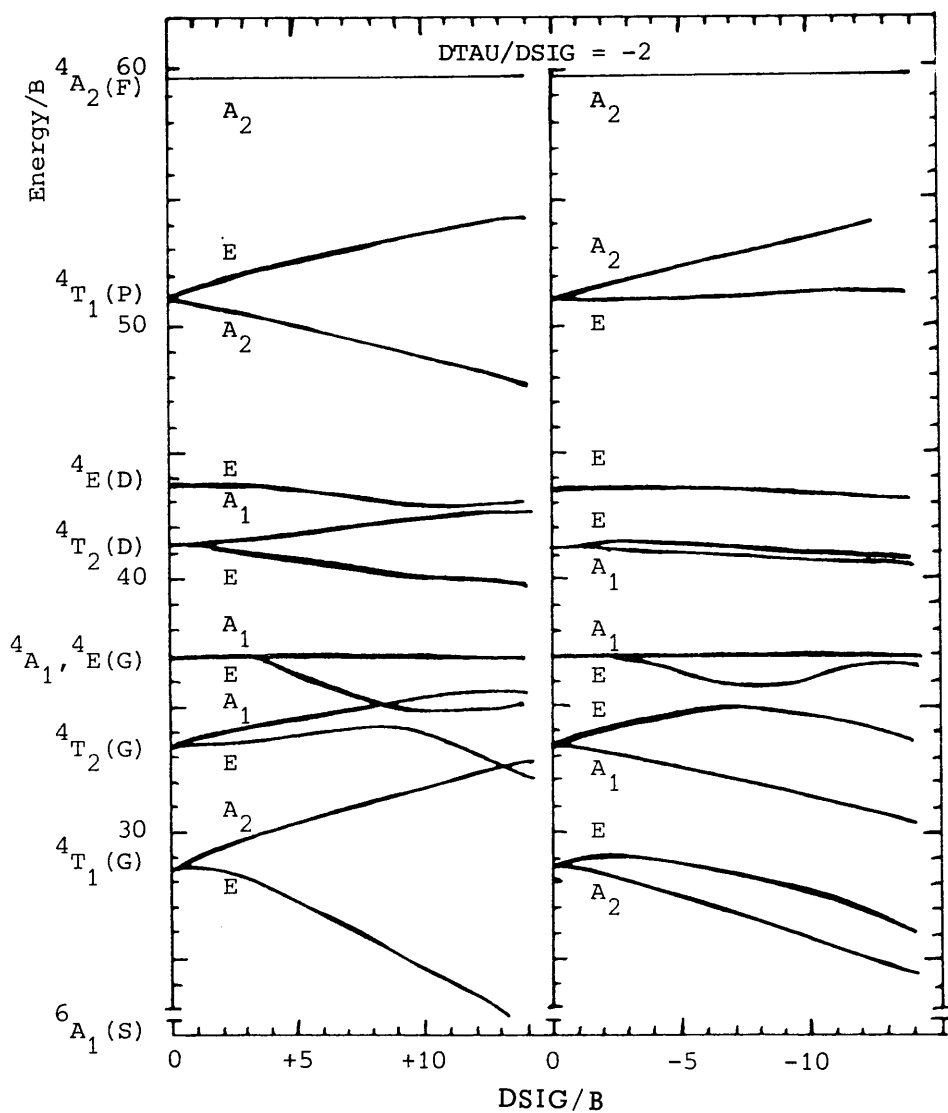


Figure 2.9). Trigonal ligand field splitting diagram for the quartet states of the nd^5 system, $B=670\text{ cm}^{-1}$, $C/B=5.4$, $DQ=26,291\text{ cm}^{-1}$ and $DTAU/DSIG=-2$.
 D_3 symmetry

A_1 or an A_2 orbital singlet: cf. Table (2.9). The energies of the quartet spin T-states calculated for $DTAU/(DSIG) = \pm 2$ for varying values of the ratio $DSIG/B$ are shown in Figures (2.8) and (2.9).

The following observations emerge from studies of the detailed results of such calculations.²⁴

- (i) When $|DTAU/DSIG| > \frac{1}{2}$, and when $DTAU/DSIG = -\frac{1}{10}$ or $-\frac{1}{2}$ the first excited ${}^4T_1({}^4G)$ state always splits, so that the 4A_2 component is lower in energy if DTAU is positive, as in Figure (2.8). However, the 4E component is lower in energy if DTAU is negative, as in Figure (2.9). The relative ordering of the energies of these components is reversed when $DTAU/DSIG = +\frac{1}{10}$ or $+\frac{1}{2}$.
- (ii) The splitting of the 4A_1 and ${}^4E({}^4G)$ levels is largest for a given parameter set when DTAU and DSIG have opposite signs and in such cases the 4E state is always shifted to lower energy.
- (iii) The energies of the ${}^4A_1({}^4G)$ and ${}^4A_2({}^4F)$ states are found to be independent of the trigonal ligand field strength.
- (iv) When higher order perturbation treatments are used, the splittings of the ${}^6A_1({}^6S)$ ground state of the nd^5 system by a trigonal distortion turn out to be a sensitive function of the sign and magnitude of DTAU, but not of DSIG. Such splittings are functions of DQ only, in so far as the DQ parameter is a function of the energy of the first excited state relative to the ground state.

Calculations⁴⁸ show that spin-orbit coupling mixes only the doublet states of the nd^5 configuration into the ground state ${}^6A_1({}^6S)$. Therefore, the zero-field-splitting calculations for complexes which have

trigonal symmetries may be restricted to the quartet and sextet manifold:
cf. chapter three.

2.7.c THE nd^5 ION IN CRYSTAL FIELDS OF POINT GROUP SYMMETRIES C_{4v} and C_{2v}

The symmetry species of the terms that are obtained when an octahedral complex is perturbed by crystal field components of point group symmetry C_{4v} or C_{2v} are listed in Table (2.9), and complete eigenfunctions for the nd^5 energy levels of such complexes have been computed using as a basis the $252 |SLJM_J\rangle$ kets.⁴⁹ In these calculations the crystal field Hamiltonian was written in the form

$$\mathcal{H}_c = \sum_{i,k,\alpha} B_{k,\alpha}' (C_{k,\alpha}')_i \quad (2.50)$$

where $B_{k,\alpha}'$ the so-called "Wybourne parameters",⁵⁰ are related to Dq , for example, $B_{4,0} = B_{4,4} \sqrt{\frac{4}{5}} = 21Dq$. The coefficients $C_{k,\alpha}'$ are functions of spherical harmonics.

Such calculations⁴⁹ show that the zero-field-splitting of the high-spin ground state in C_{4v} symmetry arises through spin-orbit and crystal field mixing of the excited states, with non-zero L-values into the ground state: cf. reference 50, chapter one. In the neighbourhood of the cross-over limit, the splitting arises mainly through mixing of the excited 4P states, but 4G states are also indirectly mixed as a result of coupling between $^4P_{5/2}$ and 4G components. The zero-field-splitting of the $^6S_{5/2}$ term is shown schematically, as a function of the values of the parameters $B_{4,0}$ and $B_{4,4}$, in Figure (2.10).

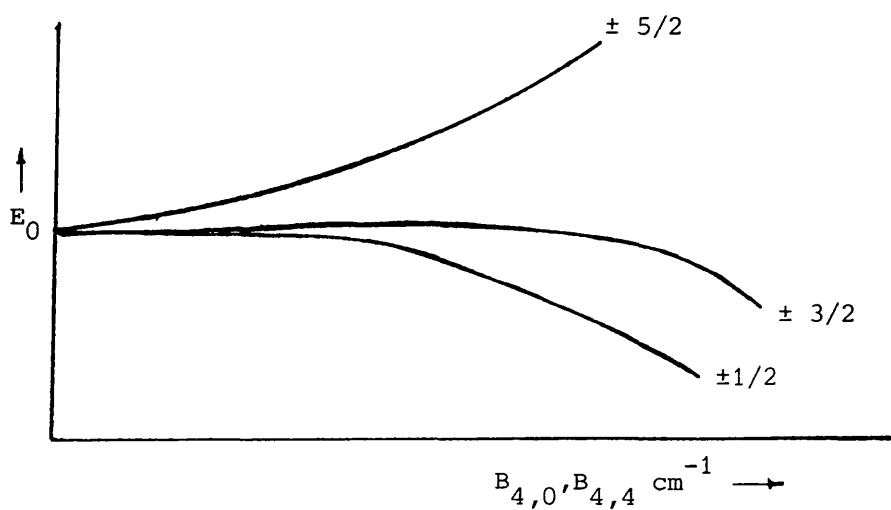


Figure (2.10)

2.7.d THE nd^5 ION IN A TETRAHEDRAL CRYSTAL FIELD

Detailed calculations on nd^5 ions in tetrahedral fields appear to have been neglected in the literature. However, Curie et al.⁵¹ have used the covalency parameters introduced by Koide, Pryce²⁵ and Pappalardo²⁶ and have reported calculations of the energy levels of nd^5 ions in tetrahedral ligand fields.

- CHAPTER THREE -

THE MAGNETIC PROPERTIES OF nd^5 IONS IN
TRANSITION METAL-ION COMPLEXES

3.1 MAGNETIC PROPERTIES OF ELECTRONS AND NUCLEI IN COMPLEXES^{1, 52, 53-59}

Electrons, protons, and neutrons undergo various kinds of closed-loop like motions, and the resultant angular momentum vector, \underline{J} , in units of \hbar , associated with any of these particles can be decomposed into its components, J_x , J_y , and J_z .

$$\underline{J}^2 = J_x J_x + J_y J_y + J_z J_z \quad (3.1)$$

along three mutually perpendicular directions x , y , and z . Some of the quantum mechanical properties of angular momentum operators have already been discussed in Chapters one and two. When a charged particle has an angular momentum it possesses a permanent magnetic dipole moment, and generally both orbital and spin angular momenta contribute to the magnetic moment of an electron. Each of the individual components of the magnetic moment is proportional to the magnitude of the corresponding angular momentum, i.e. $\underline{\mu} = \gamma \underline{J}$, where γ is the appropriate magnetogyric ratio of the motion in question. It can be shown that $\gamma = g_e e / (2mc)$, where g_e is the appropriate Landé g -factor and $g_e = 1$ or 2.00232 for electronic orbital and spin motions, respectively. For a single electron in an isolated atom where the spin and orbital angular momenta are coupled together, the total angular momentum is

$$\underline{j} = [j(j + 1)]^{\frac{1}{2}} \hbar \quad (3.2)$$

where $j = |\ell+s|, |\ell+s-1|, \dots, |\ell-s|$, and the g-factor is

$$g_j = 1 + \left[\frac{j(j+1) + s(s+1) - \ell(\ell+1)}{2j(j+1)} \right] \quad (3.3)$$

In chemically interesting situations atoms are not isolated. Then the electronic orbital motion is perturbed by the asymmetric electric fields generated by the presence of neighbouring atoms. Such fields tend to uncouple the spin and orbital angular momenta, and if the electric fields are large then the orbital contribution to electronic angular momentum is almost completely removed, and the g-factor then is very nearly the spin-only value, 2.00232. In cases where the ground state spin eigenfunction has only a second-order contribution from orbital paramagnetism, the electronic magnetic moment may be written as

$$\mu = -g_{\text{eff}} \sqrt{S(S+1)} \frac{e\hbar}{2mc} \quad (3.4)$$

$$= -g_{\text{eff}} \sqrt{S(S+1)} \beta_e \quad (3.5)$$

where β_e is the electronic Bohr magneton, 0.92731×10^{-20} erg/Gauss, the orbital contribution is taken into the effective g-factor, and the magnetic moment is assumed to arise from the "spin" of the electron only. g_{eff} is a tensor.

The component of the electron's dipole moment along the direction of an applied magnetic field, z , can be written in the form

$$\mu_z \simeq (L_z + 2S_z) \beta_e \quad (3.6a)$$

or in more general terms

$$\mu_z = -g_J \beta_e M_J \quad (3.6b)$$

The z-component of angular momentum and therefore the values allowed for μ_z are quantized. The magnetic contribution to the energy of the electron, $E_H = -\mu_z H$, is therefore quantized. The directing influence of an applied magnetic field competes against the randomizing thermal energy $\bar{k}T$ of the dipoles and the magnetization, M , i.e. the magnetic moment per unit volume, and thence the volume susceptibility, χ_V , of an assembly of electronic magnets can easily be calculated using standard statistical mechanics techniques. Suppose that unit volume contains N' similar ions, all with identical values of J , and that an atom or ion in the state i has a moment component $(\mu_z)_i$ in the field direction, then

$$\begin{aligned} M &= \sum_i (\mu_z)_i \times (\text{the number of species whose energy is } E_i) \\ &= \sum_i (\mu_z)_i \times \frac{N'}{f} \text{Exp}(-E_i/\bar{k}T) \end{aligned} \quad (3.7)$$

where f is the partition function for the assembly $= \sum_i \text{Exp}(-E_i/\bar{k}T)$, i.e.

$$M = \sum_i N' (\mu_z)_i \text{Exp}(-E_i/\bar{k}T) / \left[\sum_i \text{Exp}(-E_i/\bar{k}T) \right] \quad (3.8)$$

Provided all atomic magnets have the same J value, this last expression can be recast into the form

$$M = \frac{N' g_J \beta_e \sum_i (M_J)_i \text{Exp}[(M_J)_i x]}{\sum_i \text{Exp}[(M_J)_i x]} \quad (3.9)$$

where $x = g_J \beta_e H / \bar{k}T$.

This can now be expanded out using standard methods⁶⁰ to give

$$M = N' \mu_m B_J(\bar{Y}) \quad (3.10)$$

where $\mu_m = g_J \beta_e J$, and $B_J(\bar{Y})$ is known as the Brillouin function of the variable \bar{Y} and is given by

$$B_J(\bar{Y}) = \frac{2J+1}{2J} \coth \frac{2J+1}{2J} \bar{Y} - \frac{1}{2J} \coth \frac{\bar{Y}}{2J} \quad (3.11)$$

at all but the lowest temperatures and the highest fields,

$g_J M_J \beta_e H \ll \bar{k}T$ and equation (3.10) becomes

$$M \simeq N' \mu_{\text{eff}}^2 \beta_e H / (3\bar{k}T)$$

Thus, the volume susceptibility of the assembly of electronic magnets

χ_V , is

$$\chi_V = \frac{M}{H} = N' \mu_{\text{eff}}^2 / (3\bar{k}T) = \bar{C}/T$$

where \bar{C} is the Curie constant. μ_{eff} and the molar magnetic susceptibility are connected by the relationship

$$\begin{aligned}
 \mu_{\text{eff}} &= (3\bar{k}/\bar{N} \beta_e^2)^{1/2} (X_M T)^{1/2} \\
 &= 2.828 \sqrt{X_M T}
 \end{aligned}
 \tag{3.12}$$

where \bar{N} is Avogadro's number.

Magnetic interactions of an assembly of non-interacting ions in thermal equilibrium can also be evaluated using standard perturbation techniques. If diamagnetic terms are omitted, when carried through to second order, this leads to

$$E_H = -\mu_{jj} H - \sum_n \frac{2|\mu_{nj}|^2}{E_n - E_j} H^2 + \dots \tag{3.13}$$

where $\mu_{nj} = \int \psi_n^* \mu_z \psi_j d\tau$ is a matrix element of the permanent magnetic dipole moment operator $\mu_z = (L_z + 2S_z) \beta_e$ and is a measure of the admixture of state n in the field-induced perturbation of ψ_j . The value of the z -axis component of the magnetic dipole moment in this state is therefore,

$$\langle \mu_{nj} \rangle = - \frac{\partial E_H}{\partial H} = \mu_{jj} + \sum_i \frac{4|\mu_{nj}|^2 H}{E_n - E_j} + \dots \tag{3.14}$$

Arguments exactly analogous to those already presented then lead to the relationship⁶⁰

$$M = \frac{\sum_j [\text{Exp}(-E/\bar{k}T)] (\mu_{jj} + \sum_n \frac{4|\mu_{nj}|^2 H}{E_n - E_j})}{\sum_j \text{Exp}(-E/\bar{k}T)} \tag{3.15}$$

Nuclear magnetic behaviour can be described by sets of equations analogous to the relations (3.2)-(3.5), but using g_N and I for the nuclear g-factor and nuclear spin quantum number, respectively.

3.2 THE MAGNETIC PROPERTIES OF nd^5 SYSTEMS

3.2.a THE WEAK FIELD CASE

The ground term in a weak octahedral field, ${}^6A_{1g}$, arising from the free ion term 6S is an orbital singlet and consequently it has no orbital angular momentum. Spin-orbit coupling therefore can not raise the degeneracy of this term, and since there is no excited term with the same multiplicity as the ground term there can be no second-order mixing due to spin-orbit coupling, nor can there be any second-order Zeeman effect.¹ The magnetic dipole moment of the ${}^6A_{1g}$ term to this degree of approximation is therefore simply due to the spin contribution and

$$\begin{aligned}\mu_{\text{eff}} &\simeq [4S(S+1)]^{\frac{1}{2}} \text{ electronic B.M.} \\ &= 5.92 \text{ electronic B.M.}\end{aligned}\tag{3.16}$$

This value of μ_{eff} is independent of temperature, i.e. there is no "temperature independent paramagnetism" contributing to the magnetic moment of the ${}^6A_{1g}$ term.^{1,61}

Experimentally, it can be shown that in fact the ${}^6A_{1g}$ term does split. Weak interactions arising from various sources can cause this splitting, including higher-order spin-orbit interaction, particularly

when combined with Jahn-Teller distortion.^{38,62} Spin-spin interaction,^{63,64} section 3.4.a, can also cause extremely small zero-field splittings in a perfectly octahedral nd^5 system.

Axially distorted octahedral systems exhibit zero-field-splitting and three Kramers' doublets then appear.⁵² The combined effects of spin-orbit interaction and the low symmetry field then completely dominate the spin-spin coupling interactions,⁴¹ and spin-orbit coupling then mixes the free ion ground state 6S with 4P , section 1.3. Furthermore, in a complex which possesses less than cubic symmetry, spin-orbit coupling to the ligand-field-split components of the 4P term removes all but the Kramers' degeneracy of the ground term.

The zero-field-splitting of the ground term $^6A_{1g}$ under the influence of a tetragonal field is shown in Figure (3.1). Griffith has shown⁶⁵ that the zero-field-splitting parameter, D , in this figure, is related to the spin-orbit coefficient $\xi_{n\ell}$ and the low symmetry splitting of the 4P term by expression (3.17)

$$D = \frac{\xi_{n\ell}}{5} \left[\frac{1}{E_1} - \frac{1}{E_2} \right] \quad (3.17)$$

where E_1 and E_2 refer to the energies of the 4A_2 and 4E components of the original $^4P(^4T_1)$ term of the free ion, see Table (2.7).

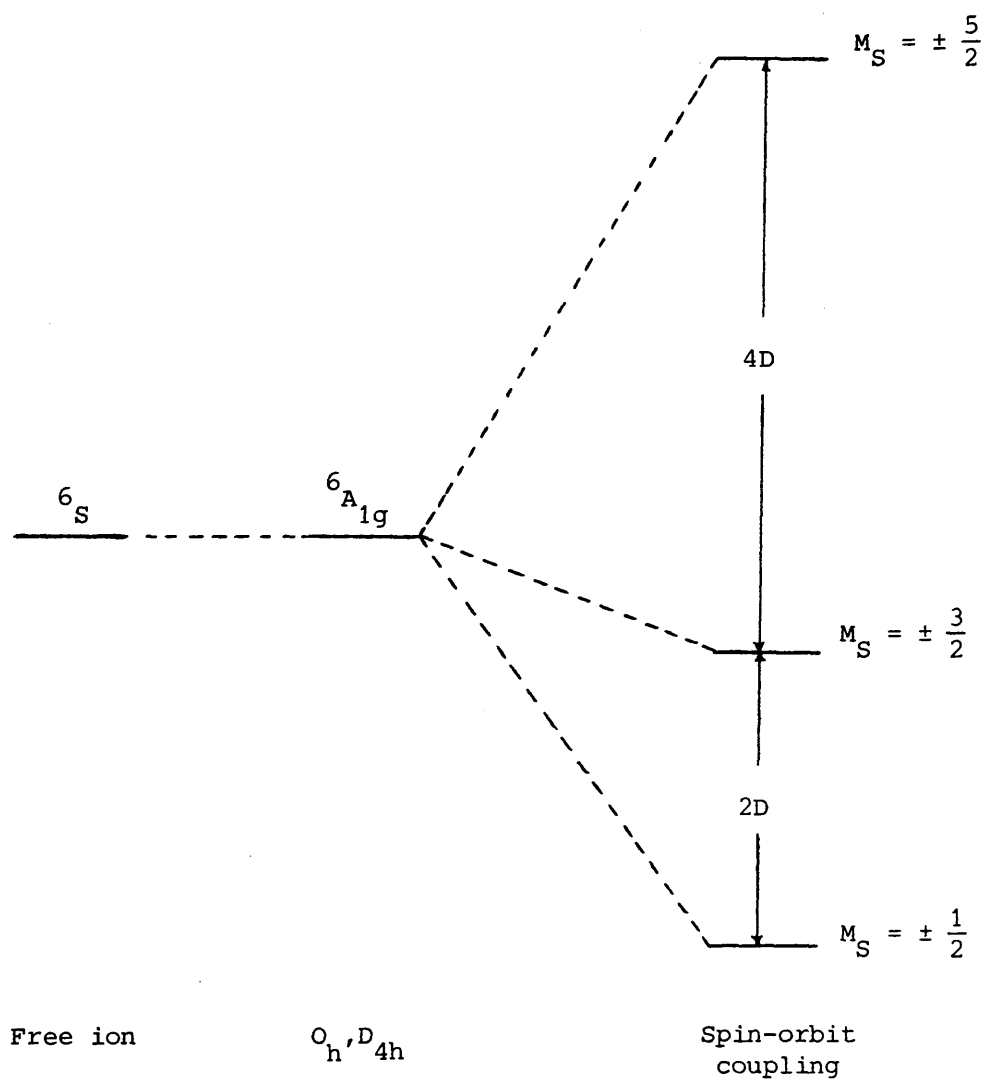


Figure (3.1). Zero-field-splitting of the ground term $6A_{1g}$, of an nd^5 ion, under the influence of a tetragonal field and spin-orbit coupling

3.2.b THE STRONG FIELD CASE

3.2.b.1 SPLITTING BY SPIN-ORBIT COUPLING

In general, magnetic moments for complexes with T ground states are obtained by summing the first- and second-order Zeeman effects, i.e. the terms on the right-hand-side of equation (3.13), outlined in section 3.1, over the states that arise after the terms have been split by spin-orbit coupling. The effect of spin-orbit coupling on T-terms can be obtained by operating with $\lambda L.S.$, equation (1.39) on the appropriate wave functions given in section (2.6.a), or an alternative procedure, that depends on the observation that there is a correspondence between the wave functions of the T-terms and those of free ion P-terms, can be used. Spin-orbit splittings of ${}^2T_{2g}$ terms can be obtained by inverting those for the P-terms arising from the same number of p-electrons as there are d-electrons, i.e.

$${}^2T_{2g} (nd^5, t_{2g}^5) \equiv \text{the inverse of } {}^2P(p^1)$$

The splittings of the ${}^2T_{2g}$ term of the nd^5 configuration by spin-orbit coupling is shown in Figure (3.2). The derivation of the diagram is considered in more detail in section (3.2.b.2).

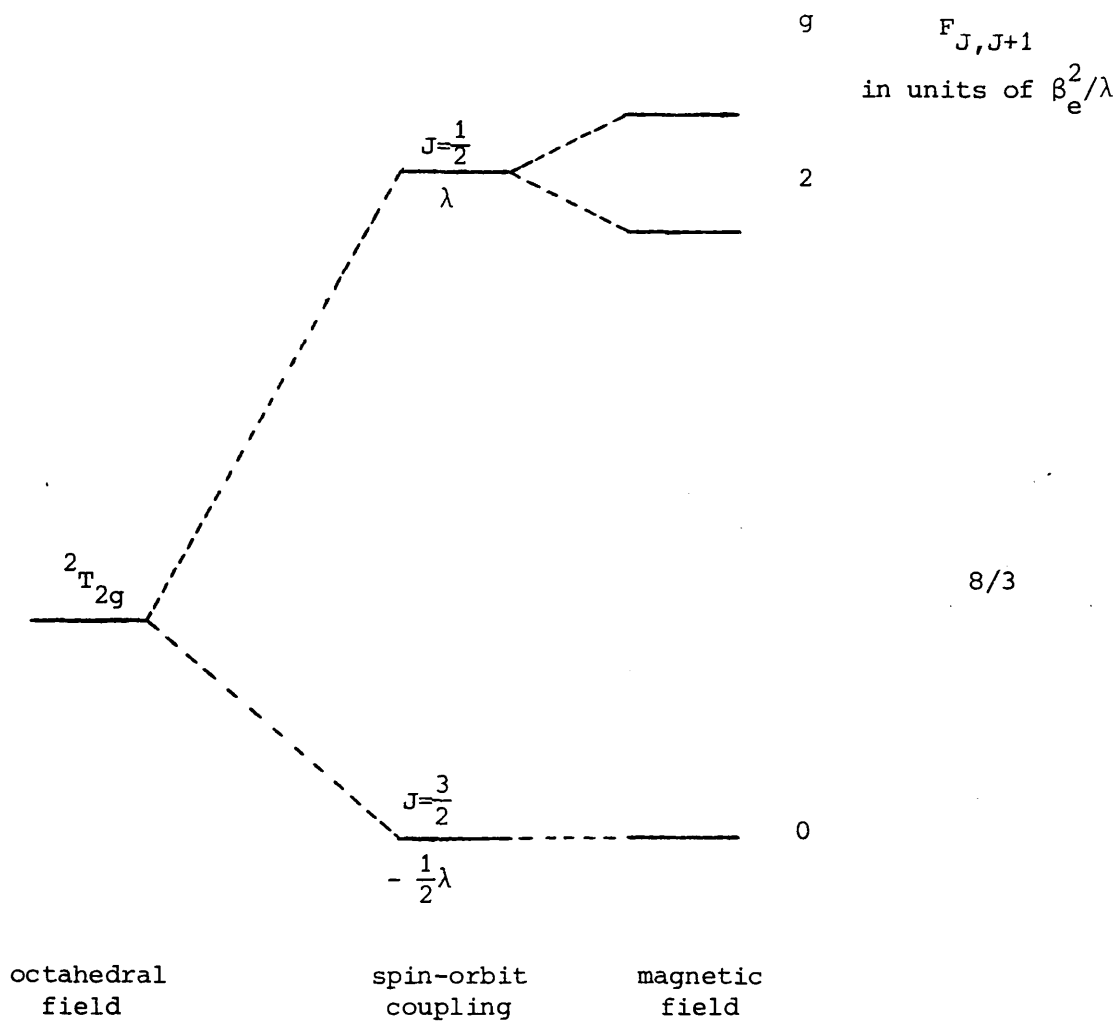


Figure (3.2). ${}^2T_{2g}$ term splitting due to spin-orbit coupling.
 λ is negative

3.2.b.2 ESTIMATION OF THE g-FACTOR, THE MOLAR MAGNETIC
SUSCEPTIBILITY, χ_M , AND THE MAGNETIC DIPOLE
MOMENT, μ_{eff} , OF THE $^2T_{2g}$ TERM

If the free ion p^n , P-terms, are used to estimate the first- and second-order Zeeman effects for $^2T_{2g}$ terms in a cubic field then the orbital angular momentum operator becomes $-A'L_z$, rather than L_z . The minus sign allows for the inversion of the spin-orbit coupling splitting on going from the p^n to the t_{2g}^n configuration, and A' is a factor whose value lies between 1.0 at the strong field limit and 1.5 at the weak field limit. The free ion expression, equation (3.3) can not be used for the g-factor. Instead, this expression becomes^{1,4}

$$g = 1 - \frac{1}{2} A' + (2+A')[S(S+1) - 2] / [2J(J+1)] \quad (3.18)$$

The coefficient of the second-order Zeeman effect, i.e. the coefficient of H^2 in equation (3.13), is given by

$$F_{J,J+1} = [(2+A')^2/A'] F_{J,J+1}^{\text{free ion P-term}} \quad (3.19)$$

where the second-order Zeeman coefficient for the free ion is given by

$$F_{J,J+1} = -(J+L+S+2)(-J+L+S)(J-L+S+1) \\ \times (J+L-S+1) \beta_e^2 / [12(J+1)^2 \lambda] \quad (3.20)$$

Equations (3.18)-(3-20) were used to obtain the results depicted on Figure (3.2).

The g-values, the J-values, and the second-order Zeeman coefficients shown in Figure (3.2) can be substituted into equation (3.15) to give the magnetization and thence the susceptibility of the $^2T_{2g}$ term and it can be shown¹ in this way that

$$\chi_M = \frac{\bar{N} \beta_e \sum_{J=|L-S|}^{|L+S|} [g_J^2 J(J+1)(2J+1) / (3\bar{k}T - 2F_{J,J+1} + 2F_{J-1,J})] \text{Exp}(-E_J/\bar{k}T)}{\sum_{J=|L-S|}^{|L+S|} (2J+1) \text{Exp}(-E_J/\bar{k}T)} \quad (3.21)$$

The corresponding expressions for the magnetic dipole moment of a $^2T_{2g}$ term turns out to be

$$\mu_{\text{eff}}^2 = \frac{8 + [3\lambda / (\bar{k}T) - 8] \text{Exp}(-3\lambda / (2\bar{k}T))}{\lambda / (\bar{k}T) [2 + \text{Exp}(-3\lambda / (2\bar{k}T))]} \quad (3.22)$$

Kotani⁶⁶ has considered in great detail the effects of varying temperature and varying spin-orbit interaction on the effective magnetic moment of the t_{2g}^5 configuration. His treatment assumed (i) that the ligand field interactions are much greater than the mutual repulsions between electrons in d-shells, (ii) that the electronic repulsions in turn are larger than the spin-orbit coupling in the ion, (iii) that the ligand field has perfect cubic symmetry, and (iv) that there are no interactions between neighbouring paramagnetic ions, i.e. anti-ferromagnetic and ferromagnetic interactions do not need to be taken into account.

His calculations show that the effective magnetic moment for the t_{2g}^5 configuration is markedly dependent on temperature and on the spin-orbit interactions.

3.2.b.3 LOW SYMMETRY CRYSTAL FIELD COMPONENTS AND MAGNETIC PROPERTIES OF nd^5 IONS¹

Ligand field components of lower than cubic symmetry lift the orbital degeneracy of T-terms and markedly affect their magnetic properties because they alter the arrangements of the energy levels over which the ions are thermally distributed. It is difficult to discuss, generally, the magnetic properties in the presence of such crystal fields since they depend on the relative magnitude of the spin-orbit coupling on the one hand and the low symmetry ligand field components on the other. When the additional ligand field component is small in comparison with spin-orbit coupling then its effects on the earlier discussion of the magnetic properties are small, but as the low symmetry ligand field component becomes larger than the spin-orbit coupling interaction, the effective magnetic moment of the ${}^2T_{2g}$ state tends towards the spin-only value, and the temperature dependence tends to decrease. When the low symmetry component of the crystal field becomes very large, the magnetic moment becomes the spin-only value and it is then independent of temperature. These effects occur because the low symmetry field component further quenches the orbital angular momentum by destroying the degeneracy of the ${}^2T_{2g}$ orbital set. These effects of the low symmetry ligand component are shown in Figure (3.3) in which μ_{eff} is plotted as a function of $\bar{k}T/|\lambda|$ for

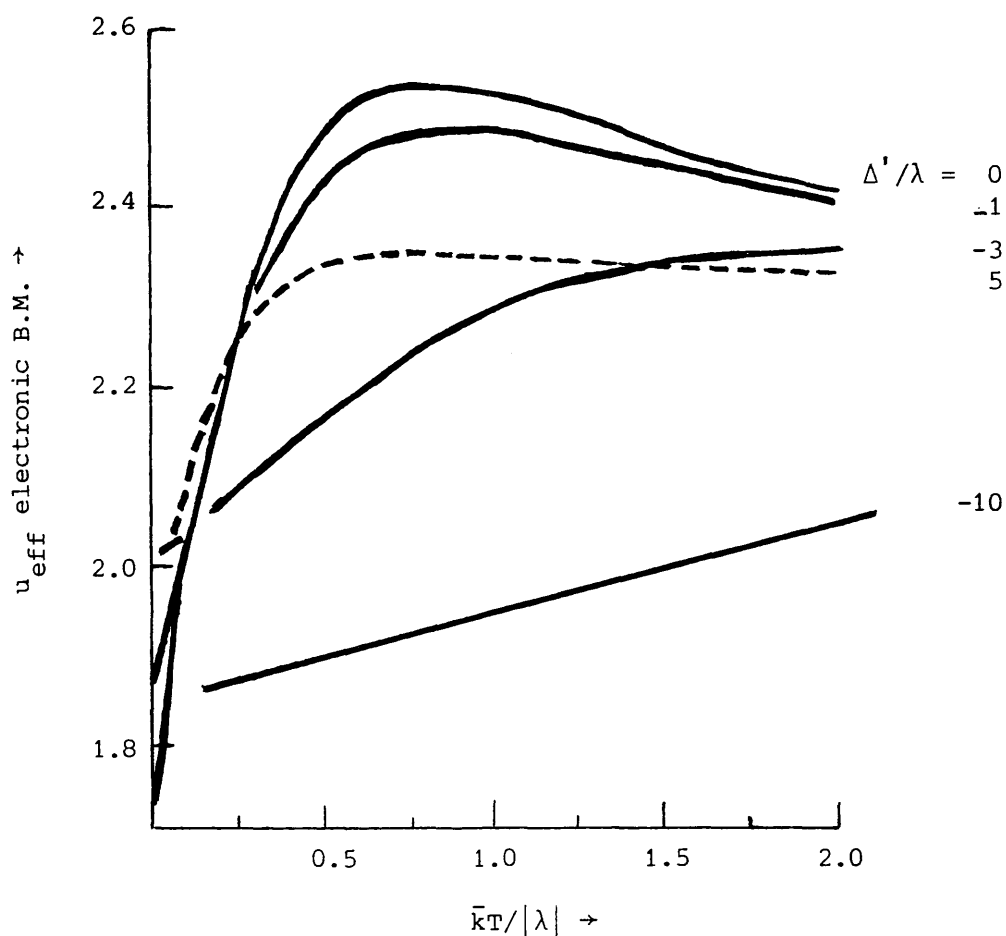


Figure (3.3). The effect of a low-symmetry ligand-field component on the magnetic moment of the ${}^2T_{2g}$ term. λ is negative, except for the dashed curve. The component is expressed as the ratio of the splitting of the t_{2g} orbitals, Δ' to the spin-orbit coupling constant, λ

several ratios of the splitting of the ${}^2T_{2g}$ orbital energy levels, Δ' , to the spin-orbit coupling constant, λ .

3.2.b.4 ELECTRON DELOCALIZATION AND MAGNETIC PROPERTIES OF ${}^2T_{2g}$ TERMS

Whenever metal-ion orbitals mix with ligand orbitals to form molecular orbitals belonging to the complex as a whole, then delocalization of the d-electrons takes place, and it becomes necessary to take account of the effective reduction of the orbital angular momentum of the electrons. It is customary to suppose that the matrix elements of the orbital angular momentum are reduced by the factor k' so that, for example, the operator for orbital angular momentum in the z-direction becomes $k'L_z$ rather than L_z . k' is a number whose value is unity when there is no delocalization, but it is in general somewhat less than unity.

Electron delocalization in the t_{2g}^5 configuration has two major effects. First, it brings the effective magnetic moment closer to the spin-only value, since it causes additional quenching of the orbital angular momentum. Second, it reduces the spin-orbit coupling constant for the T-term below the value λ_F of the free ion. The spin-orbit coupling constant λ , for the T-term in equation (3.22) becomes $\lambda = k'\lambda_F$. It has, already, been noted that introduction of the reduction factor, k' , normally causes the effective magnetic moment, μ_{eff} , to be nearer to that of the spin-only value, however, care is needed because complete calculations show that in some cases, as shown in Figure (3.4), this is not true.

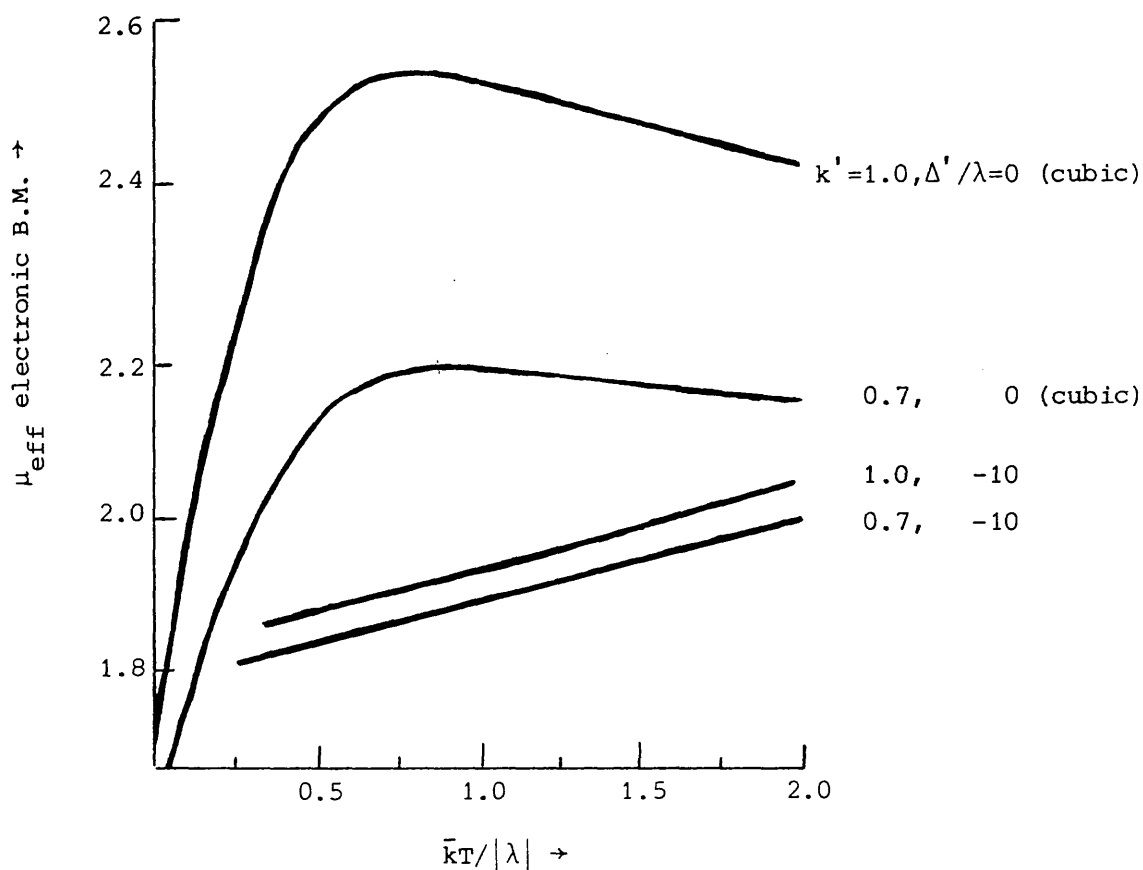


Figure (3.4). The effect of t_{2g} electron delocalization on the magnetic moment of the ${}^2T_{2g}$ term, λ is negative. $\Delta'/\lambda = -10$ means a highly distorted arrangement. λ is the spin-orbit coupling constant value which is effective in the complexed metal ion

3.2.3 SPIN FREE-SPIN PAIRED EQUILIBRIA (${}^6A_{1g} \rightleftharpoons {}^2T_{2g}$) IN AN nd^5 SYSTEM^{1,67}

In section 2.2.c, it was pointed out that for certain critical ligand field values the cross-over point is reached in Figure (2.5), and at this point there is a change in the ground term. In this case if the energies of the two terms ${}^6A_{1g}$ and ${}^2T_{2g}$ do not differ by more than $\bar{k}T$ then their relative populations become of comparable magnitude, and vary with temperature. The matrix element of the spin-orbit coupling connecting these two terms is zero. The susceptibility in this case is then the population-weighted average of the susceptibilities of the individual terms and under these circumstances it can be shown that the equilibrium susceptibility is given by

$$\chi_M = \frac{(2S'_1 + 1) \chi_{M1} + (2S'_2 + 1) \chi_{M2} \text{Exp}(-Y)}{(2S'_1 + 1) + (2S'_2 + 1) \text{Exp}(-Y)} \quad (3.23)$$

where S' is the "fictitious spin" quantum number (in many instances S' is the same as J and/or S),

$$Y = (E_{S'_2} - E_{S'_1}) / \bar{k}T$$

$E_{S'_1}$, and $E_{S'_2}$ are the energies of the terms whose degeneracies are $(2S'_1 + 1)$ and $(2S'_2 + 1)$. χ_{M1} and χ_{M2} are the respective atomic susceptibilities of these terms and they themselves may, also, be functions of temperature. In this case equation (3.23) becomes

$$\chi_M = \frac{\chi(^6A_{1g}) + \chi(^2T_{2g}) \text{Exp}(-Y)}{1 + \text{Exp}(-Y)} \quad (3.24)$$

where $\chi(^2T_{2g})$ is itself a function of temperature and may be introduced into (3.24) as a calculated quantity or as an experimental result obtained from a $^2T_{2g}$ complex with similar ligand atoms surrounding the same metal-ion, due allowance being made for the effects of electron delocalization and low symmetry ligand field components.

3.2.4 THE MAGNETIC PROPERTIES OF COMPLEXES OF Ru³⁺

As already mentioned in section (2.5), $\text{NH}_4[\text{RuNOCl}_5]$ appears to be the only Ru^{3+} complex reported to contain high-spin Ru^{3+} . Its measured magnetic moment is 5.86 electron B.M. and this value does not change when the temperature is altered.³³

All other reported³⁴ magnetic measurements carried out on Ru^{3+} cubic complexes involve the low-spin $^2\text{T}_{2g}$ ground state for the $4d^5$ ion. The effective magnetic moment for several low-spin nd^5 ions, plotted vs. $\bar{k}T/|\lambda|$ is shown in Figure (3.5), and it should be noted once more that these μ_{eff} values differ only slightly from the spin-only value, and, furthermore, that they do not change very much with changing temperature. It should also be noted that the spin-orbit coupling constant for Ru^{3+} , section 1.3, is so large that compounds containing Ru^{3+} appear close to the extreme left-hand edge of this Figure.

Measurements of μ_{eff} vs. temperature for $\text{K}_2\text{RuCl}_5 \cdot \text{H}_2\text{O}$, $(\text{NH}_4)_2\text{RuCl}_5 \cdot \text{H}_2\text{O}$, and for K_2RuCl_5 are plotted in Figure (3.6). Data for this last complex extrapolated back to $T = 0$ indicate an extrapolated μ_{eff} of 0.85 electron B.M., indicating the presence of anti-ferromagnetic metal-metal interactions in this compound.⁶⁸

A corresponding plot for the Ru^{4+} species K_2RuCl_6 is also given in Figure (3.6) for comparison.

Values of the spin-orbit coupling parameters, ξ_{4d} , obtained⁶⁹ by fitting measured room temperature moments to Kotani's curve⁶⁶ for nd^5 systems are listed in Table (3.1) for several trivalent ruthenium complexes. These values are of the correct order of magnitude but it

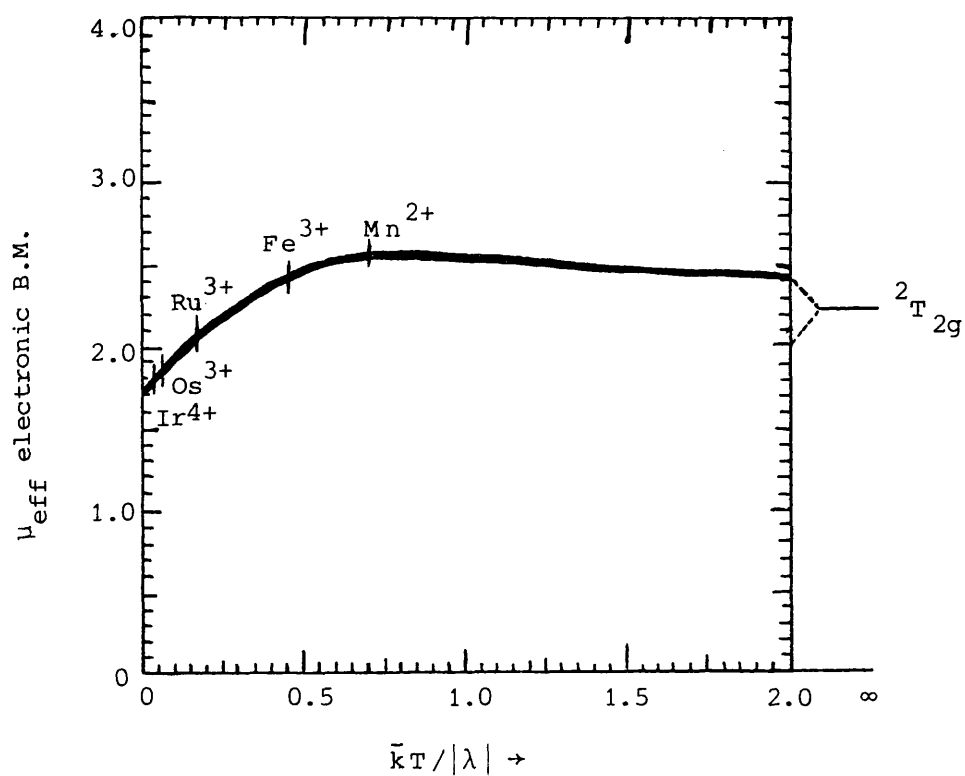


Figure (3.5). The magnetic moment of some nd^5 ions in cubic stereochemistries as a function of temperature. λ is negative

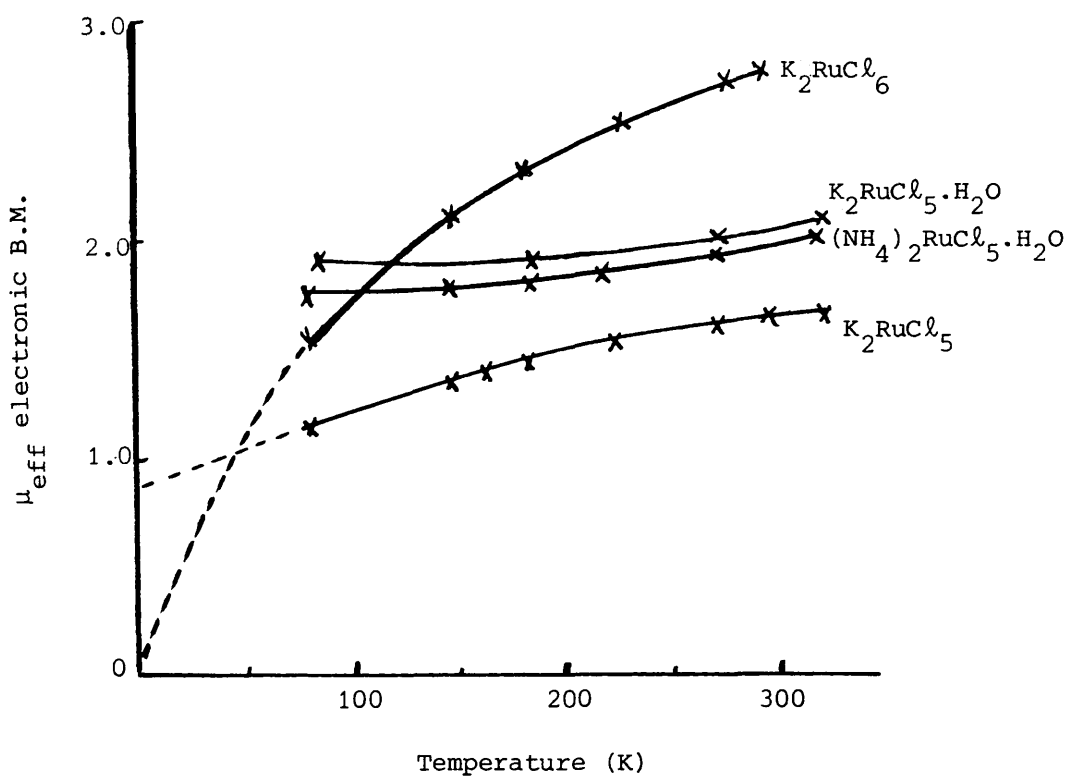


Figure (3.6)

should be noted that this method for obtaining ξ_{nd} values is inaccurate since μ_{eff} changes only slowly with $\bar{k}T/|\xi_{\text{nd}}|$. The data for $\text{Ru}(\text{NH}_3)_6\text{Cl}_3$ in this Table is consistent with Figure (3.5) .

Table (3.1)

Compound	$\sqrt{4S(S+1)}$	μ_{eff} B.M., 80K	μ_{eff} B.M., 300K	$\xi_{4d} \text{ cm}^{-1}$
$\text{Ru}(\text{NH}_3)_6\text{Cl}_3$	1.73	1.85	2.13(2.10)*	1000
$[\text{Ru}(\text{NH}_3)_6](\text{NO}_3)_3 \cdot 3\text{H}_2\text{O}$	1.73	-	2.17	1100
$\text{K}_2\text{RuCl}_5 \cdot \text{H}_2\text{O}$	1.73	-	2.10	870
$(\text{NH}_4)\text{RuCl}_5 \cdot \text{H}_2\text{O}$	1.73	-	2.00	610
$[\text{RuD}_2\text{Cl}_2]\text{ClO}_4$	1.73	-	1.95	-

* calculated employing the spin-orbit coupling constant of the free-ion, and ignoring electron delocalization and low-symmetry ligand field components.

Since the magnetic moment of low-spin Ru^{3+} is very close to the spin-only value, and since it varies only slightly over large ranges of temperature, it follows that bulk magnetic measurements in these complexes are too imprecise to provide much useful information about electron delocalization and about low symmetry ligand field components in these systems.

3.3 ADDITIONAL, WEAKER, CONTRIBUTIONS TO THE GENERAL

"THEORETICAL HAMILTONIAN"

So far, this thesis has essentially been concerned with the first three major contributions to the general "theoretical Hamiltonian", equation (1.1). However, the following, weak, contributions also ought to be taken into account.

(i) The Zeeman interaction, V_Z . This arises from the interaction between an applied magnetic field and the various magnetic moments of electrons and nuclei. Spin moments contribute an amount

$$2.00232 \beta_e H \sum_i s_i - g_N \beta_N H \sum_{i'} I_{i'} \quad (3.25)$$

$$= 2.00232 \beta_e H.S - g_N \beta_N H \sum_{i'} I_{i'}$$

where β_N is the nuclear Bohr magneton. Electronic orbital angular momentum also interacts with a magnetic field and contributes an amount

$$\beta_e H \sum_i l_i + \frac{e^2}{8mc^2} H^2 \sum_i (x_i^2 + y_i^2) \quad (3.26)$$

to the Hamiltonian, where the xy-plane is perpendicular to H, and the last term in (3.26) is usually very small compared to the first term and usually can be neglected. Combining (3.25) and (3.26), then leads to the form for total Zeeman interaction given in (3.27)

$$V_Z = \beta_e (L + 2.00232 S).H - g_N \beta_N H \sum_{i'} I_{i'} \quad (3.27)$$

(ii) The electron-electron dipolar interaction, V_{SS} . This is the sum of the interactions between pairs i, j of magnetic dipoles separated by a distance r_{ij} , and is given by

$$V_{SS} = (2.00232 \beta_e)^2 \sum_{i>j} [r_{ij}^2(s_i \cdot s_j) - 3(s_i \cdot r_{ij})(s_j \cdot r_{ij})] r_{ij}^{-5} \quad (3.28)$$

(iii) The electron spin-nuclear spin hyperfine interaction, V_{SI} ,^{55,58} which will be discussed in detail in the next chapter.

Other still weaker, interactions also contribute to the magnetic properties of complex ions, including the nuclear quadrupole interaction, $V_Q \sim 10^{-3} \text{ cm}^{-1}$; the nuclear spin-orbit interaction, V_{IL} , which provides second-order contributions to the hyperfine interactions; nuclear spin-nuclear spin dipolar interaction; and nuclear chemical-shift effects.

To obtain information, experimentally, about all these interactions, it is necessary to turn to electron paramagnetic resonance experiments, which are usually performed at temperatures at which only energy levels less than 100 cm^{-1} above the ground state are occupied.

- CHAPTER FOUR -

ELECTRON PARAMAGNETIC RESONANCE OF nd^5 IONS

IN TRANSITION METAL-ION COMPLEXES

4.1 THE GENERAL SPIN-HAMILTONIAN

Abraham and Pryce⁷⁰ showed that the complicated theoretical Hamiltonian, including all the weak interactions mentioned in the last chapter, could be recast into the form of the experimentally useful so-called "spin-Hamiltonian". They distinguished between situations involving an orbital singlet ground state on one hand and situations involving orbitally degenerate ground states on the other. Their results, carried through to second-order perturbation, for orbitally singlet ground states, showed⁶² that in such cases the spin-Hamiltonian takes the form

$$\begin{aligned} \mathcal{H}_S = & \beta_e \sum \mathbf{H} \cdot \underline{\mathbf{g}} \cdot \mathbf{S} + \sum \mathbf{S} \cdot \underline{\mathbf{D}} \cdot \mathbf{S} + \sum \mathbf{S} \cdot \underline{\mathbf{A}} \cdot \mathbf{I} + \sum \mathbf{I} \cdot \underline{\mathbf{Q}} \cdot \mathbf{I} \\ & - \gamma \beta_N \sum \mathbf{H} \cdot \mathbf{I} - \sum \mathbf{H} \cdot \underline{\mathbf{R}} \cdot \mathbf{I} - \beta_e^2 \sum \mathbf{H} \cdot \underline{\mathbf{A}} \cdot \mathbf{H} \end{aligned} \quad (4.1)$$

where the sums are overall appropriate electron-electron and electron-nuclear interactions. In equation (4.1), $\underline{\mathbf{g}}$ is the g-tensor, whose components in general differ from the "spin-only", value of 2.00232 because of the presence of orbital contributions from excited states. $\underline{\mathbf{D}}$ is the "zero-field-splitting" tensor, and the low symmetry ligand field, spin-orbit coupling, and spin-spin interactions discussed in section 3.2.a and equation (3.17) contribute to its components. The $\underline{\mathbf{A}}$ tensor characterizes the magnetic interactions between the unpaired electrons and magnetic nuclei that give rise to the hyperfine structure observed in e.p.r. spectra. The $\underline{\mathbf{Q}}$ tensor describes the quadrupole interactions. The fifth term on the right-hand side of equation (4.1)

takes the nuclear Zeeman interactions into account. The sixth term is a second order "electron-nuclear Zeeman" contribution where the tensor $(R) = 2Q\beta_e(\Lambda)$ and the ij th element of Λ is defined by

$$\Lambda_{ij} = \sum \frac{\langle 0 | L_i | \bar{n} \rangle \langle \bar{n} | L_i | 0 \rangle}{E_{\bar{n}} - E_0} \quad (4.2)$$

where $|0\rangle$ is a ground state wave function and $|\bar{n}\rangle$ is an excited state wave function. The last two terms in equation (4.1) are only important in problems involving magnetic susceptibility calculations, the last term being responsible for temperature independent paramagnetism. These last two terms are normally too small to be considered and the spin-Hamiltonian, equation (4.1), becomes

$$\begin{aligned} \mathcal{H}_S = & \beta_e \sum H_i \cdot \underline{g}_i \cdot S + \sum S \cdot \underline{D}_i \cdot S + \sum S \cdot \underline{A}_i \cdot I \\ & + \sum I \cdot \underline{Q}_i \cdot I - \gamma \beta_N \sum H_i \cdot I \end{aligned} \quad (4.3)$$

The spin-Hamiltonian must possess the local symmetry properties at the crystal site of the paramagnetic ion. When it is multiplied out, it is quite easily shown that for axial symmetry, (4.3) takes the following form

$$\begin{aligned} \mathcal{H}_S^a = & g_{11}\beta_e H_z S_z + g_{\perp}\beta_e (H_x S_x + H_y S_y) + D[S_z^2 - \frac{1}{3}S(S+1)] \\ & + AS_z I_z + B(S_x I_x + S_y I_y) + Q[I_z^2 - \frac{1}{3}I(I+1)] - \gamma \beta_N H \cdot I \end{aligned} \quad (4.4)$$

For an orthorhombic crystal field it becomes

$$\begin{aligned} \mathcal{H}_S^o = & \beta_e (g_{xx} H_x S_x + g_{yy} H_y S_y + g_{zz} H_z S_z) + D[S_z^2 - \frac{1}{3}S(S+1)] \\ & + E(S_x^2 - S_y^2) + A_{xx} S_x I_x + A_{yy} S_y I_y + A_{zz} S_z I_z \\ & + Q[I_z^2 - \frac{1}{3}I(I+1)] + Q'(I_x^2 - I_y^2) - \gamma \beta_N H \cdot I \end{aligned} \quad (4.5)$$

where Q' is the "orthorhombic quadrupole parameter". It should be noted that, in general, the principal axes of the different tensors in equation (4.3) do not coincide.

The electronic Zeeman interaction by itself produces $(2S+1)$ equally spaced, effective spin levels which lead to $2S$ allowed transitions ($\Delta M_S = \pm 1$), that coincide at the same applied magnetic field $H = h\nu / (g_{\text{eff}} \beta_e)$ giving $g_{\text{eff}} = 21.4178 / H\bar{\lambda}$, where H is in kilogauss and $\bar{\lambda}$ is the wavelength of the microwave radiation used in the electron paramagnetic resonance experiment, in cm.

(g) is a tensor, so g_{eff} is usually different for different directions of H . g_{eff} possesses the symmetry properties of the ligand field and for a general direction specified by the direction cosines, \underline{l} , \underline{m} , and \underline{n} with respect to the principal axes x, y, z of the g -tensor.

$$g_{\text{eff}} = \{ \underline{l}^2 g_{xx}^2 + \underline{m}^2 g_{yy}^2 + \underline{n}^2 g_{zz}^2 \}^{\frac{1}{2}} \quad (4.6)$$

The second term on the right-hand-side of equation (4.3) is responsible for the fine structure observed in electron paramagnetic resonance spectra and also for the initial splitting of the effective spin levels when $H=0$.

The third term, $S \cdot \underline{A} \cdot I$ on the right-hand-side of equation (4.3) is responsible for the hyperfine structure in electron paramagnetic resonance, e.p.r. spectra. It splits each e.p.r. absorption line into $(2I+1)$ hyperfine components. In general both isotropic, Fermi, interaction and anisotropic direct dipolar interaction contribute to the elements of the hyperfine tensor (A). The isotropic, Fermi, inter-

action

$$\mathcal{H}_{\text{Fer}} = \frac{8\pi}{3} g_e g_N \beta_e \beta_N \delta(r'_n) \mathbf{I} \cdot \mathbf{S}, \quad (4.7)$$

(where $\delta(r'_n)$ is the Dirac delta function) arises from electrons in orbitals possessing σ , or s -character, or from significant polarizations of inner pair s -electrons near the nucleus by unpaired valence electrons.

The anisotropic contribution to (A) is due to direct magnetic dipolar coupling between the magnetic moments of the electron and the nucleus. If the magnetic field is very strong then the electron and nuclear spin vectors, \mathbf{S} and \mathbf{I} , are effectively fully de-coupled and each is quantized separately with respect to the applied field. If θ is the angle between the vector, r' , joining the electron-nuclear dipoles and the magnetic field vector then this direct dipole contribution becomes

$$\mathcal{H}_{\text{dipole}} = g_e \beta_e g_N \beta_N \left\langle \frac{3\cos^2\theta - 1}{r'^3} \right\rangle_{\text{av}} \mathbf{I} \cdot \mathbf{S} \quad (4.8)$$

If the orbital containing the unpaired electron is spherically symmetric or if the orientation dependent term has a spherically symmetrical time average, for example, as in the Brownian motion in fluid then this direct dipole contribution to the elements of (A) tensor vanishes.

Direct dipolar interaction between the electronic orbital magnetic moment and the nuclear magnetic moment also contributes to the hyperfine coupling, but in transition-metal complexes such orbit-nucleus interaction is too small to be considered.

It should be noted that unpaired electrons in complexes can also interact with magnetic nuclei in ligands. This interaction leads to further splittings of each hyperfine line in electron paramagnetic resonance spectrum and gives rise to so-called "superhyperfine coupling".

4.2 THE ELECTRON PARAMAGNETIC RESONANCE PARAMETERS OF HIGH SPIN, $S = 5/2$, nd^5 IONS

As pointed out earlier, in section 3.2.a, in the 6A_1 state, the ground state of high spin octahedral and tetrahedral nd^5 ions, the total electronic angular momentum is zero, and so to first-order, neither ligand field nor spin-orbit coupling interactions by themselves can remove the six-fold spin degeneracy. It was also pointed out that spin-orbit coupling interactions cause the 4T_1 term to be mixed in with the ground 6A_1 term to first order, cf. p. 34. Although to first-order spin-orbit coupling cannot remove the six-fold degeneracy of the ground state nevertheless the six-fold degeneracy can be subdivided into a two-fold degenerate pair of levels, Γ_7 and a four-fold degenerate quartet of levels, Γ_8 , of the same energy. As far back as 1934 Van Vleck and Penny³⁸ found that their calculations on nd^5 systems had to be extended to fifth-order in perturbation, involving simultaneously a ligand field of cubic symmetry and spin-orbit coupling, before they were able to remove this six-fold degeneracy. Their calculations enabled them to introduce the Hamiltonian for a ${}^6S_{5/2}$ ground state ion in a cubic field in the following form

$$\begin{aligned} \mathcal{H}_{5/2} = & g\beta_e H \cdot S + \frac{1}{6} a' [S_x^4 + S_y^4 + S_z^4 - \frac{1}{5} S(S+1)(3S^2 + 3S - 1)] \\ & + AS \cdot I - \gamma\beta_N H \cdot I \end{aligned} \quad (4.9)$$

where the second term on the right-hand-side arises as a result of these higher order interactions. Van Vleck and Penny found that the constant a' in equation (4.9) is given by

$$a' \simeq \frac{K' \lambda^4}{E(^4P) - E(^6S)} \quad (4.10)$$

where K' is the ligand field matrix element, $\langle nd | V_{xl}^{\text{oct}} | nd \rangle$, λ is in cm^{-1} , and 4P and 6S are terms of the free ion. In fact the second term on the right-hand-side of equation (4.9) is an operator which is equivalent to the potential term of the fourth degree with cubic symmetry that satisfies Laplace's equation, i.e. $x^4 + y^4 + z^4 - \frac{3}{5} r^4$ of equation (2.9).

When the six-fold degeneracy is removed in the zero magnetic field, the energies of the two-fold doublet, Γ_7 , and the four-fold quartet, Γ_8 , states are $-2a'$ and $+a'$ respectively.⁵⁶ The four-fold degenerate level may show a further splitting due to Jahn-Teller distortion.⁵² However, such zero-field-splitting for octahedral nd^5 ions, $S=5/2$, is very small even in the solid state. An applied magnetic field prizes the six-fold degeneracy apart and gives rise to spin energy levels at $\pm \frac{1}{2} g\beta_e H$, $\pm \frac{3}{2} g\beta_e H$, and $\pm \frac{5}{2} g\beta_e H$, and thence a single isotropic electron paramagnetic resonance at $g = 2$ which is very easily detected.⁵²

Much later, Abragam and Pryce⁷⁰ pointed out that spin-spin coupling interaction can also contribute small amounts to the observed separations of these levels but to first-order, only if the actual ground term deviates from spherical symmetry. They introduced another zero-field-splitting term of the form $D\{S_z^2 - \frac{1}{3} S(S+1)\}$ into the spin-Hamiltonian and suggested that it arises because small ligand-field components of tetragonal and trigonal symmetries cause a slight distortion of the electron distribution within the nd^5 system. The spin-spin interaction energy then depends on the spin orientation. They found that, to second-order, interactions from this source contribute an amount $D(S_z^2 - \frac{35}{12})$, cf. section 3.2.a, equation (3.17), to the spin-Hamiltonian, where

$$D \propto \frac{U(\beta_e^2 / r^3)}{E(^6D) - E(^6S)} \quad (4.11)$$

where $U = \langle 3d | U_2^0 | 4s \rangle$, $U_2^0 = \frac{1}{4} \sqrt{\frac{5}{\pi}} A_{2,0} (3z^2 - r^2)$, and $E(^6D)$ is the energy of the 6D term arising from the excited $[nd^4(n+1)s]$ configuration.

For an nd^5 ion in an axially symmetric site, complete calculations show that other terms also contribute to the spin-Hamiltonian. The most general spin-Hamiltonian, for the nd^5 ions then becomes⁶²

$$\begin{aligned} \bar{H}_S = & g_{11} \beta_e H_z S_z + g_{\perp} \beta_e (H_x S_x + H_y S_y) \\ & + \frac{1}{6} a' [S_x^4 + S_y^4 + S_z^4 - \frac{1}{5} S(S+1)(3S^2 + 3S - 1)] \\ & + \frac{F}{180} [35 S_z^4 - 30 S(S+1) S_z^2 + 25 S_z^2 - 6 S(S+1) + 3 S^2 (S+1)^2] \\ & + D [S_z^2 - \frac{1}{3} S(S+1)] + A S_z I_z + B (S_x I_x + S_y I_y) \\ & + Q [I_z^2 - \frac{1}{3} I(I+1)] - \gamma \beta_N H \cdot I \quad , \end{aligned} \quad (4.12)$$

in this, the z-axis is the axis of distortion, and the terms in D and F correspond to axial field components of the second and fourth degree, respectively. When all the interactions are now taken into account, the 6A_1 term is finally resolved into three Kramers' doublets, usually separated by less than 1 cm^{-1} , i.e. there are small zero-field-splittings. On inserting the value $S = \frac{5}{2}$, equation (4.12) becomes^{4,71}

$$\begin{aligned} \bar{H}_S = & g\beta_e H.S + \frac{1}{6} a' (S_x^4 + S_y^4 + S_z^4 - \frac{707}{16}) + D(S_z^2 - \frac{35}{12}) \\ & + \frac{7}{36} F(S_z^4 - \frac{95}{14} S_z^2 + \frac{81}{16}) + A S.I \end{aligned} \quad (4.13)$$

The energy level diagram develops as shown in Figure (4.1). Experimentally, g is isotropic and is very close to 2, and A is isotropic, a' and D are usually very small and F is almost negligible. The final energy levels are given by the relationships, (4.14), (4.15), and (4.16)

$$E_{\pm \frac{5}{2}} = \pm \frac{5}{2} g\beta_e H + \frac{10D}{3} \quad (4.14)$$

$$E_{\pm \frac{3}{2}} = \pm \frac{3}{2} g\beta_e H - \frac{2D}{3} \quad (4.15)$$

$$E_{\pm \frac{1}{2}} = \pm \frac{1}{2} g\beta_e H - \frac{8D}{3} \quad (4.16)$$

It should be noted that because of the zero-field-splitting interactions the transitions $\Delta M_S = \pm 1$, now no longer have identical energies, and electron-electron interactions, fine interactions, cause five fine structure components to be obtained in the electron paramagnetic

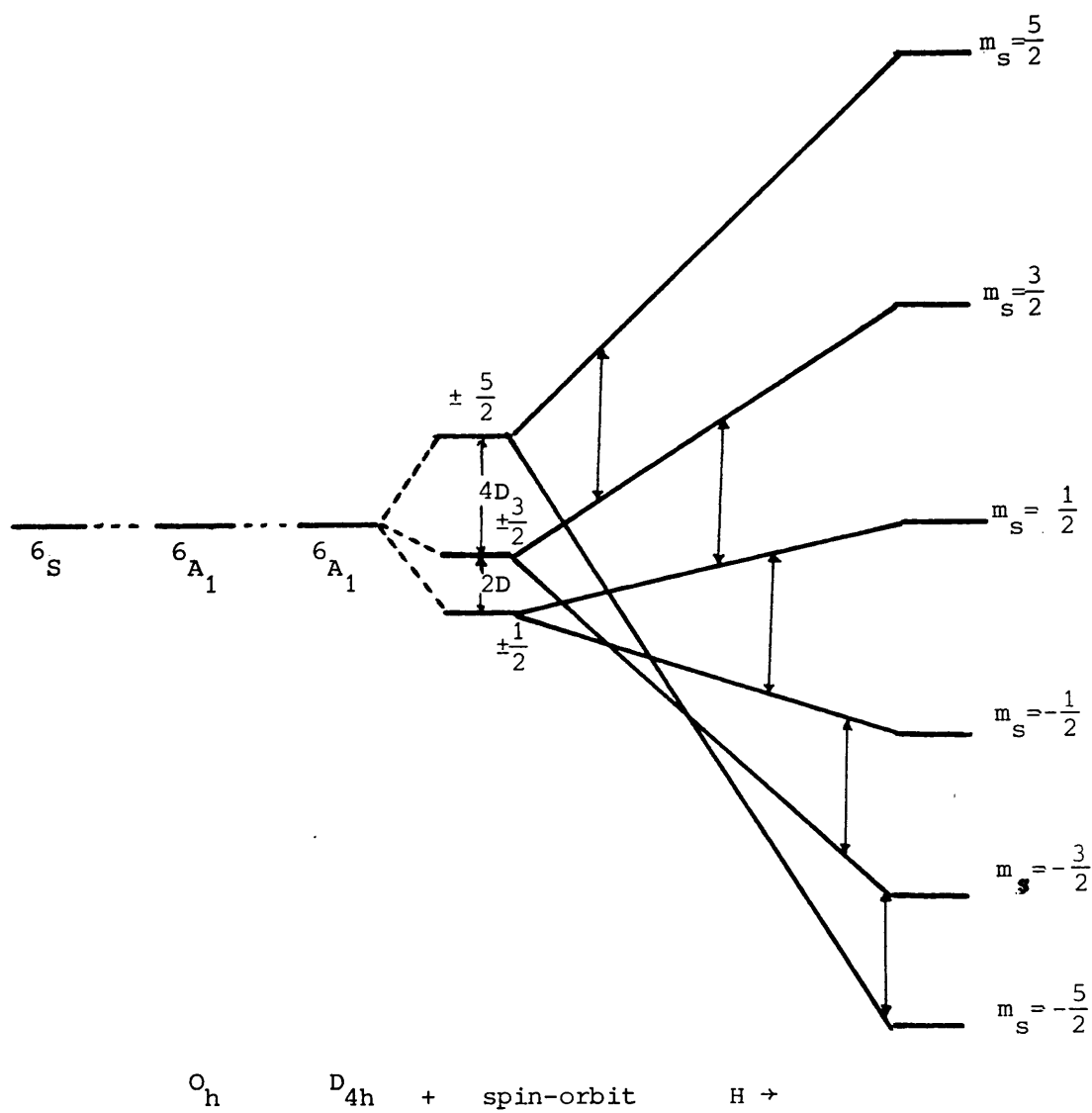


Figure (4.1). Lowest energy levels for nd^5 ions in O_h and D_{4h} symmetry. The effect of spin-orbit coupling and an applied magnetic field is indicated, along with the e.p.r. transitions

resonance spectrum. Naturally occurring ruthenium contains a number of magnetic nuclear isotopes for which $I = 5/2$, so that in principle, hyperfine interactions cause these five fine structure components to split further giving rise in general to a complex electron paramagnetic resonance spectrum pattern.

If the $S = 5/2$ ion lies in a site of orthorhombic symmetry or lower, then the spin-Hamiltonian of equation (4.13) must be modified to

$$\begin{aligned} \bar{H}_S^0 = & g\beta_e (H_x S_x + H_y S_y + H_z S_z) + \frac{1}{6} a' (S_x^4 + S_y^4 + S_z^4 - \frac{707}{16}) \\ & + D(S_z^2 - \frac{35}{12}) + E(S_x^2 - S_y^2) + A(S_x I_x + S_y I_y + S_z I_z) \end{aligned} \quad (4.17)$$

where E is the orthorhombic splitting parameter. In many $S = 5/2$ systems the second and fifth terms on the right-hand-side of equation (4.17) are small and in such cases the spin-Hamiltonian

$$\bar{H}_S^0 = g\beta_e H \cdot S + D[S_z^2 - \frac{1}{3} S(S+1)] + E(S_x^2 - S_y^2) \quad (4.18)$$

then suffices. Many studies involving this spin-Hamiltonian have been carried out,^{65,72-76} and energy level schemes derived and g -values measured. The results of these studies show that it is useful to recognise three limiting situations for high spin, $S = \frac{5}{2}$, nd^5 systems and these three cases are summarized in Figure (4.2). In the first limiting situation the zero-field-splitting parameters D and E are much smaller than the magnetic field energy, $g\beta_e H$ and then the g -factor is 2 and the spectrum already described is obtained.

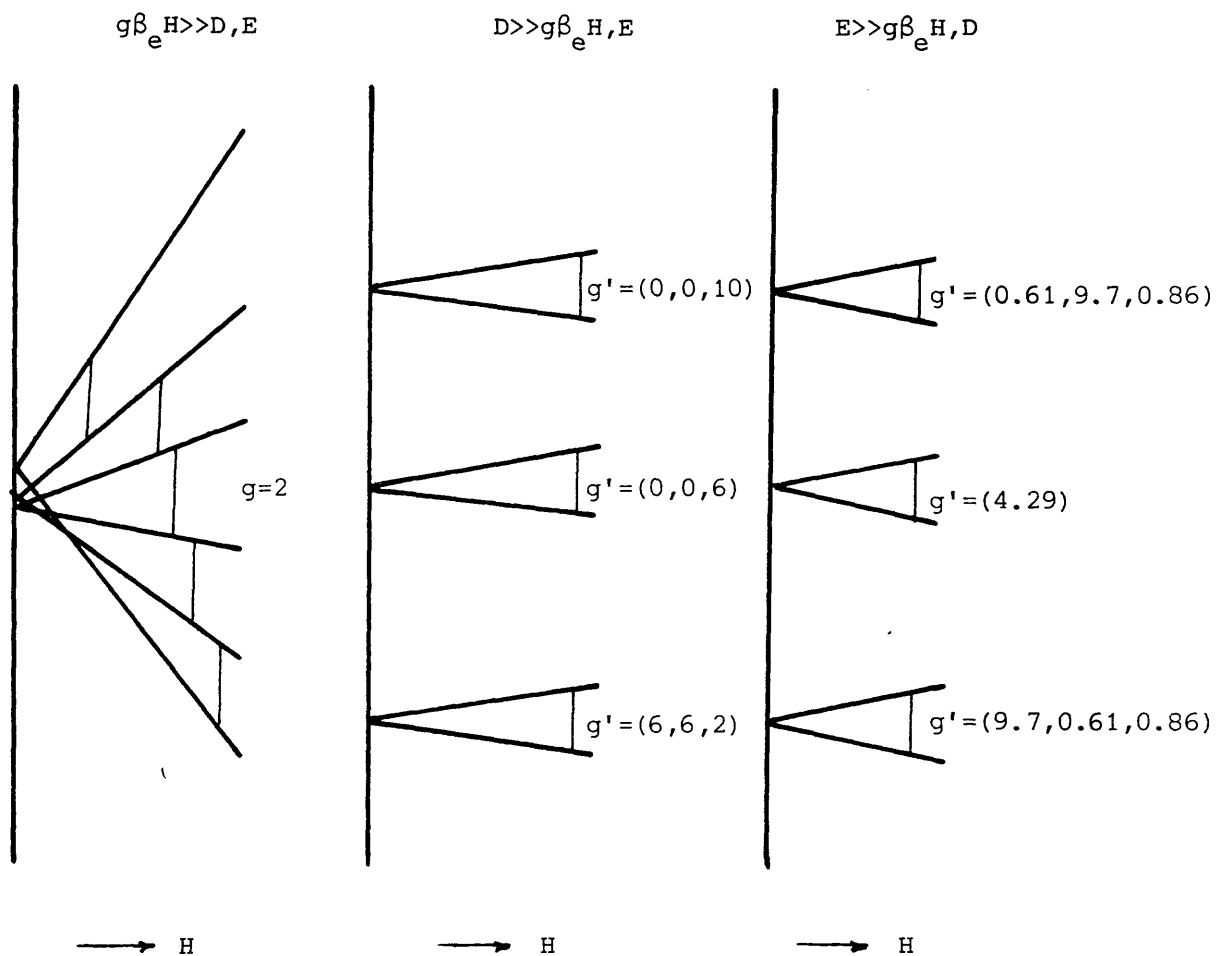


Figure (4.2). Energy levels and apparent g -values assuming that the Zeeman term (left), the axial fine structure term (centre), and the orthorhombic fine structure term (right) are much larger than the other terms.

Spin-Hamiltonian, $\bar{H}_S^0 = g\beta_e H \cdot S + DS_z^2 + E(S_x^2 - S_y^2)$

When $D \gg g\beta_e H$, then the ground doublet is well separated from the excited doublets so that if only those terms in the spin-Hamiltonian that depend on Zeeman interactions are considered then the Hamiltonian

$$\mathcal{H}_S \left(\frac{5}{2} \right) = g\beta_e H \cdot S$$

with six basis states, $|\frac{5}{2}, M_S\rangle$, may be replaced by a new effective spin-Hamiltonian with $S' = \frac{1}{2}$

$$\mathcal{H}_S \left(\frac{1}{2} \right) = g'_{11}\beta_e H_z \cdot S_z + g'_1\beta_e (H_x S_x + H_y S_y) ,$$

this has two basis states $|\frac{1}{2}, M_S\rangle$. It follows⁷⁷⁻⁷⁹ from

$$\begin{aligned} \langle \frac{1}{2} \frac{1}{2} | g'_{11}\beta_e H_z S_z | \frac{1}{2} \frac{1}{2} \rangle &= \langle \frac{5}{2} \frac{1}{2} | g\beta_e H_z S_z | \frac{5}{2} \frac{1}{2} \rangle \\ \langle \frac{1}{2} -\frac{1}{2} | g'_1\beta_e H^+ S^- | \frac{1}{2} \frac{1}{2} \rangle &= \langle \frac{5}{2} -\frac{1}{2} | g\beta_e H^+ S^- | \frac{5}{2} \frac{1}{2} \rangle \end{aligned}$$

that $g'_{11} = g \simeq 2$ and $g'_1 = 3g \simeq 6$ as noted on Figure (4.2).

A number of applications concerning the g' factor have recently appeared⁸⁰ in the literature for several nd^5 ions doped into ZrF_4 glasses. Also several reviews concerning electron paramagnetic resonance studies of high spin, $S = 5/2$, nd^5 complexes have been reported by Porte⁸¹ and Gatteschi.⁸²

4.3 THE ELECTRON PARAMAGNETIC RESONANCE PARAMETERS OF LOW-SPIN, $S = 1/2$, nd^5 IONS

In the presence of a strong octahedral crystal field, the five d-electrons in an nd^5 ion occupy the three orbitally degenerate t_{2g} -orbitals leading to an $S = \frac{1}{2}$ ground state whose spin-Hamiltonian^{52,58,62} can be written experimentally in the form (4.18)

$$\mathcal{H}_{\frac{1}{2}} = \beta_e [g_{xx} H_x S_x + g_{yy} H_y S_y + g_{zz} H_z S_z] + A_{xx} I_x S_x + A_{yy} I_y S_y + A_{zz} I_z S_z \quad (4.18)$$

In the octahedral limit the three t_{2g} -orbitals are degenerate so that the unpaired electron then possesses three-fold orbital degeneracy. The nd^5 ion in that limit therefore has a strong orbital component in its magnetic properties, which enables it to couple strongly with the vibrational modes of both the complex and its lattice. In this limit, therefore, the g-factor differs markedly from the spin-only value, 2.00232, electron spin-relaxation times are very short and e.p.r. spectra are very broad, so that very low temperatures are needed in order to study the e.p.r. phenomena of these systems. These experimental observations essentially still hold for axially distorted or even orthorhombically distorted "octahedral" nd^5 low-spin ions. Theoretical estimations relating spin-Hamiltonian parameters to electron distributions in such complexes, were carried out by Stevens,⁸³ and then in more complete form by Bleaney and O'Brien,⁸⁴ and further extended by Griffith,^{4,85} Thornley⁸⁶ and others,⁸⁷ who all used the hole formalism in which the nd^5 low-spin system is treated as a spherically symmetric t_{2g}^6 configuration containing

one positive hole, i.e. the nd^5 system is formally equivalent to an nd^1 hole.

Theoretical studies of the g-tensors of low-spin nd^5 systems whose symmetries are lower than octahedral, and even tetragonal, have been carried out by several authors,^{4,81,82,84,88-107} and their work has been extended by Hill¹⁰⁸ to incorporate effects of configuration interactions, in which the excited state configuration t_2^4e is mixed into the ground state configuration t_2^5 .

If an octahedron is compressed along its z-axis then the axial contribution, Δ' , to the crystal field interaction lowers the energy of the d_{xy} -orbital relative to the d_{xz} and d_{yz} degenerate pair, and even this degeneracy is removed by an orthorhombic contribution, V'' , to the octahedral field. Often in t_2^5 complexes the crystal field parameters Δ' , V'' and the spin-orbit coupling, ξ_{nl} , are all of the same order of magnitude so that rather than use basis function $\zeta(xy)$, $\eta(xz)$, and $\xi(yz)$ in perturbation calculations leading to spin-Hamiltonian parameters, linear combinations of these of the form

$$|1\rangle = -(\frac{1}{\sqrt{2}}) |\eta(xz) + i\xi(yz)\rangle, \quad |-1\rangle = \frac{1}{\sqrt{2}} |\eta(xz) - i\xi(yz)\rangle, \quad \text{and} \quad \zeta_1 = i\zeta(xy),$$

are used instead as basis. When the five t_2^5 electrons are fed into these orbitals, the following six basis orbital wave functions, eigenfunctions of the free-ion and octahedral crystal field interactions, and of the form $|^2T_2M_S M_L\rangle$ are obtained¹⁰⁸

$$\begin{aligned}
|{}^2T_2 \frac{1}{2} 1\rangle &= |1^+\rangle = -|1^+ -1^+ \zeta_1^+\rangle & |{}^2T_2^{-\frac{1}{2}} 1\rangle &= |\bar{1}\rangle = |\bar{1} -1^+ \zeta_1^+\rangle \\
|{}^2T_2 \frac{1}{2} 0\rangle &= |\zeta_1^+\rangle = -|\bar{1}^+ -1^+ \zeta_1^+\rangle & |{}^2T_2^{-\frac{1}{2}} 0\rangle &= |\bar{\zeta}_1\rangle = |\bar{1} -1^+ \zeta_1^-\rangle \quad (4.19) \\
|{}^2T_2 \frac{1}{2} -1\rangle &= |-1^+\rangle = |\bar{1}^+ -1^+ \zeta_1^+\rangle & |{}^2T_2^{-\frac{1}{2}} -1\rangle &= |\bar{-1}\rangle = |\bar{1} -1^+ \zeta_1^+\rangle
\end{aligned}$$

Perturbation of these simultaneously by low symmetry components of the ligand field interactions and the spin-orbit coupling leads to two identical 3×3 matrices

$$\begin{array}{c|ccc}
& |\pm 1^+ \rangle & |\bar{\zeta}_1^+ \rangle & |\mp 1^+ \rangle \\
| \pm 1^+ \rangle & 2\Delta' + (\xi_{n\ell}/2) & 0 & V''/2 \\
| \bar{\zeta}_1^+ \rangle & 0 & \Delta' & -\xi_{n\ell}/\sqrt{2} \\
| \mp 1^+ \rangle & V''/2 & -\xi_{n\ell}/\sqrt{2} & 2\Delta' - (\xi_{n\ell}/2)
\end{array} \quad (4.20)$$

It should be noted that, if the one-hole formalism is used then the perturbation matrices that are then obtained, are the same as in (4.20) but $2\Delta'$ is subtracted from the elements containing it.

Diagonalization of the two identical matrices, (4.20), then leads to eigenvalues and eigenfunctions of the free ion contribution, all the crystal field contributions, and the spin-orbit contribution to the Hamiltonian of the t_2^5 configuration. In this way the six-fold degeneracy of the 2T_2 term is resolved into three well separated Kramers' doublets.

Eigenfunctions of each of these Kramers' doublets must obviously⁹⁴ have the form

$$\begin{aligned}
\psi_+ &= A'' \left| \begin{smallmatrix} + \\ 1 \end{smallmatrix} \right\rangle + B'' \left| \begin{smallmatrix} - \\ \zeta_1 \end{smallmatrix} \right\rangle + C'' \left| \begin{smallmatrix} + \\ -1 \end{smallmatrix} \right\rangle \\
\psi_+^* &= A'' \left| \begin{smallmatrix} - \\ 1 \end{smallmatrix} \right\rangle - B'' \left| \begin{smallmatrix} + \\ \zeta_1 \end{smallmatrix} \right\rangle + C'' \left| \begin{smallmatrix} - \\ 1 \end{smallmatrix} \right\rangle
\end{aligned} \tag{4.21}$$

where A'' , B'' , and C'' are real and $A''^2 + B''^2 + C''^2 = 1$. In the case of axial symmetry $C'' = 0$. The development of the energy level scheme for these calculations is shown in Figure (4.3).

As shown in the last stage in the development of Figure (4.3), the g-tensor components for the $S = \frac{1}{2}$ system in the lowest Kramers' doublet are obtained by carrying out a standard perturbation calculation involving the Zeeman interaction $V_Z = \beta_e H(g_e S + k' L)$, where k' is the orbital reduction factor which takes account of covalent interactions in the complex. Final results for the g-tensor components turn out to be as shown in (4.22)

$$\begin{aligned}
g_{xx} &= 2[2A''C'' - B''^2 + \sqrt{2} k' B''(C'' - A'')], \\
g_{yy} &= -2[2A''C'' + B''^2 + \sqrt{2} k' B''(A'' + C'')], \\
g_{zz} &= -2[A''^2 - B''^2 + C''^2 + k'(A''^2 - C''^2)]
\end{aligned} \tag{4.22}$$

If configuration interactions, in which the $t_2^4(^1T_2)e$ and $t_2^4(^3T_2)e$ configurations are mixed in with the ground t_2^5 configuration, are taken into account, then the orbital reduction factor is modified to become K'' , where

$$K'' = \left(1 + \frac{12B}{E}\right) k' \tag{4.23}$$

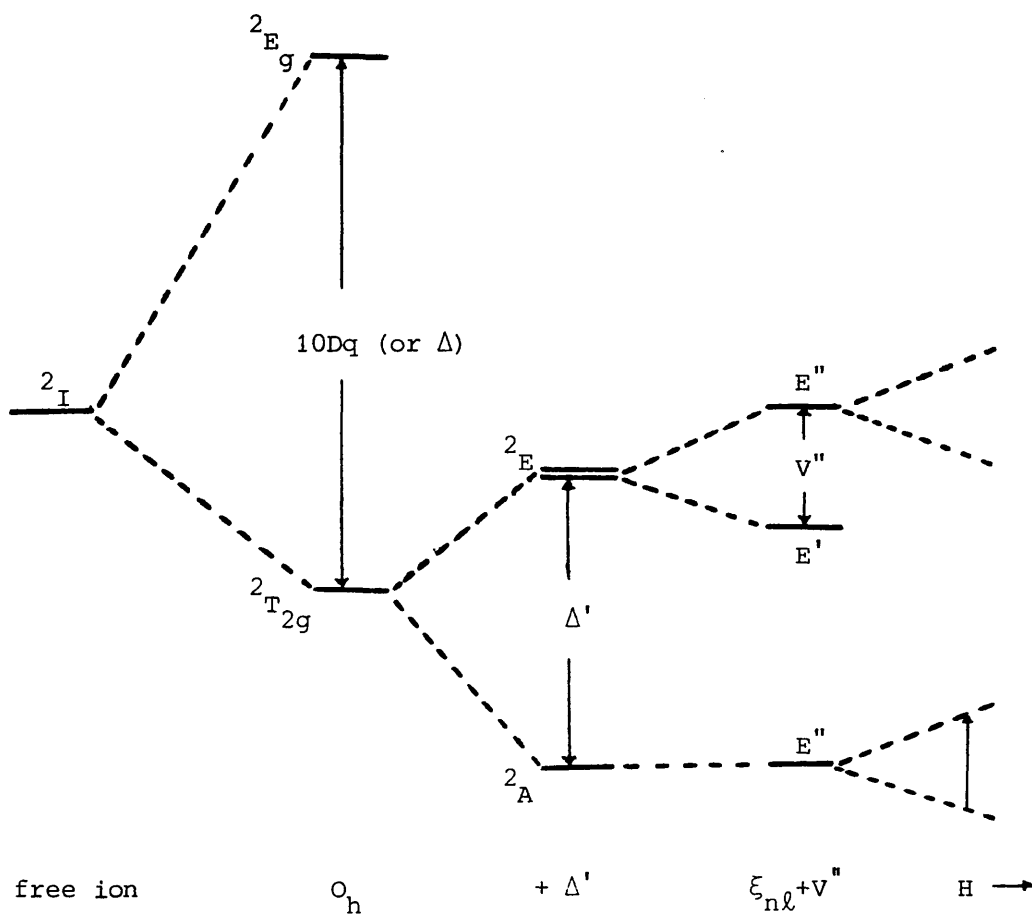


Figure (4.3). Energy level diagram for the $2T_2$ term under the combined influence of the low symmetry field, spin-orbit, and magnetic field perturbations. The positive Δ' value means that the d_{xy} ($2A$ singlet) lies lower than d_{xz} and d_{yz} ($2E$ doublet)

B is a Racah parameter and E is the average value of the d-d transition energies.

Experimental determination of the principal components of the g-tensor, when combined with the normalizing condition $A''^2 + B''^2 + C''^2 = 1$ then leads to solutions for A'' , B'' , C'' , and K'' and thence to the analytical forms of the eigenfunctions ψ_+ and ψ_+^* in (4.21). These in their turn then enable the secular equations (4.24)^{99,104}

$$\begin{aligned} V''/(6\xi_{n\ell}) &= -[(A''\sqrt{2} + B'')/3\sqrt{2}][C''/(C''^2 - A''^2)] \\ \Delta'/\xi_{n\ell} &= -A''/(B''\sqrt{2}) - \frac{1}{2} + (3A''/C'')(V''/6\xi_{n\ell}) \\ E/\xi_{n\ell} &= -A''/(B''\sqrt{2}) - (\frac{2}{3})(\Delta'/\xi_{n\ell}) \end{aligned} \quad (4.24)$$

corresponding to (4.20) to be solved, and thence values of $\Delta'/\xi_{n\ell}$, $V''/\xi_{n\ell}$, and $E/\xi_{n\ell}$ to be deduced from electron paramagnetic resonance measurements. These electron paramagnetic resonance measurements therefore lead to experimental determinations of the separations in the energy level diagram on Figure (4.3).

It should be noted that paramagnetic resonance measurements give only the magnitude of the principal components of the g-tensor. They do not give the signs of these components, nor do they correlate g_1 , g_2 , and g_3 with g_{xx} , g_{yy} , and g_{zz} . If the complex possesses three-fold or higher symmetry axes, however, the g_{zz} component may be assigned to the unique component of the measured g-tensor, and then eight possible sign permutation combinations need to be considered.^{85,91}

For an axially symmetric t_{2g}^5 complex, it can be shown,^{84,93,109,110} that the expressions for the g -tensors, equation (4.22), become

$$g_{11} = -1 + \frac{3(\Delta' - \frac{1}{2} \xi_{nl})}{X} \quad : \quad g_{\perp} = 1 + \frac{\Delta' + \frac{3}{2} \xi_{nl}}{X} \quad (4.25)$$

where $X = [(\Delta' - \frac{1}{2} \xi_{nl})^2 + 2\xi_{nl}^2]^{\frac{1}{2}}$. Elimination of the ratio Δ'/ξ_{nl} yields the theoretical plot¹¹⁰ of the g_{11} versus g_{\perp} shown in the solid curve in Figure (4.4). The experimental points shown for Ru^{3+} and Ir^{4+} fit the theoretical curve quite well and indicate, cf. expression (4.21), that in these complexes the unpaired electron lies essentially in a metal ion d_{xy} orbital.¹⁰⁸ Expressions (4.22) show that a positive g_{11} value arises if $B''^2 > A''^2 + C''^2 + k'(A''^2 - C''^2)$ i.e. the unpaired electron lies in a metal-ion d_{xy} orbital.

More complete analyses,^{84,111,112} which consider the hyperfine coupling tensor components A_{xx} , A_{yy} , and A_{zz} also enable information to be obtained about the mixing coefficients in equations (4.21). For axial symmetry $A_{xx} = A_{yy}$, and

$$\begin{aligned} A_{11} &= P'' \left[\frac{4}{7} - \left(\frac{16}{7} \right) A''^2 - \left(\frac{2\sqrt{2}}{7} \right) A''B'' + k'' (A''^2 - B''^2) \right] \\ A_{\perp} &= P'' \left[\frac{2}{7} - \left(\frac{15\sqrt{2}}{7} \right) A''B'' + k'' B''^2 \right] \end{aligned} \quad (4.26)$$

where the constant P'' is

$$P'' = 2\gamma_N \beta_e \beta_N \langle r^{-3} \rangle \quad (4.27)$$

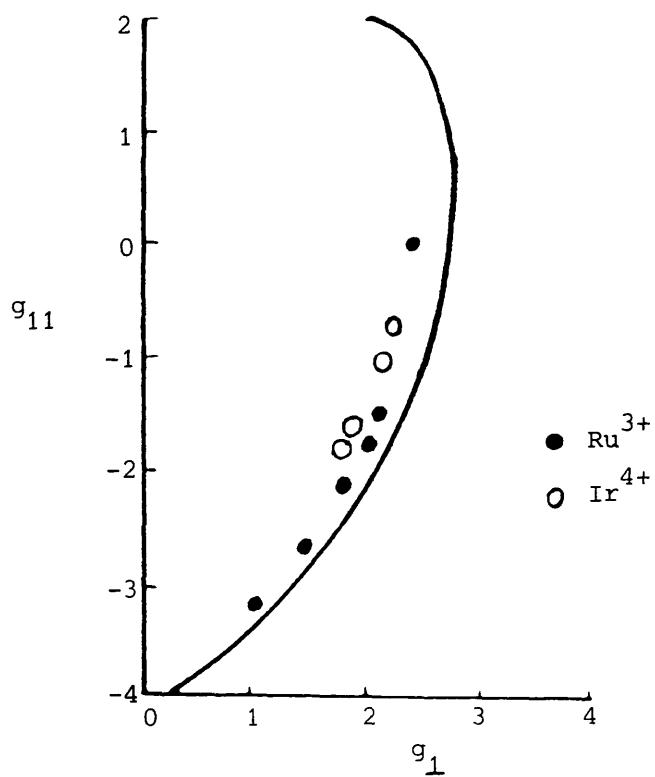


Figure (4.4). Experimental (● and ○) and theoretical (—) g -values for the configurations $4d^5$ and $5d^5$ in strong crystal fields of approximately octahedral symmetry

and k'' is the so-called core-polarization constant.^{70,113} The polarization and direct contact contributions, the Fermi contribution, to the hyperfine coupling can now be separated by means of the relationship

$$\chi'' = -\left(\frac{3}{2}\right) k'' \langle r^{-3} \rangle \quad (4.28)$$

when χ'' is the core-polarization hyperfine field per unit spin.¹¹³ For most transition-metal ions in highly symmetrical environments, the main contribution to χ'' comes from polarization of filled inner s-orbital electrons by exchange interactions with unpaired electrons in d-orbitals of the complex.¹¹⁴

4.4 THE ELECTRON PARAMAGNETIC RESONANCE SPECTRA OF THE nd^5 IONS NEAR TO THE "SPIN CROSS-OVER" POINT

The magnetic properties of octahedral nd^5 complexes in which the crystal field is close to the high spin, ${}^6\text{A}_{1\text{g}}$, \longleftrightarrow low spin, ${}^2\text{T}_{2\text{g}}$, cross-over point are very dependent on temperature, on pressure, and on minor modifications to ligands, or to the crystal-lattice, or to solvent effects.....etc., as already mentioned in section 2.2.c. In many ways the situation is now very similar to that encountered in, for example, proton exchange problems in nuclear magnetic resonance spectroscopy, and essentially two kinds of cross-over situations can be visualized.

On either side of the cross-over point one of the spin-isomers has a lower energy than the other, and in this situation thermal equilibrium, which may or may not be rapid, is set up between the high-spin and the low-spin states. In this case at any temperature the observed magnetic properties are approximately the weighted average of the corresponding high-spin and low-spin properties.⁴ In the other situation at the precise cross-over point the high-spin and low-spin forms have identical energies and then a single "mixed-spin state" exists. The spin state at this point is then some linear combination of all the possible states for which $S = 5/2$ and $S = 1/2$, and the spin quantum number of the complex is now no longer a good quantum number.¹¹⁵

4.4.a HIGH SPIN \longleftrightarrow LOW-SPIN EQUILIBRIUM IN PLANAR nd^5 COMPLEXES

The theoretical formulation of the behaviour of nd^5 systems at, and near to, the cross-over point were developed by Griffith.^{4,79} During the course of this work, he discussed the magnetic properties of some of the planar nd^5 complexes, such as the hydroxide, fluoride, and aquo-complexes.

He assumed that in these complexes the d-orbitals are split by the crystal field into four sets

$$\left. \begin{aligned} E(d_{xz}) &= E(d_{yz}) = 0 \\ E(d_{xy}) & \\ E(d_{z^2}) &= \bar{b} \\ E(d_{x^2-y^2}) &= \bar{c} \end{aligned} \right\} \quad (4.29)$$

where $0 < \bar{b} < \bar{c}$. Then in zero-field the eigenstates are

$$\begin{aligned} \psi_1^\pm &= |\pm \frac{1}{2}\rangle \\ \psi_2^\pm &= a_1 |\pm \frac{5}{2}\rangle + a_2 |\pm \frac{3}{2}\rangle \\ \psi_3^\pm &= a_2 |\pm \frac{5}{2}\rangle - a_1 |\mp \frac{3}{2}\rangle \end{aligned} \quad (4.30)$$

where a_1 and a_2 are real. These are then perturbed by the spin-Hamiltonian, referred to the above energy zero of the form¹¹⁶

$$\mathcal{H} = 2\beta_e (\gamma_1' H_x S_x + \gamma_1' H_y S_y + \gamma_2' H_z S_z) + a(S_x^4 + S_y^4 + S_z^4) + bS_z^2 + cS_z^4 \quad (4.31)$$

where γ_1' and γ_2' are coefficients, related to orbital reduction factor and their values are approximately unity.⁷⁹ If the states (4.30) have energy separations that are large compared with the interactions due to (4.31) then the g-tensor components for the three Kramers' doublets turn out to be

$$\begin{aligned} g_{11}^1 &= 2\gamma_2', & g_{\perp}^1 &= 6\gamma_1', \\ g_{11}^2 &= 2|\gamma_2'(5a_1^2 - 3a_2^2)|, & g_{\perp}^2 &= g_{\perp}^3 = \gamma_1' \sqrt{5} |a_1 a_2|, \\ g_{11}^3 &= 2|\gamma_2'(5a_2^2 - 3a_1^2)|. \end{aligned} \quad (4.32)$$

In a sufficiently strong crystal field $g_{11} = 2\gamma_2'$ and $g_{\perp} = 6\gamma_1'$.

Griffith assumed that for planar nd^5 complexes of haemoglobin, ψ_1^+ is lowest for very large zero field splittings (at least 10 cm^{-1}). This very large zero-field-splitting might originate from admixtures of excited configurations for which $S = 5/2$ (in particular $[nd^4(n+1)s]$ and $[nd^4(n+1)p]$ by the intramolecular field) or from admixture of states of nd^5 having $S = 3/2$ by the field and the spin-orbit coupling interactions. Griffith, also pointed out that the zero-field-splitting might arise from partial delocalization of d_{yz} and d_{xz} electrons into empty π -orbitals on the ligand.

Experimental measurements carried out on the acidic ferri-haemoglobin and the corresponding fluoride complexes^{117,118} agreed with this analysis and their e.p.r. spectra gave $g_{\perp} = 5.90$ and $g_{11} \sim 2.5$ with $\gamma_1' = 0.98$ and $\gamma_2' < 1.25$.

It has already been pointed out, in section 2.2.c, that the ${}^4T_{1g}$ term of the free nd^5 ion can never come lowest in energy in octahedral complexes. However, in D_4 planar compounds, Griffith⁴ very interestingly pointed out that near to their cross-over point, the 4T_1 term of the t_2^4e configuration can become the ground state for a range of Δ (or $10Dq$) values. As shown in Figure(4.5), a D_4 crystal field splits the 4T_1 term into a lower 4A_2 and an upper 4E_2 set of levels. These are separated by $\frac{7}{4} C'$, where

$$C' = \frac{\sqrt{5}}{\sqrt{14}\pi} A_4^4 - \frac{5}{14\sqrt{\pi}} A_4^0 \quad (4.33)$$

The zero-field interactions then lead to Kramers' doublets $E', M_S = \pm \frac{1}{2}$, the lower of the two doublets, and $E'', M_S = \pm \frac{3}{2}$, the higher in energy. To second-order perturbation, the energies of the two Kramers' doublets turn out to be

$$M_S = \pm \frac{1}{2} = E(|{}^4T_1 \frac{1}{2}0\rangle) = \frac{6\xi_{nl}^2}{5(E_6 - E_4)} - \frac{\xi_{nl}^2}{2(E_2 - E_4)} \quad (4.34)$$

$$M_S = \pm \frac{3}{2} = E(|{}^4T_1 -\frac{3}{2}0\rangle) = -\frac{4\xi_{nl}^2}{5(E_6 - E_4)} - \frac{3\xi_{nl}^2}{2(E_2 - E_4)}$$

where E_4 , E_2 , and E_6 are the energies of the 4T_1 , 2T_2 , and 6A_1 terms, respectively. It follows from (4.34) that the $M_S = \pm \frac{1}{2}$ doublet lies lower in energy if $2(E_2 - E_4) > 5(E_6 - E_4)$, and this condition is clearly satisfied near the $({}^6A_1 - {}^4T_1)$ cross-over point. It is not satisfied near the $({}^4T_1 - {}^2T_2)$ cross-over point.

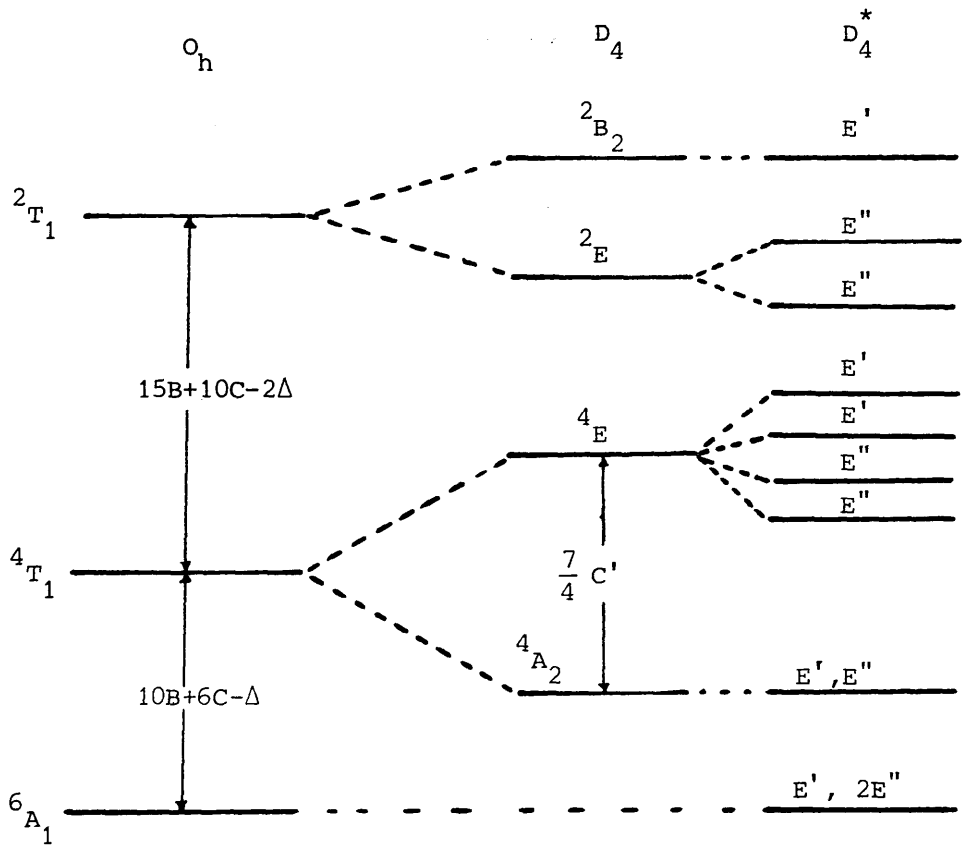


Figure (4.5). First-order electrostatic, crystal-field and spin-orbit coupling energies of the sextet, quartet and doublet states

These results are shown schematically in Figure (4.6). The ground doublet passes from being pure 6A_1 through being nearly pure 4T_1 at the region of the diagram where E'' passes below E' , and finishes up as pure 2T_2 . This figure holds the clue to understanding the complicated magnetic properties of these D_4 species.

Several authors have studied the thermal equilibrium between high-spin and low-spin systems.^{49,119-127} Nishida and his coworkers¹²² have examined, (i) high spin, (ii) low spin, and (iii) complexes near to the cross-over point of different nd^5 systems with different point-group symmetries. Their studies of the electron paramagnetic resonance spectra of high-spin complexes cover the range $1000 \ll H \ll 3000$ gauss. Spectra of low-spin complexes are observed at 3000 gauss, spectra of complexes near to the cross-over point have signals in the range $1000 \ll H \ll 2700$ gauss, and at about 3000 gauss. For this last type of complex Nishida *et al.* observed that as the temperature is lowered, the relative intensities of the different absorption regions change dramatically, but their resonant field values do not change. The intensities of the absorptions at about 3000 gauss are noticeably enhanced when the temperature is lowered. The relative populations in the high and low spin forms can be obtained from intensity measurements of these electron paramagnetic resonance spectra,¹²³ and such studies show that the population of the low-spin ground state 2T_2 increases as the temperature decreases. An upper limit for the frequency of flipping between the high-spin and low-spin forms can be obtained when distinct electron paramagnetic resonance signals are observed for both the 6A_1 and 2T_2 species.

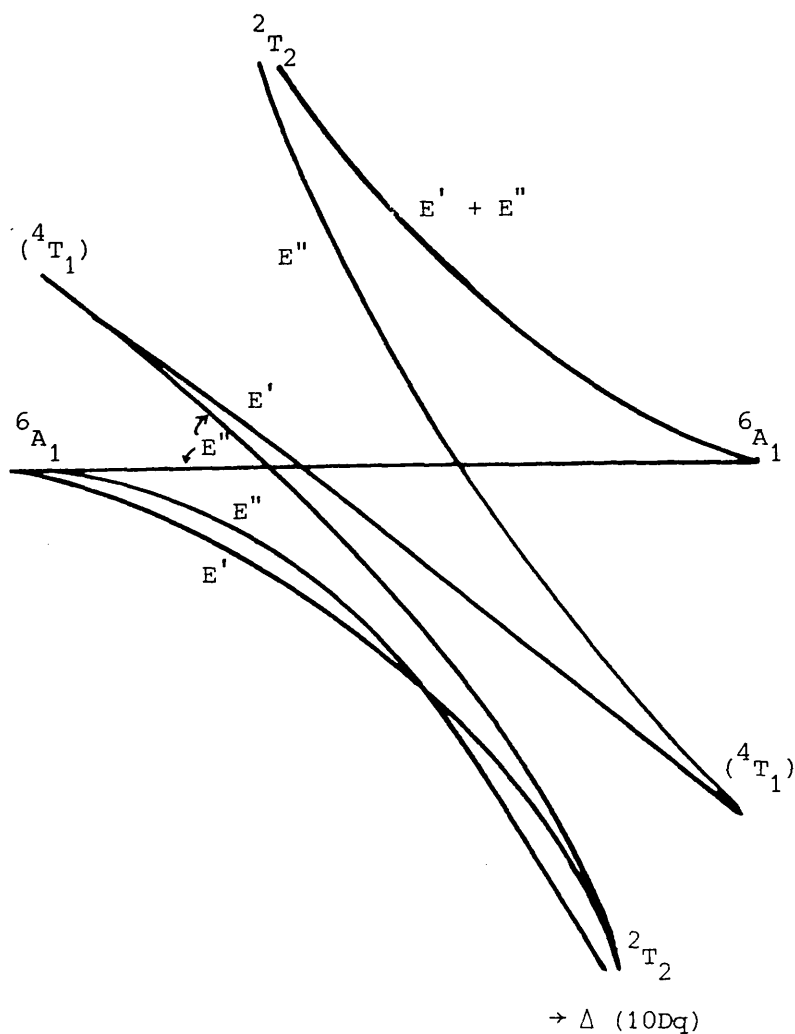


Figure (4.6). Schematic representation of the details of the cross-over in planar D_4^* , O_h and 5 complexes. At the left-hand side of the diagram the term energies are ordered as in octahedral, O_h complexes. Under the influence of D_4^* $6A_1 \rightarrow E' + 2E''$, $4A_2(4T_1) \rightarrow E' + E''$, and $2T_2 \rightarrow E' + 2E''$

4.4.b "MIXED-SPIN" SYSTEMS

The theoretical treatments of mixed-spin systems were developed by Harris.¹¹⁵ He assumed that the wave function for any mixed-spin system originating from the zero-field Kramers' doublets of an nd^5 configuration could be written as a linear combination of the twelve sextet, quartet, and doublet terms, listed in Table (4.1). The precise details of Harris's calculations are tortuous and complicated. His papers¹¹⁵ are 65 pages long and the reader is referred to them for full details. Each of the two components of the zero-field doublets does not mix with the other in the mixed-spin system, and Harris showed that the two sets of 12 x 12 matrices each factorize into linear combinations

$$\psi_{ij} = \sum_{j=1}^7 a_{ij} \phi_{ij} \quad (4.35)$$

involving the seven basis functions listed under the heading, "E" 7 x 7 matrix" shown in Table (4.1), and further linear combinations

$$\chi_{ij} = \sum_{j=8}^{12} a_{ij} \phi_{ij} \quad (4.36)$$

listed under the heading "E" 5 x 5 matrix" in the same Table.

The degeneracies of these twelve doubly degenerate linear combinations split under an applied magnetic field, and calculations of g-tensor components for each of the linear combinations, can then be carried out using the general techniques described earlier.

Table (4.1)*

E'' (7 x 7) matrix						
ϕ_i	$E''\alpha''$		$ S\Gamma O_h\rangle$	$ S\Gamma D_4\rangle$	$E''\beta''$	
	$ M_S$	$\Theta\rangle$			$ M_S$	$\Theta\rangle$
1	5/2	i	6A_1	6A_1	-5/2	i
2	-3/2	i	6A_1	6A_1	3/2	i
3	-3/2	0	4T_1	4A_2	3/2	0
4	3/2	1	4T_1	4E	-3/2	-1
5	-1/2	-1	4T_1	4E	1/2	1
6	-1/2	1	2T_2	2E	1/2	-1
7	1/2	0	2T_2	2B_2	-1/2	0
E' (5 x 5) matrix						
ϕ_i	$E'\alpha'$		$ S\Gamma O_h\rangle$	$ S\Gamma D_4\rangle$	$E'\beta'$	
	$ M_S$	$\Theta\rangle$			$ M_S$	$\Theta\rangle$
8	1/2	i	6A_1	6A_1	-1/2	i
9	1/2	0	4T_1	4A_2	-1/2	0
10	-1/2	1	4T_1	4E	1/2	-1
11	3/2	-1	4T_1	4E	-3/2	1
12	-1/2	-1	2T_2	2E	1/2	1

* The 24 basic states in this Table can be labelled by $|S\Gamma M_S \Theta\rangle$, where S is the total spin of the state, M_S is the z-component of the total spin, Γ is the irreducible representation of the group to which they belong, and Θ is the component of that representation. Complex components, 1, 0, and -1 were used for the three-fold degenerate T_i representations.

Harris showed, for tetragonal complexes, that when the field is parallel to the molecular z-axis then the g_{11} -factor associated with each of the seven ψ_{ij} eigenfunctions of the E'' states is

$$g_{11}(E'') = |-10a''^2 + 6b''^2 + 6c''^2 - 7d''^2 + 3e''^2 + 4f''^2 - 2g''^2| \quad (4.37)$$

where a'' , b'' , c'' ,etc. are the coefficients a_{ij} , $J = 1-7$, in expression (4.35). Similarly, for the five χ_{ij} eigenfunctions of the E' states, the g_{11} value is

$$g_{11}(E') = |-2h''^2 - 2i''^2 + j''^2 - 5\ell''^2| \quad (4.38)$$

where h'' , i'' ,etc. are the coefficients a_{ij} , $j = 8-12$, in expression (4.36).

Harris also deduced that, for tetragonal complexes, the corresponding expressions for perpendicular components of the g-tensors are given by

$$g_{\perp}(E'') = |2\sqrt{5}a''b'' + 2\sqrt{3}d''e'' + \sqrt{2}c''d'' - \sqrt{2}f''g'' + 2g''^2| \quad (4.39)$$

for an electron in an E'' state, and

$$g_{\perp}(E') = |6h''^2 + 4i''^2 + \sqrt{3}i''j'' + 2\sqrt{3}j''\ell''| \quad (4.40)$$

for an electron in an E' state.

The magnitudes of the mixing coefficients (4.35) and (4.36) depend on the precise details of the spin-mixing processes so that the g -components of the mixed Kramers' doublets can vary over a wide range of values. The g_{11} value of the twelve doublets range from 0 to 10.

As the tetragonal field parameter C' , in equation (4.33), is changed, mixing coefficients in (4.35) and (4.36) change, and so, therefore, do the spin-mixed g_{11} and g_{\perp} values. Plots of Harris's g_{11} and g_{\perp} values for the lowest spin-mixed Kramers' doublet versus C' are shown in Figures (4.7a) and (4.7b). These figures effectively show how spin-mixing alters g_{11} and g_{\perp} values of this doublet. The value of $g_{11} = 3.30$ at the low-spin end of Figure (4.7a), where $C' = 2000 \text{ cm}^{-1}$, reflects the fact that in this region the ground state is a pure doublet but contains some of the character of 2E and 2B states, i.e. the coefficients f'' and g'' in equation (4.37) are large. The value of g_{\perp} at this region is 1.02 due to the last two terms in equation (4.39). When C' increases, increasing mixing of the ${}^6A_1 (\pm\frac{3}{2})$ state then takes place, i.e. contribution from the terms in b'' in expressions (4.37) and (4.39) then increases. $|g_{11}|$ then increases towards the ${}^6A_1 (\pm\frac{3}{2})$ value of 6, whereas the combined effects of changes in the values of a'' and b'' in (4.39) cause the g_{\perp} value to diminish and approach the value of zero in the limit for the pure ${}^6A_1 (\pm\frac{3}{2})$ state. It should be noted that in the spin-mixed region, Harris's calculations indicate that for the ground state the g_{11} value for a sextet-doublet spin-mixed state varies from 3 to 6 and g_{\perp} from 1 to zero. Harris's calculations also predict much larger zero-field-splittings in the spin-mixed region than those that are encountered for the corresponding high-spin compounds, and lower values than encountered for the corresponding low-spin compounds.

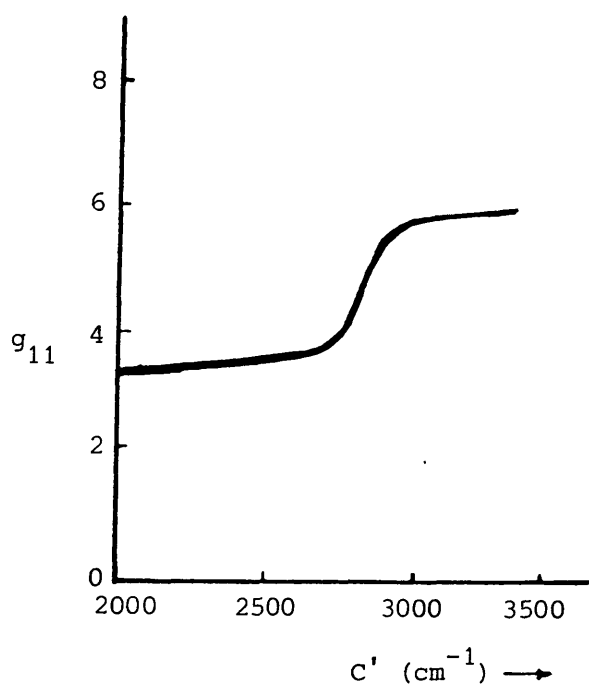


Figure (4.7a)

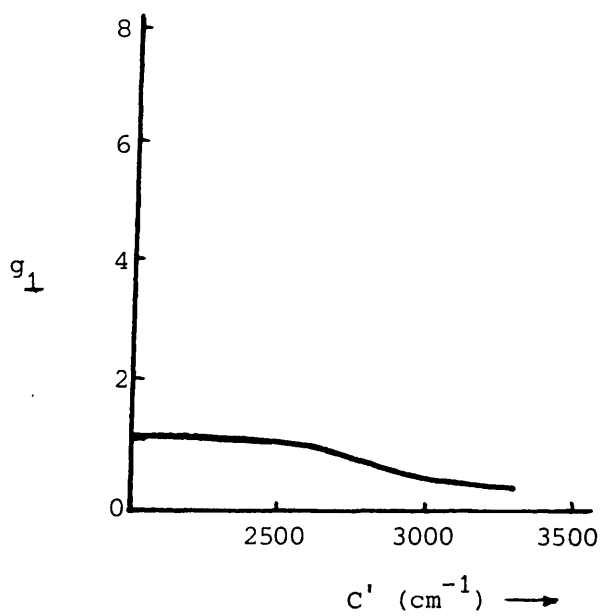


Figure (4.7b)

4.5 ELECTRON PARAMAGNETIC RESONANCE DATA FOR Ru³⁺

COMPLEXES

Electron paramagnetic resonance methods do not seem to have been used to study the electronic structure of the only reported³³ high-spin Ru³⁺ complex, NH₄[RuNOCl₅].

All e.p.r. studies of Ru³⁺ complexes, reported^{91, 93, 94, 99-105} in the literature are low-spin 4d⁵ systems, and therefore their e.p.r. properties are covered by the theory in section 4.3. For some complexes whose point group symmetries are lower than octahedral, for example, some of the complexes with sulfur-chelates,⁹⁴ β -diketones,⁹⁸ oximes,¹⁰⁰ or amines,¹⁰² the experimental data, when combined with the expressions mentioned in (4.3) yield two acceptable solutions for the electron distributions in the ground state.

(i) The hole is in the d_{xy} orbital, Figure (4.3); and $\Delta'/\xi_{n\ell}$ is large, i.e. $\Delta' > \xi_{n\ell}$, corresponding to a "large distortion". This solution requires $|g_{zz}| < |g_{xx}|, |g_{yy}|$ and g_{zz} is positive, g_{xx}, g_{yy} are negative.

(ii) The hole is in a linear combination, $\mp \frac{1}{\sqrt{2}}(d_{xz} \pm id_{yz})$ and $\Delta'/\xi_{n\ell}$ is small, corresponding to a "very small distortion". This solution requires $|g_{zz}| > |g_{xx}|, |g_{yy}|$ and $g_{zz}, g_{xx},$ and g_{yy} are all negative. Table (4.2) shows the values of $|g_1|, |g_2|, |g_3|, A'', B'',$ and C'' for some Ru³⁺ complexes. Table (4.3) shows the corresponding values of $k', \Delta'/\xi_{n\ell}, V''/\xi_{n\ell},$ and $E/\xi_{n\ell}$, cf. section 4.3.

Table (4.2)

Complex	Point group	g_{av}	$ g_1 ^{(\ell)}$	$ g_2 ^{(\ell)}$	$ g_3 ^{(\ell)}$	$A''(a)$	$B''(a)$	$C''(a)$	Reference
Ru^{3+} in $K_3InCl_6 \cdot 2H_2O$			1.0	1.22	3.24				128
Na_3RuCl_6 in $HCl\ell$		2.0							129
Ru^{3+} in $Al(acac)_3^b$	C_2		2.82	1.28	1.74				130
Ru^{3+} in YGa Garnet			3.113	-	1.148				112
$RuCl_3(PMe_2Ph)_3$	C_{2v}		2.03	1.66	2.88				91
$RuCl_3(AsPr_3)_3^c$	C_{2v}		2.06	1.64	2.93				91
$[Ru(Phen)_3]^{3-}$			1.00		-2.63				93
$[Ru(en)_3]^{3+ d}$			<0.66		2.64				106
$[Ru(C_2O_4)_3]^{3-}$			1.76	2.02	2.30	0.215	0.974	-0.067	94
$Ru(sacsac)_3^e$			1.992	2.031	2.109	0.029	0.999	-0.013	94
$[Ru(mnt)_3]^{3- f}$			1.968	2.026	2.12	0.075	0.997	-0.03	94
$Ru(dtc)_3^g$			1.979	2.109	2.156	0.074	0.997	-0.01	94
$Ru(dtp)_3^h$			1.982	2.055	2.085	0.06	0.998	-0.009	94
$[Ru(dto)_3]^{3- i}$			1.98		2.04	0.066	0.998	0.00	94

[contd.]

Table (4.2) contd.

Complex	Point group	g_{av}	$ g_1 ^{(\ell)}$	$ g_2 ^{(\ell)}$	$ g_3 ^{(\ell)}$	$A''(a)$	$B''(a)$	$C''(a)$	Reference
$[\text{Ru}(\text{NH}_3)_5\text{Cl}]^{2+}$ b			2.98	-0.99	1.51	0.384	0.920	-0.057	99,100
$[\text{RuCl}_4(\text{AsPh}_3)_2]^+$	D_{4h}	2.20	1.67		2.46	0.212	0.977	0.0	96
$\text{RuCl}_2(\text{dbm})(\text{AsPh}_3)_2^j$		2.14	-1.87		-2.27	0.154	0.988		101
$[\text{RuCl}_2(\text{HL})\text{L}]^k$	C_{2v}		1.849		-2.47	0.153	0.988		103
$\text{trans-}[\text{RuCl}_2(\text{NH}_3)_4]^+$	C_{4v}		3.33	-1.18	1.54	0.37	0.93	0.04	105
$\text{cis-}[\text{Ru}(\text{en})_2\text{Br}_2]\text{ClO}_4$			2.82	-1.02	-2.41	0.463	0.875	0.140	104

(a) Values of A'' , B'' , and C'' are those according to solution (i), p. . (b) Single crystal, (acac) \equiv acetylacetone. (c) $\text{Pr} \equiv$ propyl. (d) $\text{en} \equiv$ ethylenediamine. (e) $\text{sacsac} \equiv$ dithioacetylacetone. (f) $\text{mnt} \equiv$ 1,2-dicyanoethylene-1,2-dithiolate. (g) $\text{dte} \equiv$ dimethyldithiocarbamate. (h) $\text{dtp} \equiv$ diphenyldithiophosphoric acid. (i) $\text{dto} \equiv$ dithio oxalate. (j) $\text{dbm} \equiv$ dibenzoylmethanate. (k) $\text{L} \equiv \text{R}'\text{RC}_2\text{O}_2\text{NH}$; $\text{R}' = \text{Ph}$, $\text{R} = \text{Me}$. (ℓ) where no sign is given, the figure shown is the modulus of the value.

Table (4.3)

Complex	k'	$\Delta'/\xi_{n\ell}^*$	$V''/\xi_{n\ell}^*$	$E/\xi_{n\ell}^*$	Reference
$[\text{Ru}(\text{C}_2\text{O}_4)_3]^{3-}$	0.44	4.0	-0.48		94
$\text{Ru}(\text{sacsac})_3$	0.96	37.72	-5.36		94
$\text{Ru}(\text{dte})_3$	0.70	10.20	-0.53		94
$[\text{Ru}(\text{dto})_3]^{3-}$	0.26	11.05	0.0		94
$\text{Ru}(\text{dtp})_3$	0.46	12.56	-0.71		94
$[\text{Ru}(\text{mnt})]^{3-}$	0.41	11.94	-1.69		94
$\text{RuCl}_2(\text{acac})(\text{AsPh}_3)_2$	0.90	5.489	0.0	-5.59	101
$\text{RuCl}_2(\text{dbm})(\text{AsPh}_3)_2$	0.74	4.924	0	-5.03	101

* In units of $\xi_{n\ell}$

Very few reported e.p.r. spectra of Ru^{3+} complexes show hyperfine splitting patterns. However, an e.p.r. spectrum of an $\alpha\text{-Al}_2\text{O}_3$ crystal, containing 0.01% Ru, enriched with 91% of ^{101}Ru , does show hyperfine splittings¹³¹ as illustrated in Figure (4.8a). Di Simone⁹⁴ managed to prepare a small quantity of $^{101}\text{Ru}(\text{detc})_3$ ($\text{detc} \equiv \text{diethyldithiocarbamate}$) from 97% ^{101}Ru enriched $\text{RuCl}_3 \cdot x\text{H}_2\text{O}$, and the 77K e.p.r. spectrum of this complex exhibits the hyperfine splitting pattern due to ^{101}Ru , shown in Figure (4.8b). The six parallel components of the spectrum, due to ^{101}Ru , $I = 5/2$, are clearly resolved. However, the six perpendicular components are not. Di Simone has estimated that $A_{11} = 38 \pm 1$ gauss and $A_{\perp} = 21 \pm 3$ gauss for this complex. Table (4.4) lists hyperfine parameters for several complexes of Ru^{3+} .

The free ion values¹³³ of $\langle r^{-3} \rangle$ and χ'' for the Ru^{3+} ion, of 6.5 and -8.5 a.u. respectively, are only consistent with the measured A_{11} and A_{\perp} values for $\text{Ru}(\text{detc})_3$ if $B'' \gg A''$, and the ratio of $\frac{A_{11}}{A_{\perp}} < 0$, and the hole resides in the d_{xy} orbital of the complex. These conclusions are consistent with the presence of large low symmetry distortions in this complex. The e.p.r. data yield an estimated $\langle r^{-3} \rangle$ value of 2.7 a.u. This represents a reduction of 60% from the corresponding value of the Ru^{3+} ion, and indicates a considerable metal-ligand interaction. Spin-orbit coupling values also depend directly¹³⁴ on $\langle r^{-3} \rangle$, hence the estimated $\langle r^{-3} \rangle$ value indicates that the $\xi_{n\ell}$ value in this complex is about 480 cm^{-1} compared with the corresponding value of about 1250 cm^{-1} for the free ion. The negative value of k'' , Table (4.4), yields a value of $\chi'' = + 3.84$ a.u., and this positive polarization can only be obtained if a very small amount of direct admixture of 5s and 4d orbitals, cf.

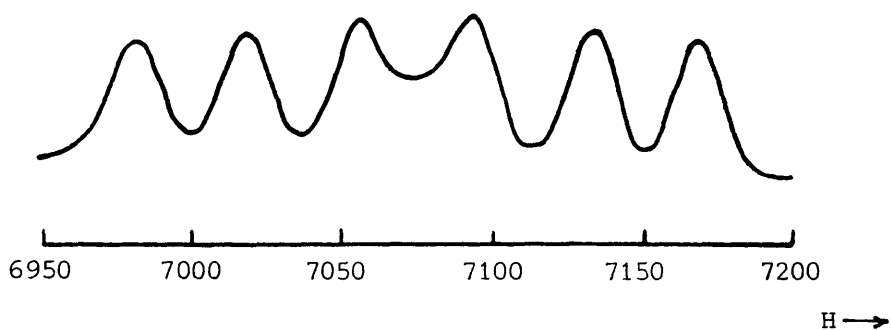


Figure (4.8a). Single crystal e.p.r. spectrum obtained from a sample of $\alpha\text{-Al}_2\text{O}_3$ doped with ^{101}Ru , enriched to 91%, at 20.4°C

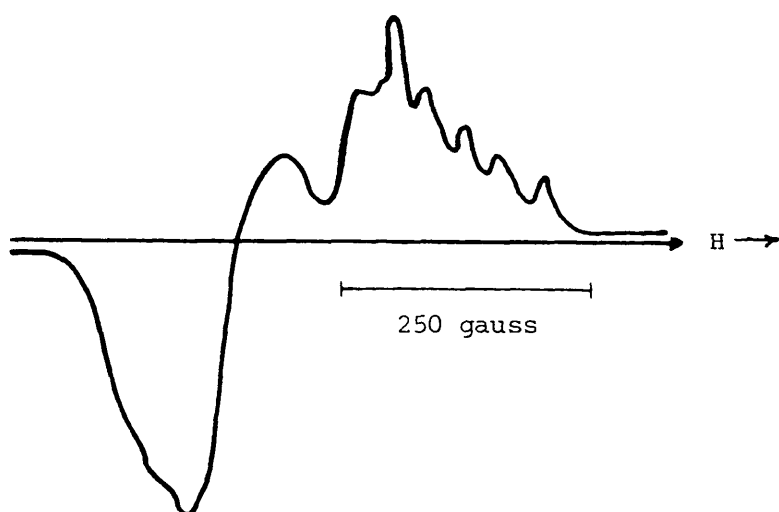


Figure (4.8b). E.p.r. spectrum of $^{101}\text{Ru}(\text{detc})_3$ at 77K , showing hyperfine splitting due to ^{101}Ru

Table (4.4)
Hyperfine interaction parameters of some of Ru^{3+} complexes

Complex	$A_{11} \times 10^4 \text{ cm}^{-1}$	$A_{\perp} \times 10^4 \text{ cm}^{-1}$	$P'' \text{ cm}^{-1}$	$k'' \text{ cm}^{-1}$	$\langle r^{-3} \rangle \text{ a.u.}$	$\chi'' \text{ a.u.}$	Reference
Ru^{3+} in YGa Garnet	63.8	38.0					112
Ru^{3+} in YAl Garnet	56.4	41.0					112
$\text{Ru}(\text{detc})_3$	38 ± 1	21 ± 3	-24×10^{-4}	-0.945	2.71	+ 3.84	94
$\text{Ru}(\text{MeC} \& \text{dtP}_i)^*$	36.0	25.0					132

* $\text{MeC} \& \text{dtP}_i \equiv \text{tris-}[\text{di}(2\text{-methyl-5-chlorophenyl})\text{dithiophosphato}]$

p.143 is present in order to offset the relatively small effect of direct polarization of the inner electron by the unpaired valence electron.

Mixing of this kind is also allowed in D_3 complexes and in most complexes of low symmetry.⁹⁴

Thiol complexes of Ru^{3+} turn out to be very covalent.⁹⁴ In them the unpaired electron is in a molecular orbital compounded from ligand group orbitals and the metal ion $4d_{xy}$ orbital. The reduced values of $\langle r^{-3} \rangle$ and $\xi_{n\ell}$, and the anisotropic covalent interactions, are natural consequences of the electron delocalization in these complexes.

- CHAPTER FIVE -

THE REACTION OF SOLID "RUTHENIUM TRICHLORIDE",

$\text{RuCl}_3 \cdot x\text{H}_2\text{O}$, AND SOLID BENZOIN, Ph-CO-CH(OH)Ph

5.1 INTRODUCTION

Most of the e.p.r. work summarized in Table (4.2) involves polycrystalline studies. Very few highly detailed magnetically-dilute single-crystal studies of Ru^{3+} complexes have been carried out, and for this reason it was decided to examine the reactions of Ru^{3+} with several oxy-chelates, and then with the corresponding thio-chelates. The oxy- and thio-chelates listed in Table (4.2) mostly involve six-membered-ring chelates and for this reason it was decided originally to concentrate attention on five-membered-ring chelates, and therefore on derivatives of benzoin and thiobenzoin.

Several attempts to prepare Ru^{3+} -chelates of benzoin and its derivatives were made, using standard methods in which buffered solutions of Ru^{3+} were refluxed with the ligands. The Ru^{3+} source used was "ruthenium trichloride", $\text{RuCl}_3 \cdot x\text{H}_2\text{O}$, purchased from "Johnson-Matthey Chemicals". These solution techniques surprisingly proved to be quite unsuccessful and so eventually the solid " $\text{RuCl}_3 \cdot x\text{H}_2\text{O}$ " and solid benzoin, Ph-COCHOH-Ph , were finally intimately mixed and heated together. This procedure caused obvious reactions to take place. After a great deal of investigation at least some of the details of these reactions were eventually unravelled. As it turned out, they certainly did not produce paramagnetic Ru^{3+} -chelates of the kind originally envisaged. Instead, some rather complex solid state reactions took place, and these form the subject matter of this chapter of this thesis. A mixture of techniques was used in this work, including microanalysis, ^1H and ^{13}C nuclear magnetic resonance spectroscopy, mass spectroscopy, infrared, visible-ultra-violet spectroscopy, electron paramagnetic resonance spectroscopy

and magnetic susceptibility measurements. These studies and their results will now be considered.

5.2 THE SOLID STATE REACTION: THE EXPERIMENTAL

PROCEDURE

Benzoin (1.4g), potassium bicarbonate (0.8g), and Johnson-Matthey Chemicals "ruthenium trichloride", $\text{RuCl}_3 \cdot x\text{H}_2\text{O}$, (0.25g) were intimately mixed and then heated carefully at 140°C under dry conditions for 40 hours. The mixture was then cooled and the dark brown residue washed with hot hexane in order to remove unreacted benzil that formed in the reaction. The residue was then extracted with dichloromethane giving an olive-green solution extract. Chloroform could also be used for this extraction. The residue was then filtered off and rejected, and the olive-green dichloromethane-extracted filtrate was then left to allow the solvent to slowly evaporate away. The olive-green residue remaining after this evaporation was then collected and purified by recrystallization several times from dichloromethane.

A solution of the purified olive-green solid in dichloromethane was then finally chromatographed using a column of neutral aluminium-oxide D. The eluant was then collected and the dichloromethane solvent evaporated to yield an olive-green solid which showed only one spot on a t.l.c. plate.

The carbon and hydrogen content of this olive-green solid was determined by microanalysis. The ruthenium content was estimated spectrophotometrically as the yellow-orange 1,10-phenanthroline

ruthenium(II) complex, $[\text{Ru}(\text{C}_{12}\text{H}_8\text{N}_2)_3]^{++}$, using $\text{Ru}(\text{acac})_3$ as standard.¹³⁵

The results listed in Table (5.1) are consistent with the empirical formula $\text{RuC}_{56}\text{H}_{42}\text{O}_2$. Corresponding calculated percentage compositions based on this formula are also given in Table (5.1).

Table (5.1)

Microanalyses and spectrophotometric results obtained from

the olive-green compound, $\text{RuC}_{56}\text{H}_{42}\text{O}_2$

Element	Calculated %	Found %
C	79.33	80.8
H	4.95	5.2
Ru	11.93	11.30

5.3 THE PROTON MAGNETIC RESONANCE SPECTRUM OF

OLIVE-GREEN RuC₅₆H₄₂O₂

A 90 MHz ^1H nuclear magnetic resonance spectrum obtained from a solution of $\text{RuC}_{56}\text{H}_{42}\text{O}_2$ in CDCl_3 , recorded on a PERKIN-ELMER spectrometer operating at room temperature, is shown in Figure (5.1). An expanded form of the same spectrum is shown in Figure (5.2).

Except for minute amounts of impurities in the olefinic region, in the range $5.24 \leq \delta \leq 5.5$, and in the aliphatic region, at $\delta \approx 1.3$, the only absorptions in this spectrum fall in the chemical shift range $6.4 \leq \delta \leq 8.4$. Furthermore, this spectrum consists of sharp resonance signals superimposed on top of a very broad background absorption.

Integration of the aromatic region of the spectrum enables it to be subdivided into two main regions, whose relative intensities are 1:2.5, or any multiple of these values, for example 12:30. Alternatively the spectrum can be described as consisting of a sharp region, decomposable into two parts whose relative intensities are 1:1.5, the latter being superimposed on a broad absorption of relative intensity 1, giving rise to three regions whose relative intensities are 12:18:12.

The expanded ^1H n.m.r. spectrum in Figure (5.2) shows these three sections of relative intensities 1:1.5:1 better, the first two figures referring to the sharp region of the spectrum and the last to the broad region.

Superimposed on the broad back-ground mentioned above is the sharp resonance from CHCl_3 in the CDCl_3 used as solvent, and two additional sharp signals in the region $7 \leq \delta \leq 7.3$ that may be

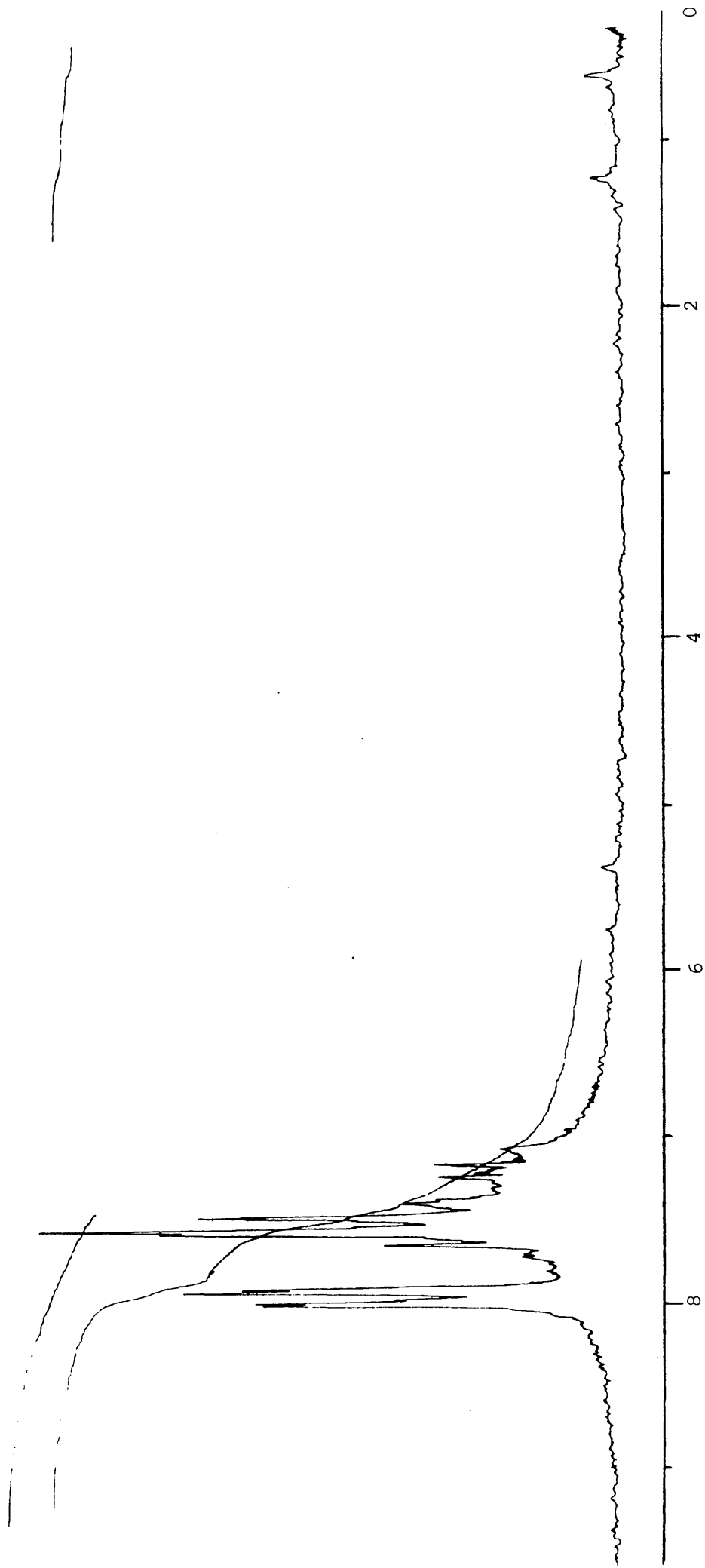


Figure (5.1). ^1H n.m.r. spectrum, $\nu = 90$ MHz, of $\text{RuC}_{56}\text{H}_{42}\text{O}_2$ in CDCl_3 solution, at 295K

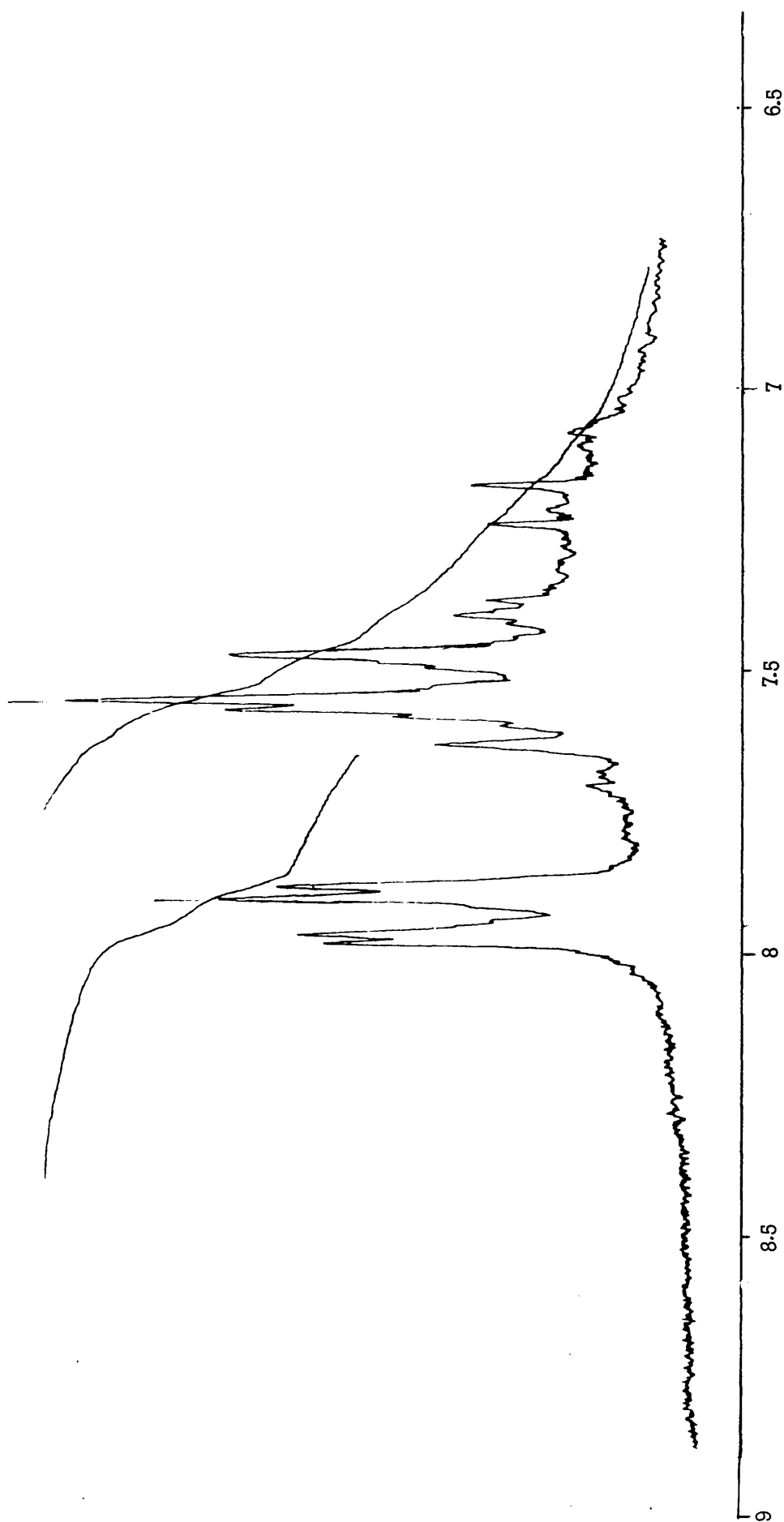


Figure (5.2). ^1H n.m.r. spectrum, $\nu = 90$ MHz, of $\text{RuC}_{56}\text{H}_{42}\text{O}_2$ in CDCl_3 solution, at 295K

assignable to highly conjugated olefinic residues.

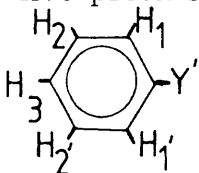
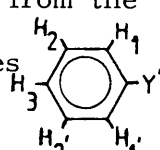
The proton resonance spectrum shows that all protons in this compound are aromatic, or are mainly aromatic along with some highly conjugated olefinic protons. The sharp pattern in the spectrum, consisting of the region of the relative intensities of 1:1.5, is exactly the pattern expected for the five protons of six equivalent mono-substituted phenyl residues  whose theoretical spectrum is constructed stepwise in Figure (5.3). Proton chemical shifts and coupling constants extracted from this spectrum are listed in Table (5.2). The broad underlying region of the ^1H n.m.r. spectrum must arise either from a further twelve aromatic protons, or from further aromatic protons and protons from a highly conjugated olefinic residue that is attached to the aromatic rings.

Table (5.2)

^1H chemical shifts and H-H coupling constants obtained from the spectrum of the mono-substituted phenyl residues 
in $\text{RuC}_{56}\text{H}_{42}\text{O}_2$

^1H Chemical shifts (δ)		^1H - ^1H Coupling constants (Hz)	
$\text{H}_1=\text{H}_{1'}$	7.945	$\text{J}_{12}=\text{J}_{23}$	8.13
$\text{H}_2=\text{H}_{2'}$	7.530	J_{13}	1.98
H_3	7.464		

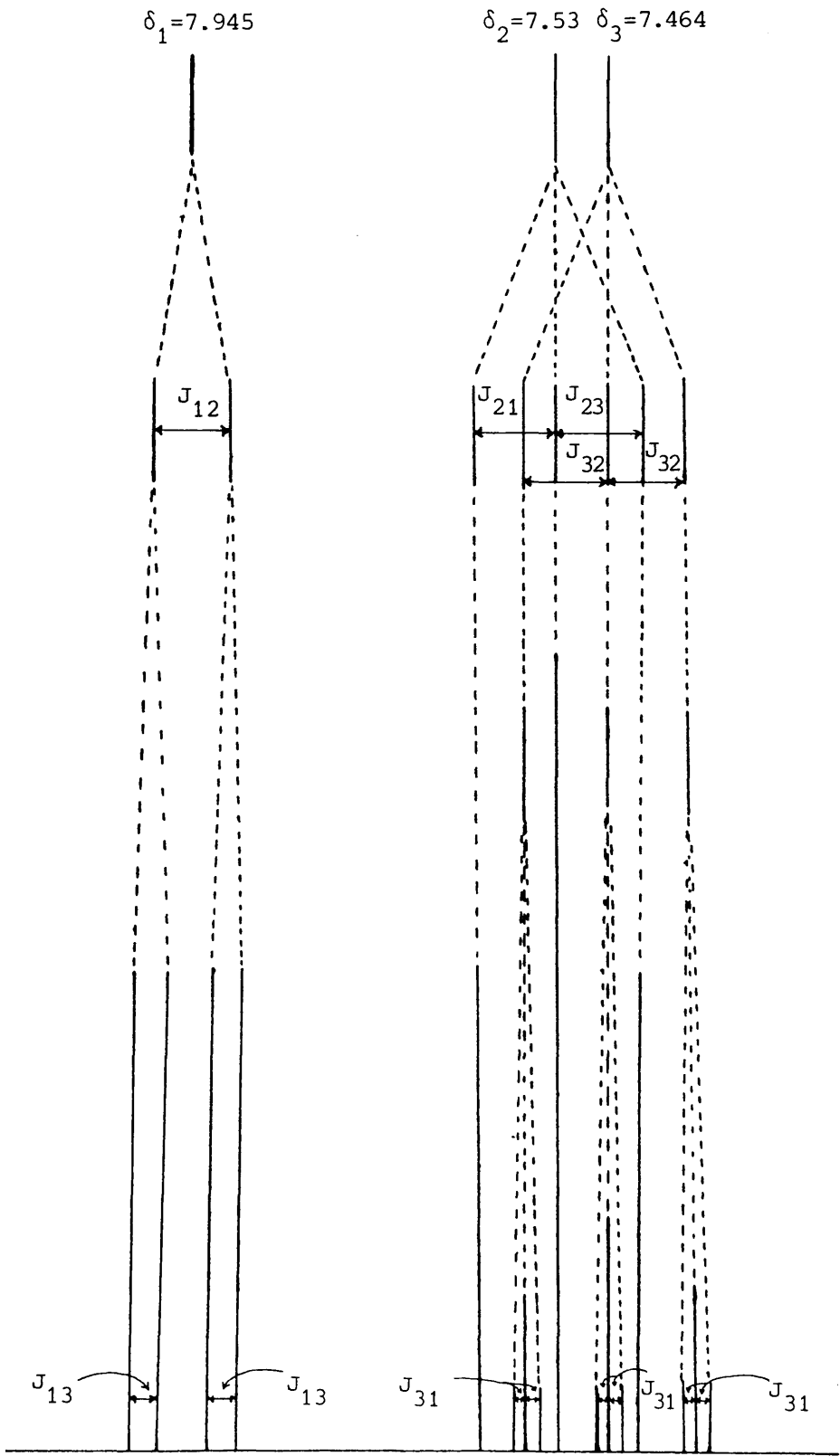


Figure (5.3)

5.4 THE ^{13}C NUCLEAR MAGNETIC RESONANCE SPECTRUM OF OLIVE-GREEN $\text{RuC}_{56}\text{H}_{42}\text{O}_2$

Fully decoupled $^{13}\text{C}-\{^1\text{H}\}$, partially decoupled $^{13}\text{C}-\{^1\text{H}\}$ and fully coupled ^{13}C nuclear magnetic resonance spectra of a solution of this compound in CDCl_3 , are shown in Figures (5.4), (5.5) and (5.6), respectively; the spectra were recorded on a VARIAN 100 n.m.r. spectrometer operating at 25.16 MHz. These spectra show quite clearly that carbonyl groups and aromatic groups, plus possibly highly conjugated olefinic residues, only are present in this compound.

In the fully decoupled $^{13}\text{C}-\{^1\text{H}\}$ spectrum shown on Figure (5.4), the relative intensity of carbonyl carbon to other ^{13}C signals turns out to be 1:(28 \pm 1), or 2:(56 \pm 2). Although Overhauser effects can seriously influence the equation of intensities with numbers of nuclei in such spectra, nevertheless the ratio of 2:(56 \pm 2), when considered in conjunction with the microanalytical results, indicates that there are two carbonyl residues and 54 other carbon atoms in this compound. Furthermore, on Figure (5.6) the ^{13}C carbonyl region consists of two peaks separated by 3.7 Hz which collapse into a single resonance in the $^{13}\text{C}-\{^1\text{H}\}$ decoupled spectra on Figures (5.4) and (5.5). The two carbonyl carbons are therefore equivalent, and each interacts weakly with one proton in the molecule.

Figure (5.4) shows that four different types of carbon atoms contribute to the aromatic region of the spectrum, and their relative abundances are in the ratios 1:1:2:2. Furthermore, one of these is a tertiary-carbon atom and all other carbons are attached to one hydrogen

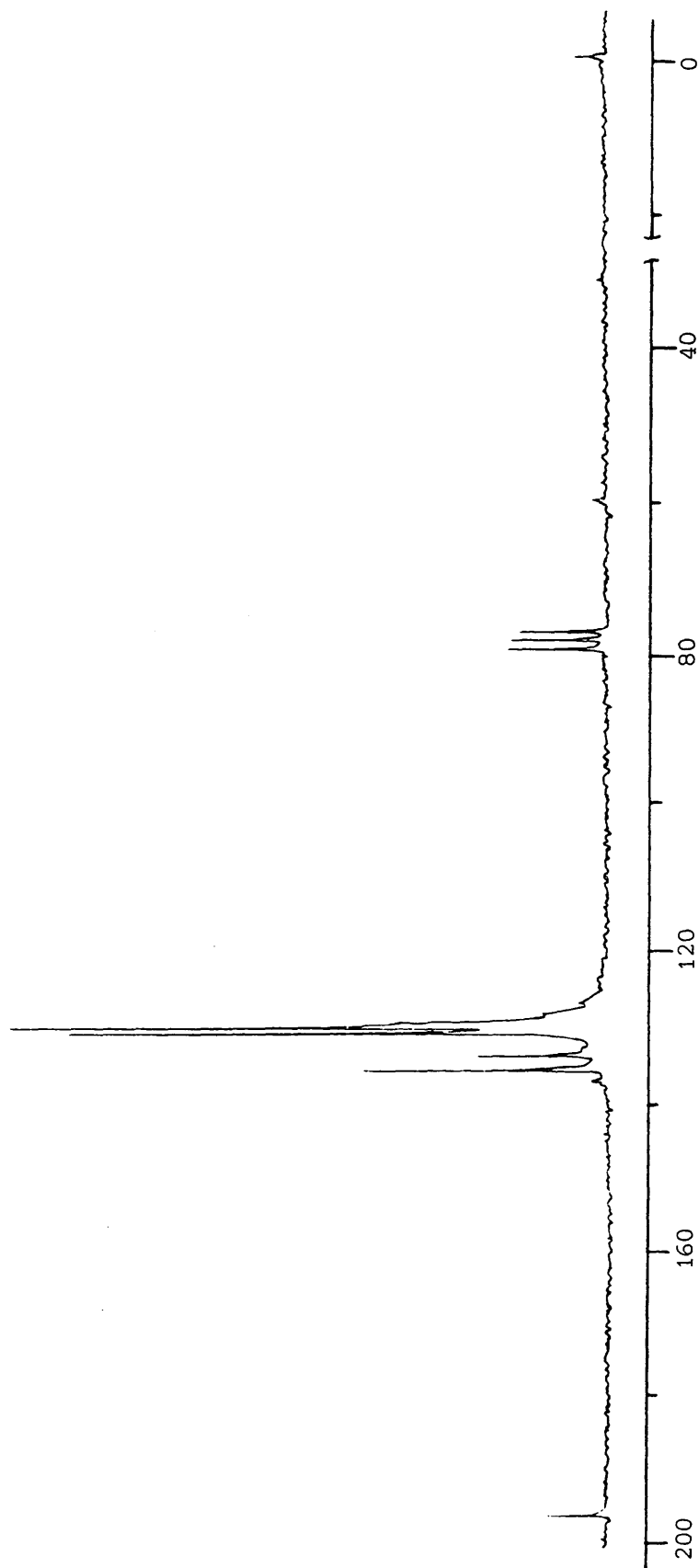


Figure (5.4). Proton-decoupled, fully, ^{13}C n.m.r. spectrum, $\nu = 25.16$ MHz, of $\text{RuC}_{56}\text{H}_{42}\text{O}_2$, in CDCl_3 solution, at 295K

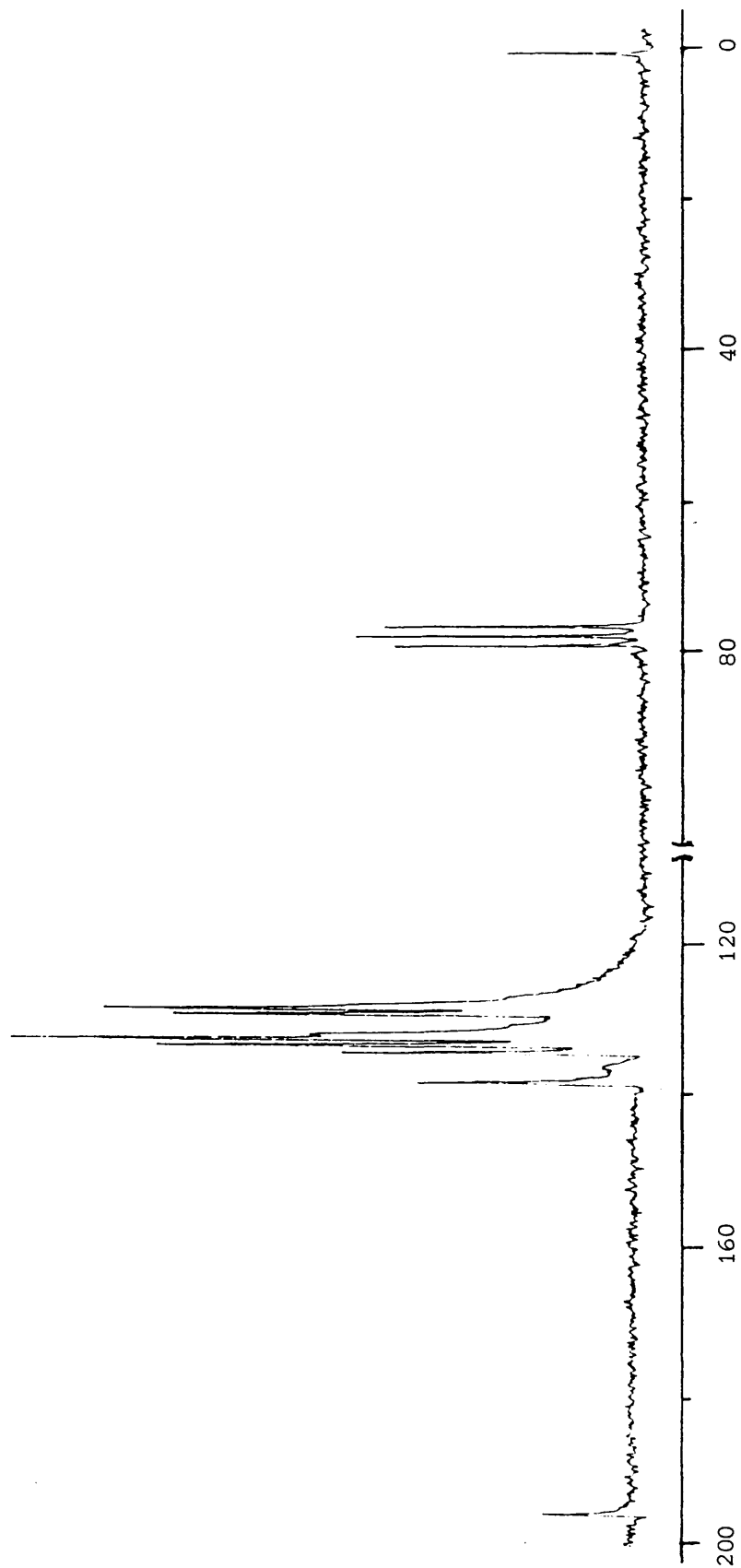


Figure (5.5). Proton-decoupled, partially, ^{13}C n.m.r. spectrum, $\nu = 25.16$ MHz, of $\text{RuC}_{56}\text{H}_{42}\text{O}_2$, in CDCl_3 solution, at 295K

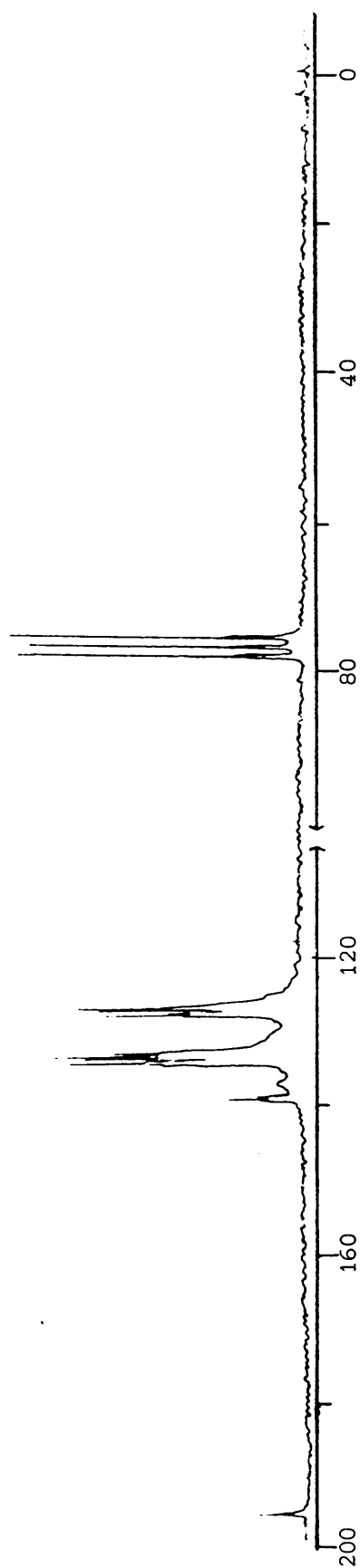
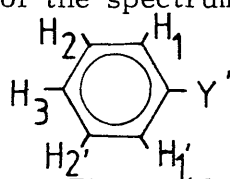


Figure (5.6). Proton-coupled ^{13}C n.m.r. spectrum, $\nu = 25.16$ MHz, of $\text{RuC}_{56}\text{H}_{42}\text{O}_2$, in CDCl_3 solution, at 295K

atom. An additional broad unresolved spectrum also underlies the aromatic carbon region, and it may indicate the existence of other aromatic ^{13}C -atoms, or else additional highly conjugated olefinic carbon atoms.

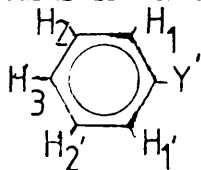
Figure (5.7) is an expanded version of the aromatic region of the ^{13}C n.m.r. spectrum of $\text{RuC}_{56}\text{H}_{42}\text{O}_2$, and Figure (5.8) shows how it can be reconstructed from a superposition of the spectrum of equivalent mono-substituted residues of the form

^{13}C chemical shifts and ^{13}C - ^1H coupling



constants for the phenyl residues extracted from Figure (5.8) are listed in Table (5.3).

The microanalytical results, the ^1H n.m.r. spectrum, and the ^{13}C n.m.r. spectrum all indicate that the formula for this substance is $\text{RuC}_{56}\text{H}_{42}\text{O}_2$. The magnetic resonance spectra show that the molecule contains six effectively "equivalent" mono-substituted phenyl residues



where y' is either a carbonyl group or is a conjugated olefinic system, or is possibly another aromatic residue, whose magnetic resonance spectra are broadened for some reason or

another. The ^{13}C n.m.r. spectrum reveals the presence of two equivalent carbonyl groups in this compound. Furthermore, there are no other functional groups present in the organic fragments in this molecule. Both the ^1H and ^{13}C n.m.r. spectra show that there are additional aromatic, and possibly highly conjugated olefinic residues present in this structure and that their spectra are broadened, presumably by molecular motions at these sites in the molecule, which

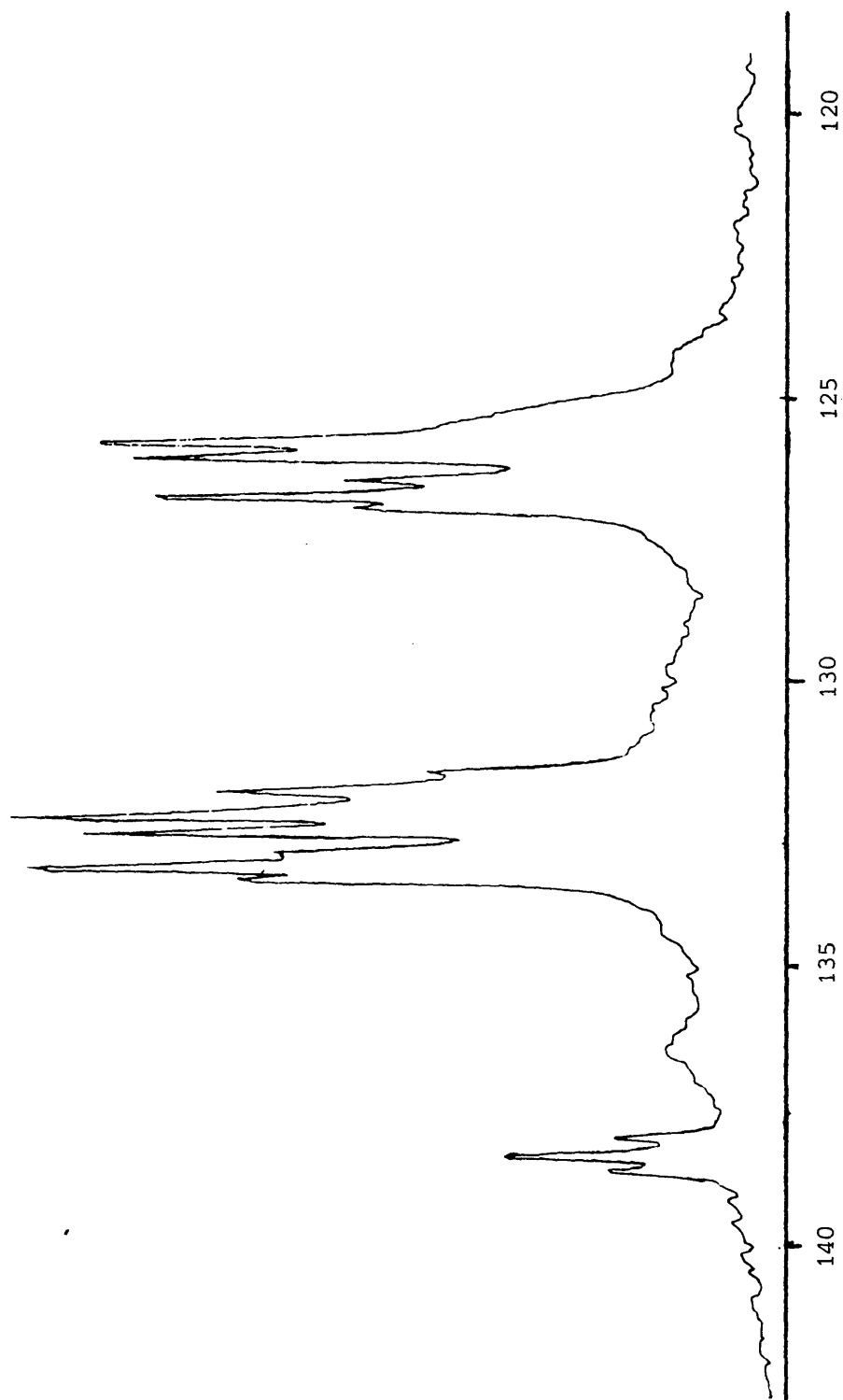


Figure (5.7). Proton-coupled ^{13}C n.m.r. spectrum, $\nu = 25.16$ MHz, of $\text{RuC}_{56}\text{H}_{42}\text{O}_2$, in CDCl_3 solution, at 295K

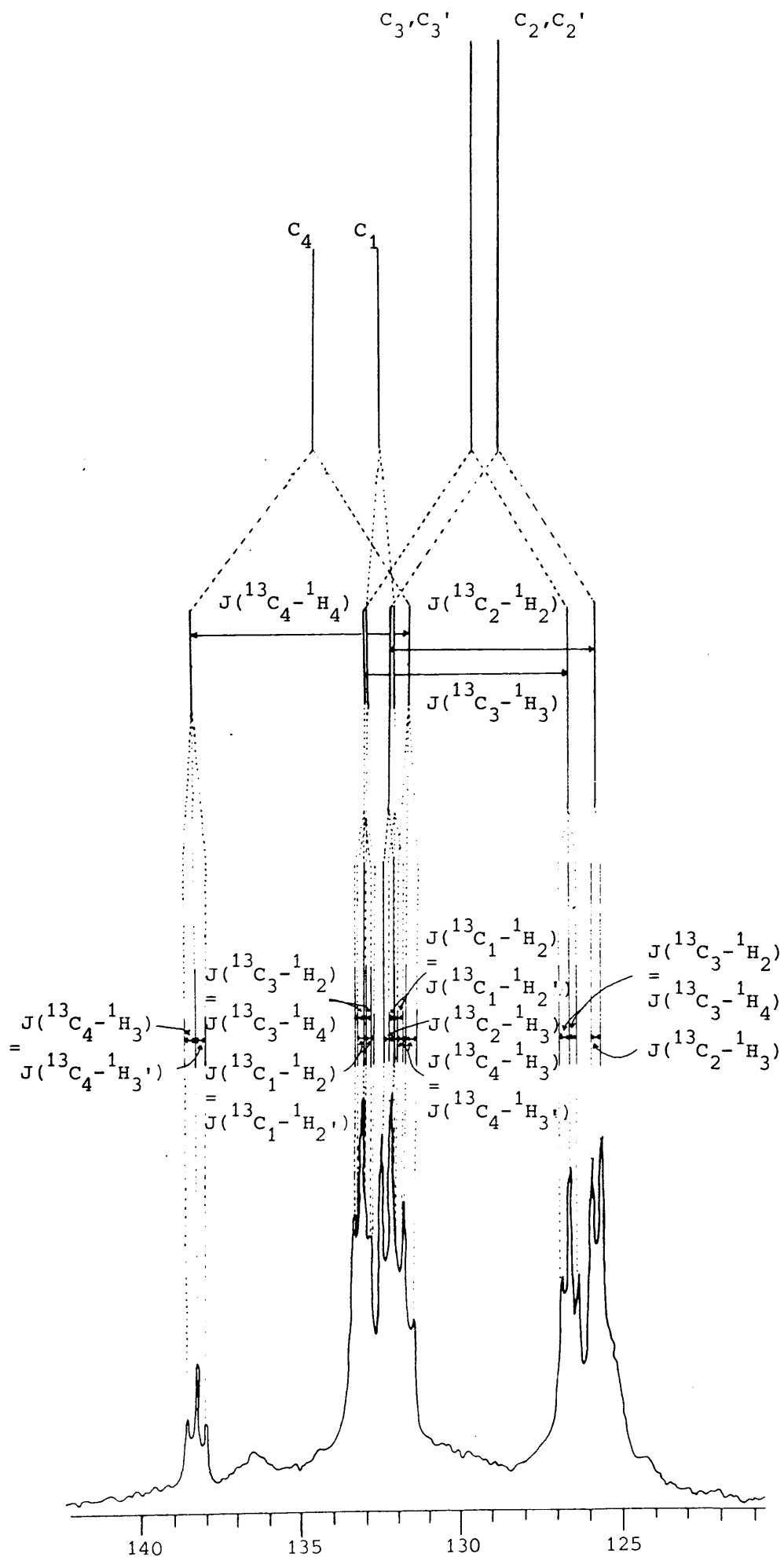
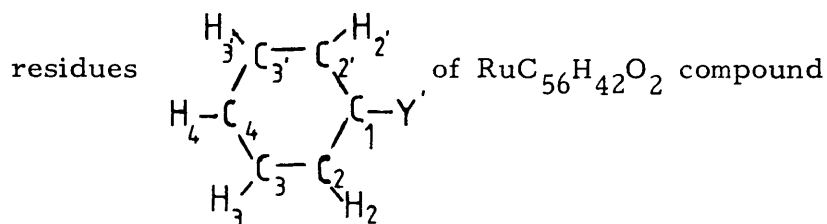


Figure (5.8)

Table (5.3)

^{13}C chemical shifts and ^{13}C - ^1H coupling constants for the phenyl



^{13}C -Chemical shifts (ppm)		^{13}C - ^1H Coupling constants (Hz)	
C_1	132.9	$\text{C}_2\text{-H}_2$	161.02
$\text{C}_2=\text{C}_{2'}$	128.9	$\text{C}_3\text{-H}_3$	159.01
$\text{C}_3=\text{C}_{3'}$	129.7	$\text{C}_4\text{-H}_4$	169.07
C_4	134.8	$\text{C}_1\text{-H}_2=\text{C}_1\text{-H}_{2'}$	8.05
		$\text{C}_2\text{-H}_3=\text{C}_{2'}\text{-H}_{3'}$	8.05
		$\text{C}_3\text{-H}_2=\text{C}_3\text{-H}_4$	8.05
		$\text{C}_{3'}\text{-H}_{2'}=\text{C}_{3'}\text{-H}_4$	
		$\text{C}_4\text{-H}_3=\text{C}_4\text{-H}_{3'}$	10.06

are slow on the magnetic resonance time scales. These broadened regions involve 12 protons and 18 carbons. The broadened region may therefore be due to two additional phenyl residues plus another six carbons which would need to be highly conjugated in order to fall into the aromatic region of ^{13}C n.m.r. spectrum.

5.5 THE INFRARED SPECTRUM OF OLIVE-GREEN $\text{RuC}_{56}\text{H}_{42}\text{O}_2$

The infrared spectrum of solid $\text{RuC}_{56}\text{H}_{42}\text{O}_2$, in a KBr disc, is shown in Figure (5.9) and the wavenumbers and the assignments of the peaks in this Figure are listed in Table (5.4); this spectrum was recorded on a PERKIN-ELMER 580 infrared spectrometer.

Figure (5.10) is a line diagram of the superimposed infrared absorptions expected¹³⁶ for, (i) a carbonyl residue,^{136a} (ii) a mono-substituted phenyl residue,^{136b} (iii) an olefinic residue,^{136c} and (iv) an acetylenic residue.^{136d} When the composite line spectrum in Figure (5.10) is compared with the experimental spectrum shown in Figure (5.9) then the following points become obvious.

I - This compound contains two carbonyl residues which are not quite equivalent in the solid. This follows because two very strong absorptions, at 1660 cm^{-1} and 1680 cm^{-1} are observed in the C=O stretch region, whereas only one strong sharp absorption is observed at 645 cm^{-1} , the region assigned to the O=C-C bending vibrational mode(s). The high intensity of the band at 645 cm^{-1} is caused either by a relatively large change in the electric dipole moment during the vibration, or by mixing with in-phase, out-of-plane ring bending modes.

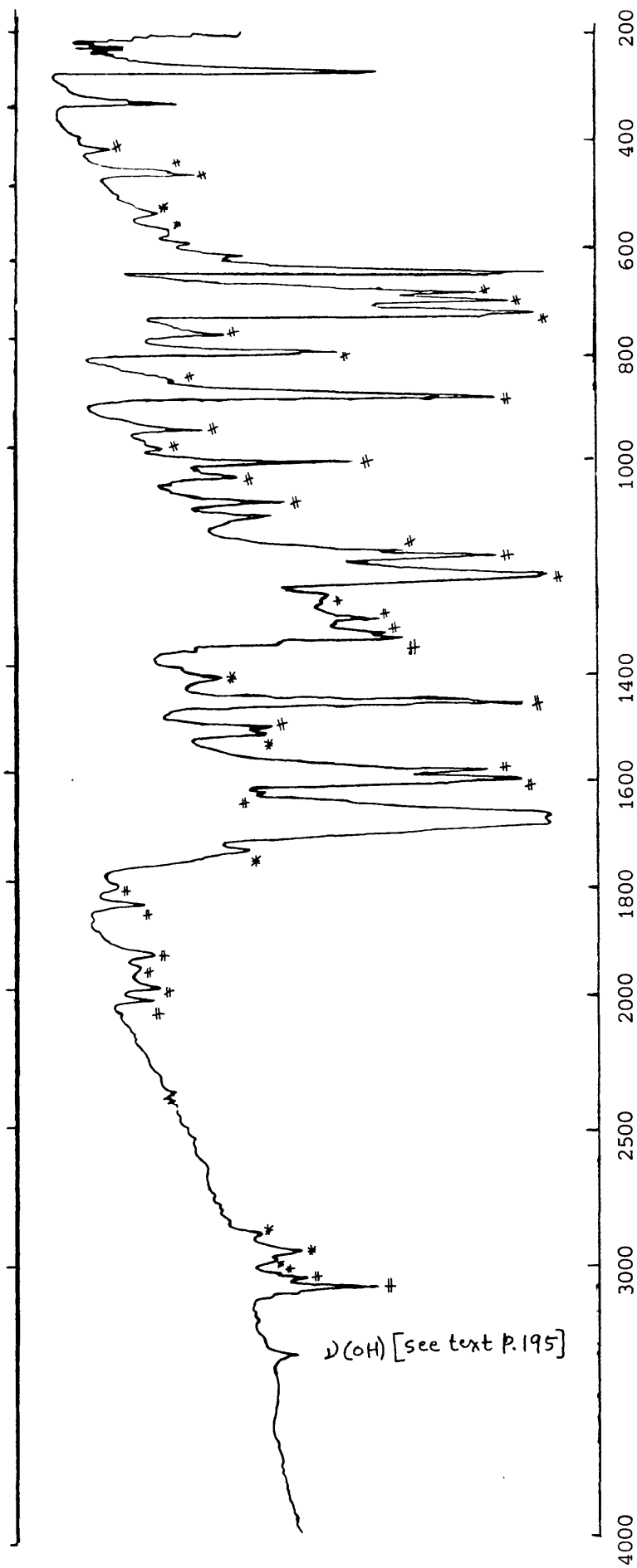


Figure (5.9). Infrared spectrum of $\text{RuC}_{56}\text{H}_{42}\text{O}_2$, KBr disc

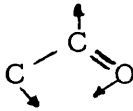
Table (5.4)

Infrared data, in wavenumber, of $\text{RuC}_{56}\text{H}_{42}\text{O}_2$ complex

band, cm^{-1}	Assignment
3060(m), 3030(vw), 3010(vw)	mono-substituted aromatic
2960(vw), 2930(m), 2860(vw)	aliphatic C-H stretching
2000(w), 1975(w), 1940(w) 1915(w), 1820(w), 1780(w)	aromatic overtone and combination bands or summation bands of $\text{x-C}_6\text{H}_5$
1720	coordinated $\text{C}\equiv\text{C}$ stretching
1680(vs), 1660(vs)	$\text{C}=\text{O}$ stretching
1615(vw), 1595(vs), 1580(s)	aromatic $\text{C}=\text{C}$ quadrant stretching
1505(m)	coordinated aliphatic $\text{C}=\text{C}$
1490(m), 1450(vs)	aromatic $\text{C}=\text{C}$ semicircle stretching
1400(w, br)	aliphatic C-C-H bending
1325(m), 1315(vw), 1290(m) 1250(vw), 1215(vs)	ring-C vibrational mode
1178(s), 1165(w)	C-H in-plane and ring deformation + C-C stretching
1100(m)	C-O stretching
1073(s), 1025(m)	$\text{C}-\text{C}-\text{H}$ in-plane bending + ring-semicircle stretching + C-C stretching
1000(s)	ring deformation
970(w, br), 940(m), 875(vs), 850(vw), 795(s), 765(m, br), 720(vs)	out-of-plane $\text{C}-\text{C}-\text{H}$ bending, five adjacent H-waging + conjugation
697(vs), 680(s)	out-of-plane $\text{C}-\text{C}-\text{H}$ in-phase bending

[contd.]

Table (5.4) contd.

band, cm^{-1}	Assignment
645(vs), 618(w), 595(w) 580(w), 570(w), 540(w,br) 468(m), 460(vw), 420(w) 335(m), 275(s)	 bending Ru-C, Ru-ring stretching ring deformation

s \equiv strong; w \equiv weak; m \equiv medium; vs \equiv very strong;

vw \equiv very weak; br \equiv broad.

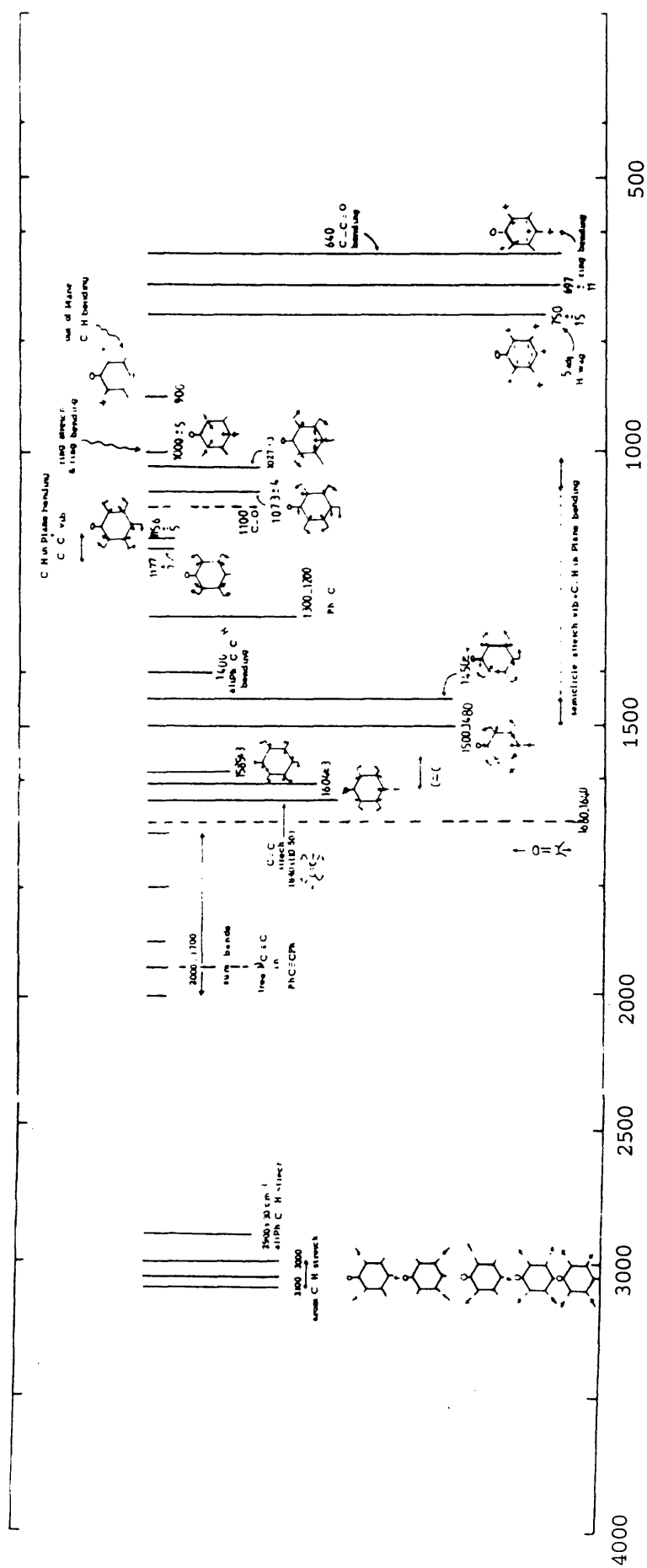




Figure (5.10)

II - Most of the other peaks in the observed i.r. spectrum arise from well-documented absorptions that are characteristic of mono-substituted phenyl residues. Absorptions that can be so assigned are denoted by (#) in Figure (5.9). Infrared absorption peaks within the range $3000 \leq \sigma \leq 3100 \text{ cm}^{-1}$ arise from C-H stretching vibrations of these mono-substituted phenyl residues, and this region of the spectrum indicates that $\text{RuC}_{56}\text{H}_{42}\text{O}_2$ contains several such residues. This deduction is consistent with the observation that within the region $1750 \leq \sigma \leq 2000 \text{ cm}^{-1}$ there appear to be two sets of four peaks of the kind normally observed as "summation bands" associated with a mono-substituted phenyl residue, again implying the presence of two major types, at least, of mono-substituted phenyl residue in this compound.

When all the i.r. absorptions assigned to C=O, C=C-C=O, and to -Y are subtracted from Figure (5.9) then the peaks labelled (*) remain, and when attention is focussed on these then the following deductions emerge.

(i) Absorptions in the range $2860 \leq \sigma \leq 2960 \text{ cm}^{-1}$ are assigned to aliphatic and conjugated olefinic C-H stretching modes of vibration.

(ii) The peak at 1720 cm^{-1} , and the nearby shoulder, may indicate the presence of coordinated diphenylacetylene $\left\{ \begin{array}{c} \text{Ph} \quad \text{Ph} \\ \diagdown \quad \diagup \\ \text{C}=\text{C} \\ \downarrow \\ \text{Ru} \end{array} \right\}$ in this compound. The $\text{C}\equiv\text{C}$ stretching vibration in $\left\{ \begin{array}{c} \text{Ph} \quad \text{Ph} \\ \diagdown \quad \diagup \\ \text{C}\equiv\text{C} \\ \downarrow \\ \text{Ru} \end{array} \right\}$ free diphenylacetylene is found at 1945 cm^{-1} , and this absorption shifts to lower frequency when the triple bond is coordinated to a transition-metal ion. The triple bond is then effectively reduced to a double bond, and the $\text{C}=\text{C}$ absorption is then found between $1700 \leq \sigma \leq 1800 \text{ cm}^{-1}$.^{137,138}

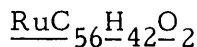


(iii) The band of medium intensity in Figure (5.9) at 1505 cm^{-1} is assigned to a C=C residue, or to a conjugated C=C residue, coordinated to ruthenium, $\text{C} \begin{array}{c} = \\ \downarrow \\ \text{Ru} \end{array} \text{C}$. A free olefinic C=C stretching mode absorbs at $(1640 \pm 50)\text{ cm}^{-1}$ whereas stretching modes of C=C residues coordinated to a transition-metal ion are known to absorb in the range $1500 \leq \sigma \leq 1565\text{ cm}^{-1}$. 136,137,139,140

(iv) The weak i.r. absorption at 1400 cm^{-1} confirms the presence of an aliphatic C-H residue: the absorption is ascribed to an aliphatic C - C^H bending mode of vibration.

(v) Weak bands at 580, 570, and 540 cm^{-1} in Figure (5.9) must come from metal-ligand modes of vibration. They imply that several kinds of ligands are present in this compound.

5.6 THE ELECTRON IMPACT MASS SPECTRUM OF OLIVE-GREEN



The microanalytical results, the ^1H and ^{13}C nuclear magnetic resonance spectra, and the infrared spectrum of this compound are all consistent, in that they show that its ligands contain,

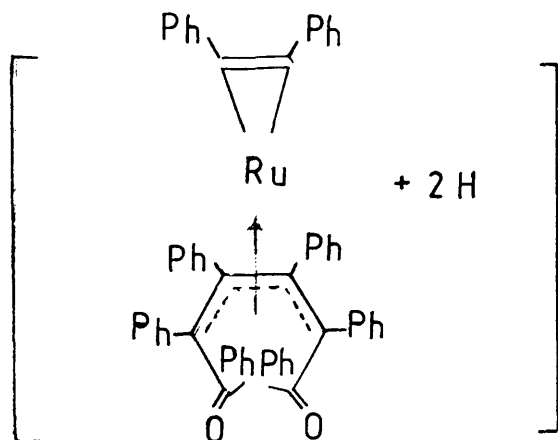
- (i) two carbonyl residues,
- (ii) at least six, and possibly eight, mono-substituted phenyl residues, and
- (iii) a further six additional carbon atoms which must be aromatic or else must form part of an extended conjugated system.

There also appear to be some aliphatic protons in this substance. The infrared spectrum of this compound is also consistent with the presence of an acetylenic and a conjugated olefinic residue in this molecule, and both of these must be coordinated to the metal ion. Furthermore, the infrared spectrum shows that the carbonyl residues are not coordinated to the ruthenium ion.

The mass spectrum cracking pattern, recorded on a KRATOS MS12 mass spectrometer, is shown in Table (5.5). It enables a number of molecular fragments to be identified and when all the bits and pieces of the jigsaw puzzle are put together, the structure of this complex is deduced to be

Table (5.5)

MASS	% A.R. BASE	MASS	% A.R. BASE	MASS	% A.R. BASE	MASS	% A.R. BASE	MASS	% A.R. BASE
41	0.9	73	0.4	102	0.3	*151	0.5	202	0.1
42	0.2	74	2.1	*103	0.2	*152	1.4	203	0.0
43	0.7	*75	1.4	*104	0.4	*153	0.5	205	0.0
44	0.7	*76	2.3	*105	100.0	*154	0.3	206	0.1
45	0.2	*77	49.3	*106	7.8	155	0.0	207	0.3
47	0.1	*78	4.9	*107	0.6	*163	0.3	*208	0.1
48	0.1	*79	0.5	108	0.1	*164	0.3	*209	0.6
*49	0.6	80	0.1	109	0.1	*165	2.1	*210	1.9
*50	6.6	81	0.3	110	0.1	*166	0.9	*211	0.5
*51	18.6	82	0.2	111	0.2	*167	1.0	*212	0.1
*52	1.4	83	0.3	113	0.2	168	0.2	213	0.1
*53	0.2	84	0.4	*115	0.4	175	0.0	215	0.2
53	0.3	85	0.3	*116	0.1	*176	0.4	223	0.0
54	0.1	86	0.2	*117	0.1	*177	0.3	224	0.0
55	0.7	*87	0.2	*118	0.4	*178	1.3	225	0.3
56	0.3	*88	0.2	*119	0.2	*179	0.9	226	0.3
57	0.7	*89	0.5	121	0.2	*180	0.7	227	0.1
60	0.1	*90	0.4	122	1.2	*181	0.7	228	0.1
*61	0.3	*91	1.5	123	0.1	*182	0.7	237	0.1
*62	0.5	92	0.2	125	0.1	*183	0.3	239	0.5
*63	0.9	93	0.1	126	0.3	189	0.2	240	0.3
*64	0.2	94	0.2	127	0.2	191	0.3	241	0.3
*65	0.7	95	0.2	128	0.3	*192	0.1	242	0.1
66	0.2	96	0.1	129	0.1	*193	0.2	250	0.2
67	0.3	97	0.3	131	0.0	*194	0.4	251	0.1
68	0.2	98	0.2	139	0.3	*195	0.3	252	0.7
69	0.4	99	0.2	141	0.2	*196	0.7	253	0.5
70	0.2	100	0.0	149	0.2	197	0.2	254	0.3
71	0.4	101	0.1	*150	0.3	200	0.0	255	0.3



The peak of highest mass number in Table (5.5) belongs to the fragment $[\text{RuC}_{42}\text{H}_{32}\text{O}_2]^+$, for which the ratio $m/e = 670$. This fragment loses its ruthenium atom to give $\{[\text{C}_{42}\text{H}_{30}\text{O}_2] \pm 2\text{H}\}^+$, $m/e = 566 \pm 2$ and this can fragment by four possible routes. As shown in Figures (5.11) and (5.12), the first route, (I), starts with the loss of $[\text{PhCO}]^+$ to give a relatively intense peak in the spectrum that arises from $\{[\text{C}_7\text{H}_5\text{O}] \pm 2\text{H}\}^+$, $m/e = 105 \pm 2$, and another much less abundant peak due to $\{[\text{C}_{35}\text{H}_{25}\text{O}] \pm 2\text{H}\}^+$, $m/e = 461 \pm 2$. This last fragment then decomposes further, as shown in Figure (5.11), to produce $\{[\text{C}_{28}\text{H}_{20}] \pm 2\text{H}\}^+$, $m/e = 356 \pm 2$, and $\{[\text{C}_{14}\text{H}_{10}] \pm 2\text{H}\}^+$, $m/e = 178 \pm 2$, respectively. This last fragment is identified as $[\text{PhCCPh}]^+$.

The decomposition pattern of diphenylacetylene is well documented in the literature,¹⁴¹ and it is known that inside the mass spectrometer it decomposes to yield the following fragments, $[\text{C}_{12}\text{H}_8]^+$, $m/e = 152$; $[\text{C}_7\text{H}_5]^+$, $m/e = 89$; $[\text{C}_6\text{H}_4]^+$, $m/e = 76$; $[\text{C}_5\text{H}_3]^+$, $m/e = 63$; $[\text{C}_4\text{H}_3]^+$, $m/e = 51$. The mass spectrum of the olive-green $\text{RuC}_{56}\text{H}_{42}\text{O}_2$, Table (5.5), shows the presence of all of these fragments

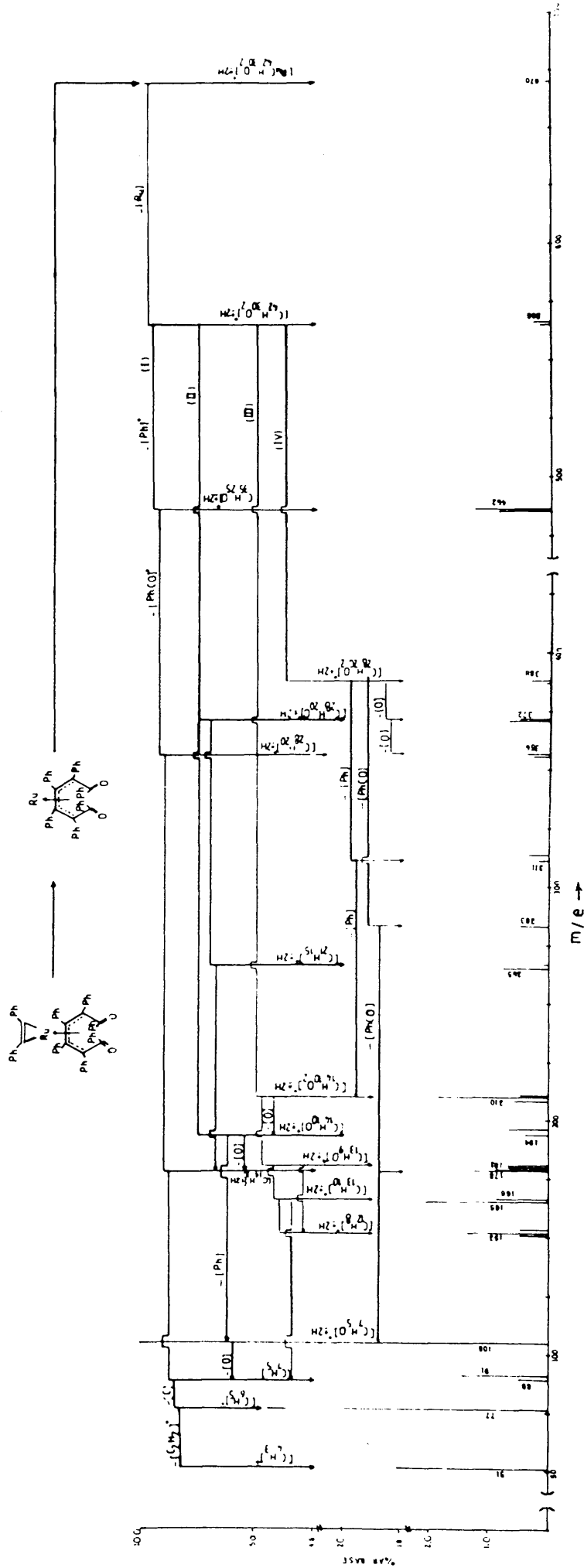


Figure (5.12). Schematic diagram of the electron impact cracking pattern of $\text{RuC}_{56}\text{H}_{42}\text{O}_2$. The normalisation of the base peak (% AR) as a function of m/e is shown in the lower part of the diagram

as relatively intense bands at ratios $m/e = 178 \pm 2$ (Parent PhCCPh) and at 152 ± 2 , 89 ± 2 , 77 ± 2 , 63 ± 2 , and 51 ± 2 , respectively.

The second most intense peak of the mass spectrum of the olive-green $\text{RuC}_{56}\text{H}_{42}\text{O}_2$, is found at $m/e=77 \pm 2$, and the third most intense peak at 51 ± 2 . The fragment $\{[\text{C}_7\text{H}_5\text{O}] \pm 2\text{H}\}^+$, $m/e = 105 \pm 2$ decomposes to give, $m/e = 89 \pm 2$ and this in its turn decomposes to give first

$\{[\text{C}_6\text{H}_5] \pm 2\text{H}\}^+$, $m/e = 77 \pm 2$, and then $\{[\text{C}_4\text{H}_3] \pm 2\text{H}\}^+$, $m/e = 51 \pm 2$.¹⁴²

The second decomposition route available to $\{[\text{C}_{42}\text{H}_{30}\text{O}_2] \pm 2\text{H}\}^+$, $m/e = 566 \pm 2$, route (II) in Figures (5.11) and (5.12) gives rise to two fragments $\{[\text{C}_{28}\text{H}_{20}\text{O}] \pm 2\text{H}\}^+$, $m/e = 372 \pm 2$, and $\{[\text{C}_{14}\text{H}_{10}\text{O}] \pm 2\text{H}\}^+$, $m/e = 194 \pm 2$. The first of these loses $[\text{PhCO}]^+$ to give $\{[\text{C}_{21}\text{H}_{15}] \pm 2\text{H}\}^+$, $m/e = 267 \pm 2$, and then $\{[\text{C}_{14}\text{H}_{10}] \pm 2\text{H}\}^+$, $m/e=178 \pm 2$ which fragments further, as already described. The second fragment $m/e=194 \pm 2$, produces $\{[\text{C}_7\text{H}_5\text{O}] \pm 2\text{H}\}^+$, $m/e=105 \pm 2$, which fragments as described above.

The mass spectrum of $\text{RuC}_{56}\text{H}_{42}\text{O}_2$ has a relatively intense peak that is assigned to a fragment $\{[\text{C}_{14}\text{H}_{10}\text{O}_2] \pm 2\text{H}\}^+$, $m/e=210 \pm 2$. It is believed that this is produced by a skeletal-rearrangement involving the fragment $\{[\text{C}_{42}\text{H}_{30}\text{O}_2] \pm 2\text{H}\}^+$, $m/e=566 \pm 2$, as shown in route (III) on Figures (5.11) and (5.12), which then fragments to produce $\{[\text{C}_{28}\text{H}_{20}] \pm 2\text{H}\}^+$, $m/e = 356 \pm 2$ and $\{\text{PhCOCOPh}\} \pm 2\text{H}\}^+$, $m/e = 210 \pm 2$. This last fragment is essentially an ion of benzil, or of a reduced benzil and both of these are known to undergo a skeletal-rearrangement¹⁴² inside the mass spectrometer $\{[\text{C}_{13}\text{H}_9\text{O}] \pm 2\text{H}\}^+$, $m/e = 181 \pm 2$;

$\{[C_{13}H_9] \pm 2H\}$, $m/e = 165 \pm 2$; and $\{[C_{12}H_8] \pm 2H\}^+$, $m/e = 152 \pm 2$, this last being the biphenylene radical.¹⁴² This decomposition route is a minor one for the olive-green solid, but nevertheless it is there, and it is important in providing information about its structure. Other investigators showed¹⁴² that the protons that are lost in the last step of this process come specifically from the ortho positions of the mono-substituted phenyl ring systems. The second fragment $\{[C_{28}H_{20}] \pm 2H\}^+$, $m/e = 356 \pm 2$ that is produced in route (III) fragments, as already described above.

The fourth decomposition mechanism available for breaking-down $\{[C_{42}H_{30}O_2] \pm 2H\}^+$, $m/e = 566 \pm 2$, route (IV) in Figures (5.11) and (5.12) involves a further skeletal-rearrangement that produces the "dimeric" $\{[C_{28}H_{20}O] \pm 2H\}^+$, $m/e = 388 \pm 2$ which fragments to form "monomeric" $\{[C_{14}H_{10}O] \pm 2H\}^+$, $m/e = 194 \pm 2$ which then breaks down, as already described above. The "dimeric" fragment, $m/e = 388 \pm 2$ also gives rise to $\{[C_{21}H_{15}O] \pm 2H\}^+$, $m/e = 283 \pm 2$, by loss of $[PhCO]^+$, and further decomposition of this fragment then gives rise to two fragments, $m/e = 105 \pm 2$ and $m/e = 178 \pm 2$, or another fragment $\{[C_{14}H_{10}O] \pm 2H\}^+$, $m/e = 194 \pm 2$ by loss of $[PhCO]^+$. This then fragments, by loss of a phenyl group to give $\{[C_8H_5O] \pm 2H\}^+$, $m/e = 117 \pm 2$. By cleavage of a phenyl group the fragment $\{[C_{28}H_{20}O_2] \pm 2H\}^+$, $m/e = 388 \pm 2$ gives rise to another fragment $\{[C_{28}H_{15}O] + 2H\}^+$, $m/e = 311 + 2$, which also produces fragments, $m/e = 194 \pm 2$, and $m/e = 117 \pm 2$.

The microanalysis results, the 1H and ^{13}C nuclear magnetic resonance spectra, the infrared spectrum and the electron impact mass spectrum of the olive-green $RuC_{56}H_{42}O_2$, are all consistent with the

5.7 THE MAGNETIC PROPERTIES OF OLIVE-GREEN $\text{RuC}_{56}\text{H}_{42}\text{O}_2$

The mass differences observed in a Gouy susceptibility experiment carried out on solid $\text{RuC}_{56}\text{H}_{42}\text{O}_2$ and corresponding mass changes for the standard, mercury tetrathiocyanato cobalt(II), $\text{HgCo}(\text{SCN})_4$, are listed in Table (5.6). The apparatus was checked by determining the magnetic susceptibility of solid ferrous ammonium sulphate hexahydrate, $\text{FeSO}_4(\text{NH}_4)_2\text{SO}_4 \cdot 6\text{H}_2\text{O}$, and was found to be in perfect working order.

As shown in Table (5.6), a small negative mass change is observed for powdered $\text{RuC}_{56}\text{H}_{42}\text{O}_2$, and this was used to calculate the gram susceptibility of this compound by means of the relationship (5.1)

$$\chi_{g2} = \chi_{g1} \left\{ \frac{(\omega_2 - \omega_0)}{(\omega_1 - \omega_0)} \frac{m_1}{m_2} \right\} \quad (5.1)$$

where, χ_{g1} is the gram susceptibility of standard, i.e. $\text{HgCo}(\text{SCN})_4$, $= 16.44 \times 10^{-6}$; χ_{g2} is the gram susceptibility of the sample $\text{RuC}_{56}\text{H}_{42}\text{O}_2$; ω_0 is the change in weight of the empty sample tube on applying a magnetic field; ω_1 is the corresponding change in weight of the sample tube plus solid $\text{HgCo}(\text{SCN})_4$; ω_2 is the change in weight of the sample tube plus solid $\text{RuC}_{56}\text{H}_{42}\text{O}_2$, and m_1 and m_2 are the masses of solid $\text{HgCo}(\text{SCN})_4$ and solid $\text{RuC}_{56}\text{H}_{42}\text{O}_2$, respectively, that were used in the experiment. Substitution of the data in Table (5.6) into equation (5.1) gives for the gram susceptibility of solid $\text{RuC}_{56}\text{H}_{42}\text{O}_2$ a value

$$\chi_{g2} = - 4.08 \times 10^{-7}$$

Table (5.6)

Magnetic susceptibility measurements of $\text{RuC}_{56}\text{H}_{42}\text{O}_2$, at
room temperature

Sample	Weight of sample in gram i=0.0 amp	Weight of sample in gram i=0.8 amp
Empty tube	1 - 1.7752	1.7752
	2 - 1.7753	1.7752
$\text{HgCo}(\text{SCN})_4$	1 - 2.7658	2.7767
	2 - 2.7656	2.7766
	3 - 2.7655	2.7766
$\text{RuC}_{56}\text{H}_{42}\text{O}_2$	1 - 2.1376	2.1375
	2 - 2.1382	2.1381
	3 - 2.1384	2.1383

The molar susceptibility of $\text{RuC}_{56}\text{H}_{42}\text{O}_2$, molecular weight = 847, is therefore

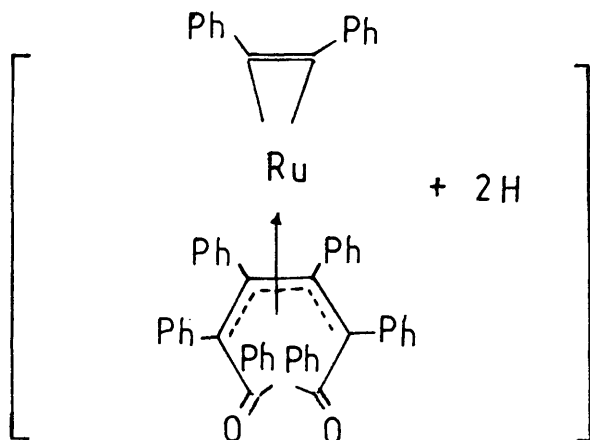
$$\chi_M = -3.46 \times 10^{-4}$$

With the balance available for the Gouy experiment masses can be measured to $\pm 0.0001\text{g}$ and therefore the limit of error in the measurement of χ_M is $\pm 6.92 \times 10^{-4}$.

The molar diamagnetic susceptibility of $\text{RuC}_{56}\text{H}_{42}\text{O}_2$ can also be calculated using Pascal's additivity law. Use of the following values for the Pascal's constants¹⁴³⁻¹⁴⁵ of the listed electrons,

Inner shell:	C($1s^2$)	-0.15×10^{-6}
	O($1s^2$)	-0.08×10^{-6}
Lone-pair:	O(sp^2)	-1.73×10^{-6}
π electrons:	C=C	-3.42×10^{-6}
	C=O	-3.05×10^{-6}
Bonds:	C(sp^3)-C(sp^3)	-3.10×10^{-6}
	C(sp^2)-C(sp^2)	-2.60×10^{-6}
	C(sp^3)-H	-4.05×10^{-6}
	C(sp^2)-O(sp^2)	-2.55×10^{-6}
Metal:	Ru	-20×10^{-6}

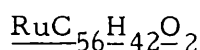
yields an estimated χ_M^D value of -5.07×10^{-4} for the structural formula



The experimental and theoretical values of the molar susceptibilities χ_M and χ_M^D , respectively are in excellent agreement and therefore this substance must be diamagnetic. It therefore follows that either the ruthenium ion in this complex is paramagnetic and the paramagnetism is exactly internally compensated, an unlikely event especially at surfaces, or the complex is diamagnetic and the ruthenium ion in it, is in the +2 oxidation state with the electronic configuration [Kr] $4d^6$, or the ruthenium ion is in zero oxidation state with the electronic configuration [Kr] $4d^8$, both of which are diamagnetic.

The silent e.p.r. responses obtained when solid and liquid (chloroform:toluene=60:40) samples of $\text{RuC}_{56}\text{H}_{42}\text{O}_2$ were examined at 295K and at 77K in a Decca e.p.r. spectrometer, over a wide range of field, confirm that this compound is diamagnetic.

5.8 THE VISIBLE-ULTRAVIOLET SPECTRUM OF OLIVE-GREEN



The visible-ultraviolet spectrum of a solution of $\text{RuC}_{56}\text{H}_{42}\text{O}_2$ in dichloromethane, recorded on a PYE-UNICAM SP800 spectrometer is shown in Figure (5.13). The measurements were carried out in a 1 cm cell and it should be noted that the olive-green solution was diluted 10-fold in recording the ultraviolet region of the spectrum, compared to measurements carried out in the visible region. Wavelengths, wave-numbers, and assignment of the peaks in Figure (5.13) are listed in Table (5.7).

The visible region of the spectrum in Figure (5.13) is very similar to the corresponding spectrum observed by Jørgensen³⁵ in his work on Ru(II)-chloride and for this reason it is believed that in olive-green $\text{RuC}_{56}\text{H}_{42}\text{O}_2$ the ruthenium ion is in the +2 rather than in the zero oxidation state.

The symmetry species of the octahedral group, O_h , correlate¹⁹ with the symmetry species of the group C_2 as shown in Figure (5.14)

O_h		C_2
A_{1g}	→	A
A_{2g}	→	A
E_g	→	2A
T_{1g}	→	A+2B
T_{2g}	→	A+2B

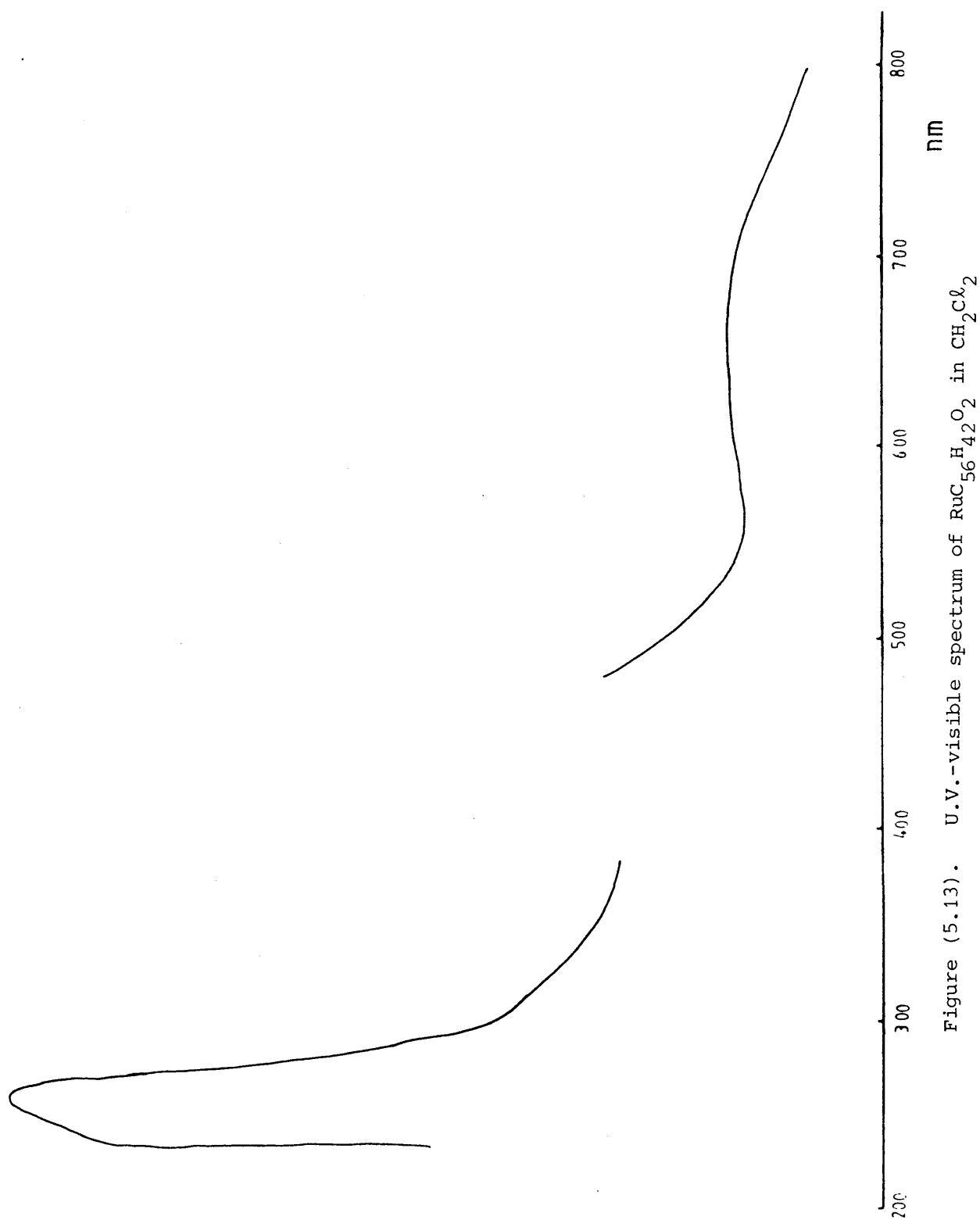


Table (5.7)

Visible-ultraviolet data for $\text{RuC}_{56}\text{H}_{42}\text{O}_2$

in CH_2Cl_2 solution

$\lambda(\text{nm})$	$\sigma(\text{cm}^{-1})$	Description	Assignment
650	15,385	very broad	$^1\text{A}(^1\text{A}_{1\text{g}}) \rightarrow ^1\text{B},(^1\text{A},^1\text{B})(^1\text{T}_{1\text{g}})$
330	30,300	shoulder	$^1\text{A}(^1\text{A}_{1\text{g}}) \rightarrow ^1\text{A},^1\text{B},^1\text{B}(^1\text{T}_{2\text{g}})$
255	39,215	sharp	charge-transfer
236	42,370	shoulder	charge-transfer

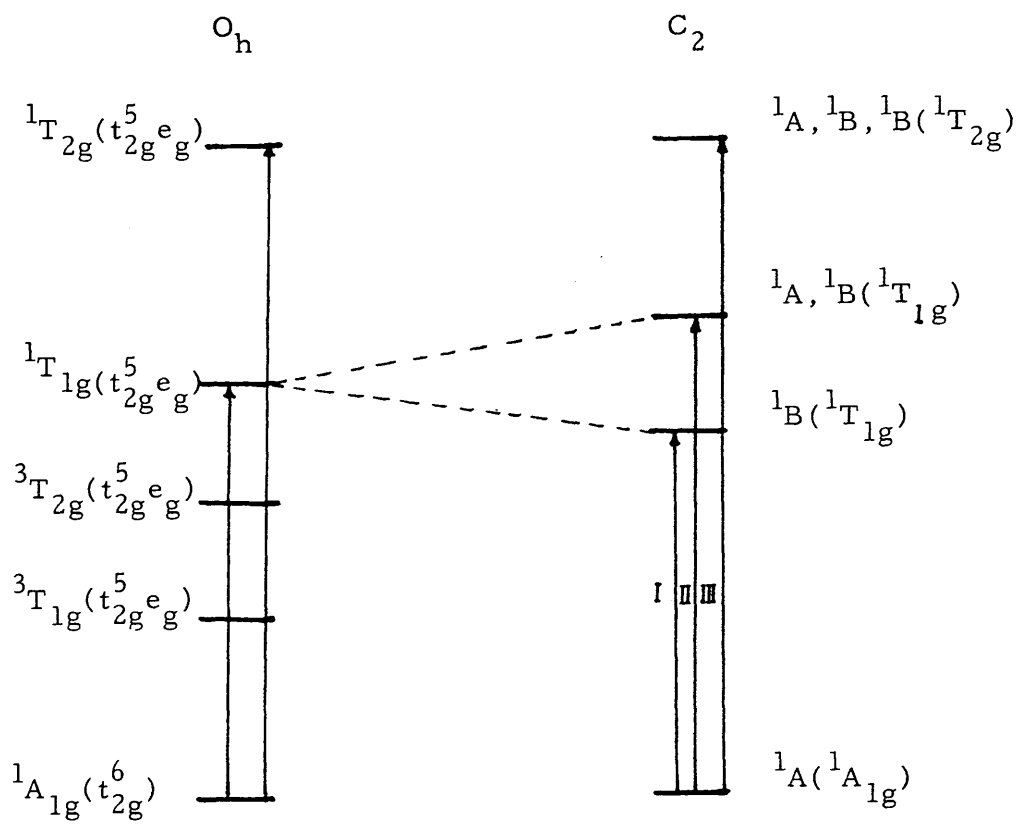


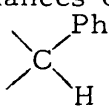
Figure (5.14)

and Orgel¹⁵⁶ and Basolo and coworkers¹⁵⁷ showed that the energy level diagram and spin-allowed transition for nd^6 transition-metal complexes correlate as shown in this same Figure.

Jørgensen in his work on the complex present in Ru(II)-chloride³⁵ reported a maximum between 660-710 nm and a shoulder between 568-578 nm in the visible absorption spectrum of this substance. These two bands have been assigned³ to transitions I, $^1A_1(^1A_{1g}) \rightarrow ^1B(^1T_{1g})$, and II, $^1A_1(^1A_{1g}) \rightarrow ^1A_1, ^1B(^1T_{1g})$. The visible region in Figure (5.13) shows a very broad absorption covering the range 600 nm ($16,600\text{ cm}^{-1}$)-740 nm ($13,500\text{ cm}^{-1}$) which might well in fact be composed of two overlapping bands arising from the transitions I and II of Figure (5.14).

The ultraviolet region of the spectrum of the complex in Ru(II)-chloride furthermore has a shoulder covering the range 370-385 nm which has been assigned³ to transition III, $^1A(^1A_{1g}) \rightarrow ^1A, ^1B, ^1B(^1T_{2g})$, in Figure (5.14). This transition has also been reported^{3,146,147} at $\sigma > 30,000\text{ cm}^{-1}$ ($\lambda < 335\text{ nm}$), in several nd^6 transition metal complexes. The shoulder at $\approx 330\text{ nm}$ ($\sigma \approx 30,300\text{ cm}^{-1}$) observed in the spectrum shown in Figure (5.13) may therefore be assigned also to transition III.

The visible and near ultraviolet spectrum of $\text{RuC}_{56}\text{H}_{42}\text{O}_2$ is consistent with the conclusion that the ruthenium ion in this complex is in the +2 rather than in the zero oxidation state. The much more intense peaks at 255 nm ($39,215\text{ cm}^{-1}$) and at 236 nm ($42,370\text{ cm}^{-1}$) in the ultraviolet region of the spectrum of $\text{RuC}_{56}\text{H}_{42}\text{O}_2$ are assigned to a charge transfer transition within the complex.

All the experimental results cited in this thesis consistently add up to indicate that the solid $\text{RuC}_{56}\text{H}_{42}\text{O}_2$ consists of a tautomeric mixture of the structures [A]-[F], shown in Figure (5.15). Additional structures, valence isomeric structures, in which the central ruthenium ion's valence fluctuates between Ru(0) and Ru(II) might also contribute. Structure [A] contributes by far the greatest amount to the structure of the solid $\text{RuC}_{56}\text{H}_{42}\text{O}_2$ and proton exchange occurs at an intermediate rate in the ^1H and ^{13}C n.m.r. time scales thereby broadening the resonances of the olefinic carbons, two of the phenyl residues and the two  protons. The tautomeric exchange must tend to make the phenyl residues attached to the olefinic carbons equivalent. The phenyl residues that give rise to the broadened region of the ^1H and ^{13}C n.m.r. spectrum must therefore be the phenyl groups in the coordinated acetylinic fragment of the molecule or they must belong to the two CPh residues. Since the olefinic carbon atoms give rise to a broad ^{13}C n.m.r. absorption, it is probable that it is the two CPh phenyl residues that are lost in the broadened region of the n.m.r. spectra.

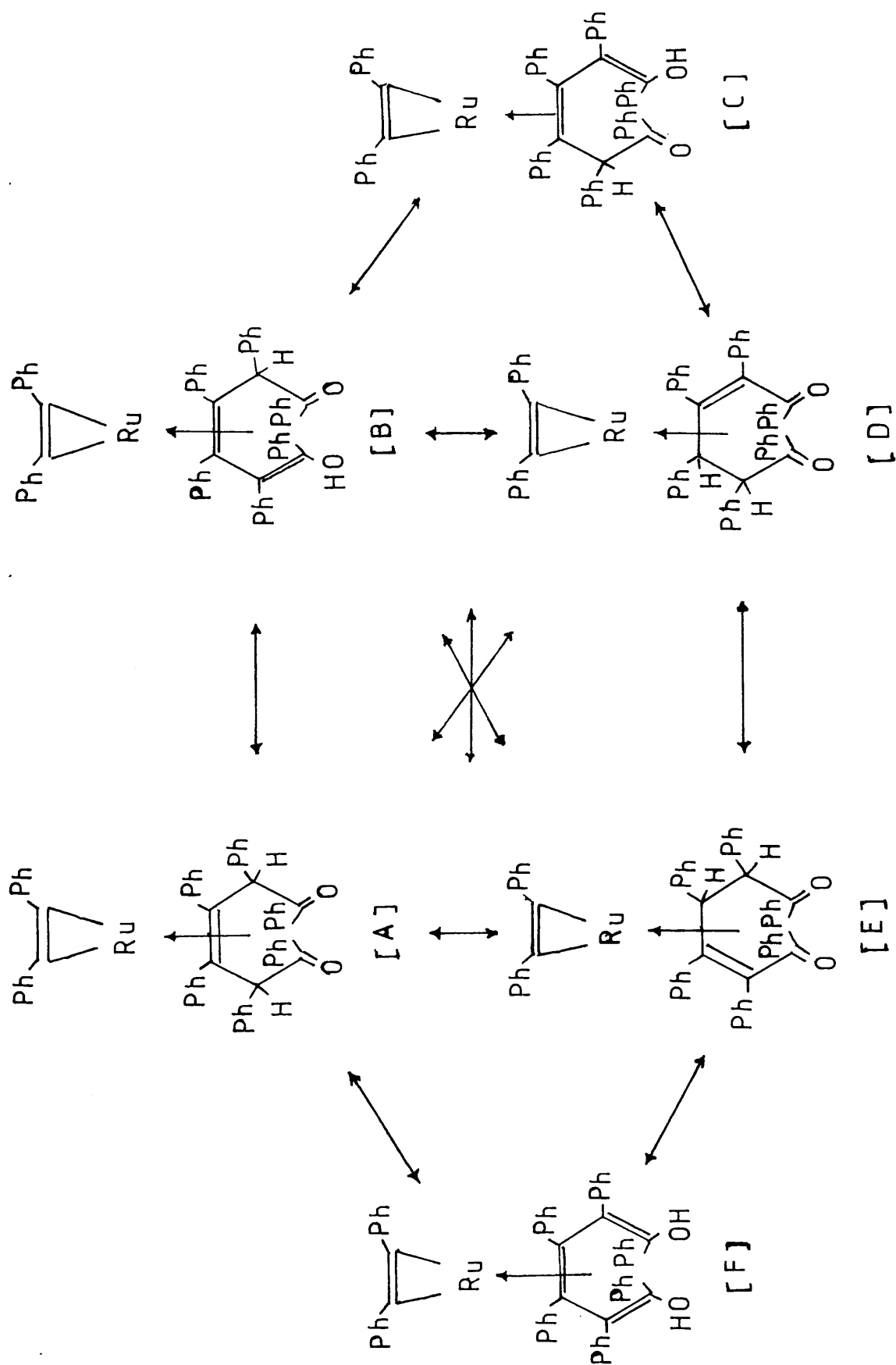


Figure (5.15)

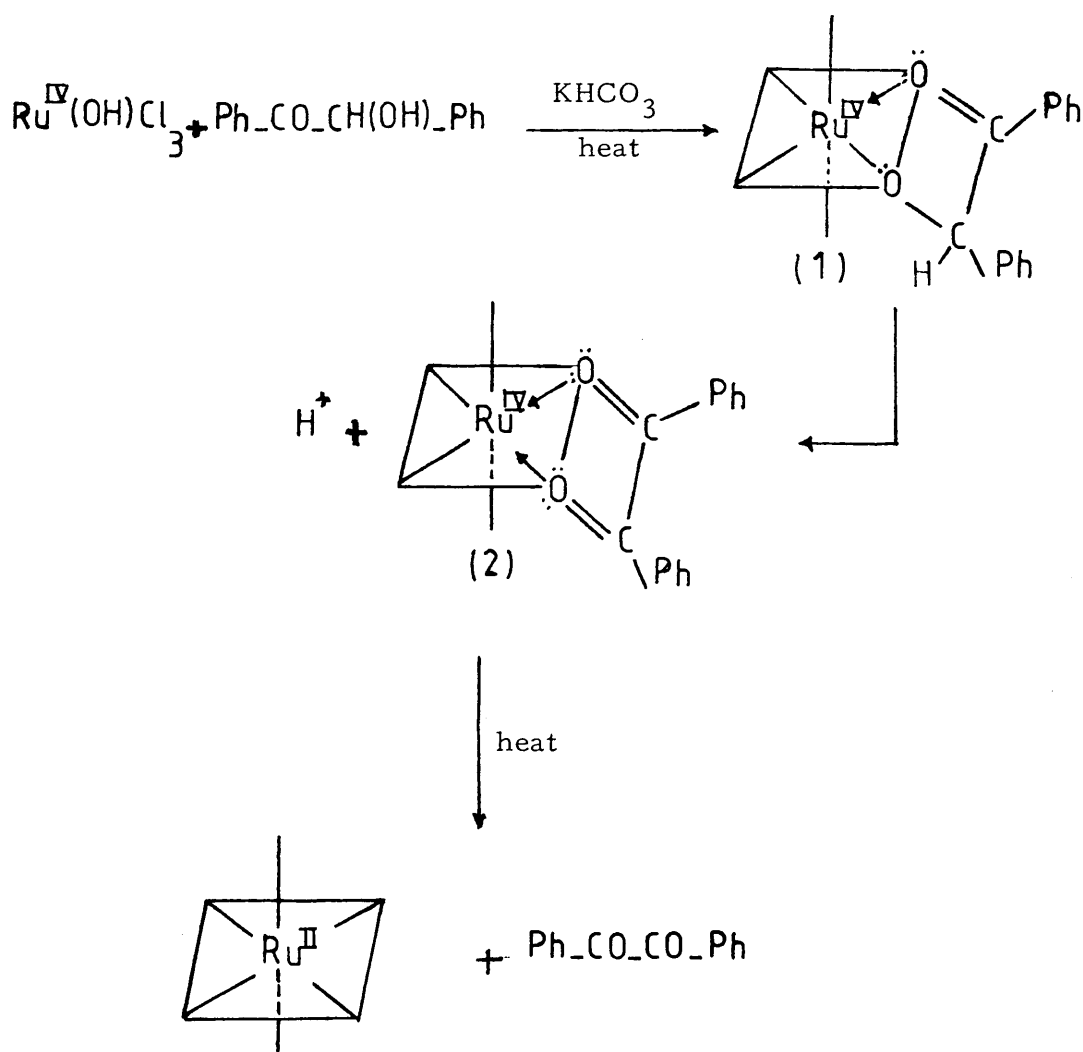
5.9 THE REACTION MECHANISMS INVOLVED IN THE FORMATION OF OLIVE-GREEN $\text{RuC}_{56}\text{H}_{42}\text{O}_2$

Anhydrous ruthenium chloride is known to exist in at least two forms, $\alpha\text{-RuCl}_3$ and $\beta\text{-RuCl}_3$. Magnetic susceptibility measurements show that $\alpha\text{-RuCl}_3$ is antiferromagnetic below 13K and $\beta\text{-RuCl}_3$ below $\sim 600\text{K}$. In the α -form, the chloride ions form a lattice with slightly distorted, dense cubic close packing, and the ruthenium ions occupy two-thirds of the octahedral sites of alternate layers.¹⁴⁸ The other alternate layers of octahedral sites are empty. The X-ray powder pattern and its infrared spectrum indicate that, in $\beta\text{-RuCl}_3$ linear chains of ruthenium ions lie in distorted octahedrons of chloride ions forming $\text{-RuCl}_3\text{-RuCl}_3\text{-RuCl}_3\text{-}$ units in the chain.¹⁴⁹

There is no doubt that in $\alpha\text{-RuCl}_3$ and in $\beta\text{-RuCl}_3$, the oxidation state of the ruthenium ion is +3, and it seemed surprising that "commercial ruthenium(III)-chloride", $\text{RuCl}_3 \cdot x\text{H}_2\text{O}$, did not form paramagnetic Ru(III)-chelates with suitable ligands. It was not until the work described in this chapter of this thesis was almost complete, that it was realized that "commercial ruthenium(III)-chloride", "hydrated ruthenium(III)-chloride", "soluble ruthenium(III)-chloride" and " $\text{RuCl}_3 \cdot x\text{H}_2\text{O}$ " are all synonyms for a heterogeneous and ill-defined mixture of ruthenium complexes of variable oxidation-state, of oxochloro- and hydroxochloro-, monomeric and polymeric substances, that even frequently contain nitrosyl derivatives. It was belatedly realized that it is not correct to regard "commercial ruthenium(III)-chloride" as a direct source of Ru(III) ions. Indeed it turns out that the average

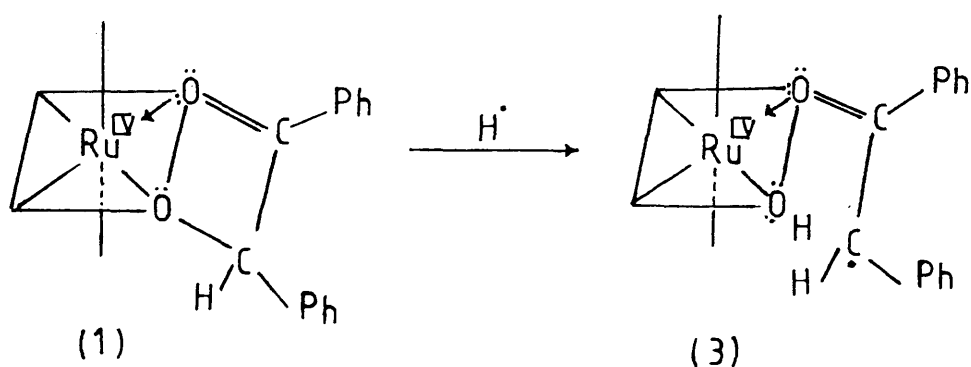
oxidation-state of this material is closer to Ru(IV) than it is to Ru(III), and the main constituent of "commercial ruthenium(III)-chloride" is $\text{Ru}^{\text{IV}}(\text{OH})\text{Cl}_3$,^{34,150} or some polymeric form of this.

This then provides the clue to possible reaction mechanisms for the formation of olive-green $\text{RuC}_{56}\text{H}_{42}\text{O}_2$, when solids " $\text{RuCl}_3 \cdot x\text{H}_2\text{O}$ ", KHCO_3 and benzoin are all heated together. It is chemically reasonable to visualize that a benzoin chelate of Ru(IV) is first formed

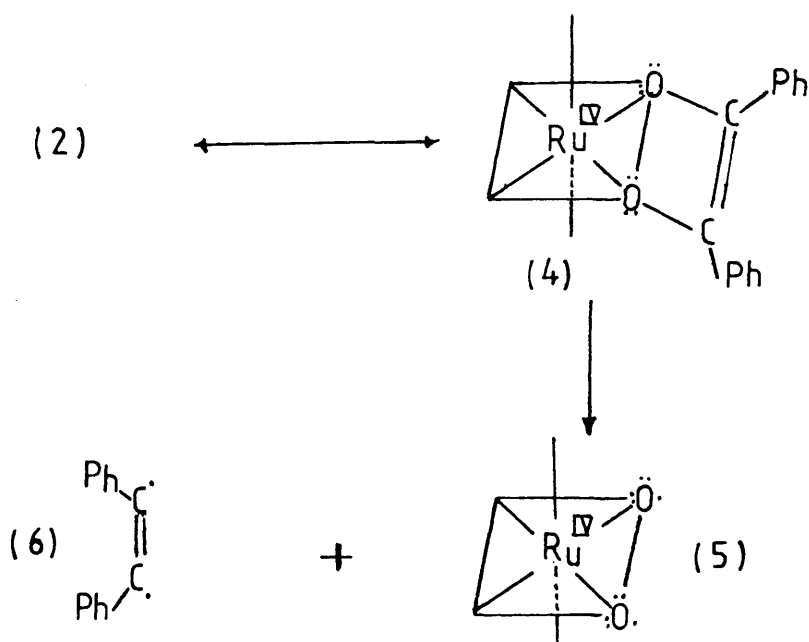


The intense-inductive influence of the Ru(IV) ion causes electrons to flow towards it. The C-H proton of the benzoin ligand ionizes off, benzoin is oxidized to benzil, and Ru(IV) is reduced to Ru(II). Large amounts of benzil are in fact isolated from the products of this reaction.

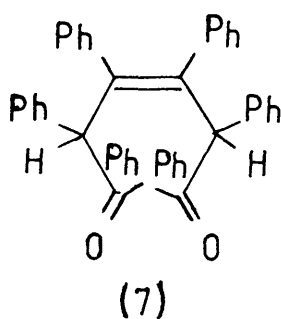
Alternatively, electron withdrawal by the Ru(IV) ion weakens a neighbouring C-O bond which undergoes homolysis to produce an aliphatic radical $\text{PhCO}\dot{\text{C}}\text{HPh}$



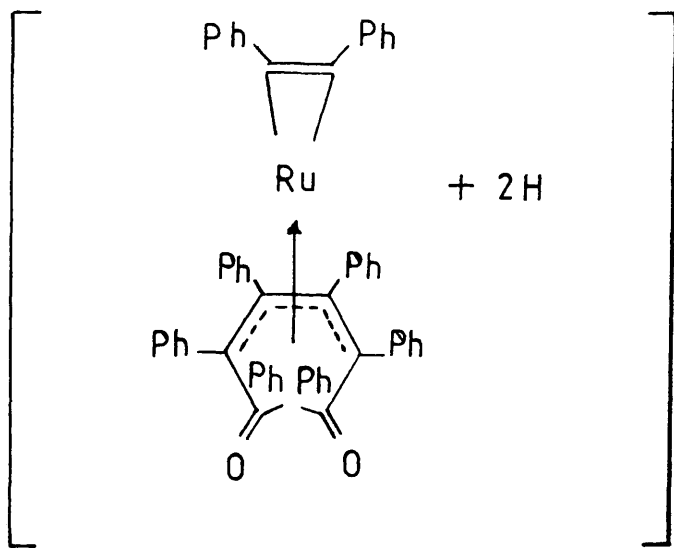
In a third possible decomposition route the intense-inductive influence of the Ru(IV) ion, acting in the resonance isomeric form (2) causes two C-O bonds to break thereby forming the biradical $\text{Ph}\dot{\text{C}}=\text{C}\dot{\text{C}}\text{Ph}$



This biradical can then stabilize to diphenylacetylene, or it can undergo some kind of "template reaction", with two equivalents of $\text{PhCO}\dot{\text{C}}\text{HPh}$ to form



The diphenylacetylene and species (7) being the ligands present in the olive-green $\text{RuC}_{56}\text{H}_{42}\text{O}_2$, i.e.



Commercial " $\text{RuCl}_3 \cdot x\text{H}_2\text{O}$ ", i.e. the Ru(IV) ion, might be a useful reagent for oxidizing hydroxyketones to diketones, or as a reagent for converting these compounds into corresponding acetylene derivatives, or possibly as a reagent for converting hydroxyketones into olefins and their polymers.

- CHAPTER SIX -

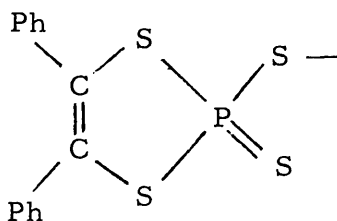
BIS[μ -THIO(1,2-DIPHENYLETHANEDITHIONE)-
RUTHENIUM(II,III)]

6.1 INTRODUCTION

Chelates, in which the sulphur atom acts as a donor, were used as far back as the early 1930's as analytical reagents for various metal ions. Such compounds were then neglected for a while, but in the last few years a renaissance of interest in them has taken place. For several reasons, there has been an enormous upsurge of interest in the chemistry of sulphur complexes of the transition metal-ions.

Sulphur-chelates are encountered in biological-inorganic chemistry, and model complexes analogous to biological systems containing transition metal-sulphur bonds are now of great interest. Transition-metal chelates containing sulphur have proved to be useful in synthesizing organometallics. Metal-sulphur systems are of wide interest, ranging from academic synthetic studies on one extreme, to large scale industrial processes on the other. Transition metal-sulphur complexes are used as highly specific analytical reagents, as chromatographic supports, as polymerization catalysts, as catalytic inhibitors, as oxidation catalysts, and as semiconductors.^{151,152}

A very extensive literature on ruthenium-sulphur chemistry exists,³⁴ but even so, very little attention has been paid to ruthenium 1,2-dithiolene complexes. Schrauzer and his co-workers have reported¹⁵³ a blue-green complex, (m.p. 225°C), which they first formulated as $\text{Ru}(\text{S}_2\text{C}_2\text{Ph}_2)_2$ and then reformulated as $\text{Ru}(\text{S}_2\text{C}_2\text{Ph}_2)_3$, though the compound has been poorly characterized. Their compound was prepared by allowing ruthenium(III)-chloride to react with the thiophosphoric ester of stilbenedithiol, [6-A]. When this work was



[6-A]

repeated by the author of this thesis, by allowing commercial " $\text{RuCl}_3 \cdot x\text{H}_2\text{O}$ " to react with [6-A], prepared by the reaction of benzoin with P_4S_{10} , a very impure, viscous, blue-green product was obtained. Extracting with dichloromethane, and then allowing the solvent to evaporate from the dichloromethane filtrate, produced a beautiful intense-blue-coloured lacquer, indicating that a polymerization reaction had taken place. The same reaction appears to take place when ruthenium(III)-chloride is used instead of the commercial " $\text{RuCl}_3 \cdot x\text{H}_2\text{O}$ ". However, reaction of [6-A] with a greenish-blue solution of ruthenium(II)-chloride in ethanol, using the procedure described later, produced as one of the products of reaction a black solid which, as shown later, turned out to be bis[μ -thio(1,2-diphenylethanedithione)ruthenium(II,III)], $\text{RuS}_2(\text{S}_2\text{C}_2\text{Ph}_2)_2$. This is analogous to the sulphur-bridged complexes of iron(III)¹⁵⁴ and copper(I)¹⁵⁵ already reported in the literature.

6.2 PREPARATION OF $\text{Ru}_2\text{S}_2(\text{S}_2\text{C}_2\text{Ph}_2)_2$

Commercial " $\text{RuCl}_3 \cdot x\text{H}_2\text{O}$ " (Johnson-Matthey Chemicals Limited) (0.56g), was dissolved in absolute ethanol (30 ml), then refluxed until the original dark-brown colour turned greenish-blue.

Benzoin (1.5g) was mixed with P_4S_{10} (1.5g), and the mixture suspended in xylene (60 ml), refluxed for 2 hours and then cooled to room temperature and filtered.

The amber filtrate was added, dropwise with stirring, to the greenish-blue solution of ruthenium(II)-chloride. The resultant mixture was then refluxed for 2 hours. During this period the greenish-blue colour turned black. The solution was then cooled and left overnight, then filtered, and the black precipitate was collected. The yield of the black solid was poor but it was improved by adding methanol. The black solid was then dried under vacuum for 24 hours.

Microanalytical results for this black powder are listed in Table (6.1) and compared with corresponding data based on the formula $\text{Ru}_2\text{S}_2(\text{S}_2\text{C}_2\text{Ph}_2)_2$.

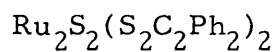
6.3 THE INFRARED SPECTRUM OF BLACK $\text{Ru}_2\text{S}_2(\text{S}_2\text{C}_2\text{Ph}_2)_2$

The infrared spectrum, KBr disc, of the black compound $\text{Ru}_2\text{S}_2(\text{S}_2\text{C}_2\text{Ph}_2)_2$, recorded on a PERKIN-ELMER 983 infrared spectrometer, is shown in Figure (6.1). Wavenumbers and functional group assignments with prominent peaks of this spectrum are listed in Table (6.2).

Absorptions that are characteristic of mono-substituted phenyl and aliphatic C-H residues in the infrared spectrum of this compound are denoted by (#) in Figure (6.1). These bands have already been assigned in detail in section (5.5).

Table (6.1)

Microanalytical results for the black powder,



Element	$\text{Ru}_2\text{S}_2(\text{S}_2\text{C}_2\text{Ph}_2)_2$ required %	Experimental %
C	44.80	44.40
H	2.66	2.59
S	25.60	25.49
*Ru	26.88	26.19

* Ruthenium was estimated spectrophotometrically as tris-1,10-phenanthroline-ruthenium(II), $[\text{Ru}(\text{C}_{12}\text{H}_8\text{N}_2)_3]^{++}$, using $\text{Ru}(\text{acac})_3$ as standard.¹³⁵

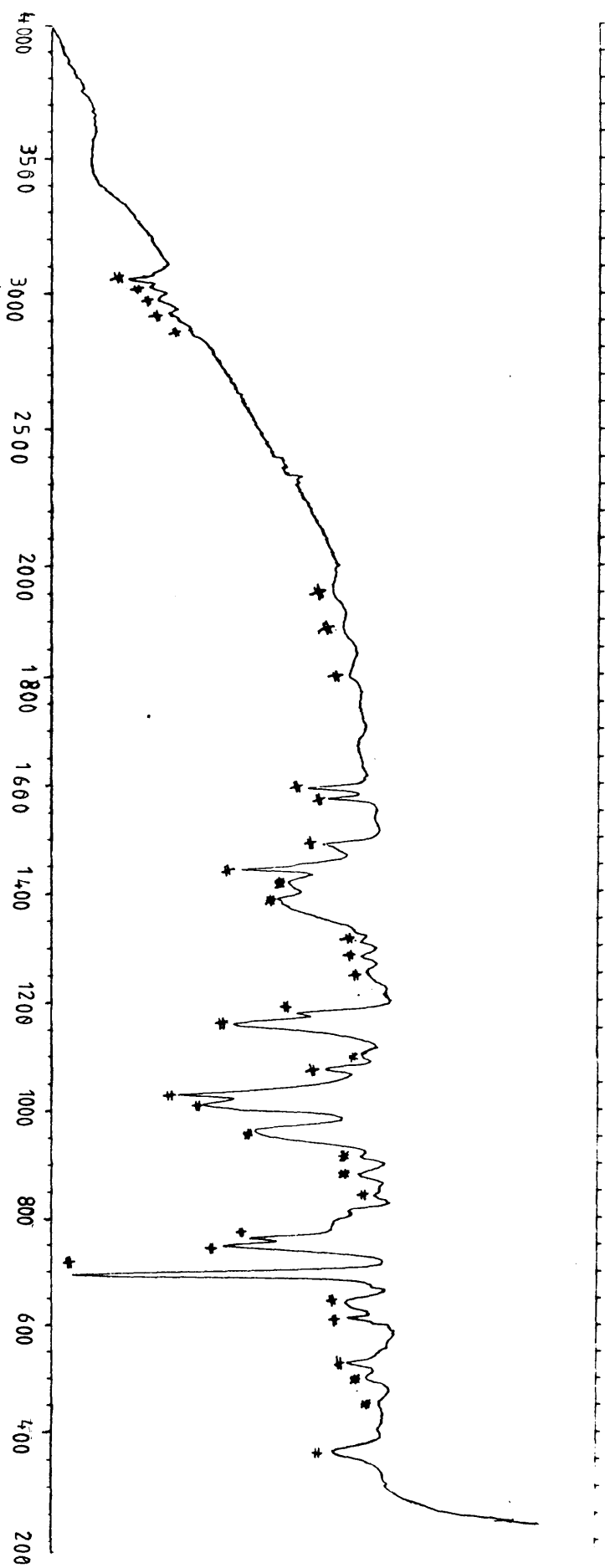


Figure (6.1) Infrared spectrum of $\text{Ru}_2\text{S}_2(\text{S}_2\text{C}_2\text{Ph})_2$, KBr disc

Table (6.2)

Infrared data, in wavenumbers, of the sulfur-bridged

dimeric complex $\text{Ru}_2\text{S}_2(\text{S}_2\text{C}_2\text{Ph}_2)_2$

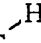
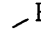
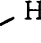

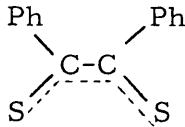
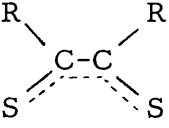
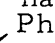
Band (cm^{-1})	Assignment
3060(m), 3030(vw)	aromatic C-H stretching
2980(w), 2930(w), 2860(vw)	aliphatic C-H stretching
1960(w), 1890(w), 1800(w)	aromatic overtone and combination bands
1592(m), 1575(m)	aromatic C=C "quadrant stretching"
1490(m), 1440(s)	aromatic C=C "semicircle stretching"
1420(m)	aliphatic C-C  bending
1390(m)	$\nu(\text{C} \cdots \text{C})$, B_{2u}
1310(w), 1280(m), 1250(m)	ring-C vibrational mode
1170(w), 1160(s)	C-H in-plane bending + C-C stretching
1100(w)	ring-C vibrational mode + $\nu(\text{C} \cdots \text{S})$, B_{3u}
1075(m), 1030(s), 1010(m)	C-C  in-plane bending + ring-semicircle stretching + C-C stretching
960(s)	ring-C vibrational mode + $\nu(\text{C} \cdots \text{S})$, B_{2u}
915(w)	out-of-plane C-C  bending
880(m)	$\nu(\text{C} \cdots \text{S})$, B_{3u}
840(w), 760(m), 747(s)	out-of-plane C-C  bending

Table (6.2) contd.

Band (cm^{-1})	Assignment
695(vs)	} in-phase, out-of-plane } ring-bending
640(m), 610(m), 527(m)	
500(w)	$\nu(\text{Ru-S}), B_{2u}$
450(vw)	$\nu(\text{Ru-S}), B_{3u}$
405(vw)	$\nu(\text{Ru-S}), B_{2u}$
365(m)	$\delta(\text{C-C-Ph}), \text{out-of-plane bending}, B_{3u}$

Figure (6.1) is consistent with the presence of bis-1,2-dithiolene residue , in this compound. Literature studies¹⁵¹ indicate that  residues characteristically absorb at $\sim 1400\text{ cm}^{-1}$, $\nu\text{ C}\equiv\text{C}$; $\sim 1110\text{ cm}^{-1}$, $\nu\text{ C}\equiv\text{S}$; and $\sim 860\text{ cm}^{-1}$, $\nu\text{ R-C}\begin{smallmatrix} \text{S} \\ \diagup \\ \text{C} \end{smallmatrix}$.

Metal-sulphur stretching frequencies, are reported to occur in the region $490\text{--}300\text{ cm}^{-1}$.^{151,152} Bis-1,2-dithiolene complexes always exhibit a number of medium and weak bands in the $500\text{--}350\text{ cm}^{-1}$ region of the infrared spectrum. Earlier work carried out by Schrauzer and Mayweg,¹⁵⁶ assigned two of these bands between $435\text{--}310\text{ cm}^{-1}$ to metal-sulphur stretching modes. However, normal coordinate analyses carried out by Siiman and Fresco,¹⁵⁷ and isotropic substitution studies carried out by Schläpfer and Nakamoto,¹⁵⁸ show that, bands in this range should not be attributed to metal-sulphur stretching modes, but on the other hand, they may be assigned to out-of-plane bending modes of the  residues. These same authors^{157,158} place the asymmetric stretching vibrations of the metal-sulphur residues in these complexes at 475 , 408 and 454 cm^{-1} respectively, where the first two of these belong to the B_{2u} vibrational species and the last belongs to the in-plane mode, B_{3u} . The motions of the atoms in these vibrational modes of bis-dithiolene complexes are shown in Figure (6.2).

Although the infrared spectrum by itself does not lead directly to the full molecular structure of $\text{Ru}_2\text{S}_2(\text{S}_2\text{C}_2\text{Ph}_2)_2$, evidence to be presented later indicates that this compound is a sulphur-bridged

dimeric complex of ruthenium. If it is assumed that this complex has D_{2h} symmetry and that the phenyl groups can be replaced by appropriate heavy point masses then the only in-plane infrared active modes of the bis-1,2-dithiolene-metal residues have B_{2u} and B_{3u} symmetry, as shown in Figure (6.2). In Figure (6.1), the absorption at 1390 cm^{-1} is assigned to a B_{2u} mode involving vibration of the $C\equiv C$ residues. The absorption peak at 960 cm^{-1} is also assigned to a B_{2u} mode involving coupling of the $(C\equiv S) + (C - Ph)$ residues: this gives a strong absorption band in the infrared spectrum. Mixed asymmetric bending vibrational modes that belong to B_{3u} representations,¹⁵⁷ and involve vibration of the $(C\equiv S) + (C - Ph)$ and $(C\equiv S)$ residues are believed to be responsible for the weak band at 1100 cm^{-1} and for the medium band at 880 cm^{-1} respectively, as shown in Figure (6.1).

Following Schl pfer and Nakamoto,¹⁵⁸ the band of medium intensity at 365 cm^{-1} , in Figure (6.1), is assigned to the out-of-plane bending mode of the $C-C\begin{smallmatrix} \nearrow \\ Ph \end{smallmatrix}$ residues. The bands at 500 and 405 cm^{-1} are attributed to ruthenium-sulphur B_{2u} stretching modes of vibration, whereas the band at 450 cm^{-1} is assigned to a ruthenium-sulphur B_{3u} vibrational mode.

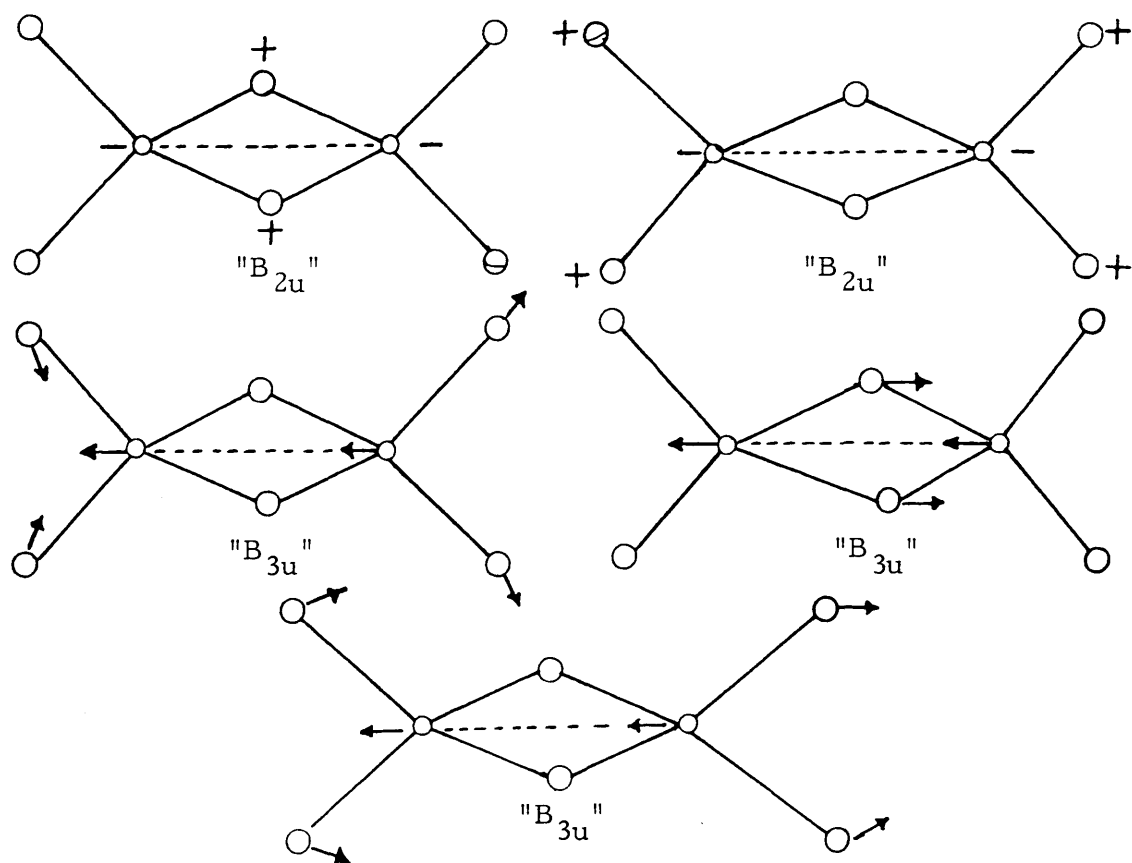
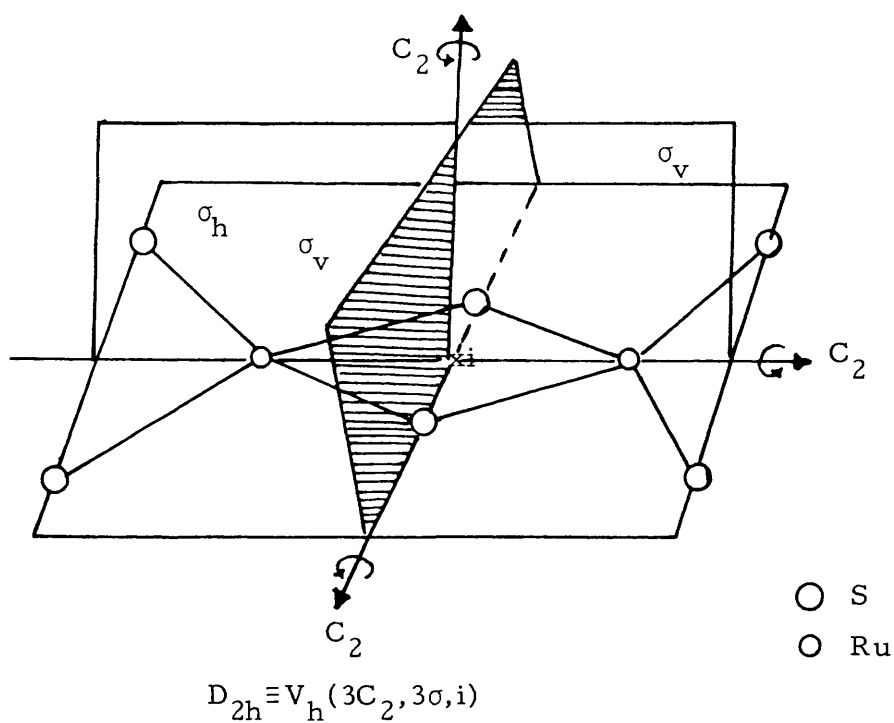
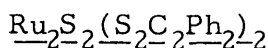


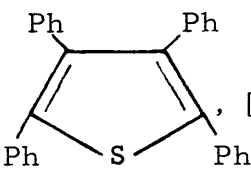
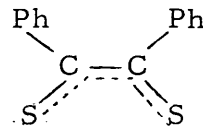
Figure (6.2). B_{2u} and B_{3u} modes of vibration of Ru₂S₂(S₂C₂Ph₂)₂,
D_{2h} symmetry

6.4 THE ELECTRON IMPACT MASS SPECTRUM OF BLACK

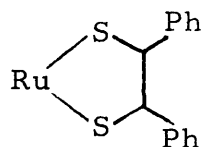


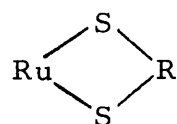
The mass spectrum of the black solid $\text{Ru}_2\text{S}_2(\text{S}_2\text{C}_2\text{Ph}_2)_2$ was recorded on a KRATOS MS12 mass spectrometer. The results are shown in Table (6.3) and line diagrams showing the decomposition pathways and the important peaks in the mass spectrum, are shown in Figures (6.3) and (6.4).

Because of decomposition within the mass spectrometer, the parent ion $[\text{Ru}_2\text{S}_2(\text{S}_2\text{C}_2\text{Ph}_2)_2]^+$ is not observed. However, the spectrum is essentially completely accounted for, on the basis of the decomposition patterns derived from ions of the following fragments.

- (i) Tetraphenyl thiophene, [6-B], (TPT), , $[\text{C}_{28}\text{H}_{20}\text{S}]^+$, $m/e = 388$.
- (ii) The chelating ligand, [6-C],  $\pm 2\text{H}$, $\{[\text{C}_{14}\text{H}_{10}\text{S}_2] \pm 2\text{H}\}^+$, $m/e = 242 \pm 2$.

In addition there are less intense peaks in the mass spectrum of this black dimer which can be identified with

- (iii) , $[\text{C}_{14}\text{H}_{11}\text{S}_2\text{Ru}]^+$, $m/e = 345$

- (iv) , $[\text{S}_2\text{Ru}_2]^+$, $m/e = 268$

- (v) $[\text{RuS}]^+$, $m/e = 134$,

Table (6.3)

MASS	% AR. BASE	MASS	% AR. BASE	MASS	% AR. BASE	MASS	% AR. BASE	MASS	% AR. BASE
*41	11.8	*71	3.9	103	3.2	*133	2.2	*166	7.2
*42	3.6	73	2.5	104	4.7	*134	4.7	*167	1.8
*43	6.1	74	18.6	*105	10.0	*135	2.5	169	3.2
*44	22.6	*75	14.3	*106	2.2	*136	0.7	170	2.5
*45	17.9	*76	19.7	*107	2.5	*137	5.4	171	4.3
*46	2.9	*77	36.2	*108	3.9	*138	5.4	172	1.1
47	11.8	*78	9.3	*109	2.9	*139	14.3	173	1.4
48	2.5	*79	4.3	*110	5.0	*140	2.2	174	2.9
*49	1.8	*80	1.1	*111	4.7	*141	2.2	175	3.9
*50	20.8	*81	3.2	*112	1.8	142	1.1	*176	26.5
*51	33.7	*82	5.4	*113	7.2	*143	1.1	*177	15.1
*52	9.0	*83	1.8	*114	4.7	*144	0.7	*178	100.0
*53	4.3	*84	1.4	*115	10.4	*145	3.6	*179	18.3
54	2.9	*85	3.9	116	2.2	*146	1.1	*180	3.2
*55	5.0	*86	10.4	117	2.9	*147	2.2	181	1.4
*56	2.5	*87	13.6	118	1.4	149	2.5	182	2.2
*57	7.5	*88	6.8	*119	2.9	*150	12.9	183	1.4
*58	6.5	*89	16.8	*120	6.8	*151	14.7	184	2.9
*59	5.0	*90	3.6	*121	31.5	*152	27.2	185	1.8
*60	4.3	*91	9.3	*122	7.5	*153	5.4	186	1.1
*61	6.1	92	3.6	*123	3.9	*154	2.2	*187	1.8
*62	20.8	93	9.0	*124	1.8	155	1.4	*188	1.1
*63	26.5	94	4.3	*125	3.2	*157	1.8	*189	4.7
*64	16.1	95	3.2	*126	14.3	*158	3.2	*190	1.8
*65	7.9	97	1.8	*127	5.7	*159	1.8	*191	2.2
*66	4.7	*98	11.1	*128	5.4	161	2.2	193	1.4
*67	3.2	*99	6.8	129	2.5	162	2.9	194	1.4
*68	1.8	*100	3.9	130	0.7	*163	11.5	195	5.7
*69	18.3	*101	3.6	131	2.9	*164	9.7	196	2.2
*70	3.9	*102	7.5	*132	1.8	*165	36.6	197	3.9

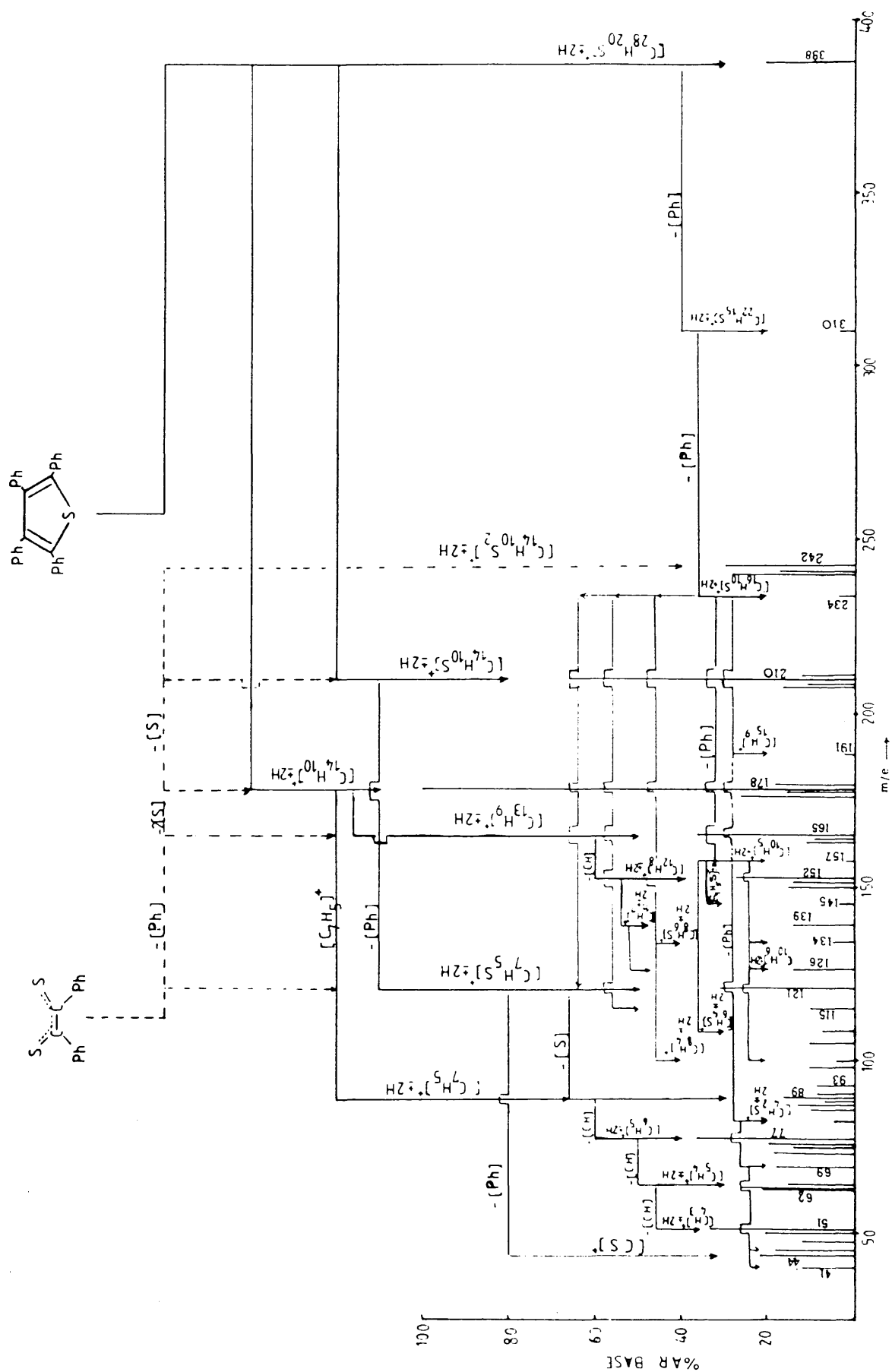
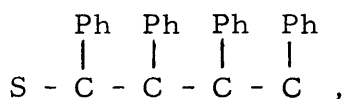


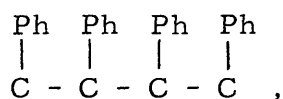
Figure (6.4). Schematic diagram of the electron impact cracking pattern of $\text{Ru}_2\text{S}_2(\text{S}_2\text{C}_6\text{Ph}_2)_2$

and with (vi) the isotopes of ruthenium itself.

The decomposition pattern from fragment [6-B], above, must arise from an ion of (TPT) rather than from an ion derived from the open-chain structure



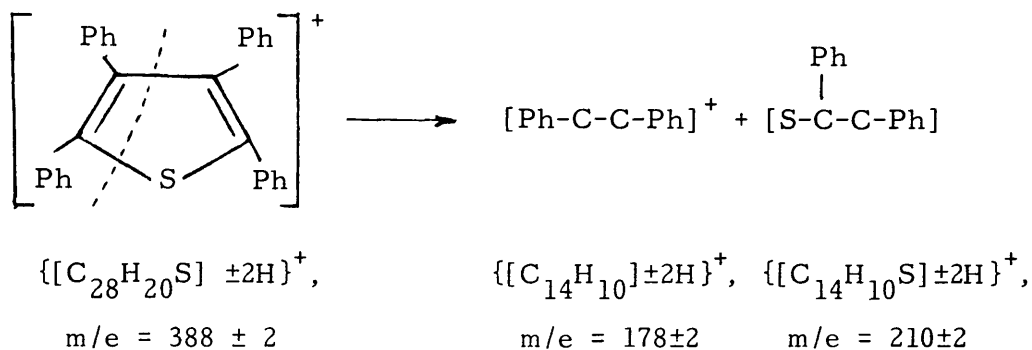
$m/e = 388$. This follows because the open-chain structure would give rise to a fragment



$m/e = 356$, which is not present in the mass spectrum of the black $\text{Ru}_2\text{S}_2(\text{S}_2\text{C}_2\text{Ph}_2)_2$, Table (6.3). The formation of the (TPT) ion on heating metal-ion complexes containing the dithiol chelating ligand [6-C], above, has already been reported by other authors.^{159,160} Furthermore, the mass spectrum of the (TPT) ion itself has already been reported,¹⁶¹ and the decomposition pattern of the (TPT) fragment obtained from black solid $\text{Ru}_2\text{S}_2(\text{S}_2\text{C}_2\text{Ph}_2)_2$ is almost identical with the fragmentation pattern reported in the literature,¹⁵⁹⁻¹⁶¹ except that the ion at $m/e = 344$, corresponding to loss of H_2S from the (TPT) fragment was not observed in the breakdown pattern of the solid $\text{Ru}_2\text{S}_2(\text{S}_2\text{C}_2\text{Ph}_2)_2$.

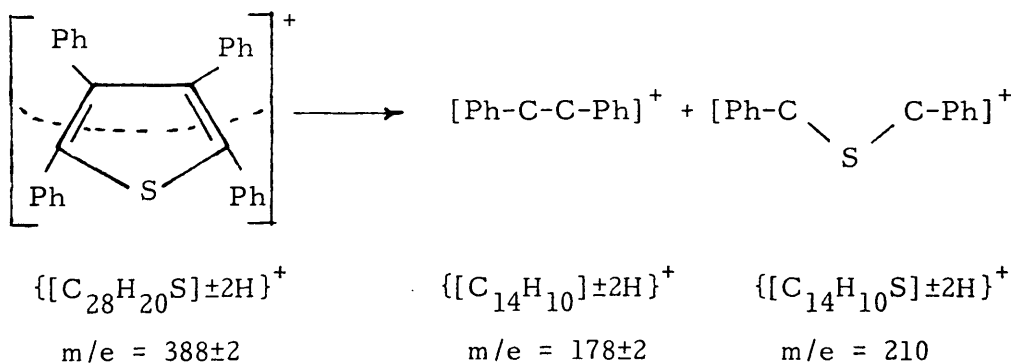
The (TPT) ion, [6-B], decomposes in several ways, as shown in Schemes [I]-[IV] below, and Figures (6.3) and (6.4).

Scheme [I] starts with the following fragmentation



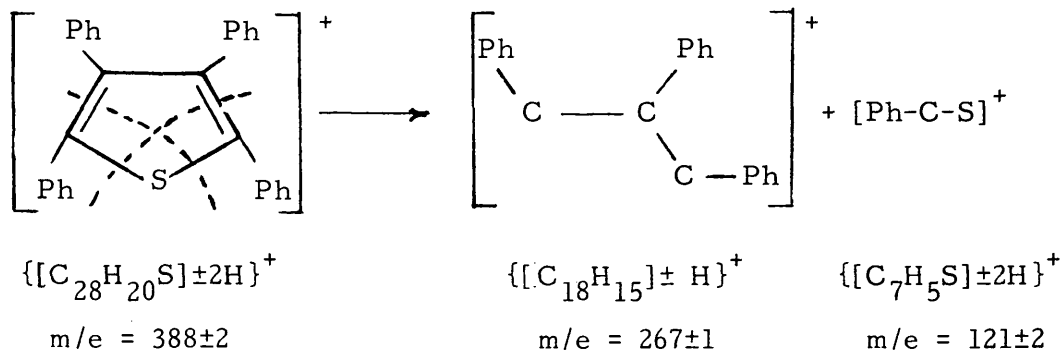
Two major fragments at $m/e = 210 \pm 2$ and $m/e = 178 \pm 2$, are produced, the peak at $m/e = 178 \pm 2$ being the most intense peak in the mass spectrum of the black solid $\text{Ru}_2\text{S}_2(\text{S}_2\text{C}_2\text{Ph}_2)_2$, and the peak at $m/e = 210 \pm 2$ being the next most intense. The successive fragmentations of these two fragments are shown in Figures (6.3) and (6.4).

Breakdown of the (TPT) fragment, [6-B], can also take place as shown in Scheme [II], Figures (6.3) and (6.4), which starts with



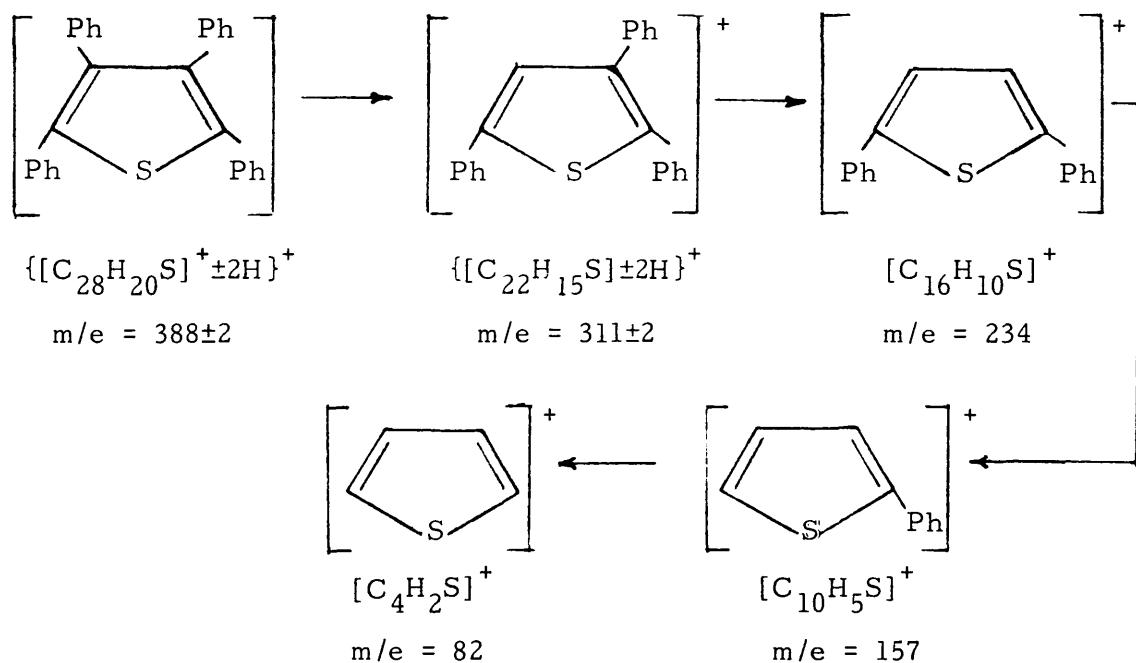
and these fragments then break down further as shown in Scheme [II], Figures (6.3) and (6.4). Break-down products of the fragments obtained for Schemes [I] and [II] are almost identical.

In Scheme [III], the first step in the fragmentation pattern is



The decomposition of these fragments produced in this manner are, also, shown in Figures (6.3) and (6.4).

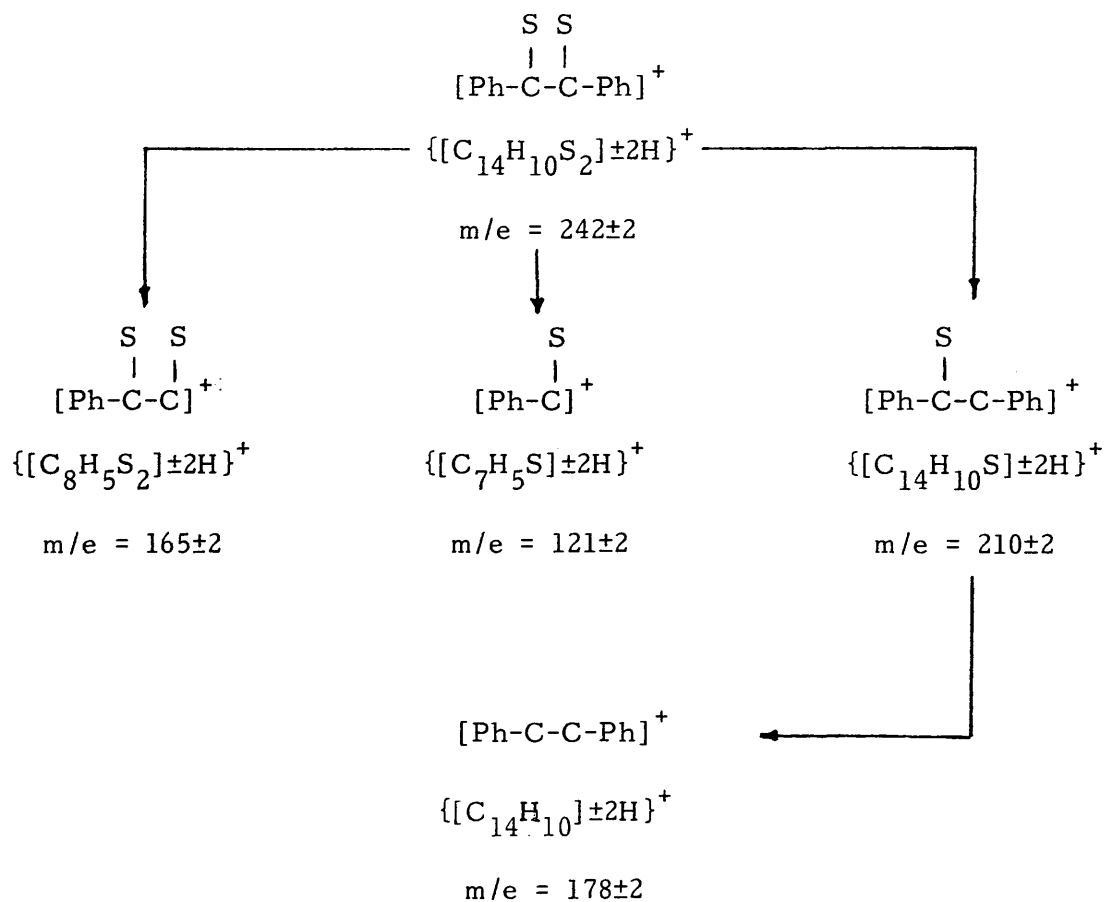
In Scheme [IV], exocyclic Ph-C bonds are cleaved to produce several dephenylated products



which then decompose in turn to give several smaller fragments as shown in Figure (6.3), all of which are identified.

Similarly, decomposition of fragment $[6-C]; \text{Ph-C(S)-C(S)Ph}$, $\{[C_{14}H_{10}S_2] \pm 2H\}^+$, $m/e = 244 \pm 2$; can also follow one or other of the several routes shown in Figures (6.3) and (6.4), and in Scheme [V]

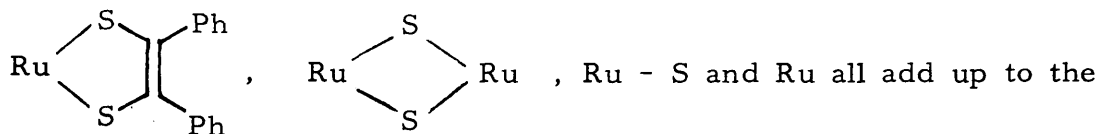
below



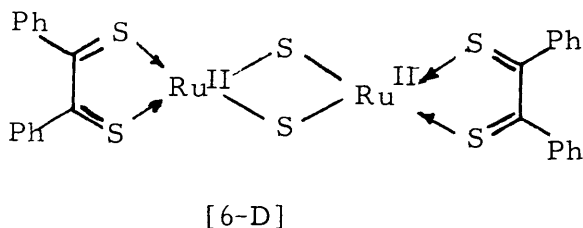
Scheme [V]

the resultant fragment-ions, then decompose into further smaller fragments, as shown in Figures (6.3) and (6.4), all of which are observed in the mass spectrum of the black solid $\text{Ru}_2\text{S}_2(\text{S}_2\text{C}_2\text{Ph}_2)_2$, Table (6.3).

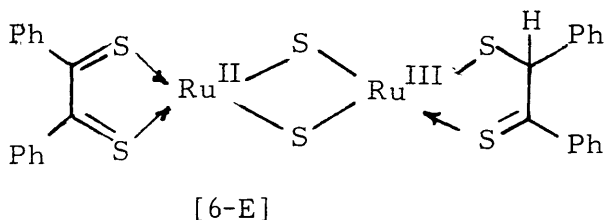
These fragmentation patterns when combined with the fragments



bridged structure



for the black compound, $\text{Ru}_2\text{S}_2(\text{S}_2\text{C}_2\text{Ph}_2)_2$, modified by the additional presence of at least a reasonable amount of analogous species containing extra hydrogen atoms, showing that at least some



is present. It seems that this substance is a mixed valence compound containing both Ru(II) and Ru(III) in planar environments, and may involve several mixed valence isomers of ruthenium, and several proton tautomers, in which electrons and protons can meander from one molecule to another in the solid. This aspect of the structure will be again considered later when the electron paramagnetic resonance spectra of the black solid are considered.

6.5 THE MAGNETIC SUSCEPTIBILITY OF BLACK $\text{Ru}_2\text{S}_2(\text{S}_2\text{C}_2\text{Ph}_2)_2$

The magnetic susceptibility of the black solid $\text{Ru}_2\text{S}_2(\text{S}_2\text{C}_2\text{Ph}_2)_2$ was measured using the Gouy method: $\text{HgCo}(\text{SCN})_4$ was used as standard, and the apparatus was tested using a solid sample of ferrous ammonium sulphate hexahydrate, $\text{FeSO}_4(\text{NH}_4)_2\text{SO}_4 \cdot 6\text{H}_2\text{O}$. The results of these measurements, Table 6.4, show that no change in mass was detected when a solid sample of $\text{Ru}_2\text{S}_2(\text{S}_2\text{C}_2\text{Ph}_2)_2$ was weighed in a magnetic field: the susceptibility balance was capable of detecting a mass difference of $> 0.0001\text{g}$.

The susceptibility measurements imply either, (i) that the black solid $\text{Ru}_2\text{S}_2(\text{S}_2\text{C}_2\text{Ph}_2)_2$ is paramagnetic, and the paramagnetic and diamagnetic contributions to the susceptibility cancel each other, OR (ii) that this solid is diamagnetic, and the balance is not sensitive enough to detect any mass change in either direction.

Pascal's constants¹⁴³⁻¹⁴⁵ give the following predicted molar diamagnetic susceptibility for the black dimer $\text{Ru}_2\text{S}_2(\text{S}_2\text{C}_2\text{Ph}_2)_2$

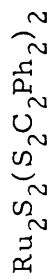
$$\begin{aligned}\chi_{\text{M}}^{\text{D}} &= -[2(\text{S}_2\text{C}_2\text{Ph}_2) + 2\text{S} + 2\text{Ru}] \\ &= -[2(150 \times 10^{-6}) + 2(15 \times 10^{-6}) + 2(20 \times 10^{-6})] \\ &= -370 \times 10^{-6}\end{aligned}$$

Therefore, if interpretation (i) is valid, the paramagnetic molar susceptibility for this dimer (molecular weight = 750) is equal to $+370 \times 10^{-6}$.

But, since the paramagnetic moment is defined by, equation (3.12),

Table (6.4)

Magnetic susceptibility measurement data for the black dimer



Sample	Weight (gm)	Weight + sample tube, (gm), at i=0 amp.	Weight + sample tube, (gm), at i=1.0 amp.
$\text{HgCo}(\text{SCN})_4$	1.0146	1- 3.9582	3.9675
		2- 3.9583	3.9677
		3- 3.9583	3.9673
$\text{Ru}_2\text{S}_2(\text{S}_2\text{C}_2\text{Ph}_2)_2$	0.2150	1- 3.1588	3.1588
		2- 3.1588	3.1588
		3- 3.1588	3.1588

$$\begin{aligned}
 |\mu_{\text{para}}| &= \sqrt{(3\bar{k}/\bar{N}\beta_e^2)(\chi_M^{\text{para}})T} && \text{electronic Bohr magnetons} \\
 &= 48.555 \sqrt{\chi_M^{\text{para}}} && \text{electronic Bohr magnetons at} \\
 &&& T = 295 \text{ K}
 \end{aligned}$$

it follows that the paramagnetic moment for the black solid

$\text{Ru}_2\text{S}_2(\text{S}_2\text{C}_2\text{Ph}_2)_2$ is

$$\begin{aligned}
 |\mu_{\text{para}}| &= 48.555 \sqrt{370 \times 10^{-6}} && \text{electronic Bohr magnetons per} \\
 &= 0.9340 && \text{molecule}
 \end{aligned}$$

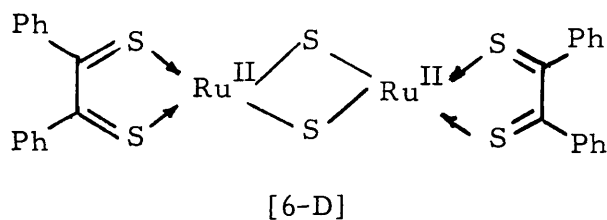
It, therefore, follows that the number of unpaired electrons, n' , in this dimer can be determined from

$$\begin{aligned}
 |\mu_{\text{para}}| &\simeq \sqrt{n'(n' + 2)} && \text{electronic Bohr magnetons} \\
 0.9340 &= \sqrt{n'(n' + 2)}
 \end{aligned}$$

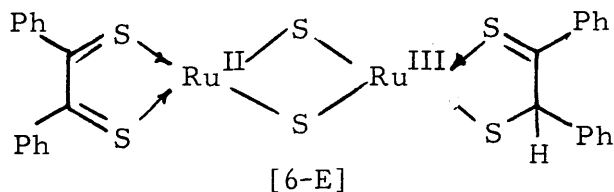
and hence

$$n' = 0.37 \text{ electrons}$$

This implies the presence of 0.37 unpaired electrons per formula unit $\text{Ru}_2\text{S}_2(\text{S}_2\text{C}_2\text{Ph}_2)_2$, i.e. an average of one unpaired electron for every 2.7 dimers of this black solid. The susceptibility results are consistent with the presence of $\sim \frac{2}{3}$ of



and $\sim \frac{1}{3}$ of



The alternative interpretation, (ii), of the susceptibility results, implies that the black dimer is diamagnetic and that

$$|\chi_M| = |\chi_M^D| = 370 \times 10^{-6}$$

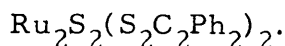
in this case $|\chi_{g2}|$ is, therefore,

$$\begin{aligned} |\chi_{g2}| &= 370 \times 10^{-6} / 750 \\ &= 0.4933 \times 10^{-6} \text{ per gram} \end{aligned}$$

Using this value and the data of Table (6.4), then substituted into equation (5.1) gives the expected weight change for the black solid $\text{Ru}_2\text{S}_2(\text{S}_2\text{C}_2\text{Ph}_2)_2$ to be $-5.90 \times 10^{-5} \text{ g}$. This mass change is too small to be detected on the balance used in the Gouy experiment.

It therefore follows that the results obtained from the Gouy experiment are not conclusive. The black dimer may be paramagnetic, or it may not be. The susceptibility experiment can not distinguish.

A careful electron paramagnetic resonance experiment in which the number of unpaired electrons can be counted, is needed to determine (a) if the substance is paramagnetic or not, and (b) if so, how many unpaired electrons are associated with each formula unit



However, the susceptibility experiment does show that each formula weight $\text{Ru}_2\text{S}_2(\text{S}_2\text{C}_2\text{Ph}_2)_2$ could possess between zero and 0.37 unpaired electrons.

6.6 THE X-BAND ELECTRON PARAMAGNETIC RESONANCE

SPECTRA OF BLACK $\text{Ru}_2\text{S}_2(\text{S}_2\text{C}_2\text{Ph}_2)_2$

The X-band electron paramagnetic resonance spectra of the black solid, at 295K and 77K, and of a solution in chloroform:toluene, (60:40), at 77K, were recorded on a Decca e.p.r. spectrometer. These spectra are shown in Figures (6.5), (6.6), and (6.7).

Spectra obtained from the solid itself are characteristic of those expected from an electron in an axially symmetric environment. In such a situation, where $S = \frac{1}{2}$ and the axis of symmetry of the paramagnetic complex lies at an angle θ with respect to the applied field, H , then the resonance field is given by⁵⁸

$$\begin{aligned} H &= h\nu_o / (g\beta_e) \\ &= h\nu_o / [\beta_e (g_{11}^2 \cos^2 \theta + g_{\perp}^2 \sin^2 \theta)^{\frac{1}{2}}] \end{aligned} \quad (6.1)$$

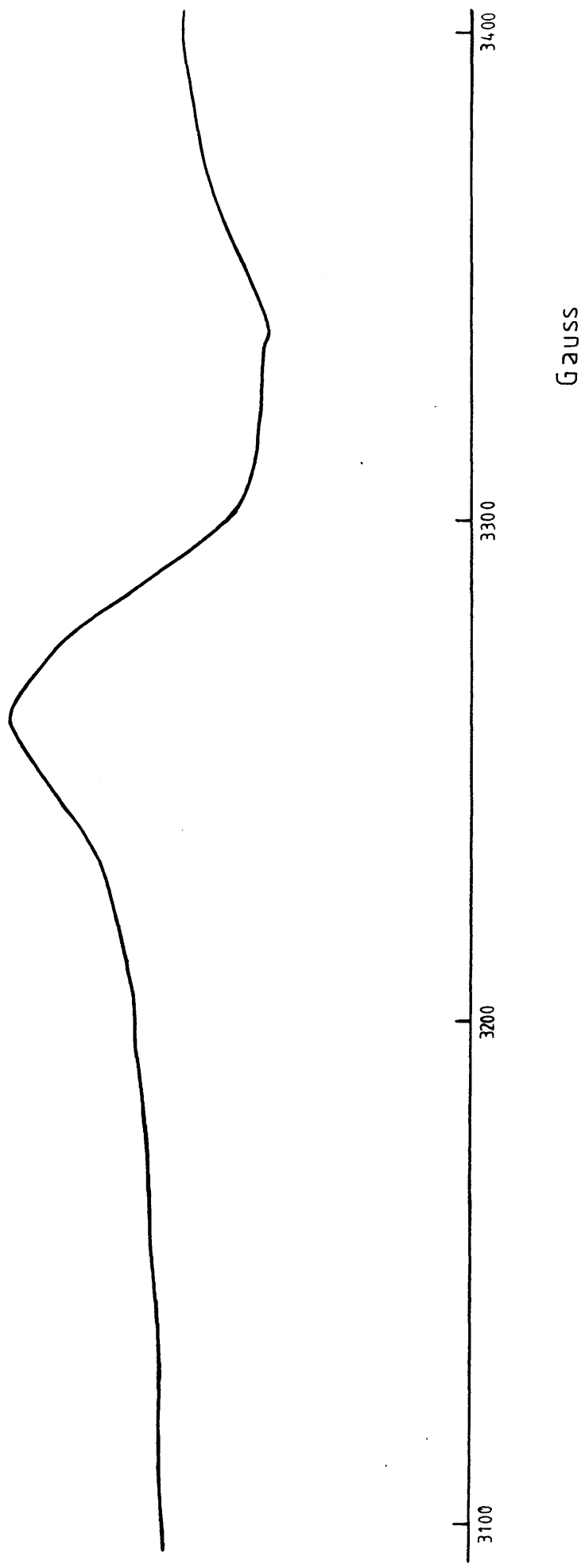


Figure (6.5). E.p.r. spectrum of solid $\text{Ru}_2\text{S}_2(\text{S}_2\text{C}_2\text{Ph}_2)_2$, at 295K

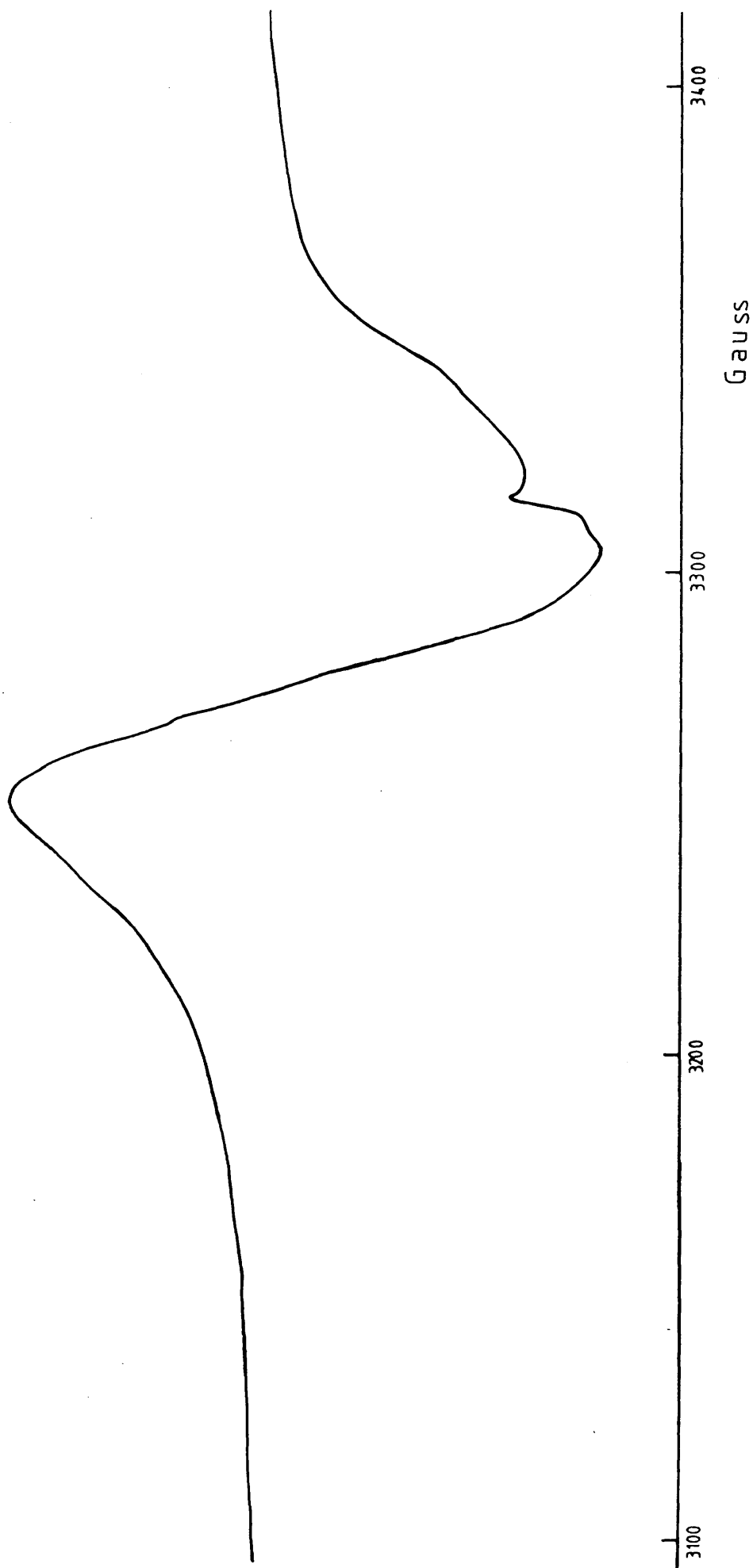


Figure (6.6). E.p.r. spectrum of solid $\text{Ru}_2\text{S}_2(\text{S}_2\text{C}_6\text{H}_4)_2$, at 77K

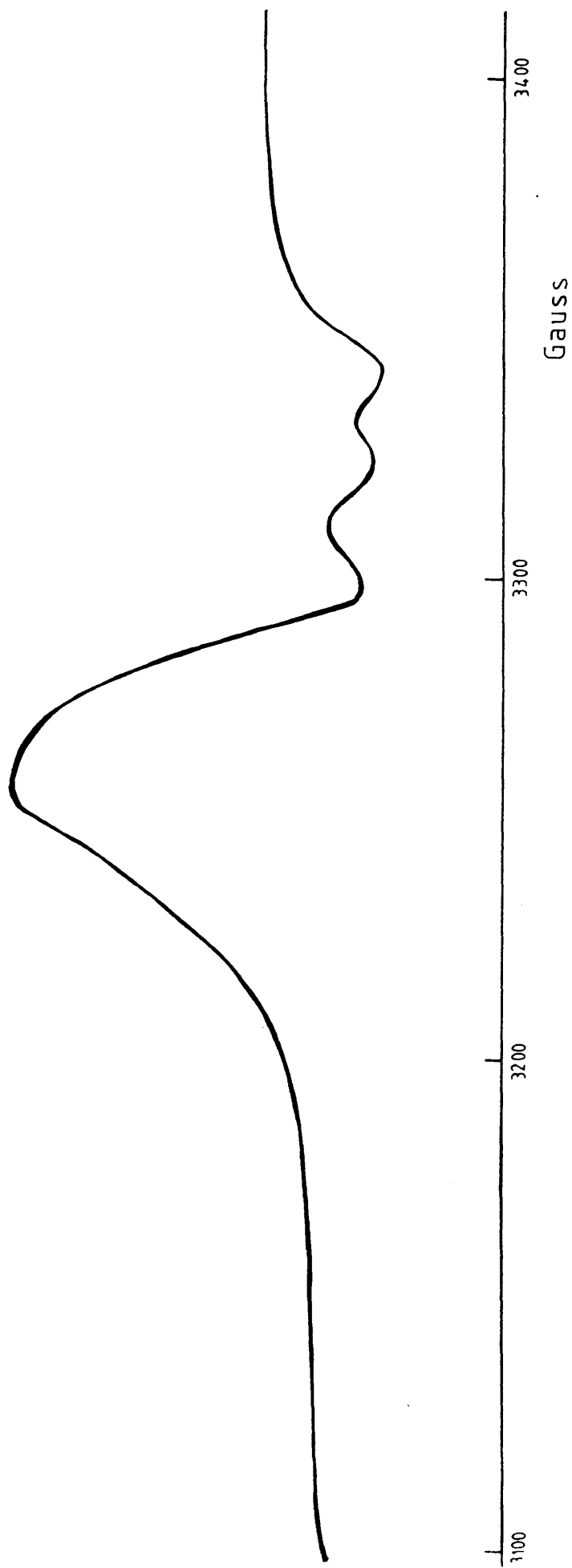


Figure (6.7). E.p.r. spectrum of a 10^{-3} M solution of $\text{Ru}_2\text{S}_2(\text{S}_2\text{C}_2\text{Ph}_2)_2$ in dichloromethane:toluene solution, at 77K

where g is the effective g -factor for the system, and ν_0 is the spectrometer's microwave frequency. In powders and in frozen solutions the paramagnetic complexes are randomly oriented and so absorb over a range of magnetic fields. The lineshape for the overall absorption curve can then be determined in the following way.^{51,162,163}

For a random distribution, the fraction of complexes that lie between θ and $\theta+d\theta$ is $d(\cos\theta)$, so if $d\bar{X}$ is the fraction of complexes whose symmetry axes lie in the interval $d\theta$, and give rise to resonance field values lying within the field interval dH , then

$$d\bar{X} = A(H)dH = d(\cos\theta) \quad (6.2)$$

therefore

$$A(H) = \frac{d(\cos\theta)}{dH} \quad (6.3)$$

and this represents the normalised line shape function, which describes the absorption intensity, as a function of magnetic field, provided the transition probability does not depend on θ .

Recasting of equation (6.1) followed by substitution into (6.3) gives

$$A(H) = -(g_{11}^2 - g_{\perp}^2)^{-\frac{1}{2}} [(\hbar\nu)^2(\beta_e H)^{-2} - g_{\perp}^2]^{-\frac{1}{2}} (\hbar\nu)^2 \beta_e^{-2} H^{-3} \quad (6.4)$$

This function is plotted as the solid line in Figure (6.8). It peaks at $H = \hbar\nu_0/(g_{\perp}\beta_e)$ and has a sharp cut-off at $H = \hbar\nu_0/(g_{11}\beta_e)$.

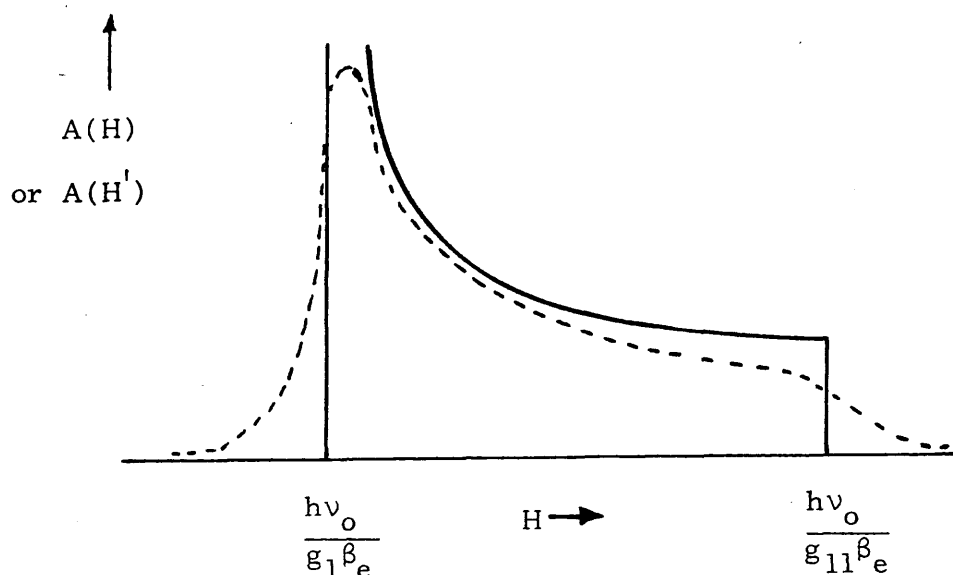


Figure (6.8)

Equation (6.4) assumes that the absorption of microwave radiation by the paramagnetic complex is infinitely sharp. When broadening effects arising from interaction with nearest neighbours are taken into account, this function must be multiplied by a suitable Gaussian function to give the observed absorption curve, the dashed curve in Figure (6.8). The analytical form of the broadened curve is given by equation (6.5)

$$A(H') = \frac{1}{\sqrt{2\pi} \bar{\beta}} \int_{H=H_1}^{H=H_2} A(H) \text{Exp}[-(H'-H)^2 (2\bar{\beta}^2)^{-1}] dH \quad (6.5)$$

where the width of each individual component line is controlled by the broadening parameter $\bar{\beta}$. The effect of $\bar{\beta}$ is to broaden the lines in the absorption spectrum so that the resonance centered at H contributes to the absorption at H' , an amount given by $A(H)dHY(H'-H)$ where $Y(H'-H)$

is the Gaussian lineshape function. The broadened absorption spectrum, equation (6.5), is plotted in the dashed curve in Figure (6.8) and its first derivative is given in Figure (6.9).

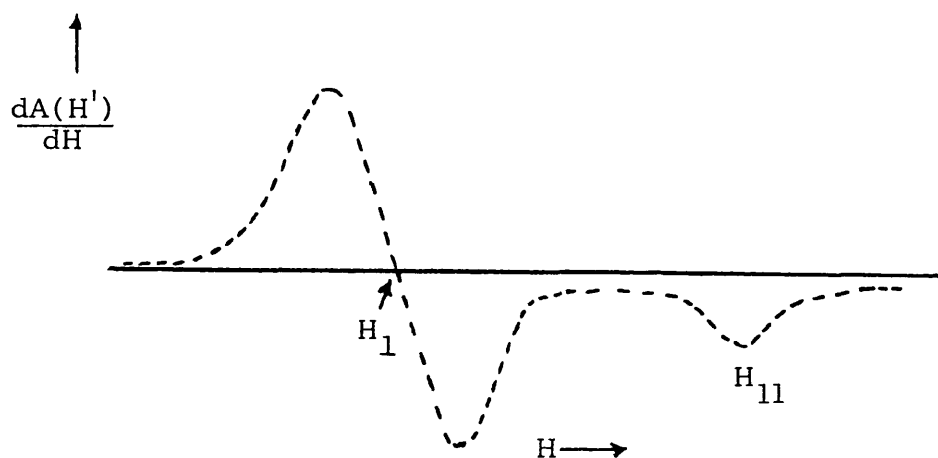
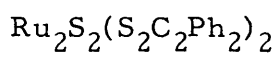


Figure (6.9)

The theoretical first derivative e.p.r. absorption spectrum in Figure (6.9) is quite similar to the derivative e.p.r. absorption spectra obtained from the black solid $\text{Ru}_2\text{S}_2(\text{S}_2\text{C}_2\text{Ph}_2)_2$, shown in Figures (6.5), (6.6), and (6.7). Electron exchange almost certainly takes place in the solid samples, Figures (6.5) and (6.6), but nevertheless on comparison of the two spectra with the frozen spectrum, Figure (6.7), it is obvious that the solid spectra (6.5) and (6.6) are broadened forms of spectrum (6.7). Spectrum (6.7), its integrated absorption spectrum and the unbroadened spectrum from which the latter is derived are shown in Figure (6.10). This comes from one electron in an axially symmetric orbital interacting anisotropically with one nucleus, $I = \frac{1}{2}$. Its spin-Hamiltonian parameters are shown in Table (6.5).

Table (6.5)

Spin-Hamiltonian parameters for the black dimer



g_{11}	g_1	A_{11}, Gauss	A_1, Gauss
1.997_4	2.027_5	19.4_4	9.5_2

The hyperfine coupling observed in the frozen e.p.r. spectrum of the black solid $\text{Ru}_2\text{S}_2(\text{S}_2\text{C}_2\text{Ph}_2)_2$, Figure (6.7), and as shown in the reconstructed diagram, Figure (6.10), can not be due to magnetic ruthenium nuclei. There are two magnetic isotopes of ruthenium, ^{99}Ru (natural abundance = 12.7%, $I = \frac{5}{2}$, $\mu = -0.63$ nuclear Bohr magnetons), and ^{101}Ru (natural abundance = 17.1%, $I = \frac{5}{2}$, $\mu = -0.69$ nuclear Bohr magnetons). These nuclei would each split the e.p.r. spectrum into six peaks, for each orientation of a crystal in a magnetic field.

The e.p.r. spectra of the black dimer show that there is no detectable interaction of the unpaired electron with ruthenium nuclei. The spin Hamiltonian, however, is very similar to those obtained from $\text{Re}(\text{S}_2\text{C}_2\text{Ph}_2)_3$ for which $g_1 = 2.0376$, $g_2 = 2.0182$, $g_3 = 1.9963$, and in which the unpaired electron has been shown to be entirely delocalized over the ligands.¹⁶⁴ Furthermore, the observed g-tensor components for $\text{Ru}_2\text{S}_2(\text{S}_2\text{C}_2\text{Ph}_2)_2$ are quite different from the values that are observed when the unpaired electron is essentially localized on a ruthenium(III) ion.^{91, 93, 94, 99, 100, 103-105, 134}

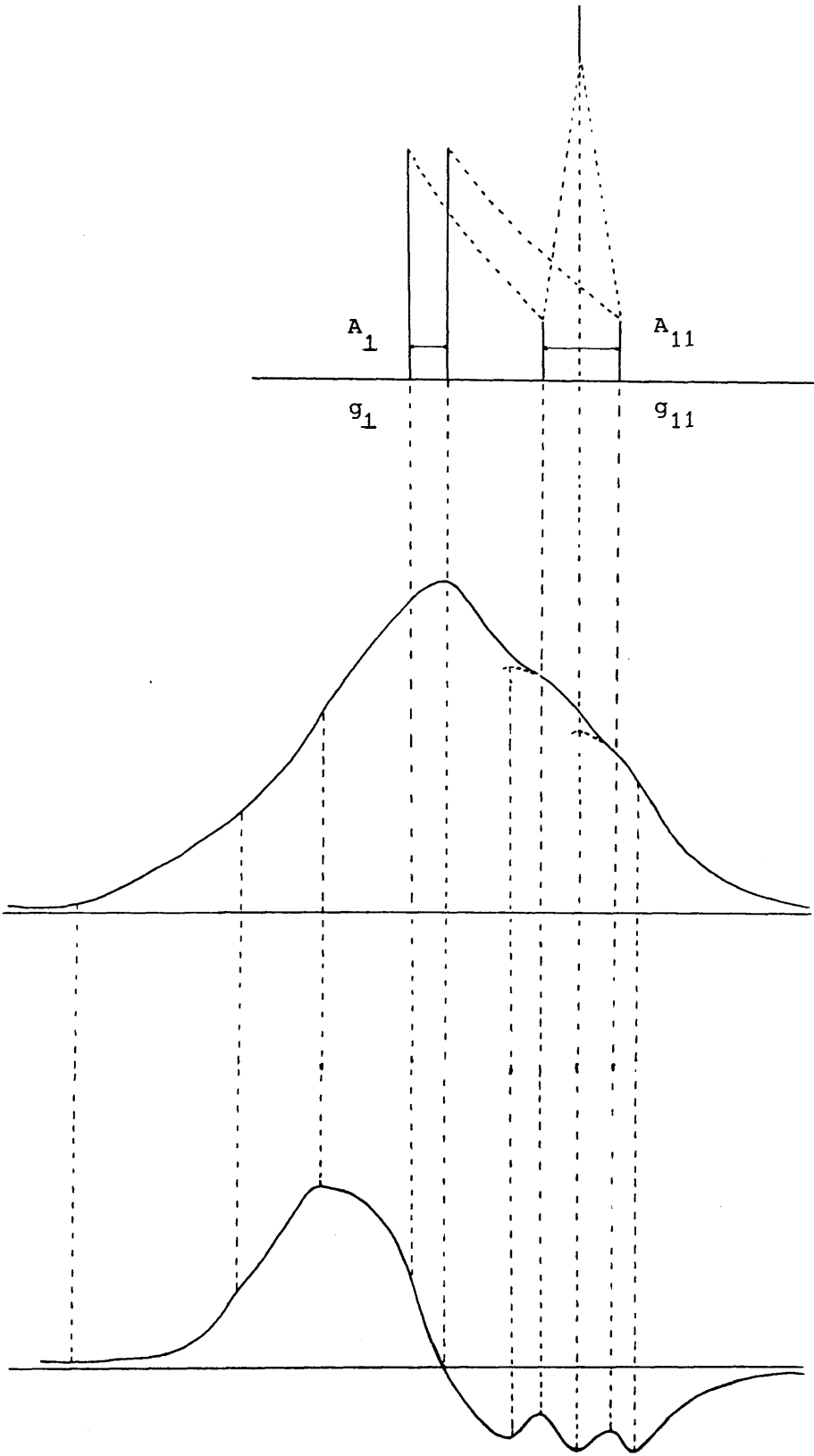
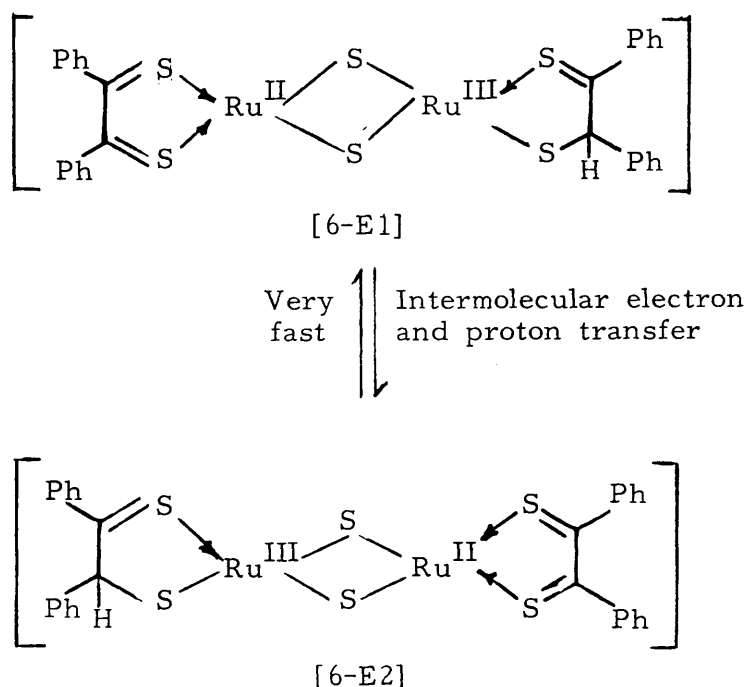


Figure (6.10)

The e.p.r. spectra of this dimer indicate that the unpaired electron is in an axially symmetric orbital delocalized over the ligands. Such spectra would be expected from structure [6-E], see sections (6.4) and (6.5),



in which the unpaired electron lies in an axially symmetric orbital and interacts with one proton.

Figures (6.5), (6.6), (6.7), and (6.10) confirm the presence of unpaired electrons in the black dimer $\text{Ru}_2\text{S}_2(\text{S}_2\text{C}_2\text{Ph}_2)_2$. In order to obtain information about the number of unpaired electrons associated with each formula unit, it is necessary to compare, carefully, the intensity of the e.p.r. absorption signal with that obtained from a suitable standard.

Bis-(acetylacetonato)copper(II), $\text{Cu}(\text{acac})_2$, was used as standard in estimating the spin concentration in the black powder, $\text{Ru}_2\text{S}_2(\text{S}_2\text{C}_2\text{Ph}_2)_2$. The e.p.r. spectra of these compounds have similar

linewidths and lineshapes. In the spectrometer, care was taken to ensure that the Klystron power supply and signal levels, modulation amplitudes and sweep rates were identical, whilst recording spectra of these two compounds. The same spectroil sample tube was filled to the same extent for each measurement, and care was also taken to position the sample tube in the same region of the cavity for all measurements. Under these conditions, the obtained results are listed in Table (6.6). These data indicate that, the number of moles of $\text{Cu}(\text{acac})_2 = \frac{0.0135}{261.54} = 5.1617 \times 10^{-5}$. Hence the number of molecules of $\text{Cu}(\text{acac})_2$ in the species examined, $= (5.1617 \times 10^{-5}) \times (6.022 \times 10^{23})$

$$= 31.0842 \times 10^{18} \text{ molecules}$$

$$= 31.0842 \times 10^{18} \text{ unpaired electrons in the species, } \text{Cu}(\text{acac})_2, \text{ examined.}$$

Similarly, the number of $\text{Ru}_2\text{S}_2(\text{S}_2\text{C}_2\text{Ph}_2)_2$ in the species examined $= 13.085 \times 10^{18}$ molecules.

The number of unpaired electrons in species, $\text{Ru}_2\text{S}_2(\text{S}_2\text{C}_2\text{Ph}_2)_2$, examined $=$ the number of unpaired electrons in species, $\text{Cu}(\text{acac})_2$, examined

$$\times \frac{\text{weight of area under the curve, } \text{Ru}_2\text{S}_2(\text{S}_2\text{C}_2\text{Ph}_2)_2}{\text{weight of area under the curve, } \text{Cu}(\text{acac})_2}$$

$$= (31.0842 \times 10^{18}) \times \frac{0.1817}{2.5796}$$

$$= 2.1462 \times 10^{18} \text{ unpaired electrons.}$$

Therefore, the number of unpaired electrons per molecule of

$$\text{Ru}_2\text{S}_2(\text{S}_2\text{C}_2\text{Ph}_2)_2 = \frac{2.1462 \times 10^{18}}{13.085 \times 10^{18}}$$

$$= 0.164 \text{ unpaired electron}$$

Table (6.6)

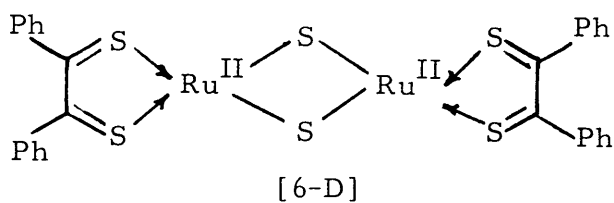
	$\text{Cu}(\text{acac})_2^*$	$\text{Ru}_2\text{S}_2(\text{S}_2\text{C}_2\text{Ph}_2)_2^{**}$
Weight of sample, in gram	0.0135	0.0163
Weight of area under the curve, at recorder gain=0.5V, in gram	2.5795	0.1817

* Molecular weight = 261.54;

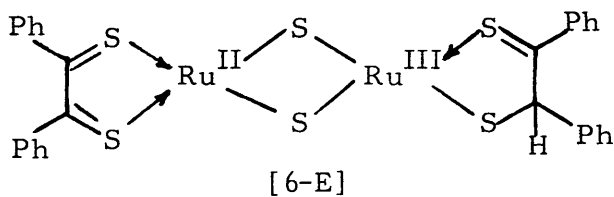
** Molecular weight = 750.14

i.e. There is one unpaired electron for every 6.097 molecules of the black dimer $\text{Ru}_2\text{S}_2(\text{S}_2\text{C}_2\text{Ph}_2)_2$.

Hence, spin counting measurements using this e.p.r. technique show that about 5/6 of the substance examined must have the, diamagnetic, structure [6-D]



and about 1/6 is the paramagnetic species, [6-E]

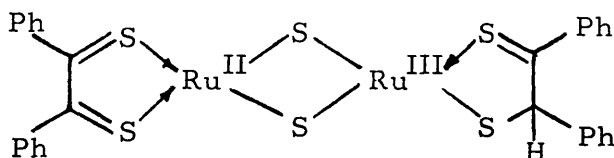


6.7 THE HIGH RESOLUTION PROTON MAGNETIC RESONANCE

SPECTRUM OF BLACK $\text{Ru}_2\text{S}_2(\text{S}_2\text{C}_2\text{Ph}_2)_2$

A 100 MHz ^1H nuclear magnetic resonance spectrum of a solution of $\text{Ru}_2\text{S}_2(\text{S}_2\text{C}_2\text{Ph}_2)_2$ in CDCl_3 , recorded on a VARIAN 100 MHz n.m.r. spectrometer, at 298K, is shown in Figure (6.11). It consists of three broad regions centred at $\delta = 7.29$, 4.26, and 1.32 of relative intensities 20:2:3 respectively. The low-field region of the spectrum, apart from broadening of the sharp structure, normally expected, is that of standard aromatic resonances in a diamagnetic system. When taken in conjunction with the other evidence already presented for this black dimeric substance, $\text{Ru}_2\text{S}_2(\text{S}_2\text{C}_2\text{Ph}_2)_2$, the two broad regions at $\delta \approx 4.26$ and $\delta \approx 1.32$ are assigned to the meta- and, ortho-plus para-, protons (relative intensities 2:3) of phenyl residues.

The intensity ratios indicate that, 0.20 of the sample is paramagnetic and 0.80 is diamagnetic. This compares reasonably favourably with the relative proportion 0.164:0.836 obtained from the e.p.r. estimates already considered. The average of the e.p.r. and n.m.r. results, lead to an estimate of 0.18 of the black dimer, $\text{Ru}_2\text{S}_2(\text{S}_2\text{C}_2\text{Ph}_2)_2$, is in the paramagnetic form, [6-E]



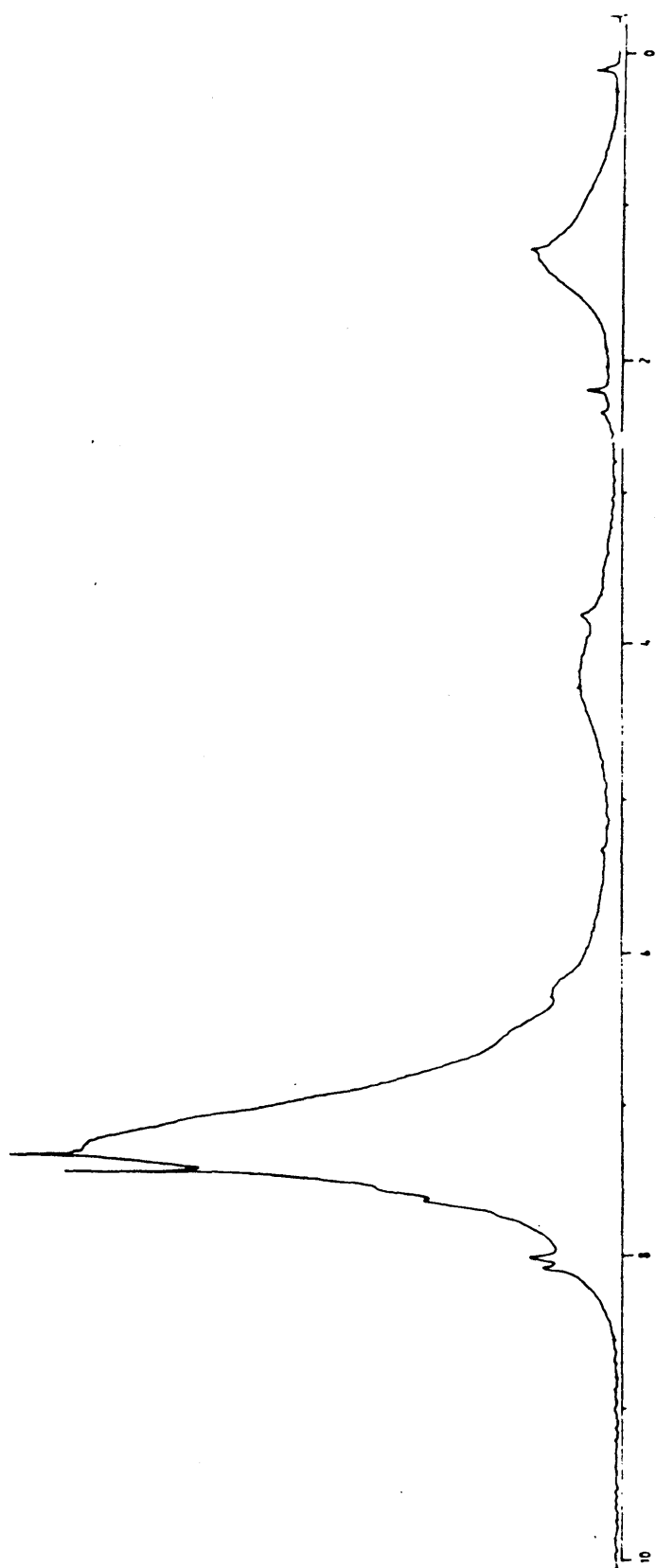
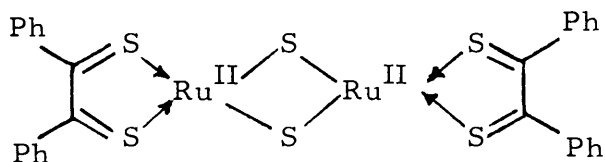
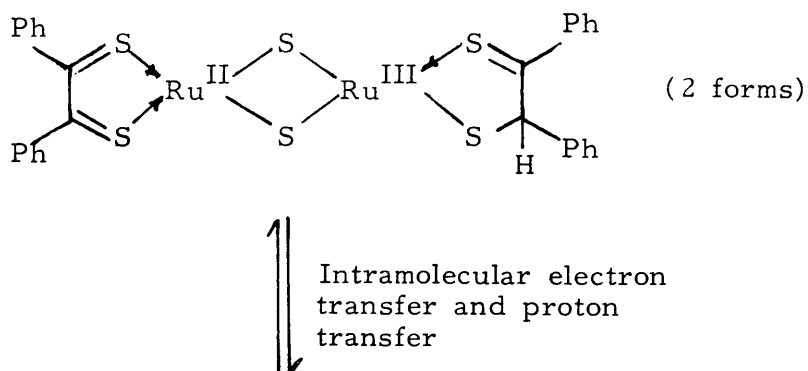


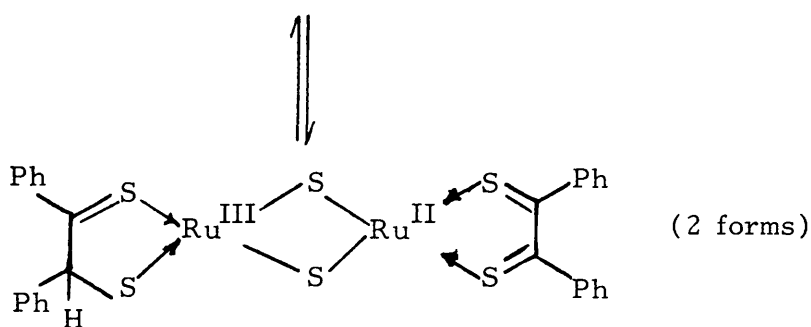
Figure (6.11). ^1H n.m.r. spectrum, $\nu = 100$ MHz, of $\text{Ru}_2\text{S}_2(\text{S}_2\text{C}_2\text{Ph}_2)_2$, in CDCl_3 , at 295K

and 0.82 in the diamagnetic form, [6-D]

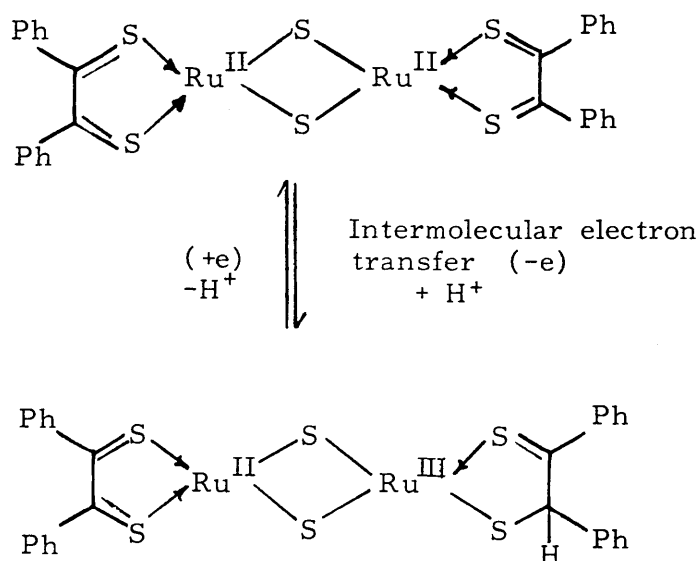


Furthermore, the relative intensities of the peaks in ^1H n.m.r. spectrum of the black dimer $\text{Ru}_2\text{S}_2(\text{S}_2\text{C}_2\text{Ph}_2)_2$ show that on the n.m.r. time scale, the two halves of the paramagnetic form, [6-E], are effectively equivalent, i.e. on the n.m.r. time scale, there is a rapid intramolecular electron transfer in the mixed valence paramagnetic form, [6-E]. A simultaneous proton transfer might also take place, i.e.





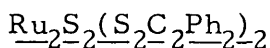
The ^1H n.m.r. spectrum of the diamagnetic form, [6-D], is also broad, implying that, intermolecular electron transfer between the diamagnetic, [6-D], and paramagnetic, [6-E], species



possibly with simultaneous proton transfer, also takes place, but at a slower rate than the intramolecular electron transfer process.

It should be noted that the ^1H n.m.r. spectrum of the black $\text{Ru}_2\text{S}_2(\text{S}_2\text{C}_2\text{Ph}_2)_2$ is also further consistent with the results obtained from the e.p.r. spectra of this dimer, in that, it shows that there is very extensive delocalization of the unpaired electron onto the ligands.

6.8 THE VISIBLE-ULTRAVIOLET SPECTRUM OF BLACK



The visible-ultraviolet spectrum of a solution of $\text{Ru}_2\text{S}_2(\text{S}_2\text{C}_2\text{Ph}_2)_2$ in dichloromethane, recorded on a PYE-UNICAM SP 800 spectrometer is shown in Figure (6.12). The measurements were carried out in a 5 mm cell and the black solution was diluted 10-fold in recording the u.v. region of the spectrum, compared to measurements carried out in the visible region. Wavelengths, wavenumbers, and assignments of the peaks in Figure (6.12) are listed in Table (6.7).

The visible region of the spectrum in Figure (6.12) is very similar to the observed spectrum of the olive-green, $\text{RuC}_{56}\text{H}_{42}\text{O}_2$, Figure (5.13). This observation is consistent with the other evidence, presented in this chapter, in that the dominant ruthenium ion in this black dimer, $\text{Ru}_2\text{S}_2(\text{S}_2\text{C}_2\text{Ph}_2)_2$, is ruthenium(II) rather than ruthenium(III).

The symmetry species of the octahedral group, O_h , correlate¹⁹ with the symmetry species of the group D_{2h} , as shown in Figure (6.13)

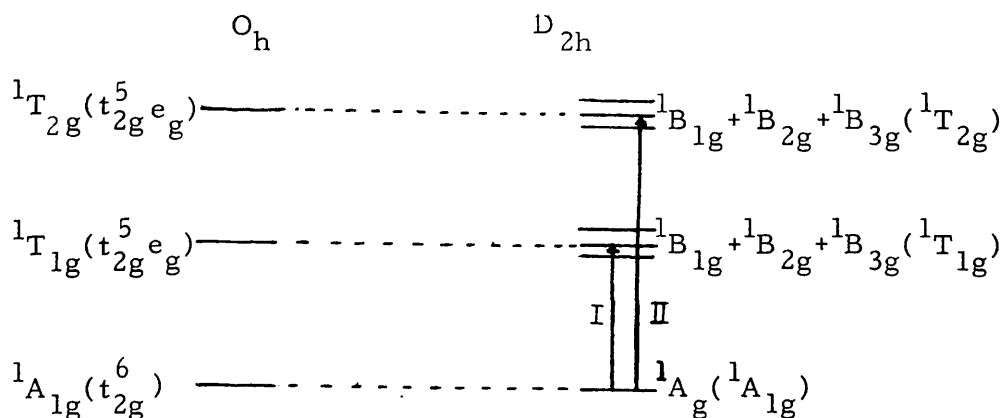


Figure (6.13)

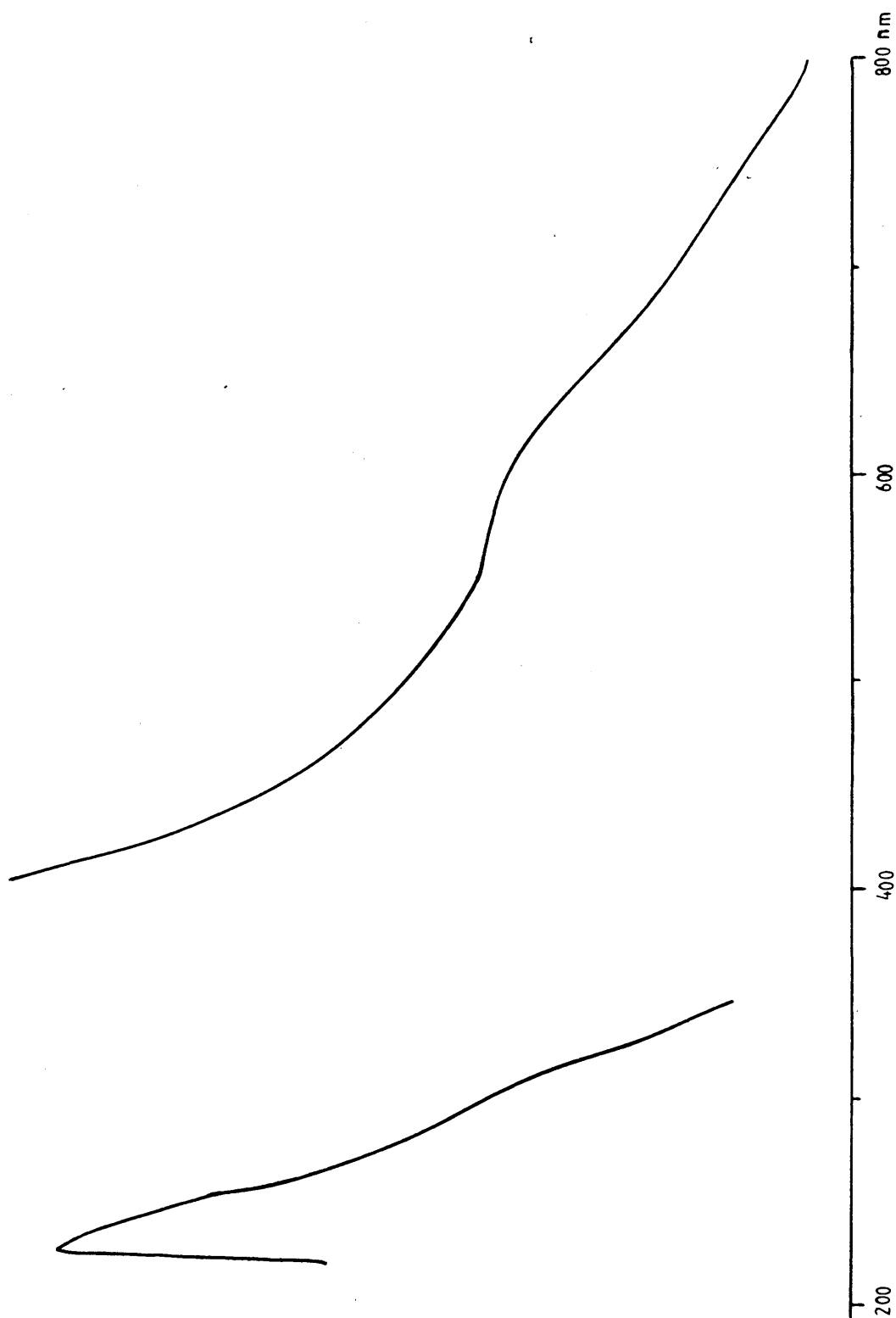


Figure (6.12). Visible-ultraviolet spectrum of $\text{Ru}_2\text{S}_2(\text{S}_2\text{C}_2\text{Ph}_2)_2$ in CH_2Cl_2 solution, at 295K

Table (6.7)

Visible-ultraviolet data for the black dimer $\text{Ru}_2\text{S}_2(\text{S}_2\text{C}_2\text{Ph}_2)_2$
in dichloromethane solution

$\lambda(\text{nm})$	$\sigma(\text{cm}^{-1})$	Description	Assignment
600 ^a	16,660	broad	$^1\text{A}_g(^1\text{A}_{1g}) \longrightarrow ^1\text{B}_{1g} + ^1\text{B}_{2g} + ^1\text{B}_{3g} (^1\text{T}_{1g})$
310 ^b	32,250	shoulder	$^1\text{A}_g(^1\text{A}_{1g}) \longrightarrow ^1\text{B}_{1g} + ^1\text{B}_{2g} + ^1\text{B}_{3g} (^1\text{T}_{2g})$
230	43,470	strong	charge-transfer

(a) Transition I in Figure (6.13); (b) Transition (II) in Figure (6.13)

6.9 The d-ELECTRON DISTRIBUTION IN BLACK $\text{Ru}_2\text{S}_2(\text{S}_2\text{C}_2\text{Ph}_2)_2$

The black dimer, $\text{Ru}_2\text{S}_2(\text{S}_2\text{C}_2\text{Ph}_2)_2$, has the nearly planar structure shown in Figure (6.14).

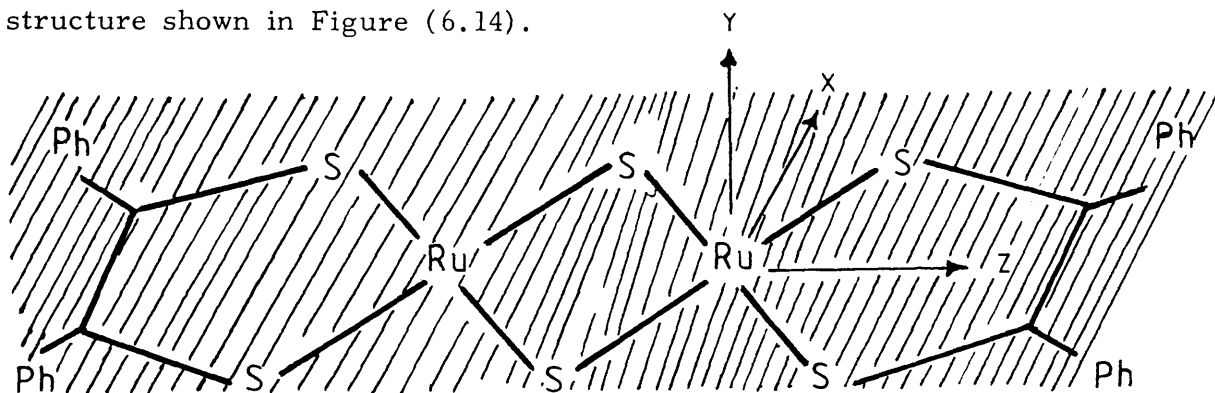


Figure (6.14)

The plane of the molecule is the xz -plane, the y -direction being at right angles to this plane, in a right-handed sense. It is assumed that the sulphur ligand atoms are sp^2 hybridized, the three σ -orbitals lying in the xz -plane, one σ -orbital in each sulphur of the SC(Ph)C(Ph)S pointing towards the neighbouring ruthenium ions, and two sp^2 σ -hybrides of each central sulphur pointing towards the neighbouring ruthenium ions. The axes of the $3p_y$ orbitals in each sulphur are parallel to the y -axis of the coordination framework.

The d-electron distribution in the black dimer, $\text{Ru}_2\text{S}_2(\text{S}_2\text{C}_2\text{Ph}_2)_2$, can be considered in three stages; in the first stage the ordering of the d-orbital energies for each of the ruthenium ions in the dimer are deduced, then the interaction of these orbitals with ligand orbitals and with orbitals on the neighbouring ruthenium ion can be considered in the second stage, and in the third stage electrons are fed into the resultant energy levels scheme.

In the first stage, a simple crystal field analysis for $S_2RuS_2C_2Ph_2$, Figure (6.15),

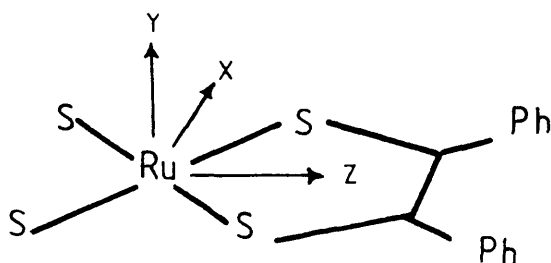


Figure (6.15)

predicts the relative d-orbital energies for each ruthenium ion in this substance to be as shown in Figure (6.16a).

The effect of covalent overlap of the d-orbitals in Figure (6.16a) with the ligand orbitals and with orbitals on the neighbouring ruthenium ion can be considered individually, in the second stage, in the following manner:

(i) $4d_{xz}$ orbital. The lobes of this orbital, of the central ruthenium ion, point directly at the four sulphur ligand atoms as shown in Figure (6.15).

$4d_{xz}$ is therefore strongly involved in σ -bonding with the four sulphur sp^2 hybrids from the ligands, each containing two electrons. Allowing for σ covalent bonding, therefore the energy of $4d_{xz}$ orbital, in Figure (6.16a), increases markedly. The $4d_{xz}$ orbital can not take part in π -bonding with the ligands: it has the wrong symmetry. Weak $d_{\pi}-d_{\pi}$ overlap; i.e. weak $4d_{xz}-4d_{xz}$ π -bonding with the neighbouring ruthenium ion can have only a slight effect on the energy of the $4d_{xz}$ orbital in Figure (6.16a) since the bridging sulphur atoms intervene.

(ii) $4d_{z^2}$ orbital. The energy of the $4d_{z^2}$ orbital is only slightly influenced by weak σ -bonding with the sulphur ligands. This orbital can not take part in π -bonding with the ligands. However, the lobes

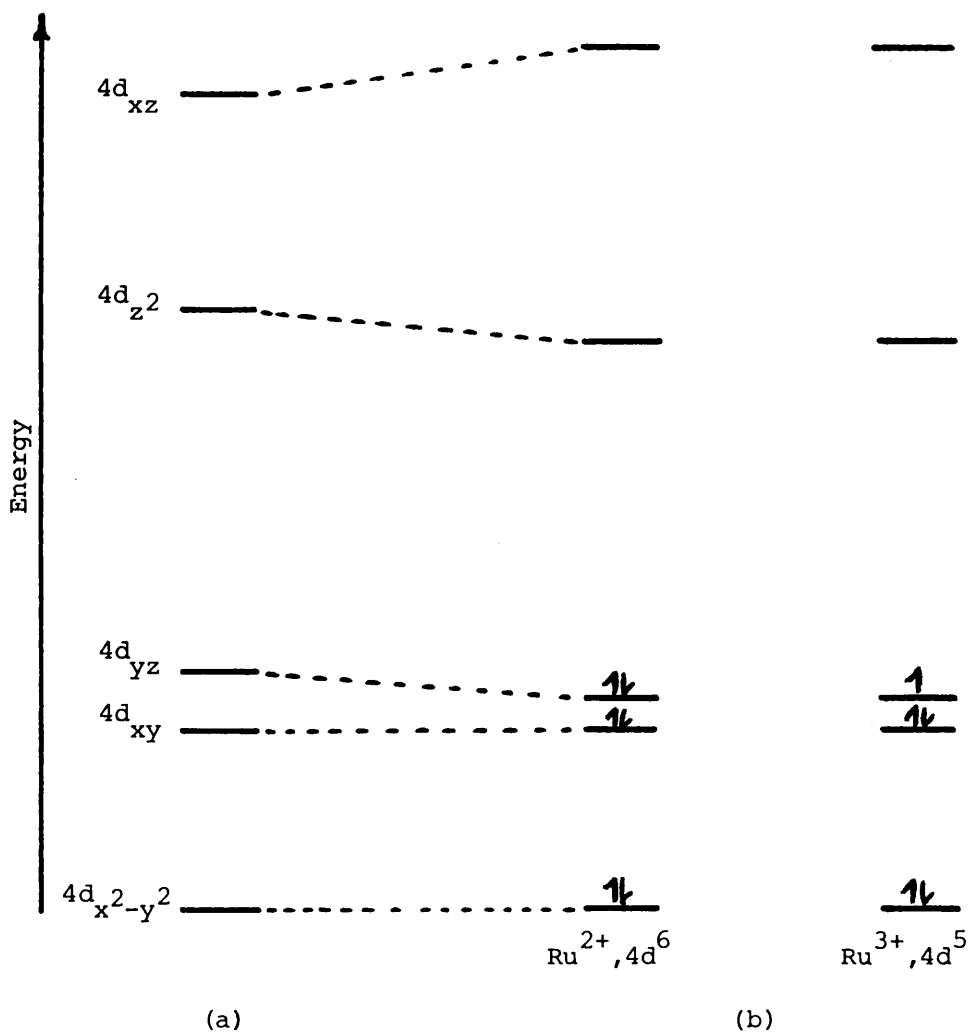


Figure (6.16) An energy level diagram showing the relative orders of the 4d-orbitals of Ru(II), III); (a) at the first stage of the analyses, (b) when the effects of covalent bonding in the black dimer $\text{Ru}_2\text{S}_2(\text{S}_2\text{C}_2\text{Ph}_2)_2$ is taken into account

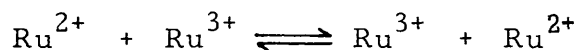
of the $4d_{z^2}$ orbitals on the neighbouring ruthenium ions point directly towards each other, and this $4d_{z^2}$ - $4d_{z^2}$ σ -bonding must lower the energy of the $4d_{z^2}$ orbital in Figure (6.16a). However, the metal ion separation must lie between 2.6 and $3.3\overset{\circ}{\text{\AA}}$, therefore the overlap integral between these two $4d_{z^2}$ orbitals is small and though the overlap will reduce the energy of the $4d_{z^2}$ orbital in Figure (6.16a), it will not lower it too much.

(iii) $4d_{yz}$ orbital. The $4d_{yz}$ orbital on each ruthenium ion can not take part in σ -bonding with the ligands but it does take part in weak side-ways π -bonding with the $3p_y$ orbitals of the neighbouring sulphur atoms. The $4d_{yz}$ orbitals on the ruthenium ions take part in d_{π} - d_{π} bonding, however, again because of the largish separation of the metal ions the net effect of covalent bonding on the $4d_{yz}$ will lower its energy only slightly in the energy level diagram in Figure (6.16a).

(iv) $4d_{xy}$ orbital. The $4d_{xy}$ orbital on each ruthenium ion can not take part in σ -bonding, but it can take part in weak side-ways π -bonding with the ligand $3p_y$ orbitals. $4d_{xy}$ - $4d_{xy}$ δ -bonding with the neighbouring ruthenium ion must be so weak that it is concluded that the relative energy of the ruthenium $4d_{xy}$ orbital is as it is in the energy level diagram, Figure (6.16a).

(v) $4d_{x^2-y^2}$ orbital. This orbital on each ruthenium ion can take part in weak σ -bonding, but it can not take part in π -bonding with the ligands. $4d_{x^2-y^2}$ δ -bonding with the neighbouring ruthenium ion is expected to be very weak, again due to the relative large separation between the two ruthenium ions. It therefore follows that the $4d_{x^2-y^2}$ orbital on the ruthenium ions must have the relative energy shown in Figure (6.16a).

In the third stage, it is concluded that when allowance is made for covalent bonding with the ligands and with the orbitals of the neighbouring ruthenium ions in the dimer, the d-orbitals energies have the relative orders shown in Figure (6.16b), compared to Figure (6.16a). Therefore the unpaired electron in the black dimer, $\text{Ru}_2\text{S}_2(\text{S}_2\text{C}_2\text{Ph}_2)_2$, lies in the $4d_{yz}$ orbital of the ruthenium(III) ions. ($4d_{yz} - 4d_{yz}$) π -bonding with the neighbouring ruthenium(II) ion enables an easy electron exchange



to take place. π -bonding of the ruthenium $4d_{yz}$ orbitals to the ligands enables delocalization of the unpaired electron onto the ligands to be easily effected. It is therefore concluded from this qualitative analysis that on a time average basis the unpaired electron is in a molecular orbital encompassing the whole framework of the molecule involving the π -frames of the ligands and the $4d_{yz}$ orbitals on each of the two ruthenium ions. This accounts qualitatively for the e.p.r. and ^1H n.m.r. results, and it is probable that the electron delocalization is also accompanied by a slower hydrogen atom delocalization of the extra hydrogen atom too.

The unpaired electron essentially migrates over the whole molecular plane, the y-direction is therefore the unique axial direction, i.e. the parallel direction in the e.p.r. experiment, and the xz-plane is the perpendicular plane for this purpose.

REFERENCES

1. B.N. Figgis, "Introduction to Ligand Fields", Interscience, New York, 1966.
2. J.C. Slater, "Quantum theory of atomic structure", McGraw-Hill, New York, 1960, Vol. I, II.
3. C.J. Ballhausen, "Introduction to Ligand Field Theory", McGraw-Hill, New York, 1962.
4. J.S. Griffith, "The Theory of Transition Metal Ions", Cambridge University Press, London, 1964.
5. E.U. Condon and G.H. Shortley, "Theory of Atomic Spectra", 2nd ed., Cambridge University Press, London, 1953.
6. H. Eyring, J. Walter and G.E. Kimball, "Quantum Chemistry", John Wiley and Sons Inc., New York, 1944.
7. H.L. Schäfer and G. Gliemann, "Basic Principles of Ligand Field Theory", Wiley-Interscience, London, 1969.
8. N.M. Gray and L.A. Wills, Phys. Rev., 1931, 38, 248.
9. M. Gerloch and R.C. Slad, "Ligand Field Parameters", Cambridge University Press, London, 1973.
10. G. Racah, Phys. Rev., 1942, 62, 438; 1943, 63, 367.
11. C.E. Moore, "Atomic Energy Levels", Nat. Bur. Standards Circ. 467, Vol.1, 1949; Vol.2, 1952; Vol.3, 1958.
12. S. Fraga, J. Karwowski and K.M.S. Saxena, "Handbook of atomic data", Elsevier, Amsterdam, 1976.
13. T.M. Dunn, Trans. Faraday Soc., 1961, 57, 1441.

14. H.A. Bethe, Ann. physik, 1929, 3 [5], 133, English Translation Consultants Bureau, N.Y., 1958.
15. W.G. Penny and R. Schlapp, Phys. Rev., 1932, 41, 194; 1932, 42, 666.
16. C.K. Jørgensen, "Modern Aspects of Ligand Field Theory", North-Holland, 1971.
17. J.N. Murrell, S.F.A. Kettle and J.M. Tedder, "The Chemical Bond", 2nd edition, John Wiley, London, 1985.
18. H.H. Schmidtke, "Physical Method in Advanced Inorganic Chemistry", ed. N.A.O. Hill and P. Day, Interscience, London, 1968.
19. B. Douglas and C.A. Hollingsworth, "Symmetry in Bonding and Spectra, an Introduction", Academic Press, 1985.
20. R. Fieschi and P.O. Löwdin: Tech. Note 4, Quantum Chemistry Group, Uppsala, 1957.
21. A.M. Clogston, J. Phys. Chem. Solids, 1958, 7, 201.
22. L.E. Orgel, J. Chem. Phys., 1955, 23, 1004 ; 1824.
23. C.K. Jørgensen, "Absorption Spectra and Chemical Bonding in Complexes", Pergamon Press, 1962, Chapter 5.
24. J.C. Hempel, J. Chem. Phys., 1976, 64, 4307.
25. S. Koide and M.H.L. Pryce, Phil. Mag., 1958, 3, 607.
26. R. Pappalardo, J. Chem. Phys., 1959, 31, 1050.
27. Y. Tanabe and S. Sugano, J. Phys. Soc. Japan, 1954, 9, 753; 766.
28. D.S. McClure, "Electronic Spectra of Molecules and Ions in Crystals", Academic Press, 1959.
29. L.E. Orgel, J. Chem. Phys., 1955, 23, 1819.
30. J.S. Griffith, Rec. Trav. Chim., 1956, 75, 676.

31. H.A. Jahn and E. Teller, Proc. Roy. Soc. (London), 1957, A161, 220.
32. J.H. Van Vleck, J. Chem. Phys., 1939, 7, 61;72.
33. K. Pandey, S. Ahuja, N. Poonia and S. Bharti, Chem. Commun., 1982, 1268.
34. E.A. Seddon and K.R. Seddon, "The Chemistry of Ruthenium", Elsevier, The Netherlands, 1984.
35. C.K. Jørgensen, Acta Chem. Scand., 1956, 10, 518.
36. R. Grobelny, B. Jezowska-Trebiatwska and W. Wojciechichowska, J. Inorg. Nucl. Chem., 1966, 28, 2715.
37. A. Gara, K. Natarajan and A. Agarwala, Indian J. Chem., 1977, 15A, 534.
38. J.H. Van Vleck and W.G. Penny, Phil. Mag., 1934, 17 (7), 961.
39. D.H. Good, J. Chem. Phys., 1965, 43, 2830.
40. M. Gerloch, J. Lewis and W.R. Smail, J. Chem. Soc., Dalton Trans., 1972, 1559.
41. K.A. Schroeder, J. Chem. Phys., 1962, 37, 1587.
42. W. Low and G. Rosengarten, J. Mol. Spectro., 1964, 12, 319.
43. J.C. Hempel, J.C. Donini, B.R. Hollebone and A.B.P. Lever, J. Am. Chem. Soc., 1974, 96, 1693.
44. C.E. Solivery, Int. J. Quantum Chem., 1973, 7, 1139.
45. J.C. Donini, B.R. Hollebone, G. London, A.B.P. Lever and J.C. Hempel, Inorg. Chem., 1975, 14, 455.
46. M.L. Ellezey, Int. J. Quantum Chem., 1973, 7, 253.
47. G.F. Koster, J.O. Dimmok, R.G. Wheeler and H. Statz, Properties of thirty-two point groups (MIT, Cambridge, MA, 1963).
48. J.C. Hempel, R.A. Palmer and M.C. Yang, J. Chem. Phys., 1976, 64, 4314.

49. P. Caro, M. Faucher, M. Sary and H. Pankowska, J. Chem. Phys., 1978, 68, 1045.
50. G. Wybourne, "Spectroscopic Properties of Rare Earths", Interscience, New York, 1965, p.164.
51. D. Curie, C. Barthou and B. Canny, J. Chem. Phys., 1974, 61, 3048.
52. B.A. Goodman and J.B. Rynor, Adv. Inorg. Chem. Radio Chem., 1970, 13, 135.
53. A.H. Al-Mowali, Ph.D. Thesis, Glasgow University, 1974.
54. A. Carrington and A.D. McLachlan, "Introduction to Magnetic Resonance", Harper and Row, New York, 1967.
55. C.P. Slichter, "Principles of Magnetic Resonance", Harper and Row, New York, 1963.
56. A. Abragam and B. Bleaney, "Electron Paramagnetic Resonance of Transition Ions", Clarendon Press, Oxford, 1970.
57. N.H. Atherton, "Electron Spin Resonance", Ellis Horwood, London, 1973.
58. B. McGarvey, "Transition Metal Chemistry", ed. Carlin, Marcel Dekker Inc., New York, 1966, Vol. 3, p.90.
59. P.B. Ayscough, "Electron Spin Resonance in Chemistry", Methuen, London, 1967.
60. D.H. Martin, "Magnetism in Solids", Illiffe Books Ltd., London, 1967, p.188.
61. F.E. Mabbs and D.J. Machin, "Magnetism and Transition Metal Complexes", Chapman and Hall, 1973, p.96.
62. E. König, "Physical Method in Advanced Inorganic Chemistry", ed. N.A.O. Hill and P. Day, Interscience, London, 1968, p.266.

63. H. Watanabe, *Progr. Theor. Phys.*, 1957, 18, 405.
64. M.J.D. Powell, J.R. Gabriel and D.F. Johnston, *Phys. Rev. Letters*, 1960, 5, 145.
65. J.S. Griffith, *Mol. Phys.*, 1964, 8, 213.
66. M. Kotani, *J. Phys. Soc. Japan*, 1949, 4, 293.
67. A. Earnshaw, "Introduction to Magnetochemistry", Academic Press, London, 1968, Ch.V.
68. A. Earnshaw, B.N. Figgis, J. Lewis and R.S. Nyholm, *Nature*, 1957, 1121.
69. B.N. Figgis, J. Lewis, R.S. Nyholm and R.D. Peacock, *Discussions Faraday Soc.*, 1958, 103.
70. A. Abragam and M.H.L. Pryce, *Proc. Roy. Soc. (London)*, Ser. A, 1951, 205, 135.
71. B. Bleaney and R.S. Tenam, *Proc. Roy. Soc. (London)*, Ser. A, 1954, 223, 1.
72. T. Castner, G.S. Newell, W.C. Holton and C.P. Slichter, *J. Chem. Phys.*, 1960, 32, 668.
73. J.S. Griffith, *Mol. Phys.*, 1964, 8, 217.
74. R. Aasa and T. Vännngard, *Arkiv Kemi*, 1965, 24, 331.
75. R.D. Dowsing and J.F. Gibson, *J. Chem. Phys.*, 1969, 50, 294.
76. R. Aasa, *ibid*, 1970, 52, 3919.
77. D.J.E. Ingram and J.E. Bennett, *Discussions Faraday Soc.*, 1955, 19, 140.
78. J.E. Bennett and D.J.E. Ingram, *Nature*, 1956, 177, 275.
79. J.S. Griffith, *Proc. Roy. Soc. (London)*, Ser. A, 1956, 235, 23.

80. E.A. Harris, XXIII Congress Ampere on Magnetic Resonance, Rome, 1986.
81. A.L. Porte, "Transition Metal Ion ESR", Specialist Periodical Reports, The Chemical Soc. (London), 1979, 5, 76; 1981, 6, 50; 1982, 7, 69.
82. D. Gatteschi, ibid, 1983, 8, 86; 1985, 9, 16.
83. K.W.H. Stevens, Proc. Roy. Soc., Ser. A, 1953, 219, 542.
84. B. Bleaney and M.C.M. O'Brien, Proc. Phys. Soc. (London) B, 1956, 69, 1216.
85. J.S. Griffith, Mol. Phys., 1971, 21, 35.
86. J.H.M. Thornley, Proc. Phys. Soc. (London) C, 1968, 1, 1024.
87. G.M. Harris Loew, Biophys. J., 1970, 10, 196.
88. J.S. Griffith, Nature, 1957, 180, 30.
89. I. Salmeen and G. Palmer, J. Chem. Phys., 1968, 48, 2049.
90. G. Harris, Theor. Chim. Acta, 1966, 5, 379.
91. A. Hudson and M.J. Kennedy, J. Chem. Soc., 1969, 1116.
92. B.F. Figgis, Trans. Faraday Soc., 1961, 57, 198.
93. R.E. DeSimone and R.S. Drago, J. Am. Chem. Soc., 1970, 92, 2343.
94. R.E. DeSimone, ibid, 1973, 95, 6238.
95. L. Rniz-Ramirez, T.A. Stephenson and E.S. Switkes, J. Chem. Soc., Dalton Trans., 1973, 1770.
96. P.T. Mandraran, P.K. Mehotra, M.M. Taquickhan and R.K. Andal, Inorg. Chem., 1973, 12, 2753.
97. S.A. Cotton and J.F. Gibson, J. Chem. Soc., A, 1971, 803.
98. R.E. DeSimone, T. Ontko, L. Wardman and E.L. Blinn, Inorg. Chem., 1975, 14, 1313.

99. S. Sakaki, N. Hagiwara, Y. Yanase and A. Ohyoshi, J. Phys. Chem., 1978, 82, 1917.
100. D. Kaplan and G. Navon, J. Phys. Chem., 1974, 78, 700.
101. O.K. Medhi and U. Agarwalaw, Inorg. Chem., 1980, 19, 1381.
102. O.K. Medhi and U. Agarwalaw, J. Inorg. Nucl. Chem., 1980, 42, 1413.
103. A.R. Chakaravarty and A. Chakaravorty, J. Chem. Soc., Dalton Trans., 1982, 615.
104. J.B. Raynor and B.A. Jeliaskowa, ibid, 1982, 1185.
105. S. Sakaki, Y. Yanase, N. Hagiwara, T. Takeshita, H. Naganuma, A. Ohyoshi and K. Ohkubo, J. Phys. Chem., 1982, 86, 1038.
106. J.A. Stanko, H.J. Peresie, R.A. Bernheim, R. Wang and P.S. Wang, Inorg. Chem., 1973, 12, 634.
107. W. Reiff and R.E. DeSimone, Inorg. Chem., 1973, 12, 1793.
108. N.J. Hill, J. Chem. Soc., Faraday Trans., 1972, 2, 427.
109. J.H.E. Griffiths, J. Owen and I.M. Word, Proc. Roy. Soc. (London), 1953, A219, 526.
110. J.W. Orton, "Electron Paramagnetic Resonance", Iliffe Books Ltd., London, 1968, p.209.
111. M. Gerloch and J.R. Miller, Prog. Inorg. Chem., 1968, 10, 1.
112. I.A. Miller and E.L. Offenbacher, Phys. Rev., 1968, 166, 269.
113. A.J. Freeman and R.E. Watson, "Hyperfine Interactions", Academic Press, New York, 1967, Chapter 2, pp.53-94.
114. B.R. McGarvey, J. Phys. Chem., 1967, 71, 51.
115. G. Harris, Theor. Chim. Acta, 1968, 10, 119, 155.
116. B. Bleaney and K.W.H. Stevens, Rep. Progr. Phys., 1953, 16, 108.
117. J.E. Bennett and D.J.E. Ingram, Nature (London), 1956, 177, 275.

118. J.E. Bennett, D.J.E. Ingram, P. George and J.S. Griffith, ibid, 1955, 176, 394.
119. J.H. Ammeter, R. Bucher and N. Oswald, J. Am. Chem. Soc., 1974, 96, 7833.
120. R.J. Bucher, J.R. Ferraro and E. Sinn, Chem. Comm., 1976, 910.
121. G.R. Hall and D.N. Hendrickson, Inorg. Chem., 1976, 15, 607.
122. Y. Nishida, S. Oshio and S. Kida, Bull. Chem. Soc. Japan, 1977, 50, 119.
123. D.P. Rininger, N.V. Duffy, R.C. Weir, E. Gelerinter, J. Sanford and D.L. Uhrich, Chem. Phys. Letters, 1977, 52, 102.
124. S. Maroie, M. Savy and J.J. Verbist, Inorg. Chem., 1979, 18, 2560.
125. M.S. Haddad, M.W. Lynch, W.D. Federer and D.N. Hendrickson, Inorg. Chem., 1981, 20, 123; 131.
126. A.K. Gregson, Inorg. Chem., 1981, 20, 81.
127. S. Neya and I. Morishima, J. Am. Chem. Soc., 1982, 104, 5658.
128. K.D. Bowers and J. Owen, J. Rep. Progr. Phys., 1955, 18, 304.
129. N.S. Garifynov and E.G. Karakhaslyan, Fiz. Tverd. Tela, 1965, 7, 1244; (Russ.), Soviet Phys.-Solid State (Engl.), 1965, 7, 1033.
130. H.S. Jarrett, J. Chem. Phys., 1957, 27, 1298.
131. S. Geschwind and J.P. Remeika, J. Appl. Phys., Suppl. No. 1, 1962, 33, 370.
132. R.N. Mukherjee and V.S. Vijaya, Indian J. Chem., 1982, 21A, 427.
133. A.J. Freeman and R.E. Watson, "Magnetism", Academic Press, New York, 1965, Vol.IIA.
134. M. Blume, A.J. Freeman and R.E. Watson, Phys. Rev., 1964, A320, 134.

135. E.B. Sandell, "Colorimetric metal analysis", 3rd edition, Interscience, 1959, p.778.
136. N. Colthup, L. Daly and S. Wiberely, "Introduction to infrared and Raman spectroscopy", 2nd edition, Academic Press, 1975,
(a) p.278; (b) p.257; (c) p.246; (d) p.237.
137. N. Nakamoto, "Infrared Spectra of Inorganic and Coordination Compound", John Wiley and Sons Inc., New York, 1963.
138. B.E. Cavit, K.R. Grundy and W.R. Roper, Chem. Comm., 1972, 60.
139. J. Collman, J. Kang, W. Little and M. Sullivan, Inorg. Chem., 1968, 7, 1298.
140. M. Michman and H.H. Zeiss, J. Organomet. Chem., 1970, 25, 161, 167.
141. "Eight Peak Index of Mass Spectra", MSDC, 1st edition, 1970, Vol.1,2.
142. J.H. Bowie, R.G. Cooks, G.E. Gream and H.H. Laffer, Aust. J. Chem., 1968, 21, 1247.
143. U.R. Myers, Rev. Mod. Phys., 1952, 24, 15.
144. B.N. Figgis and J. Lewis, "Modern Coordination Chemistry", ed. J. Lewis and R.G. Wilkens, Interscience, New York, 1960, p.400.
145. "CRC Handbook of Chemistry and Physics", CRC Press, Boca Katon, Fla., 63rd edition, 1982-1983.
146. C.K. Jørgensen, Acta Chem. Scand., 1956, 10, 500.
147. C.K. Jørgensen, ibid, 1957, 11, 151.
148. E.V. Stroganov and K.V. Ovchinnikov, Vestnik Leningrad Univ. 12, No. 22, Ser. Fiz. i Khim. No. 4, 152-7 (1957). Chem. Abs., 1957, 52, 13356.
149. J.M. Fletcher, W.E. Gardener, A.C. Fox and G. Topping, J. Chem. Soc. (A), 1967, 1038.

150. J.L. Woodhead and J.M. Fletcher, U.K. At. Energy Res. Group Rep., A.E.R.E., R-4123 (1962).
151. J.A. McCleverty, Prog. Inorg. Chem., 1968, 10, 49.
152. R.P. Burns and C.A. McAuliffe, Adv. Inorg. Chem., Radiochem., 1979, 22, 303.
153. G.N. Schrauzer, V.P. Mayweg, H.W. Finck, U. Müller-Westerhoff, and W. Heinrich, Angew. Chem., Int. Ed. Engl., 1964, 3, 381.
154. G.N. Schrauzer, V.P. Mayweg, H.W. Finck and W. Heinrich, J. Am. Chem. Soc., 1966, 88, 4604.
155. Y. Masuda, K. Koya and S. Misumi, Nippon Kagaku Kaishi, 1975, 636. Chem. Abs., 1975, 83, 36934k.
156. G.N. Schrauzer and V.P. Mayweg, J. Am. Chem. Soc., 1965, 87, 1483.
157. O. Simann and J. Fresco, Inorg. Chem., 1971, 10, 297.
158. C.W. Schlapfer and K. Nakamoto, ibid, 1975, 14, 1338.
159. G.N. Schrauzer, V.P. Mayweg and W. Heinrich, Inorg. Chem., 1965, 4, 1615.
160. S.M. Bloom and G.O. Dudeck, Inorg. Nucl. Chem. Letters, 1966, 2, 138.
161. T.A. Elwood, P.F. Rogerson and M.M. Bursey, J. Org. Chem., 1969, 34, 1138.
162. R. Neiman and D. Kivelson, J. Chem. Phys., 1961, 35, 156.
163. H.R. Gersmann and J.D. Swalen, ibid, 1962, 36 3221.
164. A. Al-Mowali and A.L. Porte, J. Chem. Soc., Dalton Trans., 1975, 250.

